

ISSN 2518-7198 (Print)
ISSN 2663-5089 (Online)



№ 2(94)/2019

ФИЗИКА сериясы

Серия ФИЗИКА

PHYSICS Series

**ҚАРАҒАНДЫ
УНИВЕРСИТЕТІНІҢ
ХАБАРШЫСЫ**

**ВЕСТНИК
КАРАГАНДИНСКОГО
УНИВЕРСИТЕТА**

**BULLETIN
OF THE KARAGANDA
UNIVERSITY**

ISSN 2518-7198 (Print)
ISSN 2663-5089 (Online)
Индексі 74616
Индекс 74616

**ҚАРАҒАНДЫ
УНИВЕРСИТЕТІНІҢ
ХАБАРШЫСЫ**

ВЕСТНИК
КАРАГАНДИНСКОГО
УНИВЕРСИТЕТА

BULLETIN
OF THE KARAGANDA
UNIVERSITY

ФИЗИКА сериясы

Серия ФИЗИКА

PHYSICS Series

№ 2(94)/2019

Сәуір–мамыр–маусым
28 маусым 2019 ж.

Апрель–май–июнь
28 июня 2019 г.

April–May–June
June, 28, 2019

1996 жылдан бастап шығады
Издается с 1996 года
Founded in 1996

Жылына 4 рет шығады
Выходит 4 раза в год
Published 4 times a year

Қарағанды, 2019
Караганда, 2019
Karaganda, 2019

Бас редакторы

химия ғыл. д-ры, профессор, ҚР ҰҒА корр.-мүшесі

А.Т. Едрисов

Бас редактордың орынбасары

Е.М. Тажбаев, хим. ғыл. д-ры, профессор,
ҚР ҰҒА корр.-мүшесі

Жауапты хатшы

Г.Ю. Аманбаева, филол. ғыл. д-ры, профессор

Редакция алқасы

Б.Р. Нүсіпбеков,

Т.Ә. Көкетайтегі,

Н.Х. Ибраев,

А.О. Сәулебеков,

Қ.М. Арынғазин,

И.В. Брейдо,

И.П. Курытник,

М. Стоев,

М.М. Кидибаев,

З.Ж. Жаңабаев,

Г.В. Климушева,

С.Е. Көмеков,

В.М. Лисицын,

И.Н. Огородников,

О.П. Пчеляков,

А.Т. Акылбеков,

А.Ж. Тұрмұхамбетов,

К.Ш. Шүңкеев,

В.Ю. Кучерук,

Л.В. Чиркова,

ғылыми редактор техн. ғыл. канд. (Қазақстан);

физ.-мат. ғыл. д-ры (Қазақстан);

физ.-мат. ғыл. д-ры (Қазақстан);

физ.-мат. ғыл. д-ры (Қазақстан);

пед. ғыл. д-ры (Қазақстан);

техн. ғыл. д-ры (Қазақстан);

техн. ғыл. д-ры (Польша);

PhD д-ры (Болгария);

физ.-мат. ғыл. д-ры (Қырғызстан);

физ.-мат. ғыл. д-ры (Қазақстан);

физ.-мат. ғыл. д-ры (Украина);

физ.-мат. ғыл. д-ры (Қазақстан);

физ.-мат. ғыл. д-ры (Ресей);

физ.-мат. ғыл. д-ры (Ресей);

физ.-мат. ғыл. д-ры (Ресей);

физ.-мат. ғыл. д-ры (Қазақстан);

физ.-мат. ғыл. д-ры (Қазақстан);

физ.-мат. ғыл. д-ры (Қазақстан);

техн. ғыл. д-ры (Украина);

жауапты хатшы техн. ғыл. канд. (Қазақстан)

Редакцияның мекенжайы: 100024, Қазақстан, Қарағанды қ., Университет к-сі, 28

Тел.: (7212) 77-03-69 (ішкі 1026); факс: (7212) 77-03-84.

E-mail: vestnick_kargu@ksu.kz; tchlv_53@mail.ru (*жауапты хатшы*)

Сайты: <https://physics-vestnik.ksu.kz/>

Редакторлары

Ж.Т. Нурмуханова, И.Н. Муртазина

Компьютерде беттеген

В.В. Бутяйкин

Қарағанды университетінің хабаршысы. «Физика» сериясы.

ISSN 2518-7198 (Print). ISSN 2663-5089 (Online).

Меншік иесі: «Академик Е.А. Бөкетов атындағы Қарағанды мемлекеттік университеті» РММ.

Қазақстан Республикасының Мәдениет және ақпарат министрлігімен тіркелген. 23.10.2012 ж. № 13111–Ж тіркеу куәлігі.

Басуға 29.06.2019 ж. қол қойылды. Пішімі 60×84 1/8. Қағазы офсеттік. Көлемі 14,5 б.т. Таралымы 300 дана. Бағасы келісім бойынша. Тапсырыс № 83.

Е.А. Бөкетов атындағы ҚарМУ баспасының баспаханасында басылып шықты.

100012, Қазақстан, Қарағанды қ., Гоголь к-сі, 38. Тел. 51-38-20. E-mail: izd_kargu@mail.ru

Главный редактор

д-р хим. наук, профессор, чл.-корр. НАН РК

А.Т. Едрисов

Зам. главного редактора **Е.М. Тажбаев**, д-р хим. наук, профессор,
чл.-корр. НАН РК

Ответственный секретарь **Г.Ю. Аманбаева**, д-р филол. наук, профессор

Редакционная коллегия

Б.Р. Нусупбеков,	научный редактор канд. техн. наук (Казахстан);
Т.А. Кокетагтеги,	д-р физ.-мат. наук (Казахстан);
Н.К. Ибраев,	д-р физ.-мат. наук (Казахстан);
А.О. Саулебеков,	д-р физ.-мат. наук (Казахстан);
К.М. Арынгазин,	д-р пед. наук (Казахстан);
И.В. Брейдо,	д-р техн. наук (Казахстан);
И.П. Курытник,	д-р техн. наук (Польша);
М. Стоев,	д-р PhD (Болгария);
М.М. Кидибаев,	д-р физ.-мат. наук (Кыргызстан);
З.Ж. Жанабаев,	д-р физ.-мат. наук (Казахстан);
Г.В. Климушева,	д-р физ.-мат. наук (Украина);
С.Е. Кумеков,	д-р физ.-мат. наук (Казахстан);
В.М. Лисицын,	д-р физ.-мат. наук (Россия);
И.Н. Огородников,	д-р физ.-мат. наук (Россия);
О.П. Пчеляков,	д-р физ.-мат. наук (Россия);
А.Т. Акылбеков,	д-р физ.-мат. наук (Казахстан);
А.Ж. Турмухамбетов,	д-р физ.-мат. наук (Казахстан);
К.Ш. Шункеев,	д-р физ.-мат. наук (Казахстан);
В.Ю. Кучерук,	д-р техн. наук (Украина);
Л.В. Чиркова,	ответственный секретарь канд. техн. наук (Казахстан)

Адрес редакции: 100024, Казахстан, г. Караганда, ул. Университетская, 28

Тел.: (7212) 77-03-69 (внутр. 1026); факс: (7212) 77-03-84.

E-mail: vestnick_kargu@ksu.kz; tchlv_53@mail.ru (*отв. секретарь*)

Сайт: <https://physics-vestnik.ksu.kz/>

Редакторы

Ж.Т. Нурмуханова, И.Н. Муртазина

Компьютерная верстка

В.В. Бутяйкин

Вестник Карагандинского университета. Серия «Физика».

ISSN 2518-7198 (Print). ISSN 2663-5089 (Online).

Собственник: РГП «Карагандинский государственный университет имени академика Е.А. Букетова».

Зарегистрирован Министерством культуры и информации Республики Казахстан. Регистрационное свидетельство № 13111–Ж от 23.10.2012 г.

Подписано в печать 29.06.2019 г. Формат 60×84 1/8. Бумага офсетная. Объем 14,5 п.л. Тираж 300 экз.
Цена договорная. Заказ № 83.

Отпечатано в типографии издательства КарГУ им. Е.А. Букетова.

100012, Казахстан, г. Караганда, ул. Гоголя, 38, тел.: (7212) 51-38-20. E-mail: izd_kargu@mail.ru

Main Editor

Doctor of Chemical sciences, Professor, Corresponding member of NAS RK

A.T. Yedrissov

Deputy main Editor

E.M. Tazhbaev, Doctor of chem. sciences, Professor,
Corresponding member of NAS RK

Responsible secretary

G.Yu. Amanbayeva, Doctor of phylol. sciences, Professor

Editorial board

B.R. Nusupbekov ,	Science editor Cand. of techn. sciences (Kazakhstan);
T.A. Kuketaev ,	Doctor of phys.-math. sciences (Kazakhstan);
N.Kh. Ibrayev ,	Doctor of phys.-math. sciences (Kazakhstan);
A.O. Saulebekov ,	Doctor of phys.-math. sciences (Kazakhstan);
K.M. Aryngasin ,	Doctor of ped. sciences (Kazakhstan);
I.V. Breido ,	Doctor of techn. sciences (Kazakhstan);
I.P. Kurytnik ,	Doctor of techn. sciences (Poland);
M. Stoev ,	PhD (Bulgaria);
M.M. Kidibaev ,	Doctor of phys.-math. sciences (Kyrgyzstan);
Z.Zh. Zhanabaev ,	Doctor of phys.-math. sciences (Kazakhstan);
G.V. Klimusheva ,	Doctor of phys.-math. sciences (Ukraine);
S.E. Kumekov ,	Doctor of phys.-math. sciences (Kazakhstan);
V.M. Lisitsyn ,	Doctor of phys.-math. sciences (Russia);
I.N. Ogorodnikov ,	Doctor of phys.-math. sciences (Russia);
O.P. Pchelyakov ,	Doctor of phys.-math. sciences (Russia);
A.T. Akylbekov ,	Doctor of phys.-math. Sciences (Kazakhstan);
A.Zh. Turmuhambetov ,	Doctor of phys.-math. sciences (Kazakhstan);
K.Sh. Shunkeyev ,	Doctor of phys.-math. sciences (Kazakhstan);
V.Yu. Kucheruk ,	Doctor of techn. sciences (Ukraine);
L.V. Chirkova ,	Secretary Cand. of techn. sciences (Kazakhstan)

Postal address: 28, University Str., 100024, Karaganda, Kazakhstan

Tel.: (7212) 77-03-69 (add. 1026); fax: (7212) 77-03-84.

E-mail: vestnick_kargu@ksu.kz; tchlv_53@mail.ru (*secretary*)

Web-site: <https://physics-vestnik.ksu.kz/>

Editors

Zh.T. Nurmukhanova, I.N. Murtazina

Computer layout

V.V. Butyaikin

Bulletin of the Karaganda University. «Physics» series.

ISSN 2518-7198 (Print). ISSN 2663-5089 (Online).

Proprietary: RSE «Academician Ye.A. Buketov Karaganda State University».

Registered by the Ministry of Culture and Information of the Republic of Kazakhstan. Registration certificate No. 13111–Zh from 23.10.2012.

Signed in print 29.06.2019. Format 60×84 1/8. Offset paper. Volume 14,5 p.sh. Circulation 300 copies. Price upon request. Order № 83.

Printed in the Ye.A. Buketov Karaganda State University Publishing house.

100012, Kazakhstan, Karaganda, Gogol Str., 38, Tel.: (7212) 51-38-20. E-mail: izd_kargu@mail.ru

МАЗМҰНЫ

КОНДЕНСАЦИЯЛАНҒАН КҮЙДІҢ ФИЗИКАСЫ

<i>Чиркова Л.В., Ермаганбетов К.Т., Маханов К.М., Рожкова К.С., Аринова Е.Т., Курмаиш А.</i> Туннельдік диодта тоқтың орнықсыздығы және электрондардың өздігінен ұйымдасуы.....	8
<i>Сакенова Р.Е., Ердыбаева Н.К., Погребняк А.Д., Кылышканов М.К.</i> Вакуумды-доғалық әдіспен алынған $\text{MoN}(\text{MoZr})\text{ZrN}$ және $(\text{TiMo})\text{N}/(\text{TiMo})$, $(\text{CrZr})\text{N}/(\text{CrZr})$ негізіндегі көпқабатты жабынды зерттеу	14
<i>Шалтаков С.Н., Кажикенова С.Ш., Нусупбеков Б.Р., Карабекова Д.Ж., Хасенов А.К., Стоев М.</i> Жақын тәртіптің табиғатын есепке ала отырып балқыманың жоғары температуралы ағынының математикалық моделі	22
<i>Глеуменов С.К., Жукенов М.К., Испулов Н.А.</i> Электрмагниттік толқындардың анизотропты магнитэлектрлік орталарда таралуы туралы.....	29
<i>Юров В.М., Архипов В.В., Ранова Г.А., Лауринас В.Ч.</i> Нанобөлшектердің термодинамикалық сипаттамаларының мөлшеріне тәуелділіктерін зерттеу	35
<i>Юров В.М., Еремин Е.Н., Лауринас В.Ч., Қасымов С.С.</i> Трибологиядағы диссипативтік үрдістер.....	42
<i>Жумабеков А.Ж., Ибраев Н.Х., Селиверстова Е.В., Камалова Г.Б.</i> $\text{TiO}_2\text{-GO}$ нанокөміршікті материалды алу мен оның электрфизикалық және оптикалық қасиеттерін зерттеу	54

ЖЫЛУ ФИЗИКАСЫ ЖӘНЕ ТЕОРИЯЛЫҚ ЖЫЛУ ТЕХНИКАСЫ

<i>Хасенов А.К., Нүсіпбеков Б.Р., Карабекова Д.Ж., Стоев М., Зейнолла Б.К., Муратова А.К.</i> Тұрғындарды жылумен және ыстық сумен жабдықтауда жылу энергиясының шығындарын үнемдеу.....	61
<i>Шаймерденова К.М., Шрагер Э.Р., Тусыпбаева А.С., Наушарбан Ж.К.</i> Тік орналасқан жылуалмастырғыштардағы жылу алмасу үрдістерін зерттеу.....	66

ТЕХНИКАЛЫҚ ФИЗИКА

<i>Гевко И., Ляшук О., Сокил М., Слободян Л., Гудь В., Вовк Ю.</i> Винттік жүктіегіштің қозғалмалы жұмыс бөлігінің резонанстық тербелісі	73
<i>Кашканов А.А., Диордица В.Н., Кучерук В.Ю., Карабекова Д.Ж., Хасенов А.К., Шарзадин А.М.</i> Шұғыл тежеу кезінде автокөлік дөңгелектерінің жолмен өзара әрекеттесуін инерциялық бағалау	82
<i>Кучерук В.Ю., Курытник И.П., Ошанов Е.З., Кулаков П.И., Семенов А.А., Карабекова Д.Ж., Хасенов А.К.</i> Асинхронды қозғалтқыштың айналмалы моментінің динамикалық сипаттамаларын компьютерлік-өлшеу жүйесі	92
<i>Нусупбеков Б.Р., Картбаева Г.Т., Стоев М., Хасенов А.К., Карабекова Д.Ж., Муратова А.К.</i> Сүйек майын алудың электрGRIDРОИМПУЛЬСТІК әдісі.....	101
<i>Танашева Н.К., Дюсембаева А.Н., Нусупбеков Б.Р., Миньков Л.Л., Нурғалиева Ж.Г., Саденова К.К.</i> Айналмалы қозғалыстағы цилиндрлердің аэродинамикалық коэффициенттерін зерттеу	108

АВТОРЛАР ТУРАЛЫ МӘЛІМЕТТЕР	114
----------------------------------	-----

СОДЕРЖАНИЕ

ФИЗИКА КОНДЕНСИРОВАННОГО СОСТОЯНИЯ

<i>Чиркова Л.В., Ермаганбетов К.Т., Маханов К.М., Рожкова К.С., Аринова Е.Т., Курмаиш А.</i> Явления неустойчивости тока в туннельном диоде и процессы самоорганизации электронов.....	8
<i>Сакенова Р.Е., Ердыбаева Н.К., Погребняк А.Д., Кылышканов М.К.</i> Исследование многослойных покрытий на основе MoN(MoZr)ZrN и (TiMo)N/(TiMo), (CrZr)N/(CrZr), полученных методом вакуумного-дугового осаждения.....	14
<i>Шалтаков С.Н., Кажикенова С.Ш., Нусупбеков Б.Р., Карабекова Д.Ж., Хасенов А.К., Стоев М.</i> Математическая модель высокотемпературного течения расплава с учетом природы ближнего порядка.....	22
<i>Тлеукиенов С.К., Жукенов М.К., Испулов Н.А.</i> О распространении электромагнитных волн в анизотропных магнитоэлектрических средах.....	29
<i>Юров В.М., Архипов В.В., Ранова Г.А., Лауринас В.Ч.</i> Исследование размерных зависимостей термодинамических характеристик наночастиц.....	35
<i>Юров В.М., Еремин Е.Н., Лауринас В.Ч., Касымов С.С.</i> Диссипативные процессы в трибологии.....	42
<i>Жумабеков А.Ж., Ибраев Н.Х., Селиверстова Е.В., Камалова Г.Б.</i> Получение и исследование электрофизических и оптических свойств нанокompозитного материала TiO ₂ -GO.....	54

ТЕПЛОФИЗИКА И ТЕОРЕТИЧЕСКАЯ ТЕПЛОТЕХНИКА

<i>Хасенов А.К., Нусупбеков Б.Р., Карабекова Д.Ж., Стоев М., Зейнолла Б.К., Муратова А.К.</i> Экономия расходов энергии тепла при обеспечении жильцов теплом и горячим водоснабжением.	61
<i>Шаймерденова К.М., Шрагер Э.Р., Тусыпбаева А.С., Наушарбан Ж.К.</i> Исследование процессов теплообмена на вертикальных теплообменниках.....	66

ТЕХНИЧЕСКАЯ ФИЗИКА

<i>Гевко И., Ляшук О., Сокил М., Слободян Л., Гудь В., Вовк Ю.</i> Резонансные колебания мобильного рабочего органа винтового загрузчика.....	73
<i>Кашканов А.А., Диордица В.Н., Кучерук В.Ю., Карабекова Д.Ж., Хасенов А.К., Шарзадин А.М.</i> Инерционная оценка взаимодействия автомобильных шин с дорогой при экстренном торможении.....	82
<i>Кучерук В.Ю., Курятник И.П., Ошанов Е.З., Кулаков П.И., Семенов А.А., Карабекова Д.Ж., Хасенов А.К.</i> Компьютерно-измерительная система динамических характеристик крутящего момента асинхронного двигателя.....	92
<i>Нусупбеков Б.Р., Картбаева Г.Т., Стоев М., Хасенов А.К., Карабекова Д.Ж., Муратова А.К.</i> Электрогидроимпульсный метод извлечения костного жира.....	101
<i>Танашева Н.К., Дюсембаева А.Н., Нусупбеков Б.Р., Миньков Л.Л., Нургалиева Ж.Г., Саденова К.К.</i> Исследование аэродинамических коэффициентов вращающихся цилиндров.....	108

СВЕДЕНИЯ ОБ АВТОРАХ.....	114
--------------------------	-----

CONTENTS

PHYSICS OF THE CONDENSED MATTER

<i>Chirkova L.V., Ermaganbetov K.T., Makhanov K.M., Rozhkova K.S., Arinova E.T., Kurmash A.</i> Current instability phenomena in a tunnel diode and electron self-organization processes	8
<i>Sakenova R.E., Erdybaeva N.K., Pogrebnjak A.D., Kylyshkanov M.K.</i> The study of multilayer coatings based on MoN(MoZr)ZrN and (TiMo)N/(TiMo), (CrZr)N/(CrZr) obtained by the method of vacuum-arc deposition.....	14
<i>Shaltakov S.N., Kazhikenova S.Sh., Nussupbekov B.R., Karabekova D.Zh., Khassenov A.K., Stoev M.</i> Mathematical model of high-temperature melt flow with account for short-range order nature ..	22
<i>Tleukenov S.K., Zhukenov M.K., Ispulov N.A.</i> Propagation of electromagnetic waves in anisotropic magnetoelectric medium	29
<i>Yurov V.M., Arkhipov V.V., Ranova G.A., Laurinas V.Ch.</i> Study of dimensional dependencies of thermodynamic characteristics of nanoparticles.....	35
<i>Yurov V.M., Eremin E.N., Laurinas V.Ch., Kasimov S.S.</i> Dissipative processes in tribology	42
<i>Zhumabekov A.Zh., Ibrayev N.Kh., Seliverstova E.V., Kamalova G.B.</i> Preparation and study of electrophysical and optical properties of TiO ₂ -GO nanocomposite material	54

THERMOPHYSICS AND THEORETICAL THERMOENGINEERING

<i>Khassenov A.K., Nussupbekov B.R., Karabekova D.Zh., Stoev M., Zeinolla B.K., Muratova A.K.</i> Saving of heat energy costs while providing residents with heat and hot water	61
<i>Shaimerdenova K.M., Schragger E.R., Tussypbaeva A.S., Nausharban Zh.K.</i> Investigation of heat exchange processes in vertically arranged heat exchangers	66

TECHNICAL PHYSICS

<i>Hevko I., Lyashuk O., Sokil M., Slobodian L., Hud V., Vovk Yu.</i> Resonant oscillation of vertical working part of conveyer-loader	73
<i>Kashkanov A.A., Diorditsa V.M., Kucheruk V.Yu., Karabekova D.Zh., Khassenov A.K., Sharzadin A.M.</i> Inertial evaluation of the tyre-road interaction during emergency braking	82
<i>Kucheruk V.Yu., Kurytnik I.P., Oshanov Ye.Z., Kulakov P.I., Semenov A.A., Karabekova D.Zh., Khassenov A.K.</i> Computer-measuring system of the induction motor's dynamical torque-speed characteristics	92
<i>Nussupbekov B.R., Kartbaeva G.T., Stoev M., Khassenov A.K., Karabekova D.Zh., Muratova A.K.</i> Electrohydroimpulse method of extracting bone grease	101
<i>Tanasheva N.K., Dyusembaeva A.N., Nussupbekov B.R., Min'kov L.L., Nurgalieva Zh.G., Sadenova K.K.</i> The study of the aerodynamic coefficients of rotating cylinders.....	108
INFORMATION ABOUT AUTHORS	114

L.V. Chirkova¹, K.T. Ermaganbetov¹, K.M. Makhanov¹,
K.S. Rozhkova¹, E.T. Arinova², A. Kurmash¹

¹*Ye.A. Buketov Karaganda State University, Kazakhstan;*

²*Gymnasium No. 1, Karaganda, Kazakhstan*

(E-mail: tchlv_53@mail.ru)

Current instability phenomena in a tunnel diode and electron self-organization processes

In the article the mechanisms of electric instability in semiconductors are considered. The origin of negative differential conductivity of different types are described. On the example of functioning of the tunnel diode the mechanism of formation of the concentrated instability in semiconductors resulting in N-shaped volt-ampere characteristic of the diode is considered. It is shown that the «semiconductor structure consisting of two layers of semiconductors with different type of conductivity and an external source of electric energy» system can be considered as an open non-equilibrium thermodynamic system in which self-organization processes are possible. Operation of the tunnel diode in terms of the theory of self-organization in semiconductor structures is analysed. Processes of self-organization are resulted by change of concentration of carriers of a charge in power zones of p- and n-semiconductors of types which make the tunnel diode and therefore the direction of streams of electrons changes. The description of the movement of carriers of a charge in the considered semiconductor structure at various values and external shift is given: in an equilibrium state, at the return shift; at the direct shift and tension which have values less peak value; and tension exceeding «voltage dip». In a thermodynamic non-equilibrium system there can be processes of self-organization of various nature — tunneling and injection of electrons. At the same time the direction of processes of self-organization is defined by features of power ranges of the semiconductors making the tunnel diode and intensity of interaction between system elements.

Keywords: self-organization, semiconductor, electric instability, tunnel diode, negative differential conductivity.

And to the arising oscillatory phenomena in them rather large number of publications and monographs is devoted to a pilot and theoretical study of instability of current in semiconductors [1–3]. Emergence of such number of works is connected with a possibility of practical use of the phenomenon of instability of current in semiconductors for creation of high-frequency generators, amplifiers, etc.

Fluctuations of current in semiconductors arises when the differential conductivity becomes negative. Emergence of the site with the negative differential conductivity (NDC) is possible on volt-ampere characteristic (VACH) with dependence of mobility and concentration of carriers of a charge in the semiconductor from electric field strength.

Differential conductivity σ_d can be written down as [4]

$$\sigma_d = \frac{dj}{dE} = e n \mu \left(1 + \frac{d \ln(n)}{d \ln(E)} + \frac{d \ln(\mu)}{d \ln(E)} \right), \quad (1)$$

where E — electric field strength; j — electric field strength; n and μ — concentration and mobility of carriers of a charge, respectively; e — electron charge.

As appears from the given expression, σ_d becomes negative if a concentration (or mobility) carrier quickly decreases with growth of electric field strength E . NDC is usually observed on a certain site VACH. At the same time VACH or N-, or S-type are observed. In these cases in VACH appears a so-called «falling» site, i.e. the site with negative differential conductivity.

If the system is on the «falling» site VACH, in a sample there can be an instability. It is usually connected with the concrete origins NDC. For example, if the negative sign third composed in the right part (1) is the reason of instability, the instability is called drift. Its mechanism caused by interval transitions was for the first time explained with Ridley, Watkins and Hilsun [2].

If NDC is connected with the second composed in (1), then it is called concentration. Concentration NDC arises as a result of sharp reduction of concentration of free carriers with increase in the field.

Both origins of NDC lead to N-shaped VACH. And both are connected with a warming up of electronic gas: in the first case the drift speed of carriers decreases with growth of the field at their constant concentration. In the second — NDC arises as result of sharp reduction of concentration of free carriers with increase in the field. There is one more origin of NDC connected with a warming up of electronic gas. Here the cause of NDC is caused by various dependence on temperature of processes of transmission of energy and an impulse to a lattice. Such NDC is implemented on the «falling» site of S-shaped VACH and carries the name of overheating imbalance. The majority of the electric non-stability leading to NDC in semiconductors can be considered as the self-organization arising in an open thermodynamic non-equilibrium system [5]. The «semiconductor structure — a power source» system acts as the last.

In the previous works of authors [6, 7] processes of self-organization in semiconductor structures in the presence in them drift NDC on the example of Gunn's generator and the avalanche and flying diode were analysed.

In the present article in terms of the theory of self-organization processes in the tunnel diode are considered in which the concentration NDC mechanism leading to N-shaped VACH (Fig. 1) is implemented.

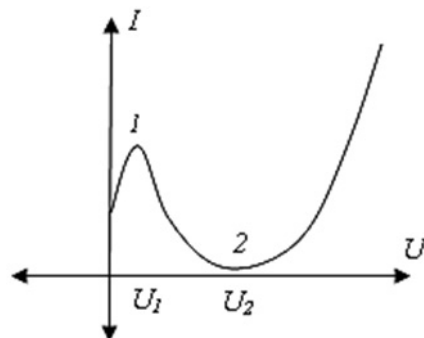


Figure 1. Static characteristic of the tunnel diode. U_1 is the peak tension, i.e. tension characteristic of the maximum current direct direction; the U_2 nd tension of «failure» characteristic of the minimum current

The tunnel diode has the special characteristics distinguishing it from ordinary diodes and stabilitrons. If diodes and stabilitrons well pass current only in one party (in the return — only in the field of breakdown), then the tunnel diode is capable to carry well current in both parties. This property is provided by features of the device of the tunnel diode: very narrow p - n transition and significant amount of impurity. It is known that for production of tunnel diodes semiconductors with high concentration of impurity are used — from 10^{18} to 10^{20} cm^{-3} . Such semiconductors are called degenerates, actually being semi-metals. In them levels of impurity atoms form the power zones merging with the main resolved zones — valent and a zone of conductivity — the semiconductor. As a result Fermi's levels will be located not in the forbidden zones of n -semiconductors and p -types, and in their resolved zones, i.e. in a valent zone of the semiconductor of p -type and in a zone of conductivity of the semiconductor of n -type (Fig. 2).

As appears from the drawing, the bottom of a zone of conductivity of the semiconductor of n -type and a ceiling of a valent zone of the semiconductor of p -type are divided by very narrow locking layer. Thus, the transition thickness (a potential barrier) in the tunnel diode is very small (about 10^{-2} microns), what are two orders less, than in ordinary semiconductor diodes. Through such thin potential barrier carriers of a charge are capable to tunnel. At the same time resultant current transition will be defined by p - n - as the difference of electronic streams from one layer of the semiconductor in another. If to consider the power source and the

tunnel diode consisting of the high-alloyed n -semiconductors and p -types, as an open non-equilibrium thermodynamic system, then the physical processes happening in it will satisfy to the basic principles of synergetic. Namely:

- in an equilibrium state when the diode is not affected by a power source, n -semiconductors and p -types exchange substance (equal quantities of electrons);
- in the presence of a power source charge carriers in semiconductors at its expense accumulate excess energy on length of a free run and transfer it due to collisions from not an ideal crystal lattice to a crystal. Temperature increase of a crystal which is transferred to the environment results, i.e. the considered system is open and is in a non-equilibrium thermodynamic state.

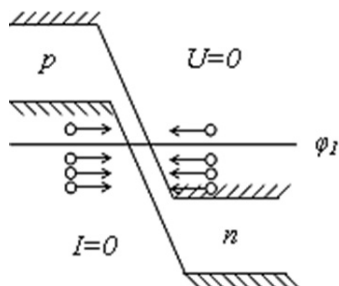


Figure 2. The power chart of the tunnel diode in an equilibrium state. By circles are designated electrons. Shooters noted the electrons capable to pass into an adjacent semiconductor layer

When the return tension is put to the diode, equilibrium state is broken and its power chart (Fig. 3) changes. At the same time there is an increase in a potential barrier and change of provision of level of Fermi: the ceiling of a valent zone of the semiconductor of p -type rises, Fermi level φ_{Fp} at the same time is displaced up, at the same time the bottom of a zone of conductivity of the semiconductor of n -type falls, and Fermi level φ_{Fn} displaced down. Electrons of a valent zone of the semiconductor of p -type which are at the power levels below Fermi level φ_{Fp} , will be located opposite to the free power levels of the semiconductor of n -type lying higher than the Fermi level φ_{Fn} (Fig. 3). Current through p - n - the transition directed from the n -type semiconductor to the p -type semiconductor results. With growth of the return tension this current increases very quickly as density of electrons in the depth of a valent zone is extremely big and even small increment of potential difference ($\varphi_{Fp} - \varphi_{Fn}$), will be followed by a significant change in a stream of electrons from the p -type semiconductor in the n -type semiconductor.

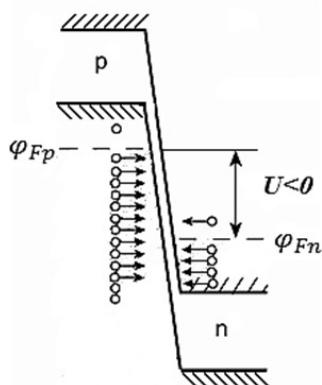


Figure 3. The power chart of the tunnel diode at the return shift

Thus, again there is an exchange of electrons of elements of a system, i.e. in a system the self-organization process having the form of the directed transfer of electric charge between semiconductors with different type of conductivity is observed. At the same time the direction of the self-coordinated process is defined by features of properties of the interacting system elements (features of power structure of semiconductors and the directions of fields of an external power source and the internal field of transition) and the

nature of interaction between them. Let's consider processes of self-organization in the tunnel diode when external tension in the direct direction is put to it. The following cases are of interest: when the size of external direct shift does not exceed peak tension, i.e. when $0 < U < U_1$ (Fig. 4), when the condition is satisfied $U_1 < U < U_2$ (Fig. 5), when $U = U_2$ and, at last, when the size of direct shift exceeds tension of «failure» $U > U_2$ (Fig. 6).

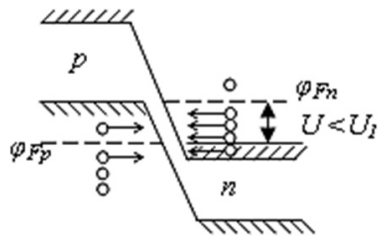


Figure 4. The power chart of the tunnel diode at a tension direct shift, there is less peak ($U < U_1$)

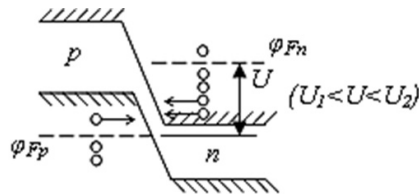


Figure 5. The power chart of the tunnel diode at a tension direct shift $U_1 < U < U_2$

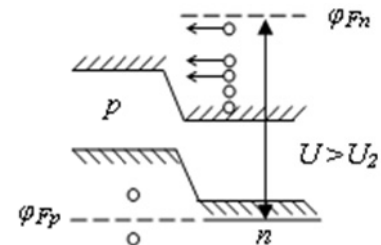


Figure 6. The power chart of the tunnel diode at a tension direct shift, exceeding tension «a failure» $U > U_2$

In the first case (Fig. 4) as a result of decrease in a potential barrier Fermi's level of the semiconductor of n -type is displaced up, and the p -type semiconductor — down. As a result, a part of electrons of a valent zone of the semiconductor of p -type will appear opposite to power levels of the forbidden n -type semiconductor zone, and a part of electrons of a zone of conductivity of the semiconductor of n -type — opposite to free power levels of a valent zone of the semiconductor of p -type. It will lead to decrease in intensity of tunneling of electrons from the p -type semiconductor in the n -type semiconductor. There will be a primary movement of electrons from n - in p -area. The direction of process of self-organization changes under the influence of features of interaction of the contacting semiconductors called by action of an external power source.

When Fermi level of the semiconductor of n -type φ_{Fn} by F_n , rising, is compared to a ceiling of a valent zone of the semiconductor of p -type, current via the tunnel diode accepts the maximum value (Fig. 1, a point 1). It corresponds to the maximum intensity of process of self-organization.

In the second case when external direct shift exceeds peak tension, but Fermi level of the semiconductor of n -type φ_{Fn} there is less than tension of «failure» (Fig. 5), being displaced up, gets to the area of the forbidden p -type semiconductor zone therefore a part of electrons of a zone of conductivity of the n -semiconductor appear opposite to power levels of the forbidden p -type semiconductor zone. It leads to reduction of current via the diode. On volt-ampere characteristic of the tunnel diode the site with a negative resistance (Fig. 1, site 1–2) appears. Again there is a change of the direction of process of self-organization of the movement of electrons in the tunnel diode.

Further increase in tension of direct shift leads to a bigger decrease in a potential barrier in the field of transition p - n -. In case the size of shift becomes equal to tension of «failure», the bottom of a zone of conductivity of the semiconductor of n -type is compared to a ceiling of a valent zone of the semiconductor of p -type. Tunnel current decreases again to zero (Fig. 1, a point 2) as electrons of a zone of conductivity of the n -semiconductor are located opposite to power levels of the forbidden p -semiconductor zone. It corresponds to reduction to zero intensity of the self-organized transition of electrons from the n -type semiconductor in the p -type semiconductor.

And, at last, at a tension of direct shift exceeding tension of «failure», the forbidden power zones of n -semiconductors and p -types become «through» (Fig. 6) and tunnel current disappears. At the same time the coordinated movement caused by tunneling of electrons through a potential barrier stops. Current via the diode increases, but already at the expense of the ordinary mechanism — overcoming by electrons of a potential barrier — injections of carriers of a charge. There is a coordinated transfer of electrons mechanism of which differs from the mechanism of the transfer connected with tunneling process.

Thus, in the thermodynamic non-equilibrium system consisting of semiconductors with different types of conductivity, and a power source there are processes of self-organization of various natures (tunneling and injection of electrons). The direction of processes of self-organization is defined by features of properties of

elements of a system (features of power ranges of semiconductors) and intensity of interaction between system elements (the sign and size of external tension).

References

- 1 Бонч-Бруевич В.Л. Доменная электрическая неустойчивость в полупроводниках / В.Л. Бонч-Бруевич, И.П. Звягин, Ф.Г. Миронов. — М.: Наука, 1972.
- 2 Шелль Э. Самоорганизация в полупроводниках / Э.Шелль. — М.: Мир, 1991.
- 3 Басс Ф.Г. Горячие электроны и сильные электромагнитные волны в плазме полупроводников и газового разряда / Ф.Г. Басс, Ю.Г. Гуревич. — М.: Наука, 1975.
- 4 Хакен Г. Синергетика / Г. Хакен. — М.: Мир, 1991.
- 5 Викулин И.М. Физика полупроводниковых приборов: учеб. пос. / И.М. Викулин, В.И. Стафеев. — М.: Сов. радио, 1980.
- 6 Ermaganbetov K.T. Physical processes in Gann diode and energybalance / K.T. Ermaganbetov, L.V. Chirkova, E.B. Skubnevsky, K.M. Machanov, E.T. Arinova, A. Omirbek // Bulletin of the Karaganda University. Physics Series. — 2017. — No. 1(85). — P. 15–21.
- 7 Ermaganbetov K.T. Electronic mechanisms of instability in semiconductor structures / K.T. Ermaganbetov, L.V. Chirkova, E.T. Arinova // Bulletin of the Karaganda University. Physics Series. — 2015. — No. 4(80). — P. 4–11.

Л.В. Чиркова, К.Т. Ермаганбетов, К.М. Маханов,
К.С. Рожкова, Е.Т. Аринова, А. Курмаш

Туннельдік диодта токтың орнық сыздығы және электрондардың өздігінен ұйымдасуы

Шалаөткізгіш электр орнықсыздығының пайда болу механизмі қарастырылған. Өртүрлі теріс дифференциалдық өткізгіштердің пайда болу механизмдері зерттелген. Туннельдік диодтың жұмыс ұстанымын талдау арқылы диодтың N-пішіндес вольтамперлік сипаттамасына әкелетін себептер талданған. Түйіскен шалаөткізгіштер мен энергия көзінен тұратын жүйені өздігінен ұйымдасатын үдерістер, пайда болатын орнықсыздықты ашық термодинамикалық жүйе ретінде қарастыруға болатындығы көрсетілген. Туннельдік диодтың жұмыс ұстанымы синергетика ұстанымдары негізінде түсіндірілген. Өздігінен жүретін үдерістер әсерінен p - және n -тектес шалаөткізгіштердің рұқсат етілген энергия жолақтарында зарядтасушылардың шоғырлану дәрежелерінің өзгерулері нәтижесінде электрондардың өздігінен тасымалдану бағыттары өзгеріске ұшырайды. Жүйені құраушы элементтердің өзара әсерлесу ерекшеліктеріне қарай электрондардың тасымалдануларында пайда болатын ерекшеліктер мұқият талданған. Қарастырылып отырған термодинамикалық жүйеде пайда болатын өздігінен ұйымдасатын үдерістердің табиғаттары өртүрлі. Өздігіне ұйымдасатын үдерістердің жүру бағыттары шалаөткізгіштердің энергия спектрлерінің ерекшеліктеріне, энергия көзінің қарқынына тәуелді.

Кілт сөздер: өздігінен ұйымдасу, шалаөткізгіш, электр орнықсыздық, туннельдік диод, теріс дифференциалдық өткізгіштік.

Л.В. Чиркова, К.Т. Ермаганбетов, К.М. Маханов,
К.С. Рожкова, Е.Т. Аринова, А. Курмаш

Явления неустойчивости тока в туннельном диоде и процессы самоорганизации электронов

Рассмотрены механизмы электрической неустойчивости в полупроводниках. Описаны механизмы возникновения отрицательных дифференциальных проводимостей различных типов. На примере функционирования туннельного диода рассмотрен механизм формирования концентрационной неустойчивости в полупроводниках, приводящей к N-образной вольт-амперной характеристике диода. Показано, что система «полупроводниковая структура, состоящая из двух слоев полупроводников с разным типом проводимости + внешний источник электрической энергии» может рассматриваться как открытая неравновесная термодинамическая система, в которой возможны процессы самоорганизации. Проанализирована работа туннельного диода с точки зрения теории самоорганизации в полупроводниковых структурах. Показано, что в результате процессов самоорганизации происходит изменение концентрации носителей заряда в разрешенных энергетических зонах полупроводников p - и

n-типов, составляющих туннельный диод, и изменяется направление потоков электронов. Приведено подробное описание движения носителей заряда в рассматриваемой полупроводниковой структуре при различных значениях и знаках внешнего смещения: в равновесном состоянии, при обратном смещении; при прямом смещении и напряжениях, меньших пикового значения; меньших напряжения «провала» и напряжениях, превышающих напряжение «провала». Показано, что в рассматриваемой термодинамической неравновесной системе могут возникать процессы самоорганизации различной природы — туннелирование и инжекция электронов. При этом направление процессов самоорганизации определяется особенностями энергетических спектров полупроводников, составляющих туннельный диод, и интенсивностями взаимодействия между элементами системы.

Ключевые слова: самоорганизация, полупроводник, электрическая неустойчивость, туннельный диод, отрицательная дифференциальная проводимость.

References

- 1 Bonch-Bruyevich, V.L., Zvyagin, I.P., & Mironov, F.G. (1972). *Domennaia elektricheskaja neustoichivost v poluprovodnikakh [Domain electric instability in semiconductors]*. Moscow: Nauka [in Russian].
- 2 Shell, E. (1991). *Samoorganizatsiya v poluprovodnikakh [Self-organization in semiconductors]*. Moscow: Mir [in Russian].
- 3 Bass, F.G., & Gurevich, Yu.G. (1975). *Horiachie elektrony i silnye elektromagnitnye volny v plazme poluprovodnikov i hazovoho razriada [Hot electrons and strong electromagnetic waves in semiconductor plasma and gas discharge]*. Moscow: Nauka [in Russian].
- 4 Khaken, G. (1991). *Sinerhetika [Synergetic]*. Moscow: Mir [in Russian].
- 5 Vikulin, I.M., & Stafeyev, V.I. (1980). *Fizika poluprovodnikovyykh priborov [Physics of semiconductor devices]*. Moscow: Sovetskoe radio [in Russian].
- 6 Ermaganbetov, K.T., Chirkova, L.V., Skubnevsky, E.B., Makhanov, K.M., Arinova, E.T., & Omirbek, A. (2017). Physical processes in Gann diode and energy balance. *Bulletin of the Karaganda University. Physics Series, 1(85)*, 15–21.
- 7 Ermaganbetov, K.T., Chirkova, L.V., & Arinova, E.T. (2015). Electronic mechanisms of instability in semiconductor structures. *Bulletin of the Karaganda University. Physics Series, 4(80)*, 4–11.

R.E. Sakenova¹, N.K. Erdybaeva¹, A.D. Pogrebnyak², M.K. Kylyshkanov³

¹*D. Serikbayev East Kazakhstan State Technical University, Ust-Kamenogorsk, Kazakhstan;*

²*Center for Priority Development «VERITAS», D. Serikbayev East Kazakhstan State Technical University, Ust-Kamenogorsk, Kazakhstan; Sumy State University, Ukraine;*

³*«Ulba Metallurgical Plant» JSC, Kazakhstan*

(E-mail: Sakenova_rimma@mail.ru)

The study of multilayer coatings based on MoN(MoZr)ZrN and (TiMo)N/(TiMo), (CrZr)N/(CrZr) obtained by the method of vacuum-arc deposition

In the article the results of experimental studies of multilayer coatings MoN(MoZr)ZrN and (TiMo)N/(TiMo), (CrZr)N/(CrZr), obtained on A570 Grade stainless steel samples with a Ra roughness of up to 0.09 μm are presented. Coatings were formed by vacuum-arc evaporation of cathodes in the installation Bulat-6. After deposition of multilayer coatings by scanning electron microscopy and microanalysis, a non-uniform distribution of zirconium, chromium, nitrogen and molybdenum was found on the surface of the samples. The research results show that good tribological properties in combination with improved physico-mechanical properties make the deposited material promising for use as a protective material for machines and tools operating in extremely difficult working conditions.

Keywords: multilayer coatings, cathode arc, microstructure, two-phase state, vacuum-arc method, microhardness, wear resistance.

1. Introduction

During the operation of machine parts, mechanisms and metal working machinery, their surface layer is subjected to mechanical, thermal and chemical influences. Thus, a significant decrease in performance in most cases occurs as a result of wear, erosion and corrosion of the surface. A significant resource for increasing the efficiency of machine parts and mechanisms is to improve the physico-mechanical properties of materials and increase their tribological properties [1–2].

The analysis of scientific publications suggests that the use of vacuum-arc magnetron installations, where highly ionized source atoms and excited target atoms allow to create microcrystalline and nanolayer coatings on the surfaces of various products, and thereby improve the operational properties of materials [3].

It has already been proved that the multilayer coatings demonstrate better properties, including magnetic and electrical, in comparison with the single-layer ones. The substitutional defects may occur along the interfaces between adjacent layers in multilayer films, when some of the elements of one layer enter the crystal lattice of the adjacent one, thus replacing its atoms. This process usually leads to generation of strain energy proportional to the shear modulus of the material. The layers with different shear modulus prevent the movement of dislocations, thus preventing the destruction of the coatings material. Firstly such type of model to describe hardness enhancement was proposed by J.S. Koehler and then approved and followed by many experimental and theoretical works, as well as by review articles. Additionally, deviations or redistribution of dislocations and cracks at the grain boundaries help to increase the coatings resistance to stress, wear and destruction. The multilayer structure significantly reduces the influence of interlayer cracking and allows it's employing under large dynamic loads. The alternation of nanoscale layers with dissimilar physical-mechanical characteristics allows to change significantly the properties of multilayer coatings, such as concentration of internal stresses, crack propagation and, hence, to increase the fracture toughness of such materials [4–6].

In work (patent RU No. 2423547, C23C 14/24, 2011) a method for obtaining a coating for the cutting tool, including vacuum ion-plasma application of a wear-resistant coating based on a complex titanium-chromium-zirconium nitride, additionally alloyed with aluminum and niobium by means of three arc evaporators arranged horizontally in one plane, connected to the drip phase separator, the following compositions of titanium-aluminum cathode made of W-5 alloy, combined zirconium-niobium cathode and chromium cathode. The disadvantage of this technology is that the coating has insufficient hardness and viscosity, as a result, the coating is more subject to wear, especially in conditions of alternating loads, as well

as at high cutting speeds, it quickly appears microcracks on the pads, which leads to its chipping and destruction during cutting.

The purpose of this work is to study the multilayer coatings MoN(MoZr)ZrN and (TiMo)N/(TiMo), (CrZr)N/(CrZr) obtained by the method of vacuum-arc deposition, as well as to study the effect of the technological settings of deposition on the formation of the microstructure of subsurface layers samples.

2. Materials and methods of the experiment

In this work, we investigated the multilayer coatings MoN(MoZr)ZrN and (TiMo)N/(TiMo), (CrZr)N/(CrZr) obtained in a vacuum arc chamber. Molybdenum and zirconium were used as cathodes. Multilayer coatings are obtained by vacuum-arc sequential evaporation of the cathodes Mo, Zr, Ti, Cr in the installation of Bulat-6 with two evaporators. Polished substrates of A 570 Grade 36 stainless steel with surface roughness Ra up to 0.09 μm were used for the deposition. The multilayer coatings were deposited by vacuum-arc evaporation of cathodes in a vacuum-arc device Bulat-6 with two evaporators, which allows deposition of nanostructured multilayer coatings. Figure 1 shows a principal scheme of the deposition system. The vacuum chamber (1) (base pressure in the chamber was 0.001 Pa) was equipped with a system of automatic nitrogen pressure control (2) and two evaporators consisting of appropriate metals for each coating (purity of metallic target was 99.8 %). The substrate holder (5) was mounted on a rotating stainless steel plate (300×300 mm) on which the substrates (6) were placed. BULAT-6 was also equipped with DC voltage source (7), the value of which can be varied between 5 and 1000 V, and high-voltage impulse generator (8) with adjustable voltage pulse amplitude of 0.5–2 kV and repetition frequency of 5–7 kHz [7–9].

The substrate cleaning process was carried out prior to coatings deposition, while applying a 1 kV substrate potential. Further, nitrogen was injected into the chamber to fabricate nitrides of appropriate refractory or transition metals.

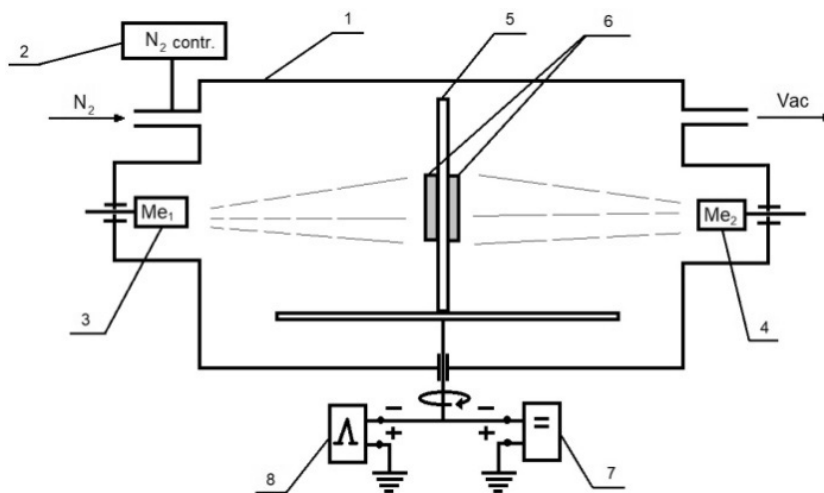


Figure 1. A principal scheme of the Bulat-6 deposition system

Rotation of the substrate holder allowed deposition of alternating layers, while injection and stopping the injection of nitrogen into the deposition chamber allowed deposition of nitride and pure metallic layers.

The structural phase state of the deposited coatings was investigated by X-ray diffraction analysis on a XPert-PRO diffract meter in Cu-K α radiation. The elemental composition of the surface and cross section of the coatings was investigated using scanning electron microscopy with the INCA microanalysis system (REM). The structure-phase state of the deposited coatings was analyzed using X-Ray diffraction (XRD) in terms of θ -2 θ scans in Bragg-Bertrano geometry. Scanning electron microscopy with Energy-dispersive spectra (SEM with EDX) was used for studies of coatings surface and elemental composition, as well as coatings cross-sections. In addition, laser digital scanning was used to study surface roughness of the coatings. Time of flight secondary ion mass-spectrometry (ToF SIMS) was used for studies of distribution of elements along the depth. Hardness of the deposited coatings was studied by micro-Vickers method. At least 10 indentations were made for each sample and for each loading [10–12].

Experimental studies were carried out in the research laboratories of Sumy State University (Ukraine), the National Research Laboratory of collective use of the East Kazakhstan State University named after

S. Amanzholov, Regional university engineering laboratory «IRGETAS» of the East Kazakhstan Technical State University named after D. Serikbayev.

3. Results and discussion

Vacuum-arc evaporation of Mo and Zr cathodes resulted in a coating with a dense structure, without obvious defects and of equal thickness (8 μm) over the entire surface of sample No. 894. Figure 2b presents the results of x-ray analysis.

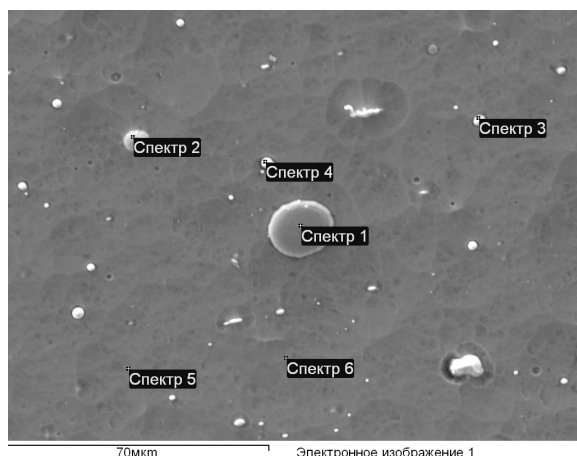


Figure 2a. RAM image

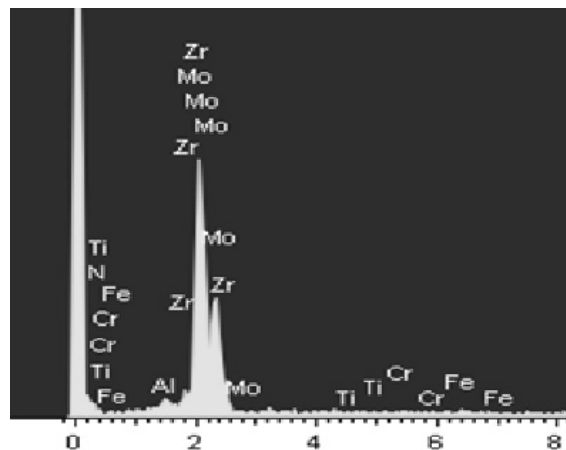


Figure 2b. EDS spectra of the sample surface with MoN(MoZr)ZrN coating

The data of scanning electron microscopy, shown in Figure 2 and Table 1 shows that the chemical composition of the coatings in the layers under study is different.

From the picture of the raster image of the multilayer coating, the selection of particles of micrometer scale is seen. Spectrum analysis shows a different quantitative distribution of elements in each layer.

Interpretation of the spectra of the layer-by-layer coating is presented in Table 1.

Table 1

The elemental composition of the coating MoN(MoZr)ZrN

Spectrum	N	Al	Ti	Cr	Fe	Zr	Mo	Sum
Spectrum 1	12.64	0.53	0.00	0.43	1.00	50.52	34.87	100.00
Spectrum 2	12.39	0.34	0.00	0.00	0.65	54.96	31.67	100.00
Spectrum 3	12.89	0.68	0.00	0.00	0.79	59.49	26.16	100.00
Spectrum 4	11.78	0.38	0.00	0.60	1.06	58.86	27.32	100.00
Spectrum 5	0.00	0.60	0.00	0.00	1.04	58.59	39.76	100.00
Spectrum 6	10.04	0.89	0.00	0.00	1.54	51.80	35.73	100.00
The average	9.96	0.57	0.00	0.17	1.01	55.70	32.58	100.00
Standard deviation	4.98	0.20	0.00	0.27	0.30	3.88	5.22	
Max.	12.89	0.89	0.00	0.60	1.54	59.49	39.76	
Min.	0.00	0.34	0.00	0.00	0.65	50.52	26.16	

In all layers there is (spectra 1–6 in Table 1) the maximum content of molybdenum, zirconium and nitrogen. The appearance of nitrogen is due to the residual gas content in the cell of the Bulat-6 unit. The data of energy dispersive analysis (Fig. 1) shows the presence of Mo and Zr in A 570 Grade steel.

Along with clear lines of phases with maximum intensity, the appearance of broadened peaks of lesser intensity is observed, which, apparently, indicate a decrease in the grain size and the formation of nanocrystallites in the coating structure. Figure 3 shows the X-ray diffraction analysis of the coating.

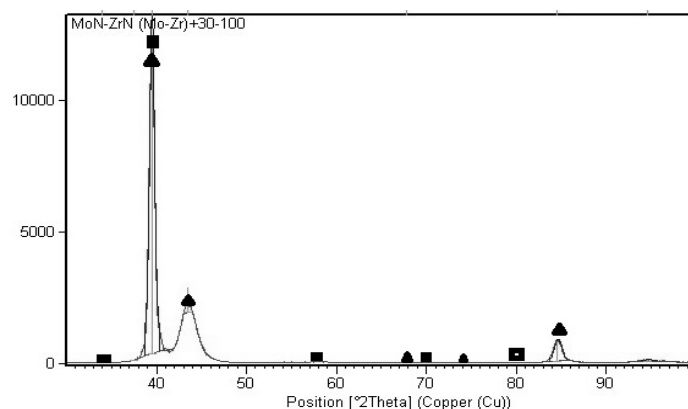


Figure 3. XRD spectors of MoN(MoZr)ZrN coatings (series 3)

Table 2

The phase composition of the multilayer coating

No.	2θ	d_{hkl} , Å	ZrN, d_{hkl} , Å	Mo ₂ N, d_{hkl} , Å
1	33.8	2.625	111	-
2	39.2	2.298	200	111
3	43.5	2.085	-	200
4	57	1.614	220	-
5	68	1.379	311	220
6	74	1.281	-	311
7	79	1.212	400	-
8	84.8	1.143	-	400

From metallographic images of the surface of the coating, you can see that the structure contains dispersed particles of predominantly spherical shape. Using the method of the ratio of the areas occupied by particles, the volume fraction of these particles was calculated, which was $\langle \phi \rangle = 3\%$. The period of the unit cell phase is $a = 4.56$ Å. X-ray diffraction analysis data (Table 2) show the appearance of zirconium and molybdenum nitride phases. The most intense peak corresponds to two phases: (200) ZrN and (111) Mo₂N.

Figure 4a presents an image of the cross section of the sample in a scanning electron microscope. Data interpretation of the spectrum of the SEM image are presented in Table 3. Spectra 4 and 5 correspond to the chemical composition of the original sample substrate steel A 570 Grade.

Spectra 1, 2 and 3, taken from a layer with a thickness of 8 μm, show the presence of Mo and Zr. According to the energy dispersive and X-ray structural analyzes, these phases are identified as ZrN, Mo₂N.

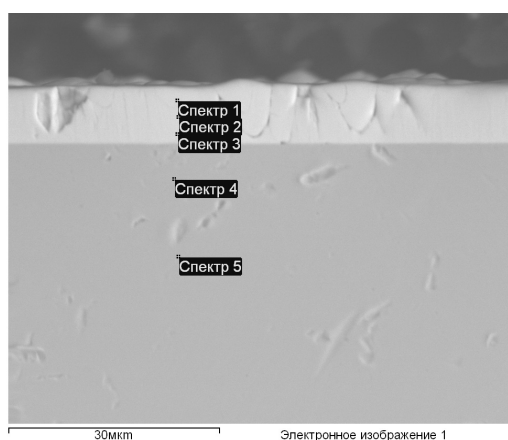


Figure 4a. SEM-image of the cross-section of the sample with a MoN(MoZr)ZrN coating

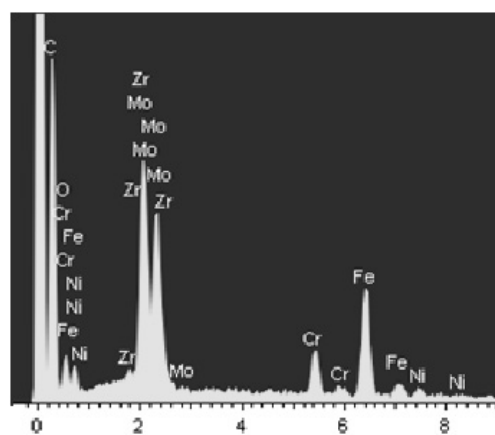


Figure 4b. Energy Dispersive Spectrum of a Section Sample Cross Section

Elemental composition of the coating and the substrate

Spectrum	O	P	S	Cr	Mn	Fe	Ni	Zr	Mo	Sum
Spectrum 1	12.98			6.78		21.83	2.53	27.99	27.89	100.00
Spectrum 2	16.46			6.93		22.82	2.18	26.82	24.78	100.00
Spectrum 3	15.28			7.85		25.29	2.53	25.83	23.23	100.00
Spectrum 4	6.18	0.42	0.46	17.30	1.53	65.94	8.16			100.00
Spectrum 5	5.45	0.38	0.37	17.27	1.94	66.68	7.91			100.00
Max.	16.46	0.42	0.46	17.30	1.94	66.68	8.16	27.99	27.89	
Min.	5.45	0.38	0.37	6.78	1.53	21.83	2.18	25.83	23.23	

The microhardness of the applied coatings was determined with a PMT-3 microhardness tester, with the Vickers method. For each sample and for each load, at least 20 holes were made. After spraying, the microhardness increased. Studies of the surface morphology of the deposited samples No. 877 and No. 891 were carried out using a Keyence VK-X100 digital microscope.

The image of the surface of sample 877 is shown in Figure 5, where it can be seen that a fairly smooth surface with droplet fractions was formed, which is characteristic of coatings applied by the vacuum-arc method. The average roughness of the samples did not exceed 0.3 microns.

In the coatings, a two-phase state is formed (nitride and metal phases), and each phase corresponds to a specific layer. In the spectrum of sample No. 877, an overlap of peaks from Ti and Mo is observed. Also the expansion of the peaks from the plane (222) is seen, indicating a high disorder of polycrystallites, probably from the molybdenum phase.

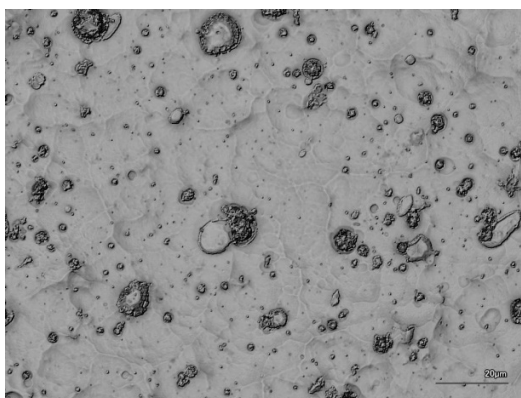


Figure 5. Surface morphology of sample 877

Typical X-ray spectra of the studied coatings are presented in Figure 6. The spectrum for each sample has a corresponding color. As can be seen from Figure 6, the most intense peaks correspond to the (111) and (200) planes, but we can also observe weaker reflections from the (311) and (220) planes.

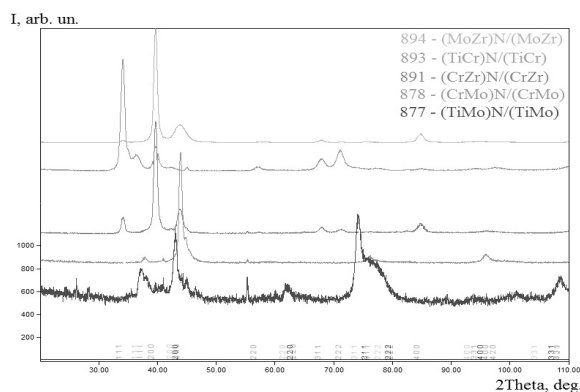
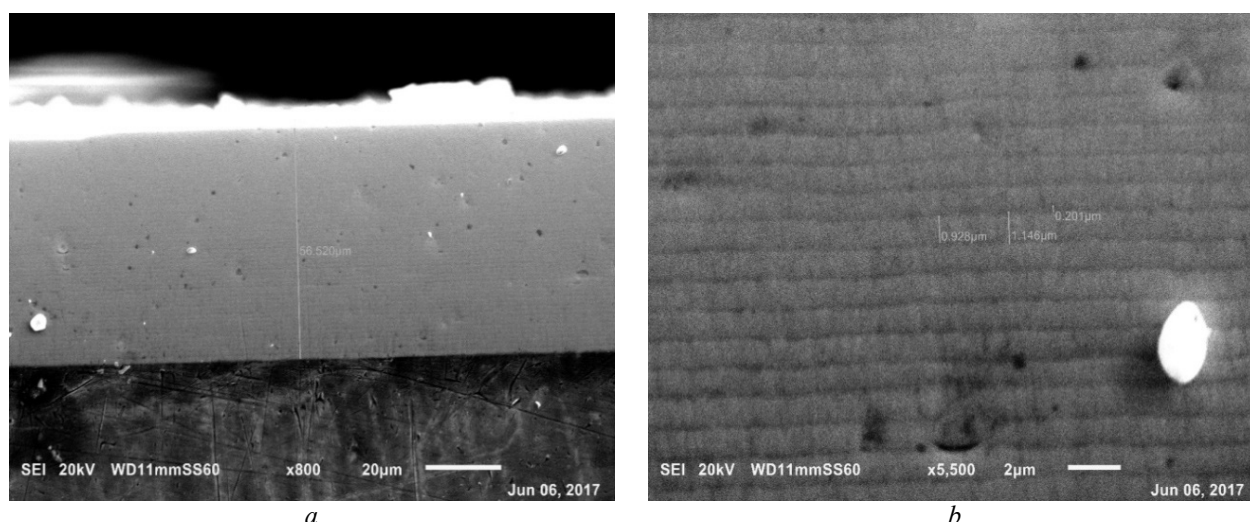


Figure 6. XRD specters of samples



a — general view; *b* — layers with a higher magnification $\times 5500$

Figure 7. SEM images of the cross section of sample 891

The cross-sectional view at magnifications of $\times 800$ (general view) and $\times 5500$ (enlarged nitride and metal layers) of sample No. 891 is shown in figures 7*a* and 7*b*, respectively. We can observe a good flatness of the layers: they do not intersect and have clear visible boundaries. The total thickness of the coating is about 54 microns, and the individual layers are about 750 nm thick (nitride layers) and 150 nm (metallic layers). The data obtained are in good agreement with the deposition parameters for nitride and pure metal layers.

The hardness of the coatings for samples № 891 and № 877 in the precipitated state was studied by the Vickers method using a TimShimadzu HMV-G Micro Vickers microhardness tester. The average hardness of the HV0.1 coatings was 2700, while the HV0.5 and HV1 coatings were 2250 and 1700, respectively, which makes them as complex as the protective coatings.

Conclusion

Vacuum-arc evaporation of Mo and Zr cathodes was obtained by coating with a dense structure, without obvious defects and of equal thickness over the entire surface of the sample. The microstructure of the coatings is represented by the cubic phases MoN and ZrN with the preferential orientation of (200) and (111), (220), respectively. The deposition of a multilayer coating on A570 Grade MoN/ZrN steel resulted in the appearance of ZrN and Mo₂N phases in the surface layers. This is evidenced by data of X-ray analysis. It was established that the particles of the nitride phase are predominantly spherical in shape with a volume fraction of 3 % and sizes of 1–3 μm and larger particles with a diameter of about 12 μm .

To determine the characteristics of the coatings, various methods of analysis were used, such as XRD, EDS, REM methods, and also hardness tests were carried out. For sample No. 877, the shape and intensity of the diffraction peaks from the nitride layers may indicate a fairly good crystal structure of the nitride layers. In accordance with the research results, the upper layers of the coatings are metals, the ratio between the metal components is in the range of 0.9–0.92.

In sample No. 891, there is a good flatness of the layers, they do not intersect and have clear visible boundaries. The total thickness of the coating is about 54 microns, and the individual layers are about 750 nm thick (nitride layers) and 150 nm (metallic layers).

Two-phase state (nitride and metallic phases) was formed in the coatings, and each phase corresponds to certain layer. For sample No. 877 we can observe overlapping of peaks from Ti and Mo (sample 877). Broadening of the peaks from (222) plane is also observed indicating at high disorder of polycrystallites, probably from molybdenum phase. Shape and intensity of diffraction peaks from nitride layers can point on pretty good crystalline structure of the nitride layers. In according to the results of the EDS studies, top layers of the coatings are metallic ones, the ratio between metallic components is in the range 0.9–0.92.

Cross-sectional view under magnification at $\times 800$ (total view) and $\times 5500$ (magnified nitride and pure metallic layers) of the sample No. 891 are presented in Figure 7*a* and 7*b* accordingly. We can observe good

planarity of layers; they do not intersect and have clear visible borders. Total thickness of the coating is around 54 μm , while alternative layers have the thickness around 750 nm (nitride layers) and 150 nm (for pure metallic layers). The obtained data is in a good agreement with the deposition parameters, where one can see 5 minutes and 1 minute deposition times for nitride and pure metallic layers.

For samples No. 877 and No. 891, the hardness of the coatings in the deposited state was studied by the Vickers method using a Tim. Shimadzu HMV-G Micro Vickers microhardness tester. The average hardness of the HV0.1 coatings was 2700, while the HV0.5 and HV1 coatings were 2250 and 1700, respectively, which makes them as complex as the protective coatings.

Hardness tests showed a maximum hardness of coatings close to 24 GPa, due to the Hall-Petch amplification effect, which is much higher than single-layer coatings. The data on microhardness measurements indicate the hardening of the surface layer by 4.3 %.

This work was carried out with the financial support of PTsF by the Science Committee of the Ministry of Education and Science of the Republic of Kazakhstan on the topic «Development of production technology for medical products from tantalum and niobium».

References

- 1 Pogrebnjak, A.D., Bagdasaryan, A.A., Yakushchenko, I.V., & Beresnev, V.M. (2014). The structure and properties of high-entropy alloys and nitride coatings based on them. *Russian Chemical Reviews*, 83, 11, 1027–1061.
- 2 Pogrebnjak, A.D., Shpak, A.P., Azarenkov, N.A., & Beresnev, V.M. (2009). Structures and properties of hard and superhard nanocomposite coatings. *Physics-Uspekhi*, 52, 1, 29–54.
- 3 Pogrebnjak, A.D., Bagdasaryan, A.A., Pshyk, A., & Dyadyura, K. (2017). Adaptive multicomponent nanocomposite coatings in surface engineering. *Physics-Uspekhi*, 60, 6, 586–607.
- 4 Pogrebnjak, A.D., et al. (2018). Experimental and theoretical studies of the physicochemical and mechanical properties of multi-layered TiN/SiC films: Temperature effects on the nanocomposite structure. *Composites. Part B: Engineering*, 142, 1, 85–94.
- 5 Bobzin, K., Brögelmann, T., Kruppe, N.C., Arghavani, M., Mayer, J., & Weirich, T.E. (2017). Plastic deformation behavior of nanostructured CrN/AlN multilayer coatings deposited by hybrid dcMS/HPPMS. *Surface and Coatings Technology*, 332, 253–261.
- 6 Pogrebnjak, A.D., Sobal, O.V., Bersenev, V.M., Turbin, P.V., Kirik, G.V., & Makhmudov, N.A., et al. (2010). Phase composition, thermal stability, physical and mechanical properties of superhard on base Zr-Ti-Si-N nanocomposite coatings. Proceedings from Nanostructured Materials and Nanotechnology IV, 34th International Conference on Advanced Ceramics and Composites, ICACC; Daytona Beach, FL; United States. January, 31, 7, 127–138.
- 7 Kasiuk, J.V. et al. (2014). Correlation between local Fe states and magnetoresistivity in granular films containing FeCoZr nanoparticles embedded into oxygen-free dielectric matrix. *J. Alloys Compd.*, 586, 1, 432–435.
- 8 Bondar, O.V., Pogrebnjak, A.D., Takeda, Y., Postolnyi, B., Zukowski, P., & Sakenova, R., et al. (2019). Structure and properties of combined multilayer coatings based on alternative triple nitride and binary metallic layers. *Lecture Notes in Mechanical Engineering*, 31–40.
- 9 Caicedo, J.C., Amaya, C., Yate, L., Nos, O., Gomez, M.E., & Prieto, P. (2010). Hard coating performance enhancement by using [Ti/TiN]_n, [Zr/ZrN]_n and [TiN/ZrN]_n multilayer system. *Materials Science and Engineering. B*, 171, 56–61.
- 10 Koshy, R.A., Graham, M.E., Marks, L.D. (2010). Temperature activated self-lubrication in Cr/Mo₂N nanolayer coatings. *Materials Science and Engineering*, 204, 9–10, 1359–1365.
- 11 Yao, S.H., & Su, Y.L. (1997). The tribological potential of CrN and Cr(C, N) deposited by multi-arc PVD process. *Wear*, 212, 1, 85–94.
- 12 Wang, Q., Zhou, F., & Yan, J. (2016). Evaluating mechanical properties and crack resistance of CrN, CrTiN, CrAlN and CrTiAlN coatings by nanoindentation and scratch tests. *Surface and Coatings Technology*, 285, 203–213.

Р.Е. Сакенова, Н.К. Ердыбаева, А.Д. Погребняк, М.К. Кылышканов

Вакуумды-доғалық әдіспен алынған MoN(MoZr)ZrN және (TiMo)N/(TiMo), (CrZr)N/(CrZr) негізіндегі көпқабатты жабынды зерттеу

Мақалада 0,09 мкм дейінгі Ra кедірі бар А570 маркалы тот баспайтын болаттың бетіне жабылған көпқабатты жабындылар MoN(MoZr)ZrN және (TiMo)N/(TiMo), (CrZr)N/(CrZr) жабуда алынған эксперименттік зерттеулердің нәтижелері келтірілген. «Бұлат-6» қондырғысында катодты вакуумды-доғалық булану әдісімен жабындар алынды. Көпқабатты жабындарды сканерлейтін электронды микроскопия және микроталдау әдісімен түсіргеннен кейін цирконийдің, хромның, азоттың және молибденнің үлгілердің бетіне біркелкі таралуы анықталды. Зерттеу нәтижелері жақсы трибологиялық қасиеттері жақсартылған физика-механикалық қасиеттермен үйлескенде балқытылған

материалды жұмыстың өте ауыр жағдайларында жұмыс істейтін машиналар мен құрал-саймандар үшін қорғау материалы ретінде қолдану үшін өте тиімді.

Кілт сөздер: көпқабатты жабындылар, катодтық доғалар, микроқұрылым, екіфазалы күй, вакуумды доғалы әдіс, микроқаттылық, тозуға төзімділік.

Р.Е. Сакенова, Н.К. Ердыбаева, А.Д. Погребняк, М.К. Кылышканов

Исследование многослойных покрытий на основе MoN(MoZr)ZrN и (TiMo)N/(TiMo), (CrZr)N/(CrZr), полученных методом вакуумного-дугового осаждения

В статье представлены результаты экспериментальных исследований многослойных покрытий MoN(MoZr)ZrN и (TiMo)N/(TiMo), (CrZr)N/(CrZr), полученных на образцах из нержавеющей стали A570 Grade с шероховатостью Ra до 0,09 мкм. Покрытия были сформированы методом вакуумно-дугового испарения катодов в установке «Булат-6». После нанесения многослойных покрытий методом сканирующей электронной микроскопии и микроанализа обнаружено неоднородное распределение циркония, хрома, азота и молибдена по поверхности образцов. Результаты исследований показывают, что хорошие трибологические свойства в сочетании с улучшенными физико-механическими свойствами делают наплавленный материал перспективным для применения в качестве защитного материала для машин и инструментов, работающих в чрезвычайно тяжелых условиях работы.

Ключевые слова: многослойные покрытия, катодная дуга, микроструктура, двухфазное состояние, вакуумно-дуговой метод, микротвердость, износостойкость.

S.N. Shaltakov¹, S.Sh. Kazhikenova², B.R. Nussupbekov¹,
D.Zh. Karabekova¹, A.K. Khasenov¹, M. Stoev³

¹Ye.A. Buketov Karaganda State University, Kazakhstan;

²Karaganda Technical University, Kazakhstan;

³Neofit Rilski South-West University, Bulgaria

(E-mail: sagyndyk613@mail.ru)

Mathematical model of high-temperature melt flow with account for short-range order nature

The problems of mathematical description of the viscous motion of the metal melt accompanied by overcoming the internal friction caused by the movement of particles and overcoming the forces of their interaction are investigated. Solutions of hydrodynamic equations involving quantum potentials of interparticle interaction of atoms in melts, and quantum effects were taken into account using correlation functions of transport coefficients such as viscosity, since they are quite closely related to the structure of matter and are the most structurally sensitive characteristics of matter. The research consists in the fact that the correlation functions of viscosity are justified from the point of view of the quantum statistical method. The correlation between correlation functions and radial distribution functions is established. A mathematical model of the flow of high-temperature melts taking into account the nature of the near order in them and the account of the second coefficient of viscosity by methods of statistical physics is described. On the basis of theoretical studies the parameters determining the relationship between viscosity and interatomic potential are calculated. The found dependences allow us to determine the average values of any physical parameters, in particular, the values of shear and volumetric viscosity.

Keywords: viscosity, potential, hydrodynamic equations, computer simulation, melt.

1. Introduction

The authors have considered the problem of solving hydrodynamic equations involving quantum potentials of the interparticle interaction of atoms in melts, and quantum effects are taken into account using the correlation functions of transfer coefficients such as viscosity, since they are rather closely related to the structure of the substance and are the most structurally sensitive characteristic of the substance. Based on extensive classical studies of A.R. Regel, V.M. Glazov [1] it can be stated that metal and semiconductor melts are spatially inhomogeneous. The spatial heterogeneity is determined by their atomic-molecular character. Therefore, the physicochemical, metallurgical properties of metal and semiconductor melts should be described taking into account the short-range order. The methods of quantum statistical physics permit to express the coefficients of shear and volume viscosities using correlation functions [1, 2].

2. Experimental Part and Results Discussion

One of the most constructive methods for studying the physical properties of melts is computer modeling [3–5]. Consider one of the options for splitting the equations of hydrodynamics [6, 7] as applied to the calculation of the melt flow in a flat channel in accordance with Figure 1.

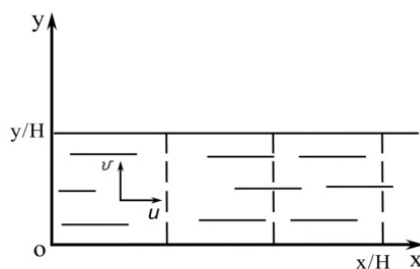


Figure 1. Model of melt flow in a flat channel

Such a melt flow can be described by the following equations of dimensionless form:

$$\frac{\partial u}{\partial x} + \frac{\partial v}{\partial y} = 0, \quad (1)$$

$$\frac{\partial u}{\partial t} + \frac{\partial u^2}{\partial x} + \frac{\partial uv}{\partial y} + \frac{\partial p}{\partial x} = \frac{1}{\text{Re}} \left(\frac{\partial^2 u}{\partial x^2} + \frac{\partial^2 u}{\partial y^2} \right), \quad (2)$$

$$\frac{\partial v}{\partial t} + \frac{\partial v^2}{\partial y} + \frac{\partial uv}{\partial x} + \frac{\partial p}{\partial y} = \frac{1}{\text{Re}} \left(\frac{\partial^2 v}{\partial x^2} + \frac{\partial^2 v}{\partial y^2} \right), \quad (3)$$

where $\text{Re} = \rho u_0 H / \mu$, H is a channel width; u_0 is speed; ρ is density; μ is viscosity.

Equations (1)–(3) are integrated under the following initial and boundary conditions:

$$\begin{aligned} \text{at } t = 0, 0 \leq x \leq \frac{\ell}{H}, 0 \leq y \leq 1: & \quad u = 1, v = 0, p = p_0, \\ \text{at } t > 0, x = 0, 0 \leq y \leq 1: & \quad u = 0, v = 0, p = p_0, \\ \text{at } t > 0, x = \frac{L}{H}, 0 \leq y \leq 1: & \quad \frac{\partial u}{\partial x} = \frac{\partial v}{\partial x} = 0, \frac{\partial p}{\partial x} = -\beta, \\ \text{at } t > 0, y = 0, y = 1, 0 \leq x \leq \frac{L}{H}: & \quad u = 0, v = 0, \frac{\partial p}{\partial y} = \frac{1}{\text{Re}} \frac{\partial^2 v}{\partial y^2}, \end{aligned}$$

where β is the preset pressure gradient; ℓ is the distance from the entrance to the ledge; L is the total length of the channel.

Equations (1)–(3) depend on t and can be solved for u, v . But the pressure p is implicitly preset, because it is not part of the equations in the form of the derivative of t . To exclude this, we write the equation of continuity (1) as follows

$$\frac{\partial w}{\partial t} + \frac{\partial u}{\partial x} + \frac{\partial v}{\partial y} = 0, \text{ where } w = p + \frac{1}{2}(v^2 + u^2), \text{ according to Bernoulli's law.}$$

Then equations (1)–(3) can be reduced to the following two independent systems of equations (4) and (5), which are given for consideration below:

$$\begin{cases} \frac{1}{2} \frac{\partial w_1}{\partial t} + \frac{\partial u}{\partial x} = 0 \\ \frac{1}{2} \frac{\partial u}{\partial t} + \frac{\partial u^2}{\partial x} + \frac{\partial p}{\partial x} = \frac{1}{\text{Re}} \frac{\partial^2 u}{\partial x^2} \\ \frac{1}{2} \frac{\partial v}{\partial t} + \frac{\partial uv}{\partial x} = \frac{1}{\text{Re}} \frac{\partial^2 v}{\partial x^2}, \end{cases} \quad (4)$$

$$\begin{cases} \frac{1}{2} \frac{\partial w_2}{\partial t} + \frac{\partial v}{\partial y} = 0 \\ \frac{1}{2} \frac{\partial v}{\partial t} + \frac{\partial v^2}{\partial y} + \frac{\partial p}{\partial y} = \frac{1}{\text{Re}} \frac{\partial^2 v}{\partial y^2} \\ \frac{1}{2} \frac{\partial u}{\partial t} + \frac{\partial uv}{\partial y} = \frac{1}{\text{Re}} \frac{\partial^2 u}{\partial y^2}, \end{cases} \quad (5)$$

where $w_1 = p + \frac{u^2}{2}$, $w_2 = p + \frac{v^2}{2}$.

Thus, these two systems of equations make it possible to model the melt flow in a flat channel. It should be noted that boundary conditions should also be split here. We represent the split boundary conditions for our case. For the system (4):

$$\begin{aligned} \text{at } x = 0: & \quad u = 1, v = 0, p = 0, \text{ for } y, \text{ at } x = \frac{L}{H}: \frac{\partial u}{\partial x} = \frac{\partial v}{\partial x} = 0, \frac{\partial p}{\partial x} = -\beta, \text{ for } y, \\ \text{at } x = \frac{\ell}{H}: & \quad u = 0, v = 0, \frac{\partial p}{\partial x} = \frac{1}{\text{Re}} \frac{\partial^2 u}{\partial x^2}, \text{ for } 0 \leq y \leq \frac{L}{H}. \end{aligned}$$

For the system (5):

$$\begin{aligned} \text{at } y = \frac{L}{H}, 0 \leq x \leq \frac{\ell}{H} : u = 0, v = 0, \frac{\partial p}{\partial y} &= \frac{1}{\text{Re}} \frac{\partial^2 v}{\partial y^2}, \\ \text{at } y = 0, \frac{\ell}{H} \leq x \leq \frac{L}{H} : u = 0, v = 0, \frac{\partial p}{\partial y} &= \frac{1}{\text{Re}} \frac{\partial^2 v}{\partial y^2}, \\ \text{at } y = 1, 0 \leq x \leq \frac{L}{H} : u = 0, v = 0, \frac{\partial p}{\partial y} &= \frac{1}{\text{Re}} \frac{\partial^2 v}{\partial y^2}. \end{aligned}$$

Now consider the melt flow in a tilting trunk. For a particular design, one can interpret and write it as follows. Direct Oz axis along the axis of the trunk, assuming that the design of the trunk is infinitely long, and the melt flow is directed along the axis of the trunk so that only w , of the three components u, v, w , remains, therefore $u = 0, v = 0$. Let the melt flow be isothermal, then ρ density and viscosity $\mu = \text{const}$.

Consequently, the hydrodynamics equation can be written as:

$$-\frac{1}{\rho} \frac{\partial p}{\partial x} = 0, -\frac{1}{\rho} \frac{\partial p}{\partial y} = 0, w \frac{\partial w}{\partial z} = -\frac{1}{\rho} \frac{\partial p}{\partial z} + \gamma \left(\frac{\partial^2 w}{\partial x^2} + \frac{\partial^2 w}{\partial y^2} + \frac{\partial^2 w}{\partial z^2} \right), \frac{\partial w}{\partial z} = 0. \tag{6}$$

Thus, as can be seen from the system of equations (6), the rate w is a function of x, y , only; in addition, the pressure function p is a function of z . On the basis of (6), we obtain the equation:

$$\frac{dp}{dz} = \mu \left(\frac{\partial^2 w}{\partial x^2} + \frac{\partial^2 w}{\partial y^2} \right). \tag{7}$$

The right side of (7) represents a function of x, y , while the left side is a function of z . From the basic principles of hydrodynamics, it follows that $\frac{dp}{dz} = -\frac{\Delta p}{\ell}$, where Δp is the pressure drop at an arbitrarily chosen section; ℓ is the length of the trunk. In addition, due to the free surface of the melt, the pressure in the channel is equal to the atmospheric pressure [8]. Since the trunk is inclined to the horizon at a certain angle α , a volume force arises, the projection of which on the axis Oz is equal to $F_z = g \sin \alpha = \frac{\Delta p}{\ell}$. Then the equation of motion (7) in the direction of Oz becomes:

$$\mu \left(\frac{\partial^2 w}{\partial x^2} + \frac{\partial^2 w}{\partial y^2} \right) + \rho g \sin \alpha = 0. \tag{8}$$

To solve the resulting equation, boundary conditions are necessary. These conditions will be determined by sticking of the melt to the bottom of the trunk and the absence of friction on the free surface of the melt. Denote the depth of the flow as h_1 , and the width of the trunk as h_2 . Then the boundary conditions of the problem can be written as follows:

$$w = 0 \text{ at } y = 0, \frac{\partial w}{\partial y} = 0 \text{ at } y = h_1, \frac{\partial w}{\partial x} = 0 \text{ at } x = h_2. \tag{9}$$

Thus, equation (8) with boundary conditions (9) will describe the process of melt flow in specific designs of the trunk type. This model is designed for the melting equipment of the SCR-2000 line; the drawing of the lower trunk section is presented in Figure 2.

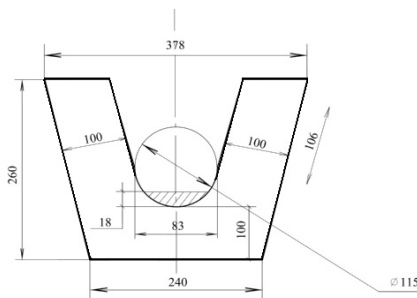


Figure 2. Lower trunk cross section

Calculations are made for the lower trunk with an inclination angle of 3° . Numerical parameters are found by the following calculations: the area of the segment $S = \frac{[lr - a(r - h)]}{2}$, $a = 83$ mm, $h = 18$ mm, $l \approx \sqrt{a^2 + (16h^2/3)} = \sqrt{83^2 + (16 \cdot 18^2/3)} = 92.8$ mm, where l is the length of the arc; a is a chord; h is a segment arrow. Consequently, $S = \frac{[92.8 \cdot \frac{115}{2} - 83(\frac{115}{2} - 18)]}{2} = 1029$ mm². Then the melt consumption per second is $Q = 3.61$ kg/s. Based on this, one can make definite the average melt flow rate, which is equal to $v_{av} = 0.45$ m/s.

In the calculations, constant step-sizes were used. The time-step in the calculations was chosen to be $\Delta t = 0.001$. The found out results for the profiles of melt flow rates v and u in the flat channel are respectively presented in Figure 3. Obtaining the steady-state flow required 3000 steps. The results show that the proposed computational scheme is quite economical and it can be easily used to calculate the flow at sufficiently low Reynolds numbers. The analysis of the data obtained shows that replacing the continuity condition by a Poisson-type pressure equation leads to a numerical scheme that is free from a complicated computational procedure.

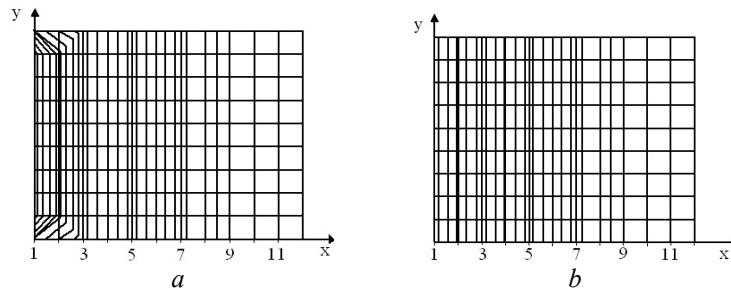


Figure 3. Profiles of a) transverse v and b) longitudinal u rates

On the basis of the compressibility sum rule, one can determine how self-consistent the adopted model of the melt system is. If the value of the volume modulus is determined correctly, then its reciprocal value is equal to compressibility. Compressibility is important when considering the physicochemical properties of molten metals. On the basis of [9], one may state that in a crystalline substance the bulk modulus of elasticity is equal to the derivative of the energy in terms of volume. At the same time, the static modulus must be consistent with the dynamic modulus. The dynamic modulus is calculated from the phonon dispersion ratio in the long wave approximation. Therefore, it is strongly linked by interatomic interaction. This statement is the essence of the compressibility rule and is well tested for crystalline metals [9]. Further studies have shown that the sum rule is not fully satisfied for the model of metals constructed using perturbation theory in the second order in empirical potentials. Then, the third and fourth order terms appearing in the dynamic matrix at $q \rightarrow 0$ bring to a second order contribution. Also, the discrepancy is obtained due to the inclusion of these contributions only when calculating static modules and neglecting them when calculating dynamic ones. The inclusion of the higher terms of the expansion in the construction of a dynamic matrix approximates the experimental data to the theoretical ones [10–12].

The data are in good agreement with experimental ones within 10 %. These assumptions make it possible to estimate the relaxation time of the structural viscosity (i.e. the volume one). According to Ya.I. Frenkel, the settled life of an atom $t = 10^{-11}$ c. This value agrees well with the found relaxation time of the volume viscosity. According to the hole theory, it can be assumed that the volume deformation of the melt consists of two types of deformation. The first is instantaneous and retarding. The second is the deformation associated with the change in the number of holes during the movement of the melt. The retarding part of compressibility can be calculated by the formula $\beta_s = \frac{\Delta V^2}{VRT} e^{-\Delta H/RT}$, where ΔV is the change in the volume of holes, ΔH is the increase in enthalpy due to the formation of holes. Then, if the retarding part of

compressibility is known, using the formula given in [11], it is possible to determine the value of the volume viscosity $\mu_V = \frac{t}{\beta_0}$, where β_0 is the equilibrium compressibility, t is the lag time. The regime of the copper melt flow is completely determined by the melt viscosity, the theoretical and experimental [12] values of which are presented in Figure 4 and Table.

Table

Experimental μ_{SE} and theoretical μ_{ST} values of the shear viscosity and the theoretical value of the volume viscosity μ_V

T, K	$\mu_{SE}, Pa \cdot s$	$\mu_{ST}, Pa \cdot s$	$\mu_V, Pa \cdot s$
1358	0.005	0.0060999	0.12354
1398	0.0046	0.005847	0.11959
1438	0.0042	0.005606	0.11578
1478	0.0038	0.005374	0.11208
1518	0.0036	0.005153	0.10851
1558	0.0033	0.00494	0.10505
1598	0.0031	0.004736	0.10117
1638	0.0029	0.00454	0.09846

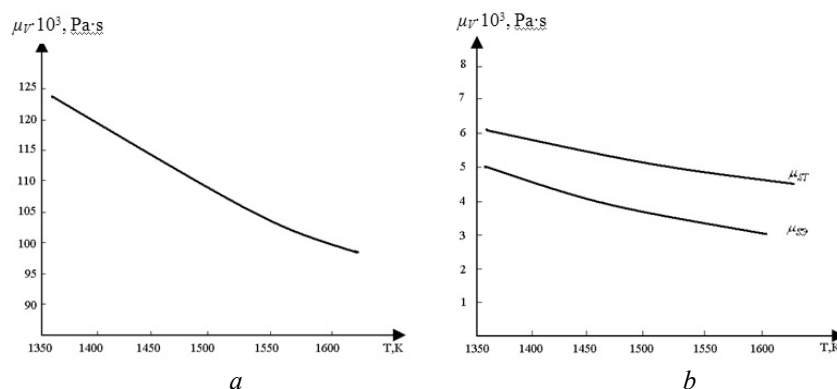


Figure 4. *a* — the theoretical value of volume viscosity and *b* — the experimental one μ_{SE} [9] and the theoretical value of shear viscosity μ_{ST}

Conclusions

Thus, the main problem of the mathematical description of a viscous motion of a metal melt, accompanied by overcoming internal friction caused by the melt particles movement and overcoming the forces of their interaction, is considered. Based on the cluster theory of the melt flow, a relationship between viscosity and interatomic potential is established.

References

- 1 Регель А.Р. Физические свойства электронных расплавов / А.Р. Регель, В.М. Глазов. — М.: Наука, 1980. — 296 с.
- 2 Anisimov V.I. First principles electronic structure calculation and simulation of the evolution of radiation defects in plutonium by the density functional theory and the molecular dynamics approach / V.I. Anisimov, V.V. Dremov, M.A. Korotin // The Physics of Metals Metallography. — 2013. — Vol. 114. — P. 1087–1122.
- 3 Kato Yasumasa. Finite-element method for three-dimensional incompressible viscous flow using simultaneous relaxation of velocity and Bernoulli function. 1st report flow in a lid-driven cubic cavity at $Re=5000$ / Kato Yasumasa, Tanahashi Takahico // Journal JSME international journal. — 1991. — Vol. 57, No. 540. — P. 2640–2647.
- 4 Kazhikenova S.Sh. Monitoring of Process Flow Diagrams in the Production of Ferrous Metals / S.Sh. Kazhikenova // Refractories and Industrial Ceramics. — 2016. — Vol. 57, No. 4. — P. 360–363.
- 5 Yan X. Wei L. Numerical Simulation of Meso-Micro Structure in Ni-Based Superalloy During Liquid Metal Cooling / Yan X. Wei L, Lei Yao, Xin Xue, Yanbin Wang, Gang Zhao, Juntao Li, Qingyan Xu // The Minerals, Metals & Materials Series: Proceedings of the 4th World Congress on Integrated Computational Materials Engineering. — 2017. — P. 249–259.

- 6 Sciubba E. A variational derivation of the Navier-Stokes equations based on the energy destruction of the flow / E. Sciubba // J. Math. and Phys. Sci. — 1991. — Vol. 25, No. 1. — P. 61–68.
- 7 Кажикенова С.Ш. Физико-химические аспекты теории металлургических процессов / С.Ш. Кажикенова, С.Н. Шалтаков, А.З. Исагулов. — Караганда: Изд-во КарГТУ, 2010. — 257 с.
- 8 Максимов Е.В. Механика жидкостей, газов и сыпучей среды / Е.В. Максимов, А.К. Торговец. — Алматы: РИК, 1997. — 254 с.
- 9 Сулейменов Т. Квантово-химическая природа ближнего порядка в неупорядоченных системах: дис. ... д-ра хим. наук: 02.00.04 / Т. Сулейменов. — Караганда, 2004. — 191 с.
- 10 Назаренко В.И. Модель жидкого металла при температуре плавления / В.И. Назаренко, В.А. Полухин, Р.М. Белякова, В.Ф. Ухов // Металлофизика. — 1981. — № 5. — С. 122–126.
- 11 Lobodyuk, V.A. Crystal-structural features of pretransition phenomena and thermo elastic martensitic transformations in alloys of nonferrous metals / V.A. Lobodyuk, Y.N. Koval, V.G. Pushin // The Physics of Metals Metallography. — 2011, Vol. 111. — P. 165–189.
- 12 Шпильрайн Э.Э. Исследование вязкости жидких металлов / Э.Э. Шпильрайн, В.А. Фомин, С.Н. Сквородько, Г.Ф. Сокол. — М.: Наука, 1983. — 244 с.

С.Н. Шалтаков, С.Ш. Кажикенова, Б.Р. Нусупбеков,
Д.Ж. Карабекова, А.К. Хасенов, М. Стоев

Жақын тәртіптің табиғатын есепке ала отырып балқыманың жоғары температуралы ағынының математикалық моделі

Бөлшектердің қозғалысынан және олардың өзара әрекеттесуінің күшінен туындаған ішкі үйкелісті жеңумен қоса жүретін металл балқымасының тұтқыр қозғалысының математикалық сипаттамасы мәселелері зерттелді. Қорытпалардағы атомдардың үлестес өзара әрекеттесуінің кванттық потенциалдарының қатысуымен гидродинамикалық теңдеулерді шешу және кванттық әсерлер тұтқырлық сияқты тасымалдау коэффициенттерінің корреляциялық функцияларын пайдалана отырып зерттелді, олар заттың құрылымымен тығыз байланысты және заттың неғұрлым құрылымдық-сезімтал сипаттамалары болып табылады. Зерттеу тұтқырлықтың корреляциялық функциялары кванттық-статистикалық әдіс тұрғысынан негізделді. Корреляциялық функциялар мен радиалды үлестіру функциялары арасында корреляция орнатылған. Жоғары температуралы балқымалар ағынының математикалық моделі, оларда жақын тәртіптің табиғатын есепке ала отырып және статистикалық физика әдістерімен екінші тұтқырлықтың коэффициентін есепке алу сипатталған. Жүргізілген теориялық зерттеулер негізінде тұтқырлық пен атомаралық потенциал арасындағы байланысты анықтайтын параметрлер есептелді. Табылған тәуелділіктер кез келген физикалық параметрлердің, атап айтқанда, жылжу және көлемдік тұтқырлықтың мәндерінің орташа мәнін анықтауға мүмкіндік береді.

Кілт сөздер: тұтқырлық, потенциал, гидродинамикалық теңдеулер, компьютерлік модельдеу, балқымалар.

С.Н. Шалтаков, С.Ш. Кажикенова, Б.Р. Нусупбеков,
Д.Ж. Карабекова, А.К. Хасенов, М. Стоев

Математическая модель высокотемпературного течения расплава с учетом природы ближнего порядка

Исследованы проблемы математического описания вязкого движения металлического расплава, сопровождающегося преодолением внутреннего трения, вызванного движением частиц и преодолением сил их взаимодействия. Решения гидродинамических уравнений с участием квантовых потенциалов межчастичного взаимодействия атомов в расплавах и квантовые эффекты учитывались с использованием корреляционных функций коэффициентов переноса, таких как вязкость, поскольку они довольно тесно связаны со структурой вещества и являются наиболее структурно-чувствительными характеристиками вещества. Исследования заключались в том, что корреляционные функции вязкости обоснованы с точки зрения квантово-статистического метода. Установлена корреляция между корреляционными функциями и функциями радиального распределения. Описана математическая модель течения высокотемпературных расплавов с учетом природы ближнего порядка в них и второго коэффициента вязкости методами статистической физики. На основании проведенных теоретических исследований рассчитаны параметры, определяющие связь между вязкостью и межатомным потенциалом. Найденные зависимости позволяют определить средние значения любых физических параметров, в частности, значений сдвиговой и объемной вязкости.

Ключевые слова: вязкость, потенциал, гидродинамические уравнения, компьютерное моделирование, расплав.

References

- 1 Regel, A.R., & Glazov, V.M. (1980). *Fizicheskie svoystva elektronnykh rasplavov [Physical properties of electron melts]*. Moscow: Nauka [in Russian].
- 2 Anisimov, V.I., Dremov, V.V., & Korotin, M.A. (2013). First principles electronic structure calculation and simulation of the evolution of radiation defects in plutonium by the density functional theory and the molecular dynamics approach. *The Physics of Metals Metallography*, 114, 1087–1122.
- 3 Kato Yasumasa, & Tanahashi Takahico (1991). Finite-element method for three-dimensional incompressible viscous flow using simultaneous relaxation of velocity and Bernoulli function. 1st report flow in a lid-driven cubic cavity at Re=5000. *Journal JSME international journal*, 57, 540, 2640–2647.
- 4 Kazhikenova, S.Sh. (2016). Monitoring of process flow diagrams in the production of ferrous metals. *Refractories and Industrial Ceramics*, 57, 4, 360–363.
- 5 Yan X. Wei L., Lei Yao, Xin Xue, Yanbin Wang, Gang Zhao, Juntao Li, & Qingyan Xu (2017). Numerical Simulation of Meso-Micro Structure in Ni-Based Superalloy During Liquid Metal Cooling. Proceedings from The Minerals, Metals & Materials Series. *The 4th World Congress on Integrated Computational Materials Engineering*, 249–259.
- 6 Sciubba, E. (1991). A variational derivation of the Navier-Stokes equations based on the energy destruction of the flow. *J. Math. and Phys. Sci.*, 25, 1, 61–68.
- 7 Kazhikenova, S.Sh., Shaltakov, S.N., & Isagulov, A.Z. (2010). *Fiziko-khimicheskie aspekty teorii metallurgicheskikh protsessov [Physico-chemical aspects of the theory of metallurgical processes]*. Karaganda: KSTU Publishing House [in Russian].
- 8 Maksimov, E.V., & Torgovets, A.K. (1997). *Mekhanika zhidkosti, hazov i sypuchei sredy [Mechanics of liquids, gases and solids]*. Almaty: RIK [in Russian].
- 9 Suleimenov, T. (2004). *Kvantovo-khimicheskaia priroda blizhneho poriadka v neuporiadochennykh sistemakh [Quantum-chemical nature of short-range order in disordered systems]*. Doctor's thesis. Karaganda [in Russian].
- 10 Nazarenko, V.I., Polukhin, V.A., Belyakova, R.M., & Ukhov, V.F. (1981). Model zhidkoho metalla pri temperature plavleniia [Model of liquid metal at melting point]. *Metallofizika — Metal Physics*, 5, 122–126 [in Russian].
- 11 Lobodyuk, V.A., Koval, Y.N., & Pushin, V.G. (2011). Crystal-structural features of pretransition phenomena and thermo elastic martensitic transformations in alloys of nonferrous metals. *The Physics of Metals Metallography*, 111, 165–189.
- 12 Spielrain, E.E., Fomin, V.A., Skovorodko, S.N., & Sokol, G.F. (1983). *Issledovanie viazkosti zhidkikh metallov [The study of liquid metals viscosity]*. Moscow: Nauka [in Russian].

S.K. Tleukenov¹, M.K. Zhukenov², N.A. Ispulov²¹L.N. Gumilyov Eurasian National University, Nur-Sultan, Kazakhstan;²S. Toraighyrov Pavlodar State University, Kazakhstan

(E-mail: marat_k_zhukenov@mail.ru)

Propagation of electromagnetic waves in anisotropic magnetoelectric medium

In the article we consider propagation and interaction of electromagnetic waves of different polarization, in anisotropic medium that is inhomogeneous along the Z axis with magnetoelectric effect of tetragonal, trigonal, and hexagonal symmetries are described by the structure of the matrix coefficients. The matricant structure of the original system of equations follows from the structure of coefficient matrix. In unlimited periodic structures, dispersion relations of electromagnetic waves are determined from the new modified conditions for the existence of non-trivial solutions which are the consequence of the matricant structure. Obvious analytical form of the matricants for the homogeneous anisotropic dielectric medium with magnetoelectric effects follows from the matricant structure. Analytical equations for homogeneous anisotropic medium with magnetoelectric effects allow one, in matrix setting, to obtain analytical solutions for the problem of reflection and refraction on the border of isotropic and anisotropic medium with magnetoelectric effect based on the matricant method. Initial relationships that describe electromagnetic wave propagation in anisotropic magnetoelectric medium are reduced to the system of linear homogeneous first order differential equations. The structure of the matricant is obtained. Dispersion equations of electromagnetic waves in periodic inhomogeneous medium with magnetoelectric effects are constructed. Averaged matricant describing the propagation of electromagnetic waves in homogeneous anisotropic medium with magnetoelectric medium are also constructed. Besides, the graphs of energy reflection coefficient of TE and TM electromagnetic waves and incident angle are plotted.

Keywords: anisotropic medium; electromagnetic waves; magnetoelectric effect; matricant method; reflection, refraction of electromagnetic waves.

Introduction

Anisotropic medium is characterized by many parameters. One of the constructive ways to overcome these difficulties is a systematic and detailed study of properties of Maxwell equations in a wide class of anisotropic medium so that the regularities of these solutions that depend on the structure of tensor quantities defining anisotropy of medium can be established. In this research, solutions of Maxwell equations in dielectric magnetoelectric medium that depend on time harmonically are considered [1].

In this work on the basis of a method of variables separation and representation of a solution in the form of plane harmonious waves of Maxwell equation and the defining ratios describing distribution of electromagnetic waves in non-isotropic mediums with magnetoelectric effect are brought to the equivalent system of ordinary differential equations of the 1st order with float factors and matrixes of coefficients for tetragonal, trigonal and hexagonal singoniya in volume and flat cases are received [2]. The structure of matrixes of fundamental solutions of a system of the differential equations of the 1st order describing distribution of electromagnetic waves in anisotropic environments of tetragonal, trigonal and hexagonal singoniya with magnetoelectric effect in volume and flat cases is constructed [3]. The equations of dispersion of electromagnetic waves in unlimited periodic structures are received. Matriciants of homogeneous anisotropic dielectric environments with magnetoelectric effect are constructed. Matrix statement is formulated and the analytical solution of a problem of reflection and refraction of electromagnetic waves on border of the isotropic environment and anisotropic environment with magnetoelectric effect is received [4]. The numerical analysis of power coefficients of reflection and refraction at reflection of electromagnetic waves on border of the isotropic environment and anisotropic environment with magnetoelectric effect is carried out. Schedules of dependence of power coefficients of reflection and refraction from a hade of electromagnetic waves are constructed [5, 6]. The value of work is that the structure of fundamental decisions and an obvious type of analytical representations of a matriciant allows to investigate periodically non-uniform anisotropic environments and average structures [7, 8].

When volume charge density, ρ , current density vectors and harmonic time dependance of wave fields are absent Maxwell equations take following form:

$$\operatorname{rot} \vec{E} = -\frac{\partial \vec{B}}{\partial t} = -i\omega \vec{B}, \quad \operatorname{rot} \vec{H} = \frac{\partial \vec{D}}{\partial t} = i\omega \vec{D}, \quad (1)$$

$$\operatorname{div} \vec{B} = 0, \quad \operatorname{div} \vec{D} = 0. \quad (2)$$

Material equations connecting \vec{B} and \vec{H} , \vec{D} and \vec{E} we obtain from free energy

$$F_{3m} = \varepsilon_0 \varepsilon_{ij} E_i E_j + \mu_0 \mu_{ij} H_i H_j - \alpha_{ij} E_i H_j, \quad (3)$$

where $\varepsilon_{ij}, \mu_{ij}$ — components of dielectric and magnetic susceptibility tensors; α_{ij} — component of non-symmetric magnetoelectric effect tensor.

Solutions of $\vec{E}, \vec{H}, \vec{B}, \vec{D}$ wave fields are taken in the following form:

$$\vec{F} = \vec{F}(z) e^{i\omega t \pm ik_x x \pm ik_y y}, \quad (4)$$

where ω — frequency; k_x, k_y — components of a wave vector. We assume that medium is inhomogeneous along the z axis. Then material equations take the following form:

$$\frac{\partial F}{\partial E_i} = \varepsilon_0 \varepsilon_{ij} E_j - \alpha_{ij} H_j = D_i; \quad \frac{\partial F}{\partial H_i} = \mu_0 \mu_{ij} H_j - \alpha_{ij} E_i = B_j. \quad (5)$$

Based on the matricant method, the system of equations describing propagation of electromagnetic waves can be reduced to equivalent system of differential equations:

$$\frac{d\vec{U}}{dz} = B\vec{U}, \quad \vec{U} = (E_y, H_x, H_y, E_x). \quad (6)$$

Then matrix coefficients of \hat{B} takes the following form:

$$\hat{B} = \begin{pmatrix} b_{11} & b_{12} & b_{13} & b_{14} \\ b_{21} & b_{11} & b_{23} & b_{24} \\ -b_{24} & -b_{14} & -b_{11} & b_{34} \\ -b_{23} & -b_{13} & b_{43} & -b_{11} \end{pmatrix}, \quad (7)$$

where

$$\begin{aligned} b_{11} &= i \frac{k_x k_y}{\beta} \alpha_{11}; & b_{12} &= i\mu_0 \left(\frac{k_y^2}{\beta} \mu_2 + \omega \mu_1 \right); & b_{13} &= -i \frac{k_x k_y}{\beta} \mu_0 \mu_2; \\ b_{14} &= -i \left(\frac{k_y^2}{\beta} \alpha_{11} + \omega \alpha_{\perp} \right); & b_{21} &= i\varepsilon_0 \left(\frac{k_x^2}{\beta} \varepsilon_2 + \omega \varepsilon_1 \right); & b_{23} &= -i \left(\frac{k_x^2}{\beta} \alpha_{11} + \omega \alpha_{\perp} \right); \\ b_{24} &= -i \frac{k_x k_y}{\beta} \varepsilon_0 \varepsilon_2; & b_{34} &= -i\varepsilon_0 \left(\frac{k_y^2}{\beta} \varepsilon_2 + \omega \varepsilon_1 \right); & b_{43} &= -i\mu_0 \left(\frac{k_x^2}{\beta} \mu_2 + \omega \mu_1 \right). \end{aligned}$$

Propagation of waves in the (xz, yz) planes is described by \hat{B} matrix:

$$\hat{B} = \begin{pmatrix} 0 & b_{12} & 0 & b_{14} \\ b_{21} & 0 & b_{23} & 0 \\ 0 & -b_{14} & 0 & b_{34} \\ -b_{23} & 0 & b_{43} & 0 \end{pmatrix} \quad (8)$$

When waves propagate in the xz ($k_y = 0$) matrix elements takes the form:

$$\begin{aligned} b_{12} &= i\omega \mu_0 \mu_1; & b_{14} &= -i\omega \alpha_{\perp}; & b_{21} &= i\varepsilon_0 \left(\frac{k_x^2}{\beta} \varepsilon_2 + \omega \varepsilon_1 \right); \\ b_{23} &= -i \left(\frac{k_x^2}{\beta} \alpha_{11} + \omega \alpha_{\perp} \right); & b_{34} &= -i\omega \varepsilon_0 \varepsilon_1; & b_{43} &= -i\mu_0 \left(\frac{k_x^2}{\beta} \mu_2 + \omega \mu_1 \right). \end{aligned}$$

When waves propagate in the yz ($k_x = 0$) matrix elements takes the form:

$$b_{12} = i\mu_0 \left(\frac{k_y^2}{\beta} \mu_2 + \omega \mu_1 \right); \quad b_{14} = -i \left(\frac{k_y^2}{\beta} \alpha_{11} + \omega \alpha_{\perp} \right); \quad b_{21} = i\omega \varepsilon_0 \varepsilon_1$$

$$b_{23} = -i\omega\alpha_{\perp}; \quad b_{34} = -i\epsilon_0 \left(\frac{k_y^2}{\beta} \epsilon_2 + \omega\epsilon_1 \right); \quad b_{12} = -i\omega\mu_0\mu_1.$$

The consequence of the matrix structure of coefficients of \hat{B} is the structure of fundamental solutions:

$$\hat{T}^{-1} = \begin{pmatrix} t_{22} & -t_{12} & -t_{42} & -t_{32} \\ -t_{21} & t_{11} & t_{41} & -t_{31} \\ -t_{24} & t_{14} & t_{44} & -t_{34} \\ t_{23} & -t_{13} & -t_{43} & t_{33} \end{pmatrix}. \quad (9)$$

Due to its wide application, inhomogeneous periodic medium is one of the important class of inhomogeneous medium. The structure of the fundamental solutions give the opportunity to find the most general dispersion equations of electromagnetic waves in inhomogeneous periodic medium with magnetoelectric effect.

When electromagnetic waves propagate in the coordinate planes dispersion equations are found from the following condition:

$$\det(\hat{P} - \hat{E} \cos \tilde{k}h) = 0, \quad (10)$$

here

$$\hat{P} = \frac{1}{2}(\hat{T} + \hat{T}^{-1}). \quad (11)$$

From the structures of T and T^{-1} the structure of P takes the form:

$$\hat{P} = \begin{pmatrix} P_{11} & 0 & P_{13} & P_{14} \\ 0 & P_{11} & P_{14} & P_{24} \\ -P_{24} & P_{14} & P_{33} & 0 \\ P_{14} & -P_{13} & 0 & P_{33} \end{pmatrix}, \quad (12)$$

taking into account (12) in (10) gives:

$$\tilde{P}_1, \tilde{P}_2 = \frac{1}{2} \left(P_{11} + P_{22} \pm \sqrt{(P_{11} - P_{22})^2 + 4(P_{14}P_{14} + P_{13}P_{24})} \right), \quad (13)$$

the general form of dispersion equations can be written in the following form:

$$\cos \tilde{k}_1 h = \tilde{P}_1, \quad \cos \tilde{k}_2 h = \tilde{P}_2. \quad (14)$$

Averaged matricant, describing the propagation of electromagnetic wave in homogeneous anisotropic medium with magnetoelectric effect, is obtained in the following analytical form

$$\hat{T}_{aver}^{\pm} = \left(\hat{\pi} + \frac{1}{2} \hat{E} \right) \left(\hat{E} \cos kz \pm \frac{\hat{B}}{k} \sin kz \right) - \left(\hat{\pi} - \frac{1}{2} \hat{E} \right) \left(\hat{E} \cos \chi z \pm \frac{\hat{B}}{\chi} \sin \chi z \right) \quad (15)$$

here

$$\hat{\pi} = \frac{\hat{P} - \tilde{P}_2 \hat{E}}{\tilde{P}_1 - \tilde{P}_2} - \frac{1}{2} \hat{E}; \quad \hat{P} = \hat{E} + \frac{1}{2} \hat{B}^2 h^2. \quad (16)$$

Matricants will have an appearance

$$\hat{T}_{aver}^{+} = \begin{pmatrix} t_{11} & t_{12} & t_{13} & t_{14} \\ t_{21} & t_{11} & t_{23} & t_{24} \\ -t_{24} & -t_{14} & t_{33} & t_{34} \\ -t_{23} & -t_{13} & t_{43} & t_{33} \end{pmatrix}; \quad (17)$$

$$\hat{T}_{aver}^{-} = \begin{pmatrix} t_{11} & t_{12} & t_{13} & -t_{14} \\ t_{21} & t_{11} & -t_{23} & t_{24} \\ -t_{24} & t_{14} & t_{33} & t_{34} \\ t_{23} & -t_{13} & t_{43} & t_{33} \end{pmatrix}, \quad (18)$$

where

$$\begin{aligned}
 t_{11} &= \frac{\text{Cos}[kz](b_{12}b_{21} - b_{34}b_{43} + \Delta)}{2\Delta}; \\
 t_{12} &= \frac{\text{Sin}[kz](b_{12}^2b_{21} - 2b_{14}^2b_{43} + b_{12}(-2b_{14}b_{23} - b_{34}b_{43} + \Delta))}{2k\Delta}; \\
 t_{13} &= \frac{\text{Cos}[kz](b_{12}b_{23} + b_{14}b_{43})}{2\Delta}; \\
 t_{14} &= \frac{\text{Sin}[kz](b_{12}(b_{14}b_{21} + 2b_{23}b_{34}) + b_{14}(b_{34}b_{43} + \Delta))}{2k\Delta}; \\
 t_{21} &= \frac{\text{Sin}[kz](b_{12}b_{21}^2 - 2b_{14}b_{21}b_{23} - b_{34}(2b_{23}^2 + b_{21}b_{43}) + b_{21}\Delta)}{2k\Delta}; \\
 t_{23} &= \frac{\text{Sin}[kz](b_{12}b_{21}b_{23} + 2b_{14}b_{21}b_{43} + b_{23}(b_{34}b_{43} + \Delta))}{2k\Delta}; \\
 t_{24} &= \frac{\text{Cos}[kz](b_{14}b_{21} + b_{23}b_{31})}{\Delta}; \\
 t_{33} &= \frac{\text{Cos}[kz](-b_{12}b_{21} + b_{34}b_{43} + \Delta)}{2\Delta}; \\
 t_{34} &= \frac{\text{Sin}[kz](-2b_{14}^2b_{21} - 2b_{14}b_{23}b_{34} + b_{34}(-b_{12}b_{21} + b_{34}b_{43} + \Delta))}{2k\Delta}; \\
 t_{43} &= \frac{\text{Sin}[kz](-b_{12}(2b_{23}^2 + b_{21}b_{43}) + b_{43}(-2b_{14}b_{23} + b_{34}b_{43} + \Delta))}{2k\Delta}, \tag{19}
 \end{aligned}$$

here

$$\Delta = \sqrt{(b_{12}b_{21} - b_{34}b_{43})^2 - 4(b_{12}b_{23} + b_{14}b_{43})(b_{14}b_{21} + b_{23}b_{34})}$$

When $z = 0$ matricant (15) can be written as:

$$\hat{T}_0^\pm = \frac{1}{2} \hat{E} \mp \hat{R} \tag{20}$$

\hat{R} matrix has the form:

$$\hat{R} = \frac{1}{2i} \left(\frac{k - \chi}{k\chi} \right) \pi \hat{B} - \frac{1}{4i} \left(\frac{k + \chi}{k\chi} \right) \hat{B}. \tag{21}$$

Assuming: \vec{U}_p — field of incident waves, \vec{U}_R — field of reflected waves and \vec{U}_t — field of refracted waves, from (6) we have:

$$T_0^p \vec{U}_p + T_0^R \vec{U}_R = T_0^t \vec{U}_t, \text{ when } z = 0. \tag{22}$$

Considering continuity of fields at the boundary:

$$\vec{U}_p + \vec{U}_R = \vec{U}_t. \tag{23}$$

We get the result for reflected waves:

$$\vec{U}_R = (R_0 + \hat{R}_t)^{-1} (\hat{R}_0 - \hat{R}_t) \vec{U}_0. \tag{24}$$

Condition (19) with consideration of continuity of solutions at the boundary (20) is the matrix form of boundary conditions which are imposed on vectors of reflected, refracted and incident waves.

Then the fields of reflected and refracted waves:

$$\vec{U}_R = \hat{G} \vec{U}_p; \tag{25}$$

$$\vec{U}_t = (\hat{G} + \hat{E}) \vec{U}_p. \tag{26}$$

Analytical equations for homogeneous anisotropic medium with magnetoelectric effects allows one, in matrix setting, to obtain analytical solutions for the problem of reflection and refraction on the border of isotropic and anisotropic medium with magnetoelectric effect based on the matricant method. Initial relation-

ships that describe electromagnetic wave propagation in anisotropic magnetoelectric medium are reduced to the system of linear homogeneous first order differential equations.

Using above algorithm, numerical calculations of energy flow density in the case of TE and TM incident waves at the boundary of two medium are conducted. The graphs of reflected energy coefficients when TE and TM electromagnetic waves are incident are plotted against incident angle.

References

- 1 Ландау Л.Д. Электродинамика сплошных сред / Л.Д. Ландау, Е.М. Лифшиц. — М.: Наука, 1982.
- 2 Тлеуменов С.К. Изучение электромагнитных полей в анизотропных средах / С.К. Тлеуменов, А.Т. Оспанов. — Алматы: Наука, 1985. — 176 с.
- 3 Тлеуменов С.К. О характеристической матрице периодически неоднородного слоя / С.К. Тлеуменов // Математические вопросы теории распространения волн. Т. 165. — Л.: Записки науч. семинара ЛОМИ, 1987. — С. 177–181.
- 4 Тлеуменов С.К. Метод матрицанта / С.К. Тлеуменов. — Павлодар: НИЦ ПГУ им. С. Торайгырова, 2004. — 148 с.
- 5 Тлеуменов С.К. О методе решения некоторых задач распространения упругих волн при наличии периодической неоднородности. Т. 148 / С.К. Тлеуменов, О. Байгонысов. — Л.: Записки науч. семинара ЛОМИ АН СССР, 1985. — С. 30–33.
- 6 Тлеуменов С.К. Электромагниттік толқындардың шағылу және сыну есептеріндегі шектік шарттардың матрицалық түрі / С.К. Тлеуменов, М.К. Жукенов, Н.К. Каратаева, Д. Жакипова // Вторые Ержановские чтения: материалы Междунар. науч. конф. — Актөбе, 2007. — С. 278–281.
- 7 Тлеуменов С.К. К вопросу отражения электромагнитной ТЕ-волны от поверхности магнитоэлектрического кристалла гексагональной сингонии классов 622, 6mm, 6m2, 6mmm / С.К. Тлеуменов, М.К. Жукенов, Т.С. Досанов, Г.М. Жумабаева // Вестн. Караганд. ун-та. Сер. Физика. — 2016. — № 3. — С. 21–27.
- 8 Тлеуменов С.К. Метод матрицанта. Единое описание волновых процессов в средах с взаимной трансформацией упругих и электромагнитных полей / С.К. Тлеуменов, М.К. Жукенов // Вестн. Казах. нац. пед. ун-та. Сер. физ.-мат. наук. — Алматы, 2016. — № 4. С. 85–91.

С.К. Тлеуменов, М.К. Жукенов, Н.А. Испулов

Электрмагниттік толқындардың анизотропты магнитэлектрлік орталарда таралуы туралы

Мақалада магнитэлектрлік эффектісі бар тетрагоналды, тригоналды және гексагоналды сингониялы Z осі бойынша анизотропты орталарда поляризациясы әртүрлі электрмагниттік толқындардың таралуы мен әсерлесуі қарастырылды. Бастапқы теңдеулер жүйесінің матрицант құрылымы коэффициенттер матрицасының құрылымынан шығады. Шексіз периодты құрылымдардағы электрмагниттік толқындардың дисперсия теңдеулері матрицант құрылымының салдары болып табылатын жаңа модификацияланған шарттардан анықталады. Біртекті анизотропты магнитэлектрлік эффектісі бар диэлектрлік орталар үшін матрицанттардың анық аналитикалық түрі матрицант құрылымынан шығады. Магнитэлектрлік эффектісі бар біртекті анизотропты орталар үшін аналитикалық теңдеулер матрицалық түрде изотропты орта мен магнитэлектрлік эффектісі бар ортаның арасындағы шекарада толқындардың шағылу және сыну есептерін аналитикалық шешуіне мүмкіндік береді. Электрмагниттік толқындардың анизотропты магнитэлектрлік орталарда таралуын сипаттайтын бастапқы қатынастар сызықты біртекті бірінші ретті дифференциалдық теңдеулердің жүйесіне келтірілді. Матрицант құрылымы шығарылды. Біртексіз магнитэлектрлік эффектісі бар орталардағы электрмагниттік толқындардың дисперсия теңдеулері жазылды. Электрмагниттік толқындардың магнитэлектрлік эффектісі бар біртекті анизотропты орталарда таралуын сипаттайтын орташаланған матрицант құрылды. Энергиялық шағылу коэффициентінің электрмагниттік ТЕ және ТМ толқындардың түсу бұрышына тәуелділік графиктері салынды.

Кілт сөздер: анизотропты орталар, электрмагниттік толқындар, магнитэлектрлік эффект, матрицант әдісі, электрмагниттік толқындардың шағылуы, сынуы.

С.К. Тлеуменов, М.К. Жукенов, Н.А. Испулов

О распространении электромагнитных волн в анизотропных магнитоэлектрических средах

В статье распространение и взаимодействие электромагнитных волн различной поляризации в неоднородных вдоль оси Z анизотропных средах с магнитоэлектрическим эффектом тетрагональной,

тригональной и гексагональной сингонии описываются структурой матрицы коэффициентов. Структура матрицант исходной системы уравнений следует из структуры матрицы коэффициентов. В неограниченных периодических структурах уравнения дисперсии электромагнитных волн определяются из нового модифицированного условия существования нетривиальных решений, являющегося следствием структуры матрицанта. Явный аналитический вид матрицантов для однородных анизотропных диэлектрических сред с магнитоэлектрическим эффектом следует из структуры матрицанта. Аналитические формулы для однородных анизотропных сред с магнитоэлектрическим эффектом позволяют в матричной постановке получить аналитическое решение задачи отражения и преломления на границе изотропной среды и анизотропной среды с магнитоэлектрическим эффектом на основе метода матрицанта. Исходные соотношения, описывающие распространение электромагнитных волн в анизотропных магнитоэлектрических средах, приведены к системе линейных однородных дифференциальных уравнений первого порядка. Получена структура матрицанта. Построены уравнения дисперсии электромагнитных волн в периодически неоднородных средах с магнитоэлектрическим эффектом, усредненный матрицант, описывающий распространение электромагнитных волн в однородных анизотропных средах с магнитоэлектрическим эффектом. Кроме того, построены графики зависимости энергетического коэффициента отражения при падении электромагнитных ТЕ и ТМ волн от угла падения.

Ключевые слова: анизотропные среды, электромагнитные волны, магнитоэлектрический эффект, метод матрицанта, отражение, преломление электромагнитных волн.

References

- 1 Landau, L.D., & Lifshitz, E.M. (1982). *Elektrodinamika sploshnykh sred* [Electrodynamics of continuous media]. Moscow: Nauka [in Russian].
- 2 Tleukenov, S.K., Ospanov, A.T. (1985). *Izuchenie elektromagnitnykh polei v anizotropnykh sredakh* [Investigation of electromagnetic fields in anisotropic medium]. Almaty: Nauka [in Kazakhstan].
- 3 Tleukenov, S.K. (1987). O kharakteristicheskoi matritse periodicheski neodnorodnogo sloia [On characteristic matrix of periodic inhomogeneous layer]. *Matematicheskie voprosy teorii rasprostraneniia voln — Mathematical questions of wave propagation theory*. Leningrad: Zapiski nauchnogo seminar LOMI AN SSSR [in Russian].
- 4 Tleukenov, S.K. (2004). Metod matritsanta [Matricant method]. Pavlodar: NITs PGU im. S. Toraighyrova [in Russian].
- 5 Baighonysov, O., & Tleukenov, S.K. (1985) *O metode resheniia nekotorykh zadach rasprostraneniia upruhikh voln pri nalichii periodicheskoi neodnorodnosti* [On the method of solving some problems on propagation of elastic waves with the presence of periodic inhomogeneity]. Leningrad: Zapiski nauchnogo seminar LOMI AN SSSR, 30–33 [in Russian].
- 6 Tleukenov, S.K., Zhukenov, M.K., Karatayeva, N.K., & Zhakipova, D. (2007) Electromagnittik tolkyndardyn shahylu zhane synu esepertindehi shektik sharttardyn matritsalyk turi [Matrix forms of boundary conditions in the problems of reflection and refraction of electromagnetic waves]. Proceedings from The second Erzhanov readings. *Mezhdunarodnaia nauchnaia konferentsiia — International scientific conference*, Aktobe, 278–281 [in Kazakh].
- 7 Tleukenov, S.K., Zhukenov, M.K., Dosanov, T.S., & Zhumabayeva, G.M. (2016). K voprosu otrazheniia elektromagnitnoi TE-volny ot poverkhnosti magnitoelektricheskogo kristalla heksahonalnoi sinhonii klassov 622, 6mm, 6m2, 6mmm [To an issue of reflection of an electromagnetic TE-wave from a surface of a magnetoelectric crystal of a hexagonal singoniya of classes 622, 6mm, 6m2, 6mmm]. *Vestnik Karahandinskoho universiteta. Seriya Fizika — Bulletin of the Karaganda University. Physics series*, 3, 21–27 [in Russian].
- 8 Tleukenov, S.K., & Zhukenov, M.K. (2016). Metod matritsanta. Edinoe opisanie volnovykh protsessov v sredakh s vzaimnoi transformatsiei upruhikh i elektromagnitnykh polei [Matriciant method. The uniform description of wave processes in environments with mutual transformation of elastic and electromagnetic fields]. *Vestnik Kazakhskoho natsionalnogo pedagogicheskoho universiteta. Seriya fiziko-matematicheskikh nauk — Bulletin of the Kazakh National Pedagogical University. Physical and Mathematical sciences Series*, 4, 85–91.

V.M. Yurov¹, V.V. Arkhipov², G.A. Ranova¹, V.Ch. Laurinas¹

¹*Ye.A. Buketov Karaganda State University, Kazakhstan;*
²*G.F. Morozov Voronezh State Forestry University, Russia*
(E-mail: exciton@list.ru)

Study of dimensional dependencies of thermodynamic characteristics of nanoparticles

In the article some approaches to the theoretical description of the deviations of thermodynamic characteristics, such as the heat capacity and the Debye temperature for nanoparticles are considered. The standard Debye inference for the heat capacity of massive crystalline solids was investigated for its modernization in order to take into account surface phenomena of considerable weight for nanoparticles. Unlike massive samples, not only the upper limit of possible frequencies but the lower one starts to matter for nanoparticles. Indeed, in principle, elastic waves with a wavelength greater than the size of the crystal itself cannot arise in a crystal. The equation obtained shows that the thickness of the surface layer of an atomically smooth solid is determined by one parameter — the atomic (molecular) volume of the element, which changes in accordance with the periodic law of D.I. Mendeleev. The equation in its final form, despite its simplicity, shows good agreement with the experimental data

Keywords: heat capacity, Debye temperature, nanostructure, crystal, atomic volume.

Introduction

The beginning of the 21st century laid the foundation for nanoscience as a whole [1–8]. The main difference from massive crystalline bodies is dimensional factors [9–13]. It is believed that a necessary condition for the manifestation of nanostructured properties of a condensed medium is the size dependence of its physical properties [14]. «Normal» size effects are associated with the contribution of surface energy to Gibbs energy. They are called size effects of the first kind (according to L.M. Scherbakov [15]). Such size effects are characteristic of any systems and are determined by the scattering of quasiparticles (electrons, phonons, etc.) at the boundaries of the system.

Phase size effects (size effects of the second kind) are determined by the entire collective of atoms in the system (collective processes). Such size effects are observed only in nanoclusters and nanostructures [16].

In addition to these classical size effects, there are quantum-size effects [17] associated with the quantization of the energy of charge carriers whose motion is limited in one, two, or three directions. The presence of quantum size effects imposes fundamental restrictions on the use of ultra-small nanoelectronic elements [18]. Quantum-size effects are observed when the size of the structure is comparable with the de Broglie wave (~ 0.01 – 0.1 nm).

In the molecular-kinetic theory of an ideal gas, the concept of temperature is closely related to the concept of thermal equilibrium. Bodies in contact with each other can exchange energy. The energy transferred from one body to another by thermal contact is called the amount of heat. Thermal equilibrium is a state of a system of bodies in thermal contact, in which heat transfer from one body to another does not occur, and all macroscopic parameters of the bodies remain unchanged. Temperature is a physical parameter that is the same for all bodies in thermal equilibrium. The possibility of introducing the concept of temperature follows from experience and is called the zero law of thermodynamics.

In this paper, we consider some approaches to the theoretical description of the deviations of thermodynamic characteristics, such as heat capacity and Debye temperature, for nanoparticles.

Heat capacity of nanoparticles

The Debye approach to deriving the heat capacity of a crystal is based on calculating the total number of phonons at a given temperature [19]. Namely, if we take into account only the harmonic approximation of the interatomic potential, then the internal energy can be represented as

$$U = \sum_i (N_i + \frac{1}{2}) h\nu_i . \quad (1)$$

Considering phonons as a gas of boson particles, and taking into account possible degeneracy, we get

$$U = \sum_i \left(\frac{1}{\exp(h\nu_i / kT) - 1} + \frac{1}{2} \right) g_i h\nu_i . \quad (2)$$

In contrast to the photon gas, in this amount there is an upper limit on the frequency due to the size of the atom. In order of magnitude, this limit should be equal to $v_{\max} = u / d$, where u is the phase velocity of the waves in the crystal, d is the size of the unit cell. More precisely, the limiting frequency is sought from the equality of the total number of phonons $N_i h\nu_i$ to the number of vibrational degrees of freedom of the crystal $3N - 6 \approx 3N$. Moving from the summation over frequencies to the integration according to the standard scheme, we obtain the following expression for the maximum frequency and the characteristic Debye temperature $\theta = h\nu_{\max} / k_B$.

$$v_{\max} = u \sqrt[3]{\frac{3N}{4\pi V}}, \quad \theta = \frac{hu^3}{k_B} \sqrt[3]{\frac{3N}{4\pi V}} . \quad (3)$$

The problem of the need for the dispersion equation Debye bypassed the introduction of some constant velocity averaged for longitudinal and transverse waves u . Thus, expression (2) is reduced to the integral:

$$U = \frac{12\pi V k_B^4 T^4}{u^3 h^3} \int_0^{\theta/T} \frac{x^3 dx}{e^x - 1} + N \frac{9}{8} k_B \theta , \quad (4)$$

where the variable $x = h\nu / k_B T$ is entered. The second term in this expression is due to the vacuum energy, or zero vibration modes. The resulting expression agrees well with the experiment in two ranges, $\theta \ll T$ and $\theta \gg T$, when the assumption made about the form of the dispersion equation turns out to be applicable. In the first case, after approximation of the exponential in the form $e^x \approx 1 + x$, we obtain for the internal energy and heat capacity of the expression:

$$U = 3Nk_B T + \frac{8}{9} k_B N \theta, \quad C_V = 3Nk_B . \quad (5)$$

In the second case, when $\theta \gg T$, the upper limit in the integral is replaced by ∞ :

$$\int_0^{\infty} \frac{x^3 dx}{e^x - 1} = \frac{\pi^4}{15} . \quad (6)$$

Accordingly, we obtain:

$$U = \frac{12\pi^5 V k_B^4 T^4}{15u^3 h^3} + N \frac{9}{8} k_B \theta, \quad C_V = \frac{48\pi^5 V k_B^4 T^3}{15u^3 h^3} . \quad (7)$$

Unlike massive samples, not only the upper limit of possible frequencies and the lower one starts to matter for nanoparticles. Indeed, in principle, elastic waves with a wavelength greater than the size of the crystal itself cannot arise in a crystal. Thus, instead of the expression (4) for nanoparticles, one would have to write

$$U = \frac{12\pi V k_B^4 T^4}{u^3 h^3} \int_{x_1}^{\theta/T} \frac{x^3 dx}{e^x - 1} + \frac{6\pi V}{u^3} \int_{x_1}^{\theta/T} v^3 dv , \quad (8)$$

where $x_1 = \frac{h\nu_{\min}}{k_B T} = \frac{hu}{k_B l T}$ is the lower limit determined by the characteristic size of the nanoparticle l . It is convenient to express this expression in the form (9):

$$U = \frac{12\pi V k_B^4 T^4}{u^3 h^3} \left(\int_0^{\theta/T} \frac{x^3 dx}{e^x - 1} - \int_0^{x_1} \frac{x^3 dx}{e^x - 1} \right) + \frac{3}{2} \frac{\pi V h}{u^3} (v_{\max}^3 - v_{\min}^3) . \quad (9)$$

For the analysis it is necessary to make some assumptions about the ratio T and θ . If we assume that $T \ll \theta$, but $T \gg h\nu_{\min} / k_B$, then we arrive at the expression

$$U = \frac{12\pi^5 V k_B^4 T^4}{15u^3 h^3} - \frac{12\pi V k_B T v_{\min}^3}{u^3} + \frac{3}{2} \frac{\pi V h}{u^3} (v_{\max}^3 - v_{\min}^3) . \quad (10)$$

For the heat capacity of nanoparticles, we obtain the expression

$$C_V = \frac{48\pi^5 V k_B^4 T^3}{15u^3 h^3} - \frac{12\pi V k_B v_{\min}^3}{u^3}. \quad (11)$$

Given that you can take $v_{\min} = u/l$, we get

$$C_V = \frac{48\pi^5 V k_B^4 T^3}{15u^3 h^3} - \frac{12\pi V k_B}{l^3}. \quad (12)$$

At high temperatures $T \gg \theta$ we get

$$C_V = 3Nk_B - \frac{12\pi V k_B}{l^3}. \quad (13)$$

However, $V/l^3 \approx 1$. Consequently, taking into account the existence of a minimum frequency leads to a «subsidence» of the heat capacity of bodies by about $12\pi k_B$.

For massive samples, this value has no practical value. However, for nanoparticles, this amendment contributes. It is easy to see that at high temperatures, it reaches 10 % with the number of atoms in the nanoparticle of the order of 100.

At temperatures well below the Debye temperature, its relative weight becomes much larger.

Note that the theory used is not a quantum one and does not allow conclusions to be made regarding ultra-low temperatures.

Debye temperature for nanoparticles

The Debye temperature is derived from the equality of the number of phonons and the number of degrees of freedom of the sample.

$$\frac{12\pi V}{u^3} \int_0^{v_{\max}} v^2 dv = 3N - 6 \approx 3N \quad (14)$$

Where we get expressions (3). In the case of nanoparticles, as noted above, this integral should have a lower bound $v_{\min} \approx u/l$. In addition, in view of the relative increase in area relative to volume, the number of degrees of freedom must also be recalculated. Roughly, the number of degrees of freedom of a spherical nanoparticle can be estimated as follows. Let d be the size of the unit cell. Then the ratio of the volume of the surface layer of the nanoparticle V_s , taken as having a thickness d , to its volume:

$$\frac{V_s}{V} = \frac{4\pi R^2 d}{(4/3)\pi R^3} = \frac{3d}{R} = \frac{N_s}{N}, \quad (15)$$

where N_s/N is the ratio of the number of atoms on the surface of the nanoparticle to the total number of atoms. If we assume that for atoms of superficiality one of the vibrational degrees of freedom is degenerate (for the time being we neglect «surface phonons»), then the total number of degrees of freedom of nanoparticles will be less by N_s . For the Debye temperature we have, therefore,

$$\frac{12\pi V}{u^3} \int_{v_{\min}}^{v_{\max}} v^2 dv \approx 3N - \frac{3d}{R} N. \quad (16)$$

After integration, we obtain the expressions for v_{\max} and the Debye temperature for nanoparticles

$$v_{\max} = \sqrt[3]{\frac{3u^3 N}{4\pi V} \left(1 - \frac{d}{R}\right) + v_{\min}^3}, \quad \theta_{nano} = \sqrt[3]{\theta^3 \left(1 - \frac{d}{R}\right) + \left(\frac{h}{k_B} v_{\min}\right)^3}. \quad (17)$$

Considering that the difference between the orders v_{\max} and v_{\min} is quite significant

$$\frac{v_{\max}}{v_{\min}} \approx \frac{l}{d} \propto 10^3 - 10^6, \quad (18)$$

We can neglect the second term in (17) and accept the expression

$$\theta_{nano} = \theta \sqrt[3]{1 - \frac{d}{R}}. \quad (19)$$

The thickness of the surface layer of crystals

In [20], we showed that the thickness of the surface layer of an atomically smooth solid is:

$$d = 0,17 \cdot 10^{-3} \cdot v. \tag{20}$$

Equation (20) shows that the thickness of the surface layer of an atomically smooth solid is determined by one parameter — the atomic (molecular) volume of the element, which changes in accordance with the periodic law D.I. Mendeleev.

The values of the parameter d for some metals are given in Table 1. The experimental value for atomically smooth surfaces of gold crystals obtained in the geometry of sliding x-rays is 2.4 nm [21]. This almost coincides with Table 1.

However, the size dependence of the physical properties of solids begins at $h \approx 10d$.

Equation (19) shows that in coordinates $^3(\theta_{nano} / \theta) - 1 \approx 1 / R$ we get a straight line giving the values of d . In Table 1, d values can be compared.

For the dimensional dependence of the physical property of a solid $A(r)$, we obtained the relations [22]:

$$A(r) = A_0 \cdot \left(1 - \frac{d}{r}\right). \tag{21}$$

Here, A_0 is equal, in particular, to the melting point T_m . According to Lindemann [23], when the oscillation amplitude reaches a certain critical (magnitude) fraction of the distance between the equilibrium positions of the atoms, the oscillations begin to interfere with each other.

As a result, the crystal becomes mechanically unstable. For the melting point, he obtained the following expression:

$$T_m = c v_E V^{2/3} \cdot M = c' \cdot \theta^2 V^{2/3} \cdot M, \tag{22}$$

where V is the molar volume, M is the mass of the atom, v_E is the characteristic frequency, θ is the Debye temperature, c and c' are constant, which are assumed to be the same for crystals with similar structures. The verification showed that the Lindemann equation (22) is justified only for metals with the structure of the HCP, FCC and partially BCC. From equation (22) it follows that $T_m \sim \theta^2$, and from equations (21) and (19) it follows that $T_m \sim \theta^3$.

Table 1

The thickness of the surface layer of some metals [20]

M	d , nm										
Li	0,7	Sr	5,8	Sn	1,4	Cd	1,3	Fe	2,2	Gd	5,3
Na	1,5	Ba	6,2	Pb	1,8	Hg	0,6	Co	2,0	Tb	5,3
K	2,6	Al	1,5	Se	1,3	Cr	2,7	Ni	1,9	Dy	5,3
Rb	2,9	Ga	0,6	Te	2,5	Mo	4,6	Ce	3,8	Ho	5,5
Cs	3,6	In	1,1	Cu	1,6	W	5,8	Pr	4,2	Er	5,5
Be	1,3	Tl	1,9	Ag	2,2	Mn	2,0	Nd	4,5	Tm	5,2
Mg	2,2	Si	3,4	Au	2,3	Tc	3,6	Sm	4,4	Yb	4,6
Ca	4,9	Ge	2,8	Zn	1,1	Re	4,6	Eu	5,8	Lu	5,7

In [24], the Lindemann equation was refined:

$$T_m = \frac{m\theta^2 V^{2/3} Z \left(1 + \frac{\Delta S_m}{2R} + \frac{\Delta S_p}{2R}\right) \cdot 3R}{d_r c_p (1+v) \cdot (1-2v)^{1/2} \cdot (1+\sigma)^2}. \tag{23}$$

From equation (23) it follows that $T_m \sim \theta^2 \sim \theta^3$, which is close to equation (19).

In nanomaterials, as shown by experimental data, the Debye temperature decreases in comparison with large-crystalline samples. The reason for this is the change in the form and boundaries of the phonon spectrum of a small crystal. A decrease in the Debye temperature associated with a decrease in particle size has

been observed in many studies [25]. The dependence of the Debye temperature of small particles on their size is shown in Table 2.

Equation (19), despite its simplicity, shows good agreement with experimental data. In this case, it is necessary to take into account equation (20) that the thickness of the surface layer of an atomically smooth solid is determined by one parameter — the atomic (molecular) volume of the element.

Table 2

Debye temperature dependence of small particles on their size

Metal	R , nm	$\theta_{\text{nano}} / \theta$, experiment [25]	$\theta_{\text{nano}} / \theta$, by equation (19)
Au	10	0,920	0,917
Ag	15	0,910	0,920
Pb	6	0,830	0,836
V	6,5	0,860	0,858

The Debye temperature divides the temperature scale into two regions: low-temperature, where not all frequencies of the lattice vibration spectrum are excited, and high-temperature, where all frequencies are excited. This division is arbitrary, since the transition from one region to another in a three-dimensional crystal is not sharp. The crystal size (in the one-dimensional case, the length of the atomic chain L) determines the wavelengths λ_j of the excitations. The energy produced by the excitation at a length λ_j depends on the number of excitation photons at this wavelength. The number of quanta is related to the magnitude of the exciting factor, for example, to temperature. The energy of a single quantum depends on both λ_j and the lattice parameters.

Conclusion

In general, the described approach is quite obvious and there is a large number of its variations. However, comparison with experimental data for all variations of this formula is rather qualitative. The problem, apparently, consists in significant abstraction of the task. The studied nanoparticles do not have an ideal spherical shape and uniform size. This circumstance should introduce significant errors.

The work was performed under the program of the MES RK. Grants № 0118PK000063 and № O.0781.

References

- 1 Wolf E.L. Nanophysics and Nanotechnology: An Introduction to Modern Concepts in Nanoscience / E.L. Wolf. — Wiley-VCH: Weinheim, Germany, 2004. — 174 p.
- 2 Dupas C. Nanoscience: Nanotechnologies and Nanophysics / C. Dupas, P. Houdy, M. Lahmani (Eds.). — Springer-Berlin Heidelberg-New York, 2007. — 823 p.
- 3 Sattler K.D. Handbook of Nanophysics: Nanoelectronics and Nanophotonics / K.D. Sattler. — CRC Press, 2011. — 780 p.
- 4 Raz J. Nanoparticles / J. Raz. — Berlin; Walter de Gruyter GmbH & Co., KG, 2015. — 283 p.
- 5 Rogers B. Nanotechnology: understanding small systems / B. Rogers, J. Adams, S. Pennathur. — Boca Raton: CRC Press, Taylor & Francis Group, 2015. — 407 p.
- 6 Ngo Ch. Our nanotechnology future / Ch. Ngo, J.B. Natowitz. — Chicago: University of Chicago Press, 2017. — 243 p.
- 7 Mokkalapati S. Nanowires for energy applications / S. Mokkalapati, Ch. Jagadish. — Cambridge, MA: Academic Press, 2018. — 536 p.
- 8 Roy S. Nanotechnology: synthesis to applications / S. Roy, Ch.K. Ghosh, Ch.K. Sarkar. — Boca Raton, FL: CRC Press, Taylor & Francis Group, 2018. — 328 p.
- 9 Fraune M. Size dependence of the exchange bias field in NiOXNi nanostructures / M. Fraune, U. Reudiger, G. Geuntherod // Applied Physics Letters. — 2000. — Vol. 77. — No. 23. — P. 3815–3817.
- 10 Sun Ch.Q. Size dependence of nanostructures: Impact of bond order deficiency / Ch.Q. Sun // Progress in Solid State Chemistry. — 2007. — Vol. 35 — P. 1–159.
- 11 Liu X.J. Correlation and size dependence of the lattice strain, binding energy, elastic modulus, and thermal stability for Au and Ag nanostructures / X.J. Liu, Z.F. Zhou, L.W. Yang, J.W. Li, G.F. Xie, S.Y. Fu, Ch.Q. Sun. // Appl. Phys. — 2011. — Vol. 109. — P. 1–5.
- 12 Albanese A. The Effect of Nanoparticle Size, Shape, and Surface Chemistry on Biological Systems / A. Albanese, P.S. Tang, W.C.W. Chan. // Annu. Rev. Biomed. Eng. — 2012. — Vol. 14. — P. 1–16.

- 13 Mikhailin N.Yu. Size Dependences of the Magnetic Properties of Superconducting Lead–Porous Glass Nanostructures / N.Yu. Mikhailin, D.V. Shamshur, R.V. Parfen'ev, V.I. Kozub, Yu.M. Gal'perin, Yu.A. Kumzerov, A.V. Fokin. // *Physics of the Solid State*. — 2018. — Vol. 60, No. 6. — P. 1068–1072.
- 14 Андриевский Р.А. Размерные эффекты в нанокристаллических материалах. I. Особенности структуры. Термодинамика. Фазовые равновесия. Кинетические явления / Р.А. Андриевский, А.М. Глезер. // *Физика металлов и металловедение*. — 1999. — Т. 88, № 1. — С. 50–73.
- 15 Щербаков Л.М. О статистической оценке избыточной свободной энергии малых объектов в термодинамике микрогетерогенных систем / Л.М. Щербаков // *Доклады АН СССР*. — 1966. — Т. 168, № 2. — С. 388–391.
- 16 Уваров Н.Ф. Размерные эффекты в химии гетерогенных систем / Н.Ф. Уваров, В.В. Болдырев. // *Успехи химии*. — 2001. — Т. 70. — С. 307–329.
- 17 Tringides M.C. Quantum size effects in metallic nanostructures / M.C. Tringides, M. Jatochowski, E. Bauer. // *Physics Today*. — 2007. — Vol. 60, No. 4. — P. 50–54.
- 18 Арутюнов К.Ю. Квантовые размерные эффекты в металлических наноструктурах / Н.Ю. Арутюнов // *ДАН ВШ РАН*. — 2015. — № 3(28). — С. 7–16.
- 19 Ziman J.M. *Electrons and phonons* / J.M. Ziman. — Oxford Univer. Press, London, 1960. — 268 p.
- 20 Юров В.М. Толщина поверхностного слоя, поверхностная энергия и атомный объем элемента / В.М. Юров, С.А. Гученко, В.Ч. Лауринас // *Физико-химические аспекты изучения кластеров, наноструктур и наноматериалов*. — Тверь: Твер. гос. ун-т, — 2018. — Вып. 10. — С. 691–699.
- 21 Guo J. *X-Rays in Nanoscience: Spectroscopy, Spectromicroscopy, and Scattering Techniques* / J. Guo. — Wiley-VCH, Verlag, 2010. — 263 p.
- 22 Юров В.М. Размерные эффекты и поверхностное натяжение чистых металлов / В.М. Юров, В.Ч. Лауринас, С.А. Гученко, О.Н. Завацкая // *Успехи современного естествознания*. — 2012. — № 7. — С. 88–93.
- 23 Lindemann F.A. The calculation of molecular vibration frequencies / F.A. Lindemann. // *Physik. Z.* — 1910. — Vol. 11. — P. 609–612.
- 24 Сачавский А.Ф. Единое уравнение состояния вещества / А.Ф. Сачавский, В.В. Евстигнеев, Н.А. Сачавская // *Тр. АлтГТУ им. И.И. Ползунова*. — Барнаул, 1998. — Вып. 8. — С. 214–222.
- 25 Анциферова И.В. Зависимость процесса уплотнения при спекании с использованием наноразмерных металлических порошков / И.В. Анциферова // *Вестн. ПНИПУ*. — 2015. — Т. 17, № 2. — С. 13–20.

В.М. Юров, В.В. Архипов, Г.А. Ранова, В.Ч. Лауринас

Нанобөлшектердің термодинамикалық сипаттамаларының мөлшеріне тәуелділіктерін зерттеу

Мақалада термодинамикалық сипаттамалардың ауытқуларының теориялық сипаттамасына қатысты кейбір көзқарастар, мысалы, жылусыйымдылығы және нанобөлшектер үшін Дебай температурасы қарастырылған. Нанобөлшектер үшін айтарлықтай салмағы бар беткі құбылыстарды есепке алу үшін оны жаңғырту үшін көлемді кристалдық денелердің жылусыйымдылығына арналған Дебайдың стандартты шығарылымы зерттелді. Көлемді үлгілерден айырмашылығы, нанобөлшектер үшін мүмкін жиіліктердің жоғарғы шегі ғана емес, төменгі шегі де маңызды. Шындығында, кристалдың мөлшерінен асатын толқын ұзындығы бар серпімді толқындар кристалда пайда болмайды. Алынған теңдеу атомарлы тегіс қатты беттік қабатының қалыңдығын бір параметрмен — Д.И. Менделеевтің периодтық заңына сәйкес өзгерту элементтің атомдық (молекулалық) көлемімен — анықталатынын көрсетеді. Қорытынды теңдеудің қарапайым түріне қарамастан, эксперименттік деректермен жақсы келісетіні көрсетілді.

Кілт сөздер: жылусыйымдылық, Дебай температурасы, нанокұрылым, кристалл, атомдық көлем.

В.М. Юров, В.В. Архипов, Г.А. Ранова, В.Ч. Лауринас

Исследование размерных зависимостей термодинамических характеристик наночастиц

В статье рассмотрены некоторые подходы к теоретическому описанию отклонений термодинамических характеристик, таких как теплоемкость и температура Дебая для наночастиц. Исследован стандартный вывод Дебая для теплоемкости массивных кристаллических тел на предмет его модернизации для учета поверхностных явлений, имеющих для наночастиц значительный вес. В отличие от массивных образцов для наночастиц начинает иметь значение не только верхний предел возможных частот, но и нижний. Действительно, в кристалле не могут возникать упругие волны с длиной волны больше размера самого кристалла. Полученное уравнение показывает, что толщина поверхностного слоя атомарно-гладкого твердого тела определяется одним параметром — атомным (молекулярным) объемом элемента, изменяющемся в соответствии с периодическим законом Д.И. Менделеева. Урав-

нение в окончательном виде, несмотря на простоту, показывает хорошее согласие с экспериментальными данными.

Ключевые слова: теплоемкость, температура Дебая, наноструктура, кристалл, атомный объем.

References

- 1 Wolf, E.L. (2004). *Nanophysics and Nanotechnology: An Introduction to Modern Concepts in Nanoscience*. Wiley-VCH: Weinheim, Germany.
- 2 Dupas, C., Houdy, P., & Lahmani M. (Eds.) (2007). *Nanoscience: Nanotechnologies and Nanophysics*. Springer-Berlin-Heidelberg-New York.
- 3 Sattler, K.D. (2011). *Handbook of Nanophysics: Nanoelectronics and Nanophotonics*. CRC Press.
- 4 Raz, J. (2015). *Nanoparticles*. Berlin; Walter de Gruyter GmbH & Co., KG.
- 5 Rogers, B., Adams, J., & Pennathur, S. (2015). *Nanotechnology: understanding small systems*. Boca Raton: CRC Press, Taylor&Francis Group.
- 6 Ngo, Ch. & Natowitz, J.B. (2017). *Our nanotechnology future*. Chicago: University of Chicago Press.
- 7 Mokkaṭi, S., & Jagadiṣh, Ch. (2018). *Nanowires for energy applications*. Cambridge, MA: Academic Press.
- 8 Roy, S., Ghosh, Ch.K., & Sarkar, Ch.K. (2018). *Nanotechnology: synthesis to applications*. Boca Raton, FL: CRC Press, Taylor&Francis Group.
- 9 Fraune, M., Reudiger, U., & Geuntherod, G. (2000). Size dependence of the exchange bias field in NiOXNi nanostructures. *Applied Physics Letters*, 77, 23, 3815–3817.
- 10 Sun, Ch.Q. (2007). Size dependence of nanostructures: Impact of bond order deficiency. *Progress in Solid State Chemistry*, 35, 1–159.
- 11 Liu, X.J., Zhou, Z.F., Yang, L.W., Li, J.W., Xie, G.F., & Fu, S.Y. et al. (2011). Correlation and size dependence of the lattice strain, binding energy, elastic modulus, and thermal stability for Au and Ag nanostructures. *J. Appl. Phys.*, 109, 1–5.
- 12 Albanese, A., Tang, P.S. & Chan, W.C.W. (2012). The Effect of Nanoparticle Size, Shape, and Surface Chemistry on Biological Systems. *Annu. Rev. Biomed. Eng.*, 14, 1–16.
- 13 Mikhailin, N.Yu., Shamshur, D.V., Parfen'ev, R.V., Kozub, V.I., Gal'perin, Yu.M., & Kumzerov, Yu.A. et al. (2018). Size Dependences of the Magnetic Properties of Superconducting Lead–Porous Glass Nanostructures. *Physics of the Solid State*, 60, 6, 1068–1072.
- 14 Andrievskii, R.A., & Glezer, A.M. (1999). Razmernye efekty v nanokristallicheskih materialakh. I. Osobennosti struktury. Termodinamika. Fazovye ravnovesiia. Kineticheskie yavleniia [Size effects in nanocrystalline materials. I. Features of the structure. Thermodynamics. Phase equilibria. Kinetic phenomena]. *Fizika metallov i metallovedenie — Metal Physics and Metallography*, 88, 1, 50–73 [in Russian].
- 15 Sherbakov, L.M. (1966). O statisticheskoi otsenke izbytochnoi svobodnoi enerhii malykh obektov v termodinamike mikroheterogenykh sistem [On the statistical evaluation of the excess free energy of small objects in the thermodynamics of microheterogeneous systems]. *Doklady AN SSSR — Reports of the USSR Academy of Sciences*, 168, 2, 388–391 [in Russian].
- 16 Uvarov, N.F., & Boldyrev, V.V. (2001). Razmernye efekty v khimii heterogenykh sistem [Size effects in the chemistry of heterogeneous systems] *Uspekhi khimii — Chemistry advances*, 70(4), 307–329 [in Russian].
- 17 Tringides, M.C., Jatochowski, M., & Bauer, E. (2007). Quantum size effects in metallic nanostructures. *Physics Today*, 60, 4, 50–54.
- 18 Arutiunov, K.Yu. (2015). Kvantovye razmernye efekty v metallicheskih nanostrukturakh [Quantum size effects in metallic nanostructures]. *DAN VSh RAN — DAN Higher School of Sciences*, 3(28), 7–16 [in Russian].
- 19 Ziman, J.M. (1960). *Electrons and phonons*. Oxford Univer. Press, London.
- 20 Yurov, V.M., Guchenko, S.A., & Laurinas, V.Ch. (2018). Tolshchina poverkhnostnogo sloia, poverkhnostnaia enerhiia i atomnyi obem elementa [The surface layer thickness, surface energy and atomic volume of the element]. *Fiziko-khimicheskie aspekty izucheniia klasterov, nanostruktur i nanomaterialov — Physico-chemical aspects of the study of clusters, nanostructures and nanomaterials*. Tver: Tver State Univ. Publ., 10, 691–699 [in Russian].
- 21 Guo, J. (2010). *X-Rays in Nanoscience: Spectroscopy, Spectromicroscopy, and Scattering Techniques*. Wiley-Vch, Verlag.
- 22 Yurov, V.M., Laurinas, V.Ch., Guchenko, S.A., & Zavatskaia, O.N. (2012). Razmernye efekty i poverkhnostnoe natiazhenie chistykh metallov [Dimensional effects and surface tension of pure metals]. *Uspekhi sovremennoho estestvoznaniia — Successes of modern science*, 7, 88–93 [in Russian].
- 23 Lindemann, F.A. (1910). The calculation of molecular vibration frequencies. *Physik. Z.*, 11, 609–612.
- 24 Sachavskii, A.F., Evstihneev, V.V., & Sachavskaia, N.A. (1998). Edinoe uravnenie sostoiianiia veshchestva [Unified equation of state of matter] *Trudy AltGTU im. I.I. Polzunova, Barnaul — Works AltSTU. I.I. Polzunov, Barnaul*, 8, 214–222 [in Russian].
- 25 Antsiferova, I.V. (2015). Zavisimost protsessa uplotneniia pri spekanii s ispolzovaniem nanorazmernykh metallicheskih poroshkov [The dependence of the compaction process during sintering using nanoscale metal powders]. *Vestnik PNIPU — Bulletin of PNIPU*, 17, 2, 13–20 [in Russian].

V.M. Yurov¹, E.N. Eremin², V.Ch. Laurinas¹, S.S. Kasimov¹¹*Ye.A. Buketov Karaganda State University, Kazakhstan;*²*Omsk State Technical University, Russia**(E-mail: exciton@list.ru)*

Dissipative processes in tribology

In the paper the dissipative process is considered as the basis of the nature of external friction in solids. It is shown that non-equilibrium processes in the tribosystem can lead to a decrease in the production of entropy and, consequently, the intensity of wear and stably proceed with the formation of dissipative structures during self-organization. It was found that the first term can reach $f_e = 10^{-3}-10^{-4}$ by using X_m , ρ_m and $W(X_m)$ in the mode of using special lubricants. In space, the effect of oil filters is absent. It uses solid lubricants which include substances applied to the surface of parts in the form of films that have a shear strength that is significantly less than that of the part material. An expression for the friction coefficient is obtained, which takes into account the surface geometry and its physical properties. It was concluded that homogeneous metal pairs should not be used in friction antifriction pairs. It is shown that a decrease in the dry friction coefficient is possible due to a decrease in surface energy. In this case, friction pairs are used, in which the electron work function differs significantly. This leads to a difference in the contact potential difference and, accordingly, to a decrease in the surface energy. It is shown that the friction coefficient depends on the fractal structure of the surface of many solids and this is their characteristic property.

Keywords: dissipative process, friction, wear, surface, entropy, fractal.

Introduction

The origins of tribology — the science of friction, wear and lubrication of machines — go into the depths of human history [1–4]. The first period of history includes the accumulation of human tribological knowledge from prehistoric times to the end of the XVI century. In the XVII–XVIII centuries, the birth of the science of friction, later called «tribology», takes place. In the XIX century, the progress of technology (above all — the development of railways) highlights the problems of a tribological nature. In a word, before the beginning of the 20th century, tribology went a long and glorious way, successfully solving the tasks put forward by practice, and the progress of technology was hardly delayed for a long time because of the impossibility of solving tribological problems [1–4].

The beginning of the XXI century is especially important for friction units operating in extreme conditions (aerospace, atomic energy, high-speed transport, equipment for the development of the Ocean, the deep bowels of the Earth, etc.) [5, 6]. The urgent task is to summarize the experimental data, predict reliability and resource in a wide range of changes in voltages, temperatures, environments, exposure to fields of different physical nature (acoustic, electromagnetic, radiation, etc.) [7].

The beginning of the XXI century laid a comprehensive study of the tribological properties of nanostructures and nanomaterials [8–11]. The use of nano-coatings can significantly reduce the coefficient of friction while maintaining wear resistance, increase the viscosity of coatings while maintaining anti-corrosion properties and increasing the operating temperature by 50 °C. All this is especially important in the field of engineering. Nanostructured materials and suspensions are used to create nanocoatings. Special additives are introduced into the coatings that modify their structure and provide the necessary properties.

Selective transference under friction (the effect of wearlessness) is a natural phenomenon, it is recognized as the scientific discovery of the USSR (D. Garkunov and I. Kragelsky) No. 41 dated September 13, 1966 [12]. In practice, the «wear-free» functioning of friction units is most often achieved by using metal-plating lubricants in real tribo-splicing: oils, grease, self-lubricating materials and coatings [13]. Historically, the first studies of the mechanism of selective transfer [14] were studies of the thickness, roughness, microhardness and microstructure formed on rubbing surfaces during friction of a copper alloy on steel in an aqueous or alcoholic solution of glycerol and a visually observed copper servo film. It has been established that the servo-film film spontaneously arising during frictional interaction has a thickness of no more than 1...2 microns, and its mechanical and physicochemical properties are significantly different from the properties of ordinary compact copper.

Considering from the standpoint of green tribology, the effect of wearlessness under friction, the first thing that attracts attention is the conceptual possibility of friction without wear, which has been repeatedly confirmed experimentally and fully corresponds to the principles of green chemistry, engineering and tribology [15]. In other words, the saving of material resources during the implementation of selective transfer is achieved automatically and not only by minimizing wear, but also by increasing the resource life of engineering products.

Secondly, the friction coefficients of 10^{-3} in the implementation of super-anti-friction properties clearly lead to energy savings, which also corresponds to the principles of green science [15].

It is noted that the nature of external friction is the dissipative process [16]. Relaxation internal friction is a dissipative process found in the study of the phenomenon of inelasticity. The intensity of relaxation processes found on the temperature-frequency dependences of the dissipation of a part of the energy of an external force field mechanical effect depends on the ratio of speed or frequency from this effect and temperature T . Depending on this ratio, the reaction of the system under investigation to external influence varies from elastic to viscoelastic.

In this paper, the dissipative process is considered as the basis of the nature of external friction in solids.

Probability of dissipative processes

Crystal defects (impurity ions, color centers, etc.) will be considered as a system of noninteracting particles immersed in a thermostat (tribological system). Quantum transitions due to the interaction of defects with a thermostat will be dissipative (with probability P) as opposed to interaction with an external field (with probability F). Dissipative processes lead to the fact that the secondary field (system response) is always smaller than the primary one, which causes the formation of defects [17, 18].

Since the subsystem of defects exchanges only energy with a thermostat, the corresponding ensemble of particles will be canonical. In this case, the expression for statistical entropy is:

$$S = -k \sum_i f_i \ln f_i, \quad (1)$$

where f_i is the distribution function; k is the Boltzmann constant.

Differentiating (1) in time and transforming, we get:

$$\frac{dS}{dt} = \frac{k}{2} \sum_{i,j} (l h f_i - \ln f_j) (P_{ij} f_i - P_{ji} f_j), \quad (2)$$

where P_{ij} is the transition probability from the initial i (with energy E_i) to the excited state j (with energy E_j).

For dissipative processes, the principle of detailed equilibrium has the form:

$$\frac{g_i P_{ij}}{g_j P_{ji}} = e^{\frac{E_j - E_i}{kT}}, \quad (3)$$

where g_i, g_j are statistical weights for levels E_i and E_j .

Then (1) takes the form:

$$\frac{dS}{dt} = \frac{k}{2} P_{ij} (\ln f_i - \ln f_j) \left(f_i - \frac{g_i}{g_j} f_j e^{\frac{E_i - E_j}{kT}} \right), \quad (4)$$

Canonical distribution function:

$$f_{ij} = \frac{1}{Z} e^{-E_{ij}/kT}, \quad (5)$$

where is the statistic sum:

$$Z = e^{-G/kT}, \quad (6)$$

where G is the Gibbs potential (free energy) of the thermostat + defect system.

We assume that the non-configuration part of the Gibbs potential linearly depends on the concentration of N defects:

$$e^{-G/kT} = \sum_N h(N), \quad (7)$$

where $h(N) = \omega(N) \cdot e^{-G/kT}$; $\omega(N)$ — statistical weight.

After simple calculations, it is easy to show that the function $h(N)$ is the Gaussian distribution near the equilibrium value with a small dispersion, i.e.:

$$h(N) = h(\bar{N})e^{-\Delta\bar{N}^2/N}. \quad (8)$$

Substituting (8) into (7), we have:

$$e^{-G/kT} = h(\bar{N}) \sum_{\Delta N} e^{-\Delta\bar{N}^2/N}. \quad (9)$$

To estimate the sum in (9), we replace it with the integral:

$$\sum_{\Delta N} e^{-\Delta\bar{N}^2/N} = \int_{-\infty}^{+\infty} e^{-x^2/\bar{N}} dx = \sqrt{\pi\bar{N}}.$$

Then (9) takes the form:

$$e^{-G/kT} = h(\bar{N})(\pi\bar{N})^{1/2}. \quad (10)$$

Using (7) and taking the logarithm from (10), we find:

$$G/kT = -\ln \omega(\bar{N}) + \frac{G(\bar{N})}{kT} + \frac{1}{2} \ln(\pi\bar{N}), \quad (11)$$

where $G(\bar{N})$ is the part of the total Gibbs potential associated with the concentration of defects. From the evaluation of the first logarithmic term follows:

$$\ln \omega(\bar{N}) = N \ln \left(1 + \frac{\bar{N}}{N} \right) + \bar{N} \ln \frac{N + \bar{N}}{N}. \quad (12)$$

By approximating the logarithm in the first term of the right-hand side of (12), the first term of its expansion in a series, and the second term, expressing through the Gibbs potential of the system of defects G^f , we get:

$$\ln \omega(\bar{N}) = \bar{N} + \bar{N}G^f/kT. \quad (13)$$

Substituting (13) into (11) and neglecting the term $1/2 \ln(\pi\bar{N})$ as compared with \bar{N} , we get:

$$G = G(\bar{N}) - \bar{N}G^f - \bar{N}kT. \quad (14)$$

As above, assuming that the thermodynamic potential $G(\bar{N})$ depends on the equilibrium number of defects C^f in a linear fashion, that is:

$$G = G^0 + \bar{N}G^f, \quad (15)$$

where G^0 is the thermodynamic potential of the thermostat, we find:

$$G = G^0 - \bar{N}kT. \quad (16)$$

Using (8), expression (6) is converted to the form:

$$Z = e^{-G^0/kT} e^{\bar{N}}. \quad (17)$$

Substituting (16) into (4), we find

$$\frac{dS}{dt} = \frac{k}{2} \sum_{i,j} P_{ij} e^{G^0/kT} e^{-\bar{N}} e^{-E_i/kT} \left(\frac{E_j - E_i}{kT} \right) \left(1 - \frac{g_i}{g_j} e^{2\frac{E_i - E_j}{kT}} \right). \quad (18)$$

Neglecting the small terms and replacing in (18) the sum with the integral we get:

$$P = \frac{2\Delta S}{k\tau} \exp \left\{ -\frac{\Delta E_m - G^0/N}{kT} \right\}, \quad (19)$$

where ΔS is the change in entropy in the dissipative process; ΔE_m is the average value of the energy of the ground state of defects; τ is the relaxation time.

Friction and entropy

In the dissipative process the friction f_m changes completely. Then follows from (19):

$$f_m = \frac{2}{k} \left(\frac{dS}{dt} \right) \exp \left\{ -\frac{\Delta E_m - G^0/N}{kT} \right\} = \frac{2\Delta S}{k\tau} \exp \left\{ -\frac{\Delta E_m - G^0/N}{kT} \right\}. \quad (20)$$

Nonequilibrium processes in the tribosystem can lead to a decrease in the production of entropy and, consequently, the intensity of wear and stably proceed with the formation of dissipative structures during

self-organization [19–23]. The process of self-organization can begin only after the system has passed through instability [19–23]. The system can lose stability with a negative excess production of entropy (according to the Lyapunov function [21]). For the tribosystem to self-organize, more than one independent process should take place in it [19–23]. The paper [24] gives the formula:

$$f_e = \left(\frac{dS}{dt} \right)_e = X_m \cdot \rho_m \cdot W(X_m), \quad (21)$$

where X_m is the thermodynamic force that causes mass transfer (stress gradients or chemical potentials, respectively, for deformation or diffusion), ρ_m is the average density of the substance involved in mass transfer, $W(X_m)$ is the average mass transfer rate, depending on X_m , will increase with X_m .

From (21) follows:

$$X_m \cdot \rho_m \cdot W(X_m) \rightarrow 0. \quad (22)$$

From (22), it follows that the first term in (20) can reach $f_e = 10^{-3} - 10^{-4}$ by using X_m , ρ_m and $W(X_m)$ in the mode of using special lubricants.

According to the method of incorporation into the lubrication system, the filters are divided into series and parallel, according to the dispersity of the filtrate filtered out — into filters of coarse and fine cleaning. Detailed classification of oil filters is shown in Figure 1.

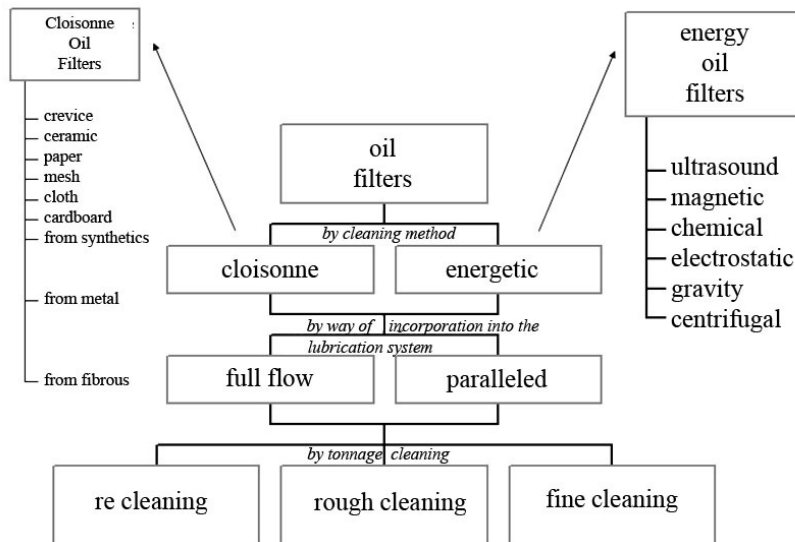


Figure 1. Classification of oil filters [25]

In space, the effect of oil filters is absent. It uses solid lubricants (TSP) which include substances applied to the surface of parts in the form of films that have a shear strength that is significantly lower than that of the part material. Films of sulfides (MoS_2 , WS_2 , PbS , NbS_2 , etc.), selenides (MoSe_2 , WSe_2 , NaSe_2 , etc.), tellurides (MoTe_2 , WTe_2 , NbTe_2 , TaTe_2), chlorides (CoCl , PbCl_2 , CdCl_2 , CuCl), fluorides (AlF_3 , CaF_2 , BaF_2 , MgF_3), iodides (CaI_2 , PbI_2 , BiI_3), metal oxides (PbO , Bi_2O_3 , $\text{PbO} + \text{SiO}_2$), graphite, boron nitride, etc. In the Table 1 the density, coefficient of friction and the operating temperature of some sulfides, selenides and metal tellurides are shown.

Table 1

Characteristics of TSP [25]

Connections	Density, g/cm^3	Coefficient friction	Maximum permissible operating temperature, $^{\circ}\text{C}$	
			vacuum	air
1	2	3	4	5
Bi_2S_3	7.40	0.07–0.14	500	–
CuS	4.28	0.17–0.41	520	–
Cu_2S	5.60	0.18	450	–
MoS_2	4.8–5.16	0.02–0.3	1100	400
NbS	5.9–6.0	0.04	1300	400

1	2	3	4	5
PbS	7.5–7.59	0.37	410	500
TaS ₂	7.16	0.06	1500	–
WS ₂	7.5–7.63	0.03–1.6	1400	500
NbSe ₂	6.25	0.06–0.17	1350	350
MoSe ₂	6.90	0.03–0.22	1350	400
WS ₂	9.0	0.02–0.18	1350	350
MoTe ₂	7.8	0.10–0.34	1240	400
WTe ₂	9.44	0.27–0.49	1020	–
VTe ₂	–	0.22	450	500

Friction and energies of the ground state of defects

We estimate the contribution of the energy of the ground state of defects:

$$f_a \approx \exp\left\{-\frac{\Delta E_m}{kT}\right\}, \quad (23)$$

Based on the concepts of the kinetic thermofluctuation concept of solid strength developed by S.N. Zhurkov and co-workers [26, 27], in [28] proposed physical and computational models of wear of friction surfaces.

The proposed models are based on a fundamental pattern [26], which relates stress, absolute temperature, and durability:

$$t = \tau_0 \exp[(U_0 - \gamma\sigma) / kT], \quad (24)$$

where σ is the breaking stress:

$$\sigma = (1/\gamma) (U_0 - kT \ln(t/\tau_0)), \quad (25)$$

where t is the time to failure (durability) of the sample under load, s; $\tau_0 = (10^{-12} \dots 10^{-13})$, c — the oscillation period of atoms in a solid; U_0 is the interatomic bond energy, J; T is the thermodynamic temperature, K; $k = 1.38 \cdot 10^{-23}$ J/K is the Boltzmann constant; γ — parameter (fitting), having the dimension of volume, m³; activation energy of destruction $\Delta U = (U_0 - \gamma\sigma)$.

For the energy of the ground state of defects in [28], it was found that for typical defects on metal surfaces it is $\Delta E \approx 2-5$ J. Then for $kT \approx 0.3$ eV, we get $\exp(-33) \approx 10^{-15} \approx 1$ and $f_a = 1$.

Friction, roughness, fracture energy of defects and Gibbs energy

Remain the third term in equation (19), which can be brought to mind:

$$f_G = \frac{A_r}{G^0} \cdot N, \quad (26)$$

where A_r is the destruction energy of defects; N — contact roughness; G^0 — Gibbs energy.

Nowadays, in mechanical engineering, high-alloyed, including stainless steels are often used for critical machine parts, the processing of which is complicated by traditional mechanical methods. Particularly problematic is obtaining accurate small holes. For this case, the most effective is the use of the EDM method of piercing a hole [29].

The mathematical model describing the dependence when using water as a working fluid has the form:

$$N = 0,11 \cdot E^{0,66} \cdot F^{-0,26}, \quad (27)$$

where E is the pulse energy, mJ; F is the pulse frequency, kHz.

GOST defined six types of directions of irregularities that are selected when recording a profilogram: parallel, perpendicular, intersecting, arbitrary, circular and radial. When removing profilograms from friction surfaces, the first two types are most often used [30]. The concepts parallel and perpendicular are related to the direction of friction during the operation of the tribo-conjugation.

The arithmetic average of the R_a profile is determined by the arithmetic average of the absolute values of the profile deviations within the base length:

$$R_a = \frac{1}{\ell} \int_0^{\ell} |y| dx \quad \text{or} \quad R_a = \frac{1}{n} \sum_{i=1}^n |y_i|, \quad (28)$$

where: ℓ is the base length, n is the number of selected profile points on the base length.

The height of the profile of irregularities at ten points R_z is defined as the sum of the average absolute values of the heights of the five largest profile protrusions and the depths of the five largest cavities of the profile within the base length:

$$R_z = \frac{\sum_{i=1}^5 |ypmi| + \sum_{i=1}^5 |yvmi|}{5}, \quad (29)$$

where $ypmi$ is the height of the i -th largest profile protrusion; $yvmi$ is the depth of the i -th largest depression of the profile.

The greatest height R_{\max} of the profile is the distance between the line of the protrusions of the profile and the line of the cavities of the profile within the base length. The average step of the irregularities of the profile S_m is the average step of the local projections of the profile within the base length. The average pitch of the local projections of the profile S is the average pitch of the local projections of the profile within the base length. The relative profile reference length t_p is the ratio of the profile length to the base length and is defined as

$$t_p = \frac{\sum_{i=1}^n b_i}{\ell}. \quad (30)$$

The cross section level of the profile p is the distance between the profile protrusion line and the line intersecting the profile equidistantly of the profile protrusion line. When studying profilograms, one should take into account that the vertical and horizontal scales of increasing the surface profile are different and real irregularities have a much smaller angle of inclination than it looks on profilograms.

Consider in (26) — A_r is the damage energy of defects [31, 32]. Work $A(J)$, spent on the destruction of contacts is proportional to the newly formed surface of the particles of the destroyed product:

$$A_r = \gamma \Delta S = K_R D^2, \quad (31)$$

where γ is the temporary compressive resistance (Nm/m^2), ΔS is the area of the newly formed surface (m^2), K_R is the proportionality coefficient (Nm/m^2); D is the characteristic size of the contact (m).

Equation (31) corresponds to the Rittinger hypothesis [33]. If during the destruction of a cubic-shaped contact, energy is expended mainly on volume deformation, then in this case the work performed is directly proportional to the change in its initial volume and is determined by the Kirpichev-Kik formula [34, 35]:

$$A_r = K \Delta V = K_K D^3, \quad (32)$$

where K and K_K are the proportionality coefficients (Nm/m^3); ΔV is the deformed volume (m^3).

Rebinder [36] combined both hypotheses and in this case the total work of destruction is equal to:

$$A = K_R D^2 + K_K D^3. \quad (33)$$

According to Bond's hypothesis [37], the total work of failure is proportional to the geometric mean between the volume and the contact surface area:

$$A = K_B \sqrt{D^2 D^3} = K_B D^{2.5}. \quad (34)$$

All formulas (31)–(34) differ in proportionality coefficients and indicators of the degree of contact diameter. This indicator is related to the dimension of the contact surface, which in the modern sense has a fractal nature [38] (Fig. 2).

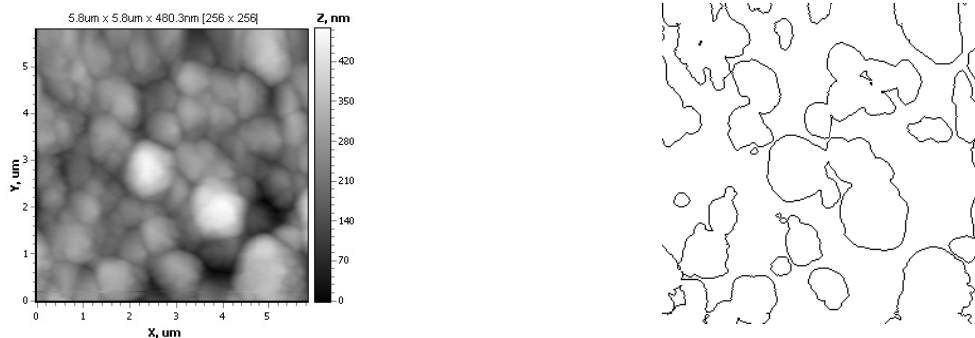


Figure 2. AFM image and the fractal structure of the Zn-Al coating ($D = 1.81$)

For pure metals, equation (26) is converted to:

$$f_G = \frac{A_r}{\mu} \cdot N, \tag{35}$$

where μ is the chemical potential of the metal.

For pure metals, the chemical potential coincides with the Fermi energy. In Table 2 these values are given for some metals [39].

Table 2

Fermi energy of some metals [39]

Metal	Fermi energy, eV	Metal	Fermi energy, eV
Cu	7,00	Zn	9,39
Ag	5,48	Al	11,63
Au	5,51	Pb	9,37
Mg	7,13	Sn	10,03
Sr	3,95	Ca	4,68

From equation (35) it follows that the coefficient of dry friction is the smaller, the greater the chemical potential (Fermi energy). Table 3 shows the dry friction coefficients for pairs of the most common materials [40]. In general, the correlation between the Table 2 and 3 is observed.

Table 3

Dry friction coefficients for homogeneous pairs of the most common materials [40]

Material combinations		Coefficient dry friction
Al	Al	1.05–1.35
Cu	Cu	1.0
Steel	Steel	0.8
Fe	Fe	1.0
Cd	Cd	0.5
Cr	Cr	0.41
Graphite	Graphite	0.5–0.8
Mg	Mg	0.6
Ni	Ni	0.7–1.1
Pt	Pt	1.2
Ag	Ag	1.4
Zn	Zn	0.6

If now we bring two dissimilar metals into contact, a contact potential difference $V_K = \mu$ will arise. Table 4 shows the values of dry friction coefficients for dissimilar pairs of the most common materials [41].

Table 4

The work function of electrons from some metals [41]

Metal	W , eV
Al	4,25
W	4,54
Fe	4,31
Cu	4,4
Ni	4,5
Sn	4,39
Pt	5,32
Ag	4,25
Zn	4,54

Table 5 shows the values of dry friction coefficients for dissimilar pairs of the most common materials [42]. Comparison of Tables 4 and 5 shows a significant decrease in the coefficient of dry friction in the case of dissimilar metals in friction pairs.

Table 5

Dry friction coefficients for dissimilar pairs of the most common materials [42]

Material combinations		Coefficient dry friction
Al	Low carbon steel	0.61
Brass	Steel	0.35
Cd	Cr	0.41
Cu	Low carbon steel	0.53
Ni	Low carbon steel	0.64
Wolfram carbide	Cu	0.35

The practical use of knowledge about the fractal structure of a solid surface has not yet been studied in detail and it is not yet known in what phenomena it will be decisive (Fig. 2).

Let us consider the well-known phenomenon of cold emission of electrons from a metal under the action of an external electric field, mainly due to the quantum tunneling effect. As is known, the current of cold emission is described by the expression:

$$j = j_0 \exp(E_0 / E), \quad (36)$$

where E is the external field strength, E_0 is the electric field of the metal surface:

$$E_0 = \frac{4\sqrt{2m}}{3e\hbar} (A - T_e)^{3/2}, \quad (37)$$

A is the electron work function, T_e is its kinetic energy.

Above, for the dependence of the electrical conductivity of the film on its thickness h , we obtained the following expression:

$$\sigma = \sigma_0 \left(1 - \frac{d}{h}\right), \quad (38)$$

where d is some critical size of the film, starting from which the bulk properties «disappear». After the transformations, we get:

$$\begin{aligned} j &= \sigma E, \quad j_0 = \sigma_0 E_0, \\ \sigma E &= \sigma_0 E_0 \exp(E / E_0), \\ \sigma_0 \left(1 - \frac{d}{h}\right) E &= \sigma_0 E_0 \exp(E_0 / E), \end{aligned}$$

$$E = E_0 \exp(E_0 / E) \left(1 - \frac{d}{h}\right) \approx E_0 \left(1 - \frac{E_0}{E}\right) \left(1 - \frac{d}{h}\right). \quad (39)$$

Denoting $E_0/E = z$, $1 - d/h = k$, where z are complex numbers, and k is real, we get the famous iterative Mandelbrot equation:

$$z = z^2 + k.$$

The solution algorithm is quite simple. Iterations are performed for each starting point from a rectangular or square area — a subset of the complex plane. The iteration process continues until z goes beyond the circumference of radius 2 whose center lies at (0,0) (this means that the attractor of the dynamical system is infinite) or after a sufficiently large number of iterations (for example, 200–500) z converge to some point of the circle. Depending on the number of iterations during which z remained inside the circle, you can set the color of point C (if z remains inside the circle for a sufficiently large number of iterations, the iteration process stops and this raster point turns black).

The following is important for us: the given example shows the fractal structure of the metal surface. Similar patterns are manifested in thermal emission, exoemission of electrons from metals and semiconductors. All this indicates that the fractal structure of the surface of many solids is a characteristic property of them.

Conclusion

Summarizing the study, we can draw the following main conclusions:

- non-equilibrium processes in the tribosystem can lead to a decrease in the production of entropy and, consequently, the intensity of wear and stably proceed with the formation of dissipative structures during self-organization;
- it is obtained that the first term from (20) can reach $f_e = 10^{-3} - 10^{-4}$ due to the use of X_m , ρm and $W(X_m)$ in the mode of using special lubricants;
- in space, the effect of oil filters is absent. It uses solid lubricants (TSP) which include substances applied to the surface of parts in the form of films, having a shear strength much lower than that of the part material;
- an expression for the friction coefficient is obtained, taking into account the surface geometry and its physical properties;
- it was concluded that homogeneous vapors of metals should not be used in friction antifriction pairs;
- it is shown that a decrease in the dry friction coefficient is possible due to a decrease in surface energy. In this case, friction pairs are used, in which the electron work function differs significantly. This leads to a difference in the contact potential difference and, accordingly, to a decrease in the surface energy;
- it is shown that the friction coefficient depends on the fractal structure of the surface of many solids and this is their characteristic property.

The work was performed under the program of the MES RK. Grants № 0118PK000063 and № Ф.0780.

References

- 1 Крагельский И.В. Развитие науки о трении. Сухое трение / И.В. Крагельский, В.С. Щедров — М.: Изд. АН СССР, 1956. — 235 с.
- 2 Современная трибология: Итоги и перспективы / под. ред. В.К. Фролова. — М.: Изд-во ЛКИ, 2008. — 480 с.
- 3 Bhushan B. Introduction to Tribology / B. Bhushan. — John Wiley & Sons. Ltd., 2013. — 711 p.
- 4 Stachowiak G. Engineering Tribology / G. Stachowiak, A. Batchelor. — Butterworth-Heinemann, 2014. — 884 p.
- 5 Маленков М.И. Конструкционные и смазочные материалы космических механизмов / М.И. Маленков, С.И. Каратушин, В.М. Тарасов. — СПб.: Балт. гос. техн. ун-т, 2007. — 54 с.
- 6 Мусалимов В.М. Основы трибоники / В.М. Мусалимов, А.А. Сизова, Е.К. Иванов, Н.А. Крылов, А.Л. Ткачев. — СПб.: СПбГУ ИТМО, 2009. — 77 с.
- 7 Одейчук Н.П. Методика трибологических испытаний углеродных материалов под воздействием ионизирующего излучения и окислительной среды / Н.П. Одейчук, В.К. Яковлев, А.И. Комир, А.Н. Одейчук. — Харьков: НТУ «ХПИ», 2018. — № 9(1285). — С. 62–69.
- 8 Овчаренко В.Е. Трибологические свойства наноструктурированной поверхности металлокерамического сплава на основе карбида титана / В.Е. Овчаренко, Ю.Ф. Иванов // Изв. Томск. политехн. ун-та. — 2008. — Т. 313, № 2. — С. 114–118.
- 9 Бакларь В.Ю. Трибологические свойства наноуглерода, полученного электроразрядным методом / В.Ю. Бакларь, Н.И. Кускова, В.В. Тихонович, А.Н. Грипачевский // Электронная обработка материалов. — 2009. — № 4. — С. 30–37.
- 10 Седалищев В.Н. Обзор существующих методов неразрушающего контроля качества поверхностей с наноструктурированными покрытиями / В.Н. Седалищев, С.П. Пронин, Е.М. Крючков, А.В. Новичихин, М.Ю. Ларионов // Ползуновский альманах. — 2012. — № 2. — С. 176–179.
- 11 Ермакова С.Ф. Трибология жидкокристаллических наноматериалов и систем / С.Ф. Ермакова // Белорусская наука. — 2014. — 381 с.
- 12 Гаркунов Д.Н. Триботехника (износ и безызносность) / Д.Н. Гаркунов. — М.: Изд-во МСХА, 2001. — 616 с.
- 13 Кужаров А.С. Свойства и применение металлоплакирующих смазок / А.С. Кужаров, Н.Ю. Онищук. — М.: Наука, 1985. — 60 с.
- 14 Гаркунов Д.Н. О механизме избирательного переноса при трении меди и медных сплавов в среде глицерина / Д.Н. Гаркунов, А.А. Поляков // Контактное взаимодействие твердых тел и расчет сил трения и износа. — М., 1968. — С. 63–72.
- 15 Кужаров А.С. Концепция безызносности в современной трибологии / А.С. Кужаров // Изв. вузов. Северо-Кавказский регион. Технические науки. — 2014. — № 2. — С. 23–31.
- 16 Шелева В.В. Трибохимия и реология износостойкости / В.В. Шелева, В.П. Александренко. — Хмельницкий: ХНУ, 2006. — 278 с.
- 17 Юров В.М. Температурные эффекты в спектрах поглощения и люминесценции экситонов в галогенидах аммония / В.М. Юров, Т.А. Кукетаев // Вестн. Караганд. ун-та. Сер. Физика. — 2004. — № 1(33). — С. 46–51.
- 18 Юров В.М. Безызлучательные процессы и фазовые переходы в кристаллах галогенидов аммония / В.М. Юров // Вестн. науки и образования. — 2008. — № 3. — С. 6–12.

- 19 Валиев Р.З. Наноструктурные материалы, полученные интенсивной пластической деформацией / Р.З. Валиев, И.В. Александров. — М.: Логос, 2000. — 272 с.
- 20 Бершадский Л.И. Структурная термодинамика трибосистем / Л.И. Бершадский. — Киев: Знание, 1990. — 31 с.
- 21 Пригожин И. Современная термодинамика / И. Пригожин, Д. Кондипуди. — М.: Мир, 2002. — 461 с.
- 22 Гершман И.С. Реализация диссипативной самоорганизации поверхностей трения в трибосистемах / И.С. Гершман, Н.А. Буше // Трение и износ. — 1995. — Т. 16, № 1. — С. 61–70.
- 23 Гершман И.С. Синергетика процессов трения / И.С. Гершман // Трение, износ, смазка. — 2006. — Т. 8, № 4(29). — С. 71–80.
- 24 Чертовских С.В. Анализ трения и изнашивания ультрамелкозернистых материалов с позиций термодинамики / С.В. Чертовских, Л.Ш. Шустер // Вестник УГАТУ. — 2016. — Т. 20, № 2(72). — С. 55–60.
- 25 Могилевский В.А. Смазочные материалы и присадки. Способы и системы смазывания / В.А. Могилевский, А.М. Лубягов, Е.С. Окулова, Н.А. Глотова. — Ростов н/Д., 2005. — 24 с.
- 26 Журков С.Н. К вопросу о физической основе прочности / С.Н. Журков // Физика твердого тела. — 1980. — Т. 22, Вып. 11. — С. 3344–3349.
- 27 Регель В.Р. Кинетическая теория прочности твердых тел / В.Р. Регель, А.Б. Слуцкер, В.Д. Томашевский. — М.: Наука, 1974. — 302 с.
- 28 Ковшов А.Г. Расчетно-экспериментальная идентификация активационных параметров модели изнашивания поверхностей трения / А.Г. Ковшов // Изв. Самарск. НЦ РАН. — 2016. — Т. 18, № 4(2). — С. 341–346.
- 29 Блинова Т.А. Зависимость шероховатости поверхности малых отверстий от типа рабочей среды и режимов электроэрозионной обработки / Т.А. Блинова, А.А. Погонин, А.Ф. Бойко // Изв. Самарск. НЦ РАН. — 2010. — Т. 12, № 1(2). — С. 301–303.
- 30 Колесников В.И. Взаимодействие контактирующих поверхностей при трении / В.И. Колесников, А.В. Челохьян, П.Г. Иванович, Е.А. Луговой, А.А. Порческо. — Ростов н/Д., 2000. — 136 с.
- 31 Юров В.М. Определение коэффициента трения скольжения / В.М. Юров, С.А. Гученко, Н.Х. Ибраев // Междунар. журн. прикл. и фундамент. исследований. — 2010. — № 8. — С. 148–152.
- 32 Юров В.М. Температурная зависимость коэффициента трения / В.М. Юров // Междунар. журн. прикл. и фундамент. исследований. — 2010. — № 8. — С. 151–152.
- 33 Rittinger P.V. Lenbruch fur Aufbereitungskunde / P.V. Rittinger. — Berlin, 1967. — 234 s.
- 34 Кирпичёв В.Л. Конспект лекций по прикладной механике / В.Л. Кирпичёв. — СПб.: Политехн. ин-т, 1911. — 160 с.
- 35 Kick F. Das Gesetz der proportionalen widerstande und seine Anwendung Dingers / F. Kick. — Berlin, 1885. — 167 p.
- 36 Ребиндер П.А. Понизители твердости породы при бурении / П.А. Ребиндер, Л.А. Шрейнер, К.Ф. Жигач. — М.: АН СССР, 1944. — 204 с.
- 37 Бонд Ф.С. Законы дробления / Ф.С. Бонд // Тр. Европейского совещ. по измельчению. — М., 1966. — С. 195–208.
- 38 Guchenko S.A. Fractal structure of multi-element coating / S.A. Guchenko, O.N. Zavatskaya, V.M. Yurov, S.S. Kasymov, V.Ch. Laurinas // Eurasian Physical Technical Journal. — 2018. — Vol. 15, No. 1(29). — P. 8–17.
- 39 Киттель Ч. Введение в физику твердого тела / Ч. Киттель. — М.: Наука, 1978. — 792 с.
- 40 Крагельский И.В. Трение и износ / И.В. Крагельский. — М.: Машиностроение, 1968. — 480 с.
- 41 Крагельский И.В. Коэффициенты трения / И.В. Крагельский, И.Э. Виноградова. — М.: Машгиз, 1962. — 220 с.
- 42 Суриков Вал. И. Основы теории твердого тела / Вал.И. Суриков, Вад. И. Суриков. — Омск: Изд-во ОмГТУ, 2016. — 95 с.

В.М. Юров, Е.Н. Еремин, В.Ч. Лауринас, С.С. Қасымов

Трибологиядағы диссипативтік үрдістер

Мақалада диссипативті үрдіс қатты денелердегі сыртқы үйкелістің табиғи негізі ретінде қарастырылды. Трибожүйенің тепе-тең емес үрдістері энтропия өндірісінің төмендеуіне әкеліп соғуы мүмкін, демек, тозу қарқындылығы және өзін-өзі ұйымдастыру кезінде диссипативті құрылымдардың қалыптасуымен тұрақты түрде жүруі мүмкіндігі көрсетілген. Арнайы майлауларды пайдалану режимінде X_m , ρ_m және $W(X_m)$ арқылы алғашқы мүшесі $f_e = 10^{-3} - 10^{-4}$ жетуі мүмкін екендігі анықталды. Ғарышта май сүзгілерінің әсері жоқ. Мұнда, бөлшек материалдарына қарағанда, ығыспалы беріктілігі анағұрлым төменірек бөлшектердің бетіне қабықша түрінде жағылған заттар түрінде қатты майлау материалдары пайдаланды. Беттің геометриясын және оның физикалық қасиеттерін ескеретін үйкеліс коэффициентіне арналған өрнек алынды. Антифрикционды жұптарда біртекті металл жұптардың үйкелісі қолданылмауы керек деген қорытынды жасалды. Беттік энергияның төмендеуіне байланысты құрғақ үйкеліс коэффициентінің төмендеуі мүмкін екенін көрсетті. Бұл жағдайда электрондардың шығу жұмысы айтарлықтай ерекшеленетін үйкеліс жұбы қолданылды. Бұл контактілік потенциалдар айырымының айырмашылығына және тиісінше беттік энергияның төмендеуіне әкеледі. Үйкеліс коэффициенті қатты заттардың беттік фракталдық құрылымына тәуелді және бұл оларға тән қасиет екенін көрсетті.

Кілт сөздер: диссипативті үрдіс, үйкеліс, тозу, бет, энтропия, фрактал.

Диссипативные процессы в трибологии

В статье диссипативный процесс рассмотрен как основа природы внешнего трения в твердых телах. Показано, что неравновесные процессы в трибосистеме могут приводить к снижению производства энтропии и, следовательно, интенсивности изнашивания и устойчиво протекать с образованием диссипативных структур при самоорганизации. Получено, что первый член может достигать $f_e = 10^{-3} - 10^{-4}$ за счет использования X_m , ρ_m и $W(X_m)$ в режиме использования специальных смазок. В космосе эффект масляных фильтров отсутствует. Здесь используют твердосмазочные материалы, к которым относятся вещества, наносимые на поверхность деталей в виде пленок, имеющие сдвиговую прочность значительно меньшую, чем у материала детали. Получено выражение для коэффициента трения, учитывающее геометрию поверхности и ее физические свойства. Сделан вывод о том, что нельзя использовать в антифрикционных парах трения однородные пары металлов. Показано, что уменьшение коэффициента сухого трения возможно за счет уменьшения поверхностной энергии. При этом используются пары трения, у которых значительно различается работа выхода электронов. Это приводит к различию в контактной разности потенциалов и, соответственно, к уменьшению поверхностной энергии. Показано, что коэффициент трения зависит от фрактальной структуры поверхности многих твердых тел и это является их характерным свойством.

Ключевые слова: диссипативный процесс, трение, износ, поверхность, энтропия, фрактал.

References

- 1 Kragelskii, I.V., & Shchedrov, V.S. (1956). *Razvitie nauki o trenii. Suhoe trenie [The development of the science of friction. Dry friction]*. Moscow: Izd. AN SSSR [in Russian].
- 2 Frolov, V.K. (Ed.). (2008). *Sovremennaiia tribolohiia: Itohi i perspektivy [Modern Tribology: results and prospects]*. Moscow: Izdatelstvo LKI [in Russian].
- 3 Bhushan, B. (2013). *Introduction to Tribology*. John Wiley & Sons. Ltd.
- 4 Stachowiak, G., & Batchelor, A. (2014). *Engineering Tribology*. Butterworth-Heinemann.
- 5 Malenkov, M.I., Karatushin, S.I., & Tarasov, V.M. (2007). *Konstruktivnye i smazochnye materialy kosmicheskikh mekhanizmov [Structural and lubricant space mechanisms]*. Saint Petersburg: Baltiiskii gosudarstvennyi tekhnicheskii universitet [in Russian].
- 6 Musalimov, V.M., Sizova, A.A., Ivanov, E.K., Krylov, N.A., & Tkachev, A.L. (2009). *Osnovy triboniki [Tribonics Basics]*. Saint Petersburg: SPbGU ITMO [in Russian].
- 7 Odeichuk, N.P., Yakovlev, V.K., Komir, A.I., & Odeichuk, A.N. (2018). *Metodika tribolohicheskikh ispytaniy uhlernykh materialov pod vozdeistviem ioniziruiushchego izlucheniia i oksiditelnoi sredy [Methods of tribological testing of carbon materials under the influence of ionizing radiation and oxidizing environment]*. Kharkov: NTU «KhPI», 9(1285), 62–69 [in Russian].
- 8 Ovcharenko, V.E., & Ivanov, Yu.F. (2008). Tribolohicheskie svoistva nanostrukturirovannoi poverkhnosti metallokeramicheskogo splava na osnove karbida titana [Tribological properties of nanostructured surface of metal-ceramic alloy based on titanium carbide]. *Izvestiia Tomskogo politehnicheskogo universiteta — News of Tomsk Polytechnic University*, 313, 2, 114–118 [in Russian].
- 9 Baklar, V.Iu., Kusikova, N.I., Tikhonovich, V.V., & Gripachevskii, A.N. (2009). Tribolohicheskie svoistva nanouhlernogo, poluchennogo elektrorazriadnym metodom [Tribological properties of nanocarbon produced by the electric discharge method]. *Elektronnaia obrabotka materialov — Electronic material processing*, 4, 30–37 [in Russian].
- 10 Sedalishchev, V.N., Pronin, S.P., Kryuchkov, E.M., Novichikhin, A.V., & Larionov, M.Yu. (2012). Obzor sushchestvuiushchikh metodov nerazrushaiushchego kontrolya kachestva poverkhnostei s nanostrukturirovannymi pokrytiiami [Review of existing methods of non-destructive quality control of surfaces with nanostructured coatings]. *Polzunov's almanach*, 2, 176–179 [in Russian].
- 11 Ermakova, S.F. (2014). Tribolohiia zhidkokristallicheskh nanomaterialov i sistem [Tribology liquid crystal nanomaterials and systems]. *Belorusskaia nauka — Belarusian science*, 381 [in Russian].
- 12 Garkunov, D.N. (2001). *Tribotekhnika (iznos i bezyznosnost) [Tribotech (wear and wearlessness)]*. Moscow: Izdatelstvo MSHA [in Russian].
- 13 Kuzharov, A.S., & Onishchuk, N.Yu. (1985). *Svoistva i primenenie metalloplakiruiushchikh smazok [Properties and application of metal cladding greases]*. Moscow: Nauka [in Russian].
- 14 Garkunov, D.N., & Poliakov, A.A. (1968). O mekhanizme izbiratel'nogo perenosu pri trenii medi i mednykh splavov v srede hlitserina [On the mechanism of selective transfer during friction of copper and copper alloys in glycerol medium]. *Kontaktnoe vzaimodeistvie tverdykh tel i raschet sil treniia i iznosa — Contact interaction of solids and calculation of friction and wear forces*. Moscow [in Russian].
- 15 Kuzharov, A.S. (2014). Kontseptsii bezyznosnosti v sovremennoi tribolohii [The concept of wearlessness in modern tribology]. *Izvestiia vuzov. Severo-Kavkazskii rehion. Tekhnicheskii nauki — News of universities. North Caucasus region. Technical science*, 2, 23–31 [in Russian].
- 16 Shelevia, V.V., & Oleksandrenko, V.P. (2006). *Tribokhimiia i reolohiia iznosostoikosti [Tribology chemistry and rheology of wear resistance]*. Khmel'nitskii: HNU [in Russian].

- 17 Yurov, V.M., & Kuketaev, T.A. (2004). Temperaturnye efekty v spektrakh pohloshcheniia i liuminesentsii eksitonov v halohenidakh ammoniia [Temperature effects in the absorption and luminescence spectra of excitons in ammonium halides]. *Vestnik Karahandinskogo universiteta. Seriya Fizika — Bulletin of the Karaganda University. Physics series*, 1(33), 46–51 [in Russian].
- 18 Yurov, V.M. (2008). Bezyzluchatelnye protsessy i fazovye perekhody v kristallakh haloidov ammoniia [Nonradiative processes and phase transitions in ammonium halide crystals]. *Vestnik nauki i obrazovaniia — Bulletin of science and education*, 3, 6–12 [in Russian].
- 19 Valiev, R.Z., & Aleksandrov, I.V. (2000). *Nanostrukturnye materialy, poluchennnye intensivnoi plasticheskoi deformatsiei* [Nanostructured materials obtained by severe plastic deformation]. Moscow: Logos [in Russian].
- 20 Bershadskii, L.I. (1990). *Strukturnaia termodinamika tribosistem* [Structural thermodynamics of tribosystems]. Kiev: Znanie [in Russian].
- 21 Prigozhin, I., & Kondipudi, D. (2002). *Sovremennaia termodinamika* [Modern thermodynamics]. Moscow: Mir [in Russian].
- 22 Gershman, I.S., & Bushe, N.A. (1995). Realizatsiia dissipativnoi samoorhanizatsii poverkhnosti treniia v tribosistemakh [Implementation of dissipative self-organization of friction surfaces in tribosystems]. *Trenie i iznos — Friction and wear*, 16, 1, 61–70 [in Russian].
- 23 Gershman, I.S. (2006). Sinerhetika protsessov treniia [Synergy of friction processes]. *Trenie, iznos, smazka — Friction, wear, lubrication*, 8, 4(29), 71–80 [in Russian].
- 24 Chertovskikh, S.V., & Shuster, L.Sh. (2016). Analiz treniia i iznashivaniia ultramelkozernistykh materialov s pozitsii termodinamiki [Analysis of rhenium and wear of ultrafine-grained materials from the standpoint of thermodynamics]. *Vestnik UGATU — Bulletin of UGATU*, 20, 2(72), 55–60 [in Russian].
- 25 Mogilevskii, V.A., Lubiagov, A.M., Okulova E.S., & Glotova N.A. (2005). *Smazochnye materialy i prisadki. Sposoby i sistemy smazyvaniia* [Lubricants and additives. Methods and lubrication systems]. Rostov-on-Don [in Russian].
- 26 Zhurkov, S.N. (1980). K voprosu o fizicheskoi osnove prochnosti [On the physical basis of strength]. *Fizika tverdoho tela — Solid state physics*, 22, 11, 3344–3349 [in Russian].
- 27 Regel, V.R., Slutsker, A.B., & Tomashevskii, V.D. (1974). *Kineticheskaia teoriia prochnosti tverdykh tel* [Kinetic theory of the strength of solids]. Moscow: Nauka [in Russian].
- 28 Kovshov, A.G. (2016). Raschetno-eksperimentalnaia identifikatsiia aktivatsionnykh parametrov modeli iznashivaniia poverkhnosti treniia [Calculated and experimental identification of the activation parameters of the friction surface wear model]. *Izvestiia Samarskogo nauchnogo tsentra RAN — News of Samara scientific centre of RAS*, 18, 4(2), 341–346 [in Russian].
- 29 Blinova, T.A., Pogonin, A.A., & Boiko, A.F. (2010). Zavisimost sherohovatosti poverkhnosti mal'kh otverstii ot tipa rabochei sredy i rezhimov elektroerozionnoi obrabotki [The dependence of the surface roughness of small holes on the type of working medium and modes of EDM treatment]. *Izvestiia Samarskogo nauchnogo tsentra RAN — News of Samara scientific centre of RAS*, 12, 1(2), 301–303 [in Russian].
- 30 Kolesnikov, V.I., Chelohian, A.V., Ivanochkin, P.G., Lugovoi, E.A., & Porchesko, A.A. (2000). *Vzaimodeistvie kontaktiruiushchikh poverkhnostei pri trenii* [Interaction of contacting surfaces during friction]. Rostov-on-Don [in Russian].
- 31 Yurov, V.M., Guchenko, S.A., & Ibraev, N.H. (2010). Opredelenie koeffitsienta treniia skolzheniia [Determination of the coefficient of sliding friction]. *Mezhdunarodnyi zhurnal prikladnykh i fundamentalnykh issledovaniia — International Journal of Applied and Basic Research*, 8, 148–152 [in Russian].
- 32 Yurov, V.M. (2010). Temperaturnaia zavisimost koeffitsienta treniia [Temperature dependence of friction coefficient]. *Mezhdunarodnyi zhurnal prikladnykh i fundamentalnykh issledovaniia — International Journal of Applied and Basic Research*, 8, 151–152 [in Russian].
- 33 Rittinger, P.V. (1967). *Lenbruch fur Aufbereitungskunde*. Berlin.
- 34 Kirpichyov, V.L. (1911). *Konspekt lektsii po prikladnoi mekhanike* [Lectures on applied mechanics]. Saint Petersburg: Politekhnikeskii institut [in Russian].
- 35 Kick, F. (1885). *Das Gesetz der proportionalen widerstande und seine Anwendung Dinglers*. Berlin.
- 36 Rebinder, P.A., Shreiner, L.A., & Zhigach, K.F. (1944). *Poniziteli tverdosti porody pri bureanii* [Rock hardness reducers while drilling]. Moscow: AN SSSR [in Russian].
- 37 Bond, F.S. (1966). Zakony drobleniia [Laws of Crushing]. *Trudy Evropeiskogo soveshchaniia po izmelcheniiu — Proceedings of the European Grinding Conference* (pp. 195–208). Moscow [in Russian].
- 38 Guchenko, S.A., Zavatskaya, O.N., Yurov, V.M., Kasymov, S.S., & Laurinas, V.Ch. (2018). Fractal structure of multi-element coating. *Eurasian Physical Technical Journal*, 15, 1(29), 8–17.
- 39 Kittel, Ch. (1978). *Vvedenie v fiziku tverdoho tela* [Introduction to Solid State Physics]. Moscow: Nauka [in Russian].
- 40 Kragelskii, I.V. (1968). *Trenie i iznos* [Friction and wear]. Moscow: Mashinostroenie [in Russian].
- 41 Kragelskii, I.V., & Vinogradova, I.E. (1962). *Koeffitsienty treniia* [Friction coefficients]. Moscow: Mashgiz [in Russian].
- 42 Surikov, Val. I., & Surikov, Vad. I. (2016). *Osnovy teorii tverdoho tela* [Fundamentals of the theory of solids]. Omsk: OmGTU Publ. [in Russian].

A.Zh. Zhumabekov, N.Kh. Ibrayev, E.V. Seliverstova, G.B. Kamalova

*Ye.A. Buketov Karaganda State University, Kazakhstan
(E-mail: almar89-89@mail.ru)*

Preparation and study of electrophysical and optical properties of TiO₂-GO nanocomposite material

Nanocomposite material TiO₂-GO was synthesized by hydrothermal method. The formation of nanocomposite was confirmed by FTIR analysis. It is shown that the functional groups characteristic of graphene oxide partially disappear in TiO₂-GO, which indicates its partial reduction during synthesis. In addition, the appearance of a wide band below 1000 cm⁻¹ also indicates the formation of bonds between TiO₂ and GO. EDS analysis showed the presence of titanium, oxygen and carbon in the powder of nanocomposite material. Raman spectra of nanocomposite contain peaks typical for both TiO₂ and graphene oxide. Measurements of the optical characteristics of the synthesized material showed that the absorption spectrum of the nanocomposite shifted in the long-wave region relative to the absorption spectrum of the original components, which may be the result of changes in the band gap of the semiconductor. Measurements of electrophysical characteristics showed that the resistance to electronic transport of nanocomposite material is much less than the value of this parameter obtained for pure TiO₂, which leads to an increase in the efficiency of the photocurrent conversion.

Keywords: titanium dioxide, graphene oxide, TiO₂-GO, nanocomposite material, impedance spectra.

Introduction

Titanium dioxide (TiO₂) occupies a special place among semiconductor materials due to its physical and optical properties, such as high melting point, chemical inertness, high efficiency of phototransformation and photostability [1–3]. Titanium dioxide with a band gap of 3.2 eV is only sensitive to light with wavelengths below 380 nm, which are in the UV range. However, it is one of the most popular photocatalysts [4] due to its high oxidation capacity and chemical stability in relation to the high acidity environment.

Semiconductor nanoparticles are aggregated, which leads to a decrease in the generation and transport of charge carriers to the counter electrodes in photocatalytic and photodetecting cells. When used with graphene, this problem can be solved. In this case, TiO₂ nanoparticles are evenly distributed in graphene and easily form chemical bonds along the folds of graphene sheets or other defects.

Graphene with sp² hybridization has recently been widely used in almost all branches of science due to its high mobility of charge carriers, high specific surface area and the possibility of chemical functionalization and mechanical strength. Graphene also absorbs both UV radiation and 1–2 % of light in the visible spectrum [5–8].

In this paper, a nanocomposite material based on TiO₂ and graphene oxide was synthesized. It is assumed that the addition of graphene oxide will improve the electrophysical properties of the semiconductor material, which can be used for photocatalysis and photovoltaics.

Method of experiment

Preparation of TiO₂-GO nanocomposite material by hydrothermal synthesis was carried out as follows: 10 mg of graphene oxide (GO, Cheaptubes, USA) was mixed with 30 ml of deionized water purified by Aquamax water purification system and 10 ml of ethanol in ultrasonic bath for 1 hour. Then, 1 g of TiO₂ was added to the suspension of graphene oxide and the sonication and stirring were sequentially alternated for 2 hours, for each procedure for 30 minutes, until a uniform suspension of light gray color was achieved. After that, the suspension is poured into a Teflon coated 100 ml autoclave and heated at 120 °C during 24 hours for the synthesis of the composite. This process simultaneously restores graphene oxide (GO) to reduced graphene oxide (rGO) by «taking» the electron from ethanol and forming Ti–O–C bonds of TiO₂ and rGO. After cooling to room temperature, the suspension was filtered several times with deionized water and the product was dried at 60 °C [9]. Under these conditions the ratio of GO to TiO₂ was equal to 1 % in nanocomposite material.

To measure the electrophysical properties of the TiO₂-GO nanocomposite material, films were prepared by the «spin-coating» method (Vacuum Spin Coater, MTI Co, USA). The finished paste was applied to the surface of a rotating substrate with a conductive layer of FTO. The substrate was rotating at a constant speed. Speed mode was varied from 500 to 4000 rpm, rotation time — 10 s. It allowed to change the thickness of the films obtained by varying the speed of rotation of the substrates. After application and drying, the film was annealed in Ar atmosphere for 2 hours. Under the same conditions, films based on pure TiO₂ paste were obtained.

The surface of morphology of the obtained nanocomposite materials was studied using a scanning electron microscope (SEM) Tescan Mira3. Also EDS of the samples was carried out on the SEM. The Confotec MR520 microscope (3D Scanning Raman Confocal Microscope, Sol Instruments) with laser excitation at a wavelength of 632.8 nm was used to record the Raman spectrum. The FTIR spectra were recorded using the Fourier spectrometer FSM 1201 and the electronic absorption spectra were recorded using the Cary-300 spectrophotometer (Agilent). To measure the absorption of nanocomposite films, the samples were deposited on quartz substrates.

The method of impedance spectroscopy was used to study the kinetics of transport and recombination of charge carriers. Measurement of impedance spectra was carried out under illumination of samples by xenon lamp light with radiation power of 100 mV/cm² (Cell Tester Model # CTAAA, Photo Emission Tech. Inc., USA) on Z-500PRO impedancemeter (Elins, Russia). The amplitude of the applied signal was 25 mV, and the frequency was ranged from 1 MHz to 100 mHz.

Platinum films deposited by an electrochemical method from an ethanol solution of H₂PtCl₆ on glass substrates with a conductive layer of FTO were used as a counter electrode. The electrodes were glued together. The 25 μm thick polymer film Meltonix (Solaronix, Switzerland) served as a gasket between the working electrode and the counter electrode in the cell. The electrolyte used was Iodolyte H30 (Solaronix, Switzerland).

Results and its discussion

Figure 1 shows SEM images of neat materials and nanocomposites. The figure shows that nanoparticles aggregated in the bulk sample of titanium dioxide. However, in the pictures a small number of micropores can be distinguished. Graphene oxide has a layered structure, which is formed by separate sheets. In the synthesis of nanocomposite material, titanium dioxide particles tend to be less aggregated. In the picture the interparticle pores can be distinguished.

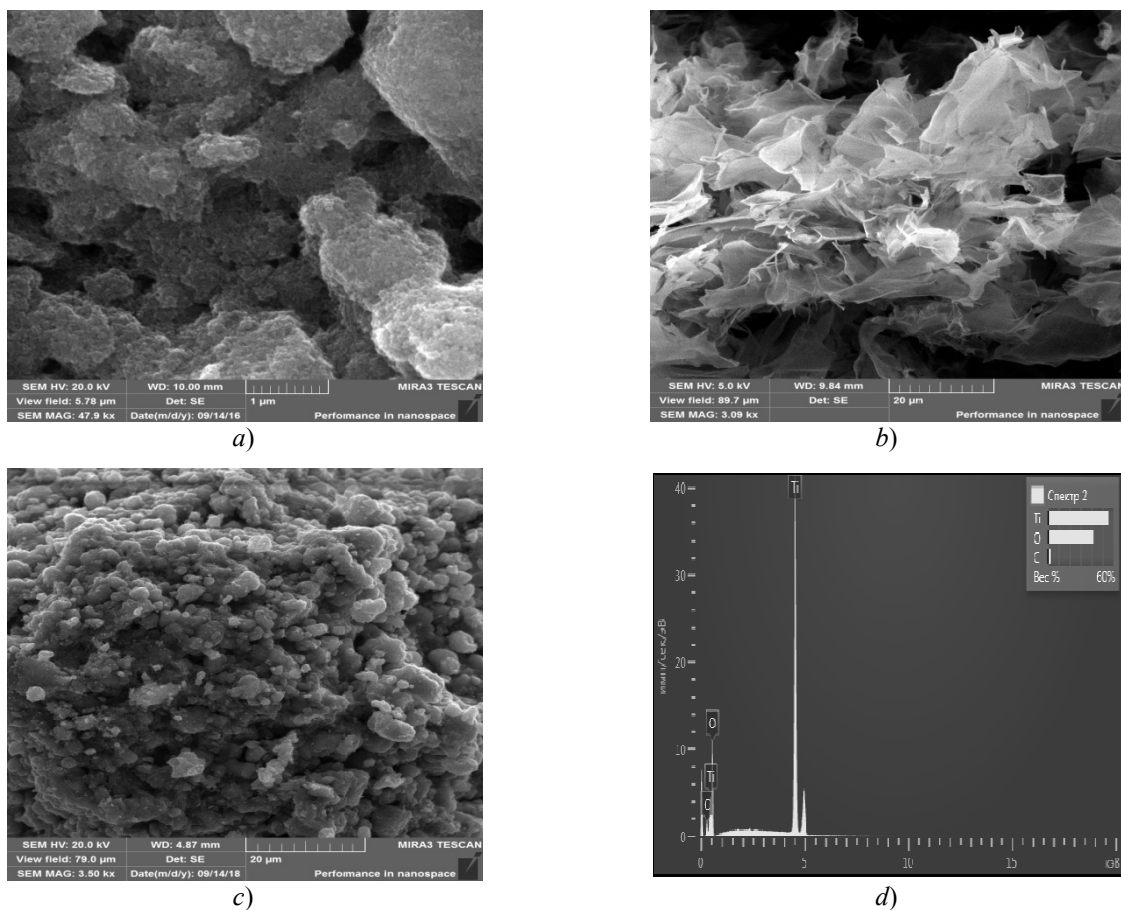
The presence of graphene oxide in the synthesized sample can be confirmed both visually and according to the EDS analysis (Fig. 1d). Figure 1d shows that most part of the studied sample is represented by atoms of titanium and oxygen. The carbon content of the sample is low, due to the low GO concentration relative to TiO₂ (1:100) in the sample.

The measured Raman spectra are shown in Figure 2. Titanium dioxide with anatase structure has six combination-active peaks in the vibrational spectrum (Fig. 2a): three E_g peaks centered at about 149, 183 and 630 cm⁻¹ (E_g(1), E_g(2) and E_g(3) peaks respectively), and two B_{1g} peaks at 397 and 506 cm⁻¹ (denoted by B_{1g}(1) and B_{1g}(2)), and A_{1g} peaks at 481 cm⁻¹ [10].

In the Raman spectra of graphene oxide several bands can be clearly distinguished: D-band, which characterizes the degree of defectiveness of graphene ($\bar{\nu} = 1350 \text{ cm}^{-1}$), G-band, which characterizes the graphene in-plane vibrational modes of sp² hybridization — this parameter displays the degree of crystallization of the material ($\bar{\nu} = 1586 \text{ cm}^{-1}$) and 2D band, which indicates the degree of graphitization and displays the number of graphene layers ($\bar{\nu} = 2700 \text{ cm}^{-1}$) [11].

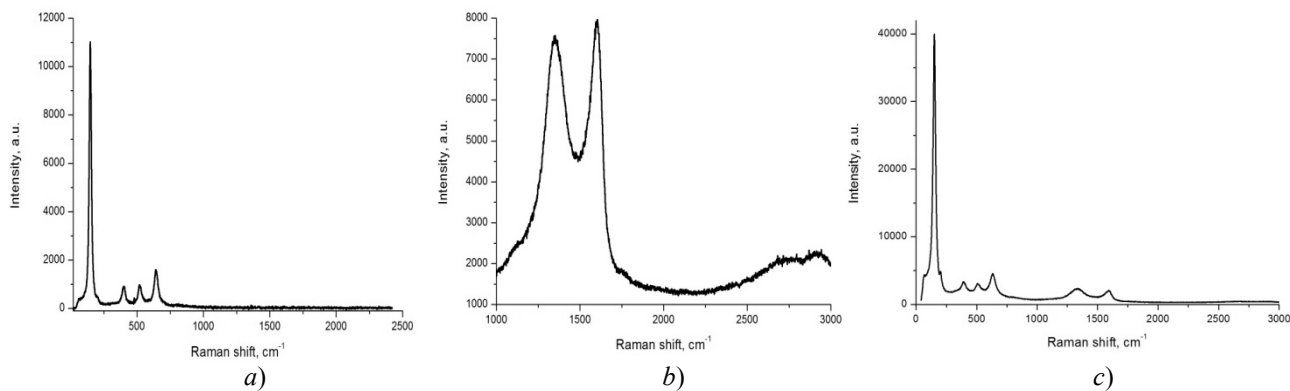
Both TiO₂ and graphene oxide peaks are present in the Raman spectra of the synthesized material. This confirms by the data obtained by EDS analysis of the samples.

Figure 3 shows the FTIR spectra for pure TiO₂ and graphene oxide powders, as well as for the TiO₂-GO nanocomposite material. FTIR spectra of graphene oxide shows the oscillations of bonds characteristic of chemical groups: C-O (1095 cm⁻¹), C-O-C (1261 cm⁻¹), C-OH (1454 cm⁻¹), C=O (1728 cm⁻¹). The intense peak at 3000–3500 cm⁻¹ (3441 cm⁻¹) characterizes fluctuations of O-H groups in the composition of C-OH and water. The peak at 1628 cm⁻¹ is called skeletal vibration of graphene oxide [12]. Figure 3 shows that the functional groups characteristic for graphene oxide are absent.



a — TiO₂; *b* — graphene oxide; *c* — TiO₂-GO

Figure 1. SEM images of powders

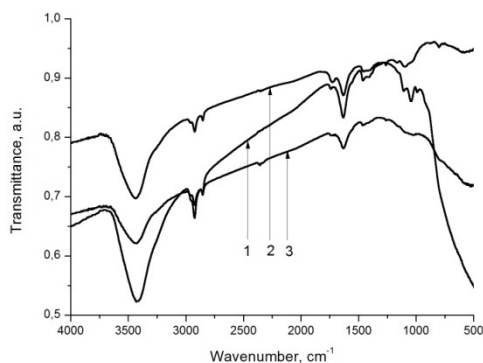


a — TiO₂; *b* — graphene oxide; *c* — TiO₂-GO

Figure 2. Raman spectra of powders

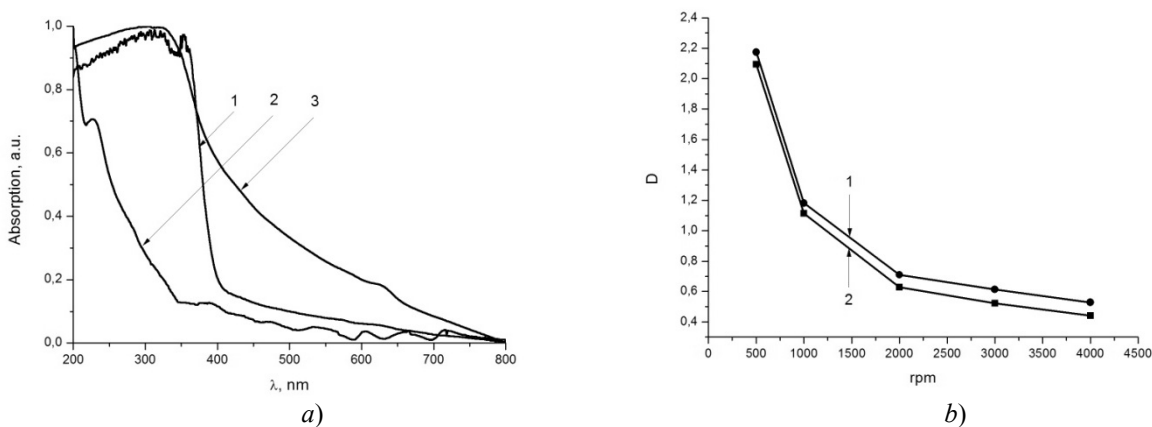
The pure powder TiO₂ has a low-frequency mode of about 500 cm⁻¹, which corresponds to the vibration of Ti-O-Ti bonds. Also, as can be seen from the spectrum, at 3440 cm⁻¹ there is an intense band, which indicates that on the surface of titanium dioxide particles adsorbed OH group.

The nanocomposite material TiO₂-GO exhibits absorption below 1000 cm⁻¹. This peak can be considered as a combination of oscillations of Ti-O-Ti and Ti-O-C bonds (about 792 cm⁻¹). The presence of Ti-O-C bonds indicates that during hydrothermal reduction graphene oxide with residual functional groups of carboxylic acid strongly interacts with surface hydroxyl groups of TiO₂ nanoparticles and, ultimately, a TiO₂-GO nanocomposite material is formed.



a — TiO₂; *b* — graphene oxide; *c* — TiO₂-GO

Figure 3. FTIR spectra of powders



a) 1 — TiO₂; 2 — graphene oxide; 3 — TiO₂-GO; *b*) at 1 — 390 nm; 2 — 700 nm

Figure 4. Absorption spectra (*a*) and the dependence of the optical density of nanocomposite films on the substrate rotation speed (*b*)

As is known, the edge of the TiO₂ absorption band appears in the UV region of the spectrum about 380 nm. Graphene oxide also absorbs in the UV region, the maximum of its absorption spectrum is 230 nm. GO films are practically transparent in the wavelength range from 400 to 800 nm [8, 13]. Figure 4*a* shows that the TiO₂-GO nanocomposite actively absorbs light in the UV region of the spectrum. Along with this, there is a broadening of the absorption band in the visible range of the spectrum. As shown in [14], this is due to the fact that nanocomposite materials shift the edge of the band gap of the material in the long-wavelength region of the spectrum.

Figure 4(*b*) shows the dependence of the optical density of TiO₂-GO nanocomposite films on the substrate rotation speed. As can be seen from the figure, the increase in speed leads to a decrease in the optical density of the samples, which indicates a decrease in the thickness of the films.

Next, the electrophysical characteristics of the material of the nanocomposite of TiO₂-GO and pure TiO₂ were studied. To obtain an equivalent circuit, the data of the measured impedance spectra were processed in the EIS analyzer program. The resulting equivalent electrical circuit of the electrochemical cell is shown in Figure 5 [15].

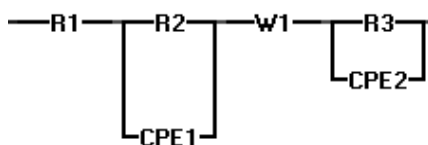
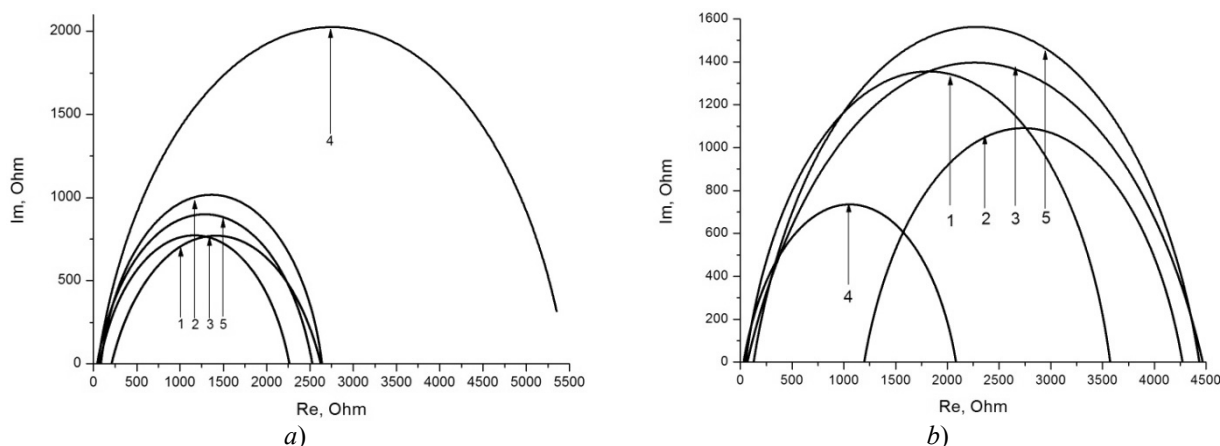


Figure 5. Equivalent electric diagram

On the basis of the obtained data (Fig. 6) the basic electrotransport properties of films were calculated, where: k_{eff} — effective rate constant for recombination, τ_{eff} — effective lifetime of the electron, electron transport resistance in the film of titanium dioxide is R_w , charge-transfer resistance R_k ($R_k = R_{w\max} - R_{w\min}$), related to recombination of electron.



a) TiO₂; b) TiO₂-GO: 1 — 500 rpm; 2 — 1000 rpm; 3 — 2000 rpm; 4 — 3000 rpm; 5 — 4000 rpm

Figure 6. Impedance of spectra

Table 1

Values of electrophysical parameters of TiO₂ films

Film speed	k_{eff}, s^{-1}	τ_{eff}, s	R_k, Ohm	R_w, Ohm
500 rpm	10	0.1	2417.4	208.3
1000 rpm	13.895	0.072	2554.5	84.9
2000 rpm	13.895	0.072	2194.0	69.3
3000 rpm	5.1795	0.193	5411.7	48.2
4000 rpm	26.822	0.037	2485.5	42.3

From Table 1 it is seen that the best electro transport and conducting properties were recorded for TiO₂ film deposited at a speed of 2000 rpm. For this sample, there is a minimum resistance value of the electro transport 2194 Ohm. The maximum value of the resistance of electro transport are films deposited at a speed of 3000 rpm.

Table 2

Values of electrophysical parameters of TiO₂-GO films

Film speed	k_{eff}, s^{-1}	τ_{eff}, s	R_k, Ohm	R_w, Ohm
500 rpm	10	0.1	3521.5	48.4
1000 rpm	26.822	0.037	3075.9	1196
2000 rpm	7.1969	0.139	4400.7	66.9
3000 rpm	51.767	0.02	2052.9	30.5
4000 rpm	10	0.1	4307.2	127.5

Table 2 shows the electrophysical parameters of the TiO₂-GO nanocomposite material. As can be seen from Table 2, that in films deposited at a rotation speed of 3000 rpm, the resistance of electronic transport is equal to $R_k = 2052.9$ Ohm, which is the minimum value compared to other samples. The minimum value of the resistance of electronic transport when measuring the impedance means that the films have large values of electrical conductivity, since the resistance is inversely proportional to the conductivity. R_w — in the film TiO₂-GO 3000 rpm is 30.5 Ohms and shows that in the nanocomposite material resistance to electronic transport is negligible. And in the sample applied at a speed of 1000 rpm, R_w is equal to 1196 Ohm, which is

much more than the above value. This suggests that electronic transport in thick films is carried out with low efficiency.

Effective lifetime of the electron (τ_{eff}) in a sample of 2000 rpm is more than in the other samples. For films deposited at a speed of 4000 rpm, the electrophysical parameters are close in value to that, obtained at 2000 rpm. Studies have shown that the best mode for deposition of TiO₂-GO films is the rotation speed of 3000 rpm.

Thus, studies have shown that hydrothermal synthesis forms a bond between the particles of TiO₂ and graphene oxide sheets, which indicates the production of nanocomposite material. This was confirmed by the EDS analysis data on the presence of titanium, oxygen and carbon in the powder of nanocomposite material. The Raman spectra of the nanocomposite show peaks characteristic of both TiO₂ and graphene oxide. According to the FTIR spectra in TiO₂-GO functional groups characteristic of graphene oxide partially disappear, which confirms its partial recovery during synthesis. In addition, the appearance of a wide band below 1000 cm⁻¹ indicates the formation of a connection between TiO₂ and GO.

Measurements of the optical characteristics of the synthesized material have shown that the absorption spectrum of the TiO₂-GO nanocomposite is shifted to the long-wave region relative to the absorption spectrum of the initial components, which may be the result of changes in the band gap of the semiconductor.

Measurements of the electrophysical characteristics of the nanocomposite material showed that the resistance to electronic transport is much less than in pure TiO₂, which leads to an increase in the efficiency of the photocurrent conversion.

This work was performed within the framework of the research grant AP05132443, funded by the Ministry of education and science of the Republic of Kazakhstan.

References

- 1 Zhang, X.-Y., Li, H.-P., Cui, X.-L., & Lin, Y. (2010). Graphene/TiO₂ nanocomposites: synthesis, characterization and application in hydrogen evolution from water photocatalytic splitting. *Journal of Materials Chemistry*, *20*, 2801–2806.
- 2 Serp, P., & Figueiredo, J.L. (2009). *Carbon Materials for Catalysis*. Hoboken, N.J.: John Wiley & Sons.
- 3 Hummers, Jr. W.S., & Offeman, R.E. (1958). Preparation of graphitic oxide. *Journal of the American Chemical Society*, *80*, 1339–1347.
- 4 Hashimoto, K., Irie, H., & Fujishima, A. (2005). TiO₂ photocatalysis: A historical overview and future prospects. *Japanese Journal of Applied Physics*, *44*, 8269–8285.
- 5 Williams, G., Seger, B., & Kamat, P.V. (2008). TiO₂-Graphene Nanocomposites. UV-Assisted Photocatalytic Reduction of Graphene Oxide. *ACS Nano*, *2*, 7, 1487–1491.
- 6 He, M., Jaehan, J., & Feng, Q. (2012). Graphene-based transparent flexible electrodes for polymer solar cells. *Jour. Materials Chem.*, *22*, 46, 24254–24264.
- 7 Roy-Mayhew, J.D., Bozym, D.J., Punckt, C., & Aksay, I.A. (2010). Functionalized Graphene as a Catalytic Counter Electrode in Dye-Sensitized Solar Cells. *ACS Nano*, *4*, 10, 6203–6211.
- 8 Zheng, Q.B., Gudarzi, M.M., & Wang, Sh.J. (2011). Improved electrical and optical characteristics of transparent graphene thin films produced by acid and doping treatments. *Carbon*, *49*, 2905–2916.
- 9 Zhang, Y., Tang, Z.-R., Fu, X., & Xu, Y.-J. (2010). TiO₂ Graphene Nanocomposites for Gas-Phase Photocatalytic Degradation of Volatile Aromatic Pollutant: Is TiO₂ Graphene Truly Different from Other TiO₂ Carbon Composite Materials? *ACS Nano*, *4*, 12, 7303–7314.
- 10 Swamy, V., Kuznetsov, A., Dubrovinsky, L.S., Caruso, R.A., Shchukin, D.G., & Muddle B.C. (2005). Finite-size and pressure effects on the Raman spectrum of nanocrystalline anatase TiO₂. *Phys. Rev. B*, *71*, 18, 184302/1–11.
- 11 Zhang, W., Cui, J., Tao, C.-an, Wu, Y., Li, Z., & Ma, L. (2009). A strategy for producing pure single-layer graphene sheets based on a confined self-assembly approach. *Angew. Chem. International Edition*, *48*, 5864–5868.
- 12 Zhang, H., Lu, X., Li, Y., Wang, Y., & Li, J. (2010). P25-graphene composite as a high performance photocatalyst. *ACS Nano*, *4*, 1, 380–386.
- 13 Ibrayev, N., Seliverstova, E., & Zhumabekov, A. (2018). Preparation of graphene nanostructured films for photovoltaics. *IOP Conf. Series: Materials Science and Engineering*, *6*.
- 14 Gao, P., Li, A., Sun, D.D., & Ng, W. (2014). Effects of various TiO₂ nanostructures and graphene oxide on photocatalytic activity of TiO₂. *Journal of Hazardous Materials*, 96–104.
- 15 Adachi, M., Murata, Y., Takao, J., & Jinting, J. (2004). Highly efficient dye-sensitized solar cells with a titania thin-film electrode composed of a network structure of single-crystal-like TiO₂ nanowires made by the «oriented attachment» mechanism. *J. Am. Chem. Soc.*, *126*, 14943–14949.

А.Ж. Жумабеков, Н.Х. Ибраев, Е.В. Селиверстова, Г.Б. Камалова

TiO₂-GO нанокompозиттік материалды алу мен оның электрфизикалық және оптикалық қасиеттерін зерттеу

TiO₂-GO нанокompозиттік материалы гидротермалды әдіспен синтезделді. Нанокompозиттің құрылуы ИК-талдау мәліметтері арқылы расталды. TiO₂-GO нанокompозитінде графен оксидіне тән функционалды топтар жарым-жартылай жоғалады, яғни синтез барысында оның жартылай қалпына келетіні көрсетілген. Сонымен қатар 1000 см⁻¹ төмен кең жолақтың пайда болуы да, TiO₂ және GO арасында байланыстың құрылуын дәлелдейді. ЭДС талдау нанокompозитті материалдың ұнтағында титанның, көміртектің және оттегінің бар болуын көрсетті. Синтезделген материалдың оптикалық сипаттамаларының өлшеулері нанокompозиттің жұтылу спектрі, бастапқы компоненттердің жұтылу спектрлеріне қарағанда, ұзынтолқынды аймаққа қарай жылжығанын көрсетті, яғни оның нәтижесі жартылайөткізгіштің тыйым салу зонасының өзгеруі болуы мүмкін. Электрфизикалық сипаттамаларының өлшеулері кезінде нанокompозиттік материалдың электрон тасымалдануы кедергісі таза TiO₂ мәндерімен салыстырғанда көп есе төмендігін көрсетті және фототокты түрлендіруде тиімділігін жоғарылатуға әкеліп соқтырады.

Кілт сөздер: титан диоксиді, графен оксиді, TiO₂-GO, нанокompозиттік материал, импеданс спектрі.

А.Ж. Жумабеков, Н.Х. Ибраев, Е.В. Селиверстова, Г.Б. Камалова

Получение и исследование электрофизических и оптических свойств нанокompозитного материала TiO₂-GO

Гидротермальным методом синтезирован нанокompозитный материал TiO₂-GO. Образование нанокompозита было подтверждено данными ИК-анализа. Показано, что в TiO₂-GO частично исчезают функциональные группы, характерные для оксида графена, что свидетельствует о его частичном восстановлении в ходе синтеза. Кроме того, появление широкой полосы ниже 1000 см⁻¹ также свидетельствует о формировании связи между TiO₂ и GO. ЭДС анализ показал наличие титана, кислорода и углерода в порошке нанокompозитного материала. В Раман спектрах нанокompозита имеются пики, характерные как для TiO₂, так и оксида графена. Измерения оптических характеристик синтезированного материала показали, что спектр поглощения нанокompозита сдвинут в длинноволновую область относительно спектра поглощения исходных компонентов, что может являться результатом изменения ширины запрещенной зоны полупроводника. Измерения электрофизических характеристик показали, что сопротивление электронному транспорту нанокompозитного материала намного меньше значения этого параметра, полученного для чистого TiO₂, что приводит к повышению эффективности преобразования фототока.

Ключевые слова: диоксид титана, оксид графена, TiO₂-GO, нанокompозитный материал, импеданс спектры.

ЖЫЛУ ФИЗИКАСЫ ЖӘНЕ ТЕОРИЯЛЫҚ ЖЫЛУ ТЕХНИКАСЫ ТЕПЛОФИЗИКА И ТЕОРЕТИЧЕСКАЯ ТЕПЛОТЕХНИКА THERMOPHYSICS AND THEORETICAL THERMOENGINEERING

DOI: 10.31489/2019Ph2/61-65

UDC 536.68; 697.1

A.K. Khassenov¹, B.R. Nussupbekov¹, D.Zh. Karabekova¹,
M. Stoev², B.K. Zeinolla¹, A.K. Muratova¹

¹*Ye.A. Buketov Karaganda State University, Kazakhstan;*
²*Neofit Rilski South-West University, Blagoevgrad, Bulgaria*
(E-mail: ayanbergen@mail.ru)

Saving of heat energy costs while providing residents with heat and hot water

In the article data on the amount of heat while providing consumers with heat and hot water are presented. The installation of heat meters is necessary to improve the standard of living of the population through the efficient use of heat energy. Various devices are used to take account of the consumption of heat in heat supply and hot water supply to consumers. Heat metering devices have been started to be installed in residential buildings in recent years. Questions connected to account of heat consumption and its cost is very important these days. The considered commercial heat metering station includes a heat meter, a mass meter or a heat carrier volume, pressure and temperature sensors. We only need to calculate the meter to save energy for heat energy because we only have to pay for the heat we consume. While equipping a residential house with heat metering devices, it was observed that payment for heat energy and consumed hot water was beneficial for consumers.

Key words: heat metering, heat energy, heat supply, flow meter, heat carrier.

Heating systems are an important part of the engineering of energy and industrial facilities. Special productions are created in large cities in order to organize the use of these systems. One of the key issues of operation is the organization of reliable heat supply to consumers [1].

Heating systems in heating facilities operate only during heating season from October to April, while hot water supply is provided throughout the year. Seasonal thermal loads depend on climatic conditions as they are subjected to changes in the heated period due to the external air temperature of the heat loss. Main seasonal heat loads include heat loads used for heating, venting and air conditioning of buildings. Heat loads for heating during the year are considered by the hot water supply systems, technological needs of communal and industrial enterprises of public buildings [2].

The accounting and controlling of heat energy consumed in heating of buildings is a topical issue both for housing and communal services and ordinary consumers. Large losses in heat grids are excluded as long as introduce effective methods of heat metering. At present, 20 % of heat loss is lost in the network, while 30 % of all dispatched energy is lost during transportation. Heat loads in heat exchangers are not regulated and as a result heat is consumed at home [3].

In addition, installation of thermal energy meters is essential to ensure the improvement of the living standards of the population by utilizing thermal energy effectively. We only need to calculate the meter to save energy for thermal energy because we only have to pay for the heat used. Equipping multi-storey apartment housing with computing equipment:

- pay only for the amount of heat energy consumed;
- refuse to invest in poor municipal resources;

– will give the opportunity to profitably use communal resources.

Calculation of payments to consumers without metering devices is carried out according to consumption norms. Therefore, the installation of heat energy meters will help to optimize the system of requirements for the use of thermal energy, and at the discretion of the customer allows to organize and distribute thermal energy in the building.

In connection with the above problems buildings connected to centralized heating networks must be equipped with commercial heat metering devices consumed at heating points. A commercial heat metering station includes a heat meter, a device for calculating the amount of heat based on input information about the mass, temperature and pressure of the coolant. Registration, collection, storage, processing of quantities of energy consumed, their processing and delivery, information quality, information storage, recorders, timers, registers. These elements provide a high level of reliability, accuracy, independence of measurements, fast response of the device and a wide range of measurements of the dimensions of the coolant flow. Domestic or foreign heat meters included in the State Register of Measuring Instruments and meeting the requirements of technical conditions can be used in the accounting units [4–7].

Choosing a computational tool requires careful consideration of its technical data, installation procedures, service rules. The principle of operation is to determine the amount of heat at the entrance, fix the temperature and determine the amount of heat exchanger consumed. The calculation is based on the coolant and the heat input scheme. Heaters can predict heat transfer costs. The building is equipped with a heat transfer pipe.

Thermal energy is determined by measuring the volume, temperature and pressure of the thermal media. The heat transfer medium is calculated using the computing device. Home computing tools can perform additional operations. They store and record the consumed heat information. The main differences between the heat meters are dependent on the measurement methods, installation and operation conditions, and their cost. It is advisable to automate the data collection system in the selection of heat metering devices in buildings. Automated data transmission systems are implemented by modem. Connection of the modems dependent on the type of heat meter is carried out by connecting the heat exchanger to the digital port, as well as to the interface or radio transceiver converters.

Due to the above mentioned issues the consumers were able to determine the cost of heating and hot water supply and determine its cost and reduce costs. The object of the research is a 5-storey, 80-apartment house. In the dwelling house since 2015 special tools for heating and hot water are installed.

As for the main issues of using heat energy, the VKT-7 heat meter was used to regulate heat consumption and heat conductor parameters. The VCT-7 can be connected to a printer, personal computer, battery pack, and a RS232S or RS485 interface modem. The NP-4A battery is used to extract data from calculators. The NP-4A battery is widely used when reading and indicating loss values in an electromagnetic flow sensor, reading and indicating pressure values in a heat calculator database.

Information on thermal energy in heat and hot water supply during heating season are presented in Figures 1 and 2.

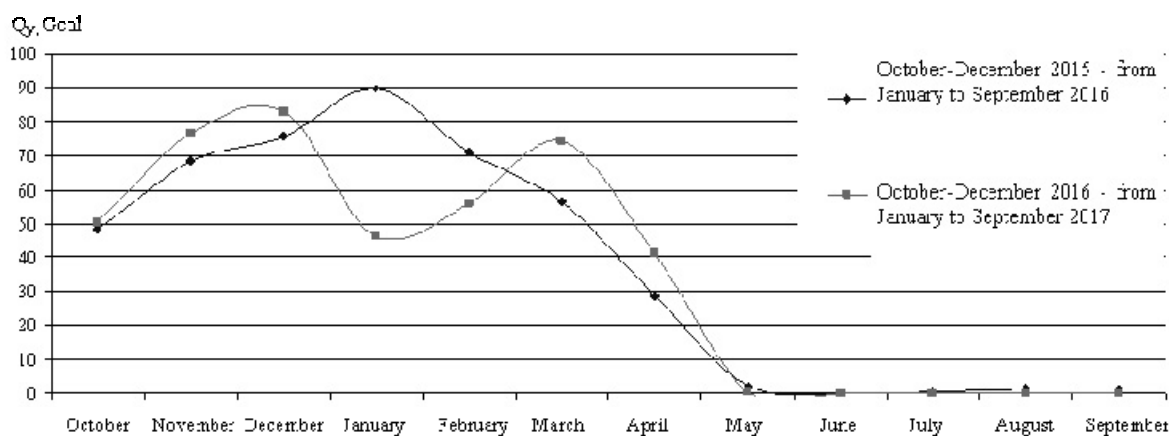


Figure 1. Heating energy in heating season

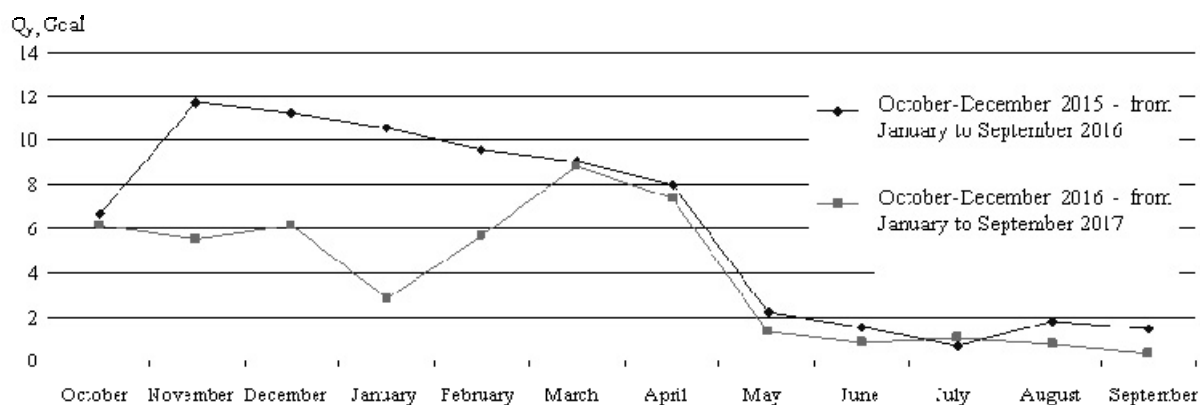
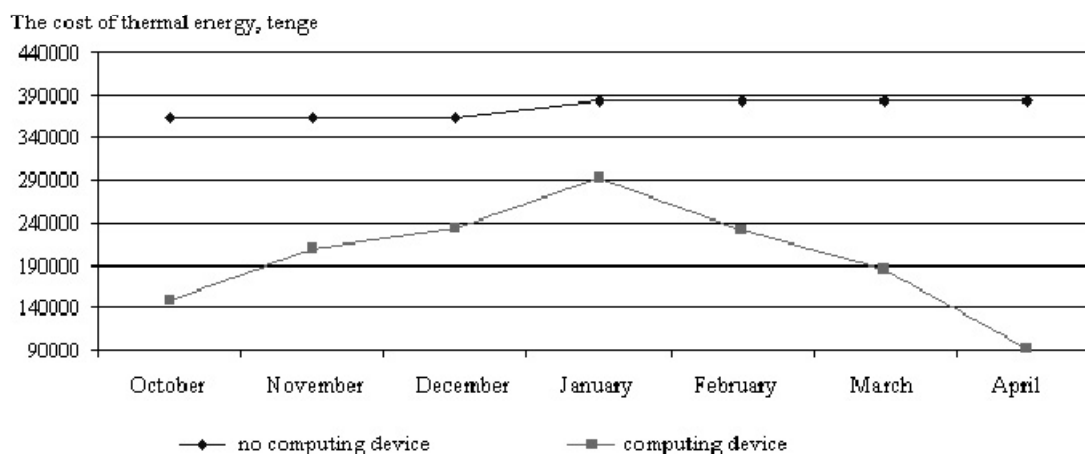


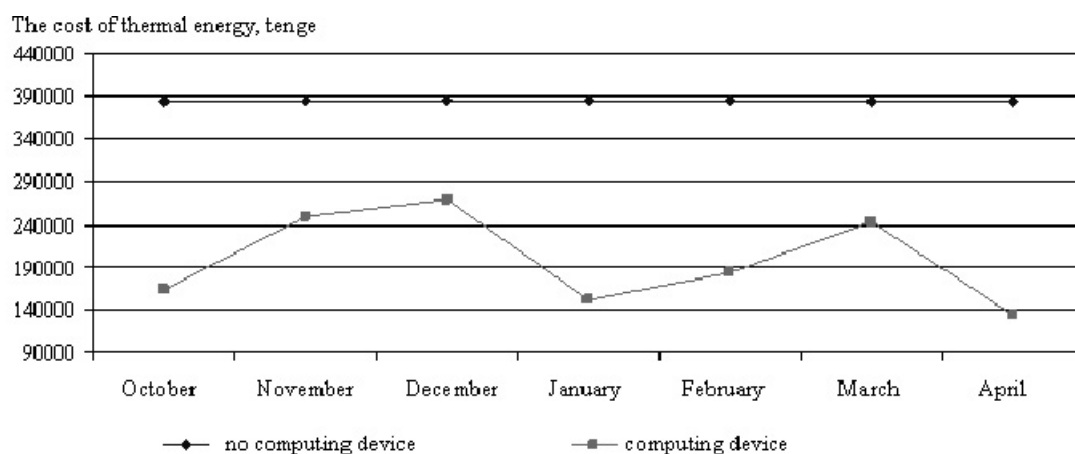
Figure 2. Heat energy relative to hot water

During the heating season, the reduction in the population's heat energy data is associated with a decrease in heat supply and hot water supply from heat energy in May-September, stopping the supply of hot water during the end of the heating season and preparation for the heating season.

The results of the research were compared before and after commercial heat metering installation. Data on thermal energy cost at hot water supply in November-December 2016 and January-September 2017 are shown in Figures 3 and 4.

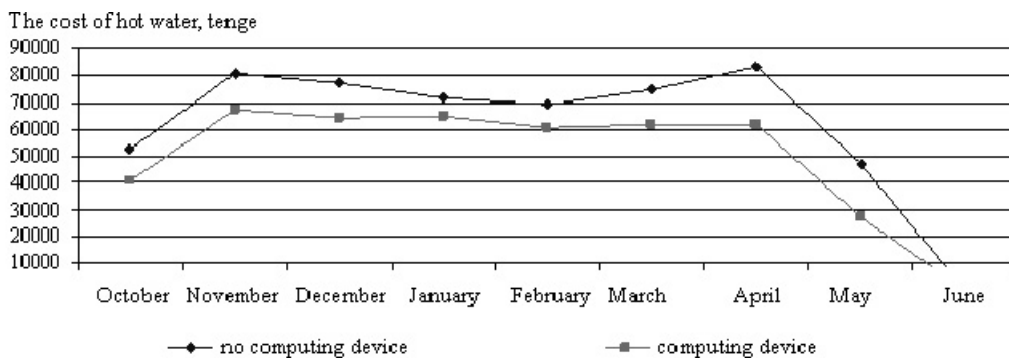


a) Period from November-December, 2015 to January-September, 2016

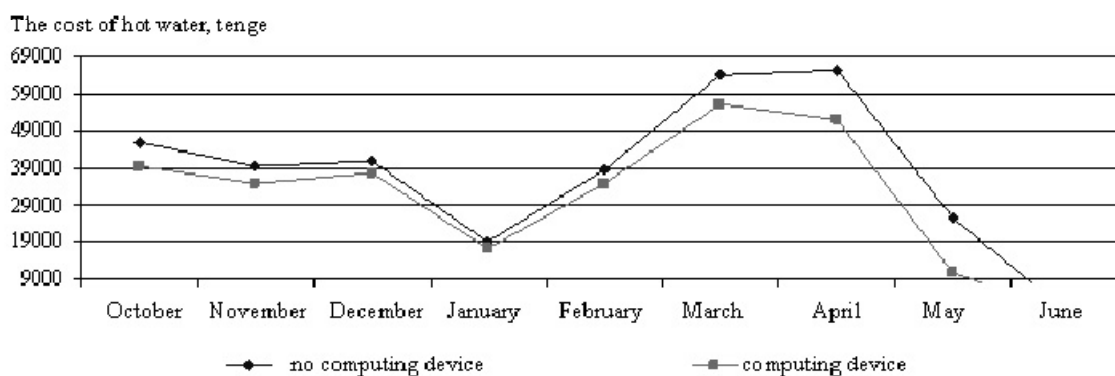


b) Period from November-December, 2016 to January-September, 2017

Figure 3. The value of thermal energy in the heat supply of consumers



a) Period from November-December, 2015 to January-September, 2016



b) Period from November-December, 2016 to January-September, 2017

Figure 4. The cost of consumed hot water

In the absence of computing equipment data for consumers during the heat supply period, we see that in January, the cost of heat energy increased. This is due to the increase in heating costs per 1 m²: 93,3 tenge/m², 2015 — 104.73 tenge/m², 2016 — 110.98 tenge/m². The dependence on the device data showed that a sharp decline in the cost of heat energy in April was due to the end of the heating season.

The following conclusions are drawn from the dependence of the thermal energy cost during heat supply:

- about 2,623,000 tenge were spent for the total thermal energy in the absence of computing tools, while during the period from November-December of 2015 to January-September of 2016 the installation of the counting device amounted to 1,393,700 tenge;
- about 2,688,200 tenge were spent in the absence of computing tools during the period from November-December of 2016 to January-September of 2017, when 1393000 tenge were spent on the installation of heat metering devices.

It is proved that consumers are provided with heat energy and hot water for the consumers when using housing computing devices.

References

- 1 Дегтяренко А.В. Теплоснабжение / А.В. Дегтяренко. — Томск: ТГАСУ, 2010. — 185 с.
- 2 Магадеев В.Ш. Источники и системы теплоснабжения / В.Ш. Магадеев. — М.: Энергия, 2013. — 272 с.
- 3 Приборы учёта тепловой энергии. [Электронный ресурс]. Режим доступа: <https://vodavdome.website/santehnika-i-vodoprovod/schetchiki/pribory-uchyota-teplovoj-energii.html>
- 4 Высоцкая Н.В. Теплоснабжение / Н.В. Высоцкая. — Ухта: УГТУ, 2010. — 119 с.
- 5 Еремкин А.И. Тепловой режим зданий / А.И. Еремкин, Т.И. Королева. — М.: АСВ, 2000. — 368 с.
- 6 Шарапов В.И. Регулирование нагрузки систем теплоснабжения / В.И. Шарапов, П.В. Ротов. — М.: Новости тепло-снабжения, 2007. — 164 с.

7 Методические указания по выбору, монтажу и эксплуатации приборов коммерческого учета в системах теплоснабжения. [Электронный ресурс]. Режим доступа: [http://www.zhkh.kz/ntd/ntd-2011/24 %20Издание_титул%20Приборы%20комерч%20учета.pdf](http://www.zhkh.kz/ntd/ntd-2011/24%20Издание_титул%20Приборы%20комерч%20учета.pdf)

А.К. Хасенов, Б.Р. Нүсіпбеков, Д.Ж. Карабекова,
М. Стоев, Б.К. Зейнолла, А.К. Муратова

Тұрғындарды жылумен және ыстық сумен жабдықтауда жылу энергиясының шығындарын үнемдеу

Мақалада тұтынушыларды жылумен және ыстық сумен қамтамасыз ету кезіндегі жылу мөлшері туралы деректер келтірілді. Жылу энергиясын есептегіштерді орнату жылу энергиясын тиімді пайдалану есебінен халықтың өмір сүру деңгейін арттыру үшін қажет. Тұтынушыларды жылумен және ыстық сумен жабдықтау кезінде жылу шығынын есептеуде әртүрлі аспаптар пайдаланылады. Тұрғын үйлерде жылу энергиясын есептеу құралдарын соңғы жылдары орната бастады. Жылу шығынын және оның құнын есепке алу мақсатына байланысты мәселелер қазіргі уақытта өте маңызды. Қарастырылып отырған коммерциялық жылу есептеу торабы жылу есептегішпен, масса немесе жылу тасымалдағыштың көлемі есептегішімен, қысым және температура датчиктерімен қамтылған. Жылу энергиясы үшін энергияны үнемдеуде біз тек есептеуіштің көрсеткіші бойынша есептеу жүргізуіміз керек, себебі тек пайдаланылған жылу үшін төлеуіміз қажет. Тұрғын үйді жылу есептеу құралдарымен жабдықтау кезінде жылу энергиясы мен пайдаланылған ыстық судың төлем ақысы тұтынушылар үшін тиімді болғаны анықталды.

Кілт сөздер: жылуды есепке алу, жылу энергиясы, жылумен жабдықтау, шығын есептеуіші, жылутасымалдаушы.

А.К. Хасенов, Б.Р. Нусупбеков, Д.Ж. Карабекова,
М. Стоев, Б.К. Зейнолла, А.К. Муратова

Экономия расходов энергии тепла при обеспечении жильцов теплом и горячим водоснабжением

В статье приведены данные о количестве тепла при обеспечении потребителей теплом и горячей водой. Установка счетчиков тепловой энергии необходима для повышения уровня жизни населения за счет эффективного использования тепловой энергии. Для учета расхода тепла при теплоснабжении и горячем водоснабжении потребителей используются различные приборы. В жилых домах приборы учета тепловой энергии начали устанавливать в последние годы. Вопросы, связанные с целью учета расхода тепла и его стоимости, в настоящее время очень важны. Рассматриваемый коммерческий узел учета тепла включает в себя: теплосчетчик, счетчик массы или объема теплоносителя, датчики давления и температуры. Чтобы сэкономить энергию для тепловой энергии, нам нужно только рассчитать счетчик, потому что мы должны платить только за использованное тепло. При оснащении жилого дома приборами учета тепла наблюдалось, что оплата за тепловую энергию и использованную горячую воду для потребителей была выгодной.

Ключевые слова: учет тепла, тепловая энергия, теплоснабжение, счетчик расхода, теплоноситель.

References

- 1 Degtiarenko, A.V. (2010). *Teplosnabzhenie [Heat supply]*. Tomsk: TSUAB [in Russian].
- 2 Magadeev, V.Sh. (2013). *Istochniki i sistemy teplosnabzheniia [Heat sources and systems]*. Moscow: Enerhiia [in Russian].
- 3 Pribory ucheta teplovoi ennerhii [Metering devices of thermal energy]. *vodavdome.website* Retrieved from <https://vodavdome.website/santehnika-i-vodoprovod/schetchiki/pribory-uchyota-teplovoj-energii.html>
- 4 Vysotskaia, N.V. (2010). *Teplosnabzhenie [Heat supply]*. Ukhta: USTU [in Russian].
- 5 Eremkin, A.I., & Koroleva, T.I. (2000). *Teplovoi rezhim zdanii [Thermal regime of buildings]*. Moscow: ASV [in Russian].
- 6 Sharapov, V.I., & Rotov, P.V. (2007). *Rehulirovanie nahrzki sistem teplosnabzheniia [Load regulation of heat supply systems]*. Moscow: Novosti teplosnabzheniia [in Russian].
- 7 Metodicheskie ukazaniia po vyboru, montazhu i ekspluatatsii priborov kommercheskoho ucheta v sistemakh teplosnabzheniia [Guidelines for the selection, installation and operation of commercial metering devices in heat supply systems]. *www.zhkh.kz* Retrieved from [http://www.zhkh.kz/ntd/ntd-2011/24 %20Издание_титул%20Приборы%20комерч%20учета.pdf](http://www.zhkh.kz/ntd/ntd-2011/24%20Издание_титул%20Приборы%20комерч%20учета.pdf)

K.M. Shaimerdenova¹, E.R. Schragger², A.S. Tussypbaeva¹, Zh.K. Nausharban¹

¹*Ye.A. Buketov Karaganda State University, Kazakhstan;*

²*National Research Tomsk State University, Russia*

(E-mail: gulzhan.0106@mail.ru)

Investigation of heat exchange processes in vertically arranged heat exchangers

Today, in many countries, electricity is produced in a variety of ways, depending on current trends. The use of heat pump technology in heat energy development is one of the most efficient energetic methods. In order to save energy, it makes possible to use heat of subsurface water, reservoirs, natural water flows, etc. The environmental effectiveness of this technology is that it helps to prevent greenhouse gas emissions caused by combustion. Therefore, it is the use of gas and liquid fuel in the system that is one of the main and actual problems of operating heat pumps, but not replacement of old boilers. It will not only reduce fuel consumption, but also reduce carbon dioxide emissions to the atmosphere. In the laboratory of «Unconventional Energy Sources», experiments were conducted on an assembled test bench to study heat exchange processes taking place in a ground heat exchanger. The temperature distribution data in the vicinity of a U-shaped ground heat exchanger was experimentally specified. They showed temperature changes around the pipe in the ground. Using the obtained data, dependency graphs were constructed. The temperature change depending on different moisture content of the sand was determined. The temperature variation dependency graph with temperature difference of different moisture content was plotted.

Keywords: heat transfer, heat exchange, ground, temperature sensor, heat exchanger, energy.

Introduction

At present, the search and active use of new alternative energy sources in many developed countries of the world are considered as vital, strategically necessary resources ensuring the prospective development of the economies of these countries. Therefore, the modern development of the energy sector of the Republic of Kazakhstan is characterized by a radical rearrangement of the fuel and energy sector structure. This is due to the increase in prices of fossil fuel in the world market, the aggravation of environmental problems. One of the effective ways to solve this problem is the introduction of less energy-consuming new technology, which will be a source of non-traditional renewable energy.

The advantage of applying heat supply technology using non-conventional energy sources over technologies with traditional energy sources is the reduction of energy consumption during heat supply, new opportunities for an environmentally friendly and autonomous heat supply system.

To use low-grade ground heat it is necessary to prepare well holes to install heat exchangers of a heat pump. Various drilling methods can be used to obtain horizontal and vertical wells. A horizontal ground heat exchanger is installed near the building, at a shallow depth. The use of such ground heat exchangers is limited by the size of the available area. The vertical ground heat exchanger works effectively in almost all types of geological media, with the exception of low thermal conductivity grounds, for example, dry sand or dry gravel. Systems with vertical ground heat exchangers got widespread use.

The most effective and widely used among such devices are heat pumps [1]. Heat pumps are our source of energy for heating and hot water supply. Heat carrier is a very convenient, cost-effective and environmentally friendly heating system. The main difference from other generators is that they generate thermal energy using, for example, electricity, gas, and so on. In the production of heat using heat pumps, 75 % of the energy comes from the environment, and the remaining 25 % is electrical energy for the operation of the heat pump compressor. In other words, the owner of the heat pump saves 70 % of the costs.

Today, heat pumping units are an effective tool for energy saving, as prices for various types of fuel and electricity have increased. The use of heat pumping units for the needs of heat supply makes it possible to use significant economic and environmentally friendly technologies that do not cause carbon dioxide and other harmful substances emission to the atmosphere. Since the first use of heat pumps in a heating system, gas boilers have proved that they are economically unable to compete. As a result, heat-absorbing units have tended to replace other types of heat supply.

As a low-cost heat source in heat pumping units, industrial and clarified domestic wastewater, geothermal and artesian heat, subsurface heat and solar energy heat and so on are used.

The heat carrier is installed horizontally and vertically under the ground. Vertical heat exchangers in the depths make it possible to use low grade thermal energy of the ground (10–20 m from the ground level). The heat carrier circulates through pipelines laid in the ground at a depth of 25–200 m. The heat of the environment is supplied with water and antifreeze. The solidification point is approximately 13 °C. This keeps the solution from freezing during the process of operation [2].

The solution is pumped by a circulating pump and is used to heat the building using a heat pump and heat insulation, therefore the surface of the heat exchanger must be adapted to the influence of sunlight. It is made of heat-exchanging polyethylene or metal-reinforced plastic pipes below the surface. Their diameter ranges from 25 to 40 mm.

In this regard, the purpose of the work is to study the temperature pattern of sandy soil around the heat exchange tubes. To achieve the goal, the time-temperature change was studied at different mass concentrations of water. The time history graphs of experimental works on dry sandy ground of different moisture content are presented.

Research technique

The research methods were the analysis of domestic and foreign methods of using heat pumps, obtaining parameters of drilling well holes by mechanical and electric pulse method intended for the installation of heat exchangers by an experimental method and the method for research of the heat exchange process of underground heat exchangers. Heat exchanger well holes, made by means of electric hydropulse technology, can improve heat exchange processes in heat exchangers and increase heat removal [3].

Installed in ready-made well holes using electric hydropulse technologies, exchanger in the laboratory of «Unconventional energy sources» experiments were conducted on the assembled test bench to study heat exchange processes in the ground heat exchanger. The initial parameters were as follows:

Initial ground temperature: $t = 10$ °C;

Environment temperature: $t = 23$ °C;

The diameter of the U-shaped vertical ground heat exchanger: $D/d = 32/25$ mm.

The experiments were carried out at different ground conditions for a closer approximation to the natural conditions of the ground heat exchanger.

The main requirements for the quality of the experimental setup were uninterrupted power supply sources of constant thermal energy at the well and the possibility of taking high temperature accuracy and heat consumption metering. In order to monitor the temperature, heat sensors were installed vertically along the pipe and in the middle of the U-shaped heat exchanger. They show temperatures in the ground and in the vicinity of the pipe. During the experiment, heat sensors measured the temperature in several locations, in particular at different distances from the U-shaped pipe, at the outlet and at the U-bend pipe turn.

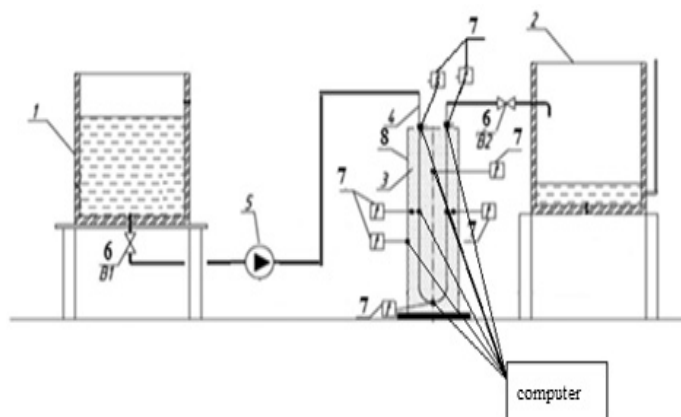
The readings of temperature sensors inside the well hole were found using the Temp Keeper program. The Temp Keeper program is designed to monitor and control the temperature and moisture content of various objects or environments in which sensors will be placed. This program makes it possible to visually observe the changes taking place, as well as to monitor whether the specified parameters are normal, warning you with an audible signal if necessary.

Figure 1 shows a test bench for studying the process of heat transfer in vertical heat exchangers.



Figure 1. The experimental test bench

Figure 2 shows a diagram of the test bench for studying the heat exchange processes in ground heat exchangers.



1 — water storage tank; 2 — tank for measurements; 3 — ground; 4 — U-shaped vertical heat transfer section with ground; 5 — circulation pump; 6 — valve (B1, B2); 7 — electronic sensors for temperature control; 8 — wooden case

Figure 2. The diagram of the test bench for studying heat exchange processes in ground heat exchangers

Investigation results

Initially, the temperature change at different radial distances in dry soil was determined. During the flow of cold water through the U-shaped pipe at a speed of 0.098 m/s, readings of thermal sensors located at different distances were taken every 10 minutes. They showed temperature changes around the pipe in the ground. Using the data obtained during the tests, dependency graphs were constructed. Figure 3 shows the change in temperature history distribution [4].

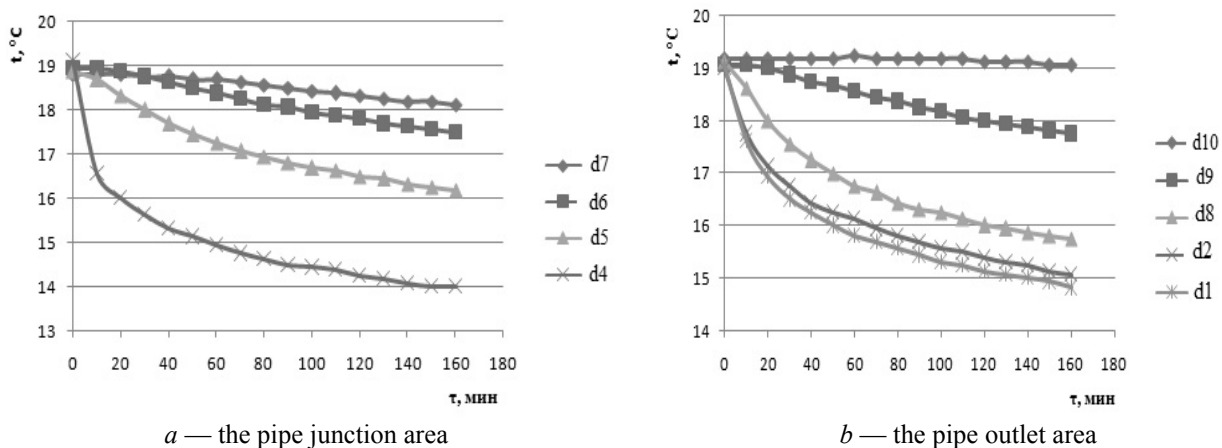


Figure 3. Change in temperature history distribution (dry soil)

The ground temperature around the pipe over the course of time falls relatively faster than the ground temperature at a distance from the pipe. The temperature at the pipe outlet is higher than the temperature at its inlet; this is due to heat transfer from the ground to the pipe.

The ground of the surface layers of the Earth is actually a heat accumulator of unlimited capacity, the thermal conditions of which is formed under the influence of two main factors: solar radiation and the flow of radiogenic heat coming from the earth's interior. When heat is removed, the temperature of the ground around the ground heat exchanger decreases. Particular attention should be paid to the influence of the moisture content of the soil mass and the migration of moisture in its pore space on the thermal processes that determine the characteristics of the ground as a source of low-grade heat energy [5].

Since the heat in the ground is transmitted mainly through solid particles, water and air, as well as upon contact of the particles, the heat conduction largely depends on the mineralogical and granulometric composition, moisture and air content and density. It is known that the heat conduction increases sharply with increasing soil moisture content, since the heat conduction of air, displaced by water from the pores of the rock, is approximately 30 times less than the heat conduction of water. When all the pores are completely filled with water, the thermal conductivity of the soil reaches its maximum value. The larger the mechanical elements, the greater the thermal conductivity. Thus, the thermal conductivity of coarse-grained sand with the same porosity and moisture content twice as much as the coarse dust fraction. In terms of thermal conductivity, the solid phase of the soil is about 100 times greater than air; therefore, loose ground has a lower thermal conductivity coefficient.

The thermal conductivity of soil to a lesser extent depends on the temperature change; in the temperature range from -50 to $+50$ °C it affects the interporous convection; in addition, the thermal conductivity coefficient can change by 25 %, while increase in the grain size from dust to coarse sand results in the rise of thermal conductivity by 2 times. For this reason, the experiment was repeated in the ground with a mass concentration of water of 1 %, 3 % and 7 %.

Figures 4–6 show temperature history distributions in a U-shaped pipe located in the ground with a mass concentration of moisture of 1 %, 3 % and 7 %.

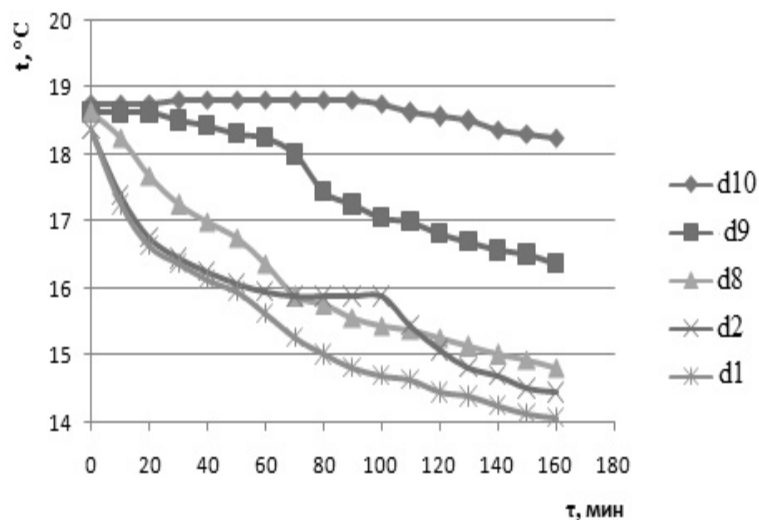


Figure 4. Temperature history distribution (moisture content of 1 %)

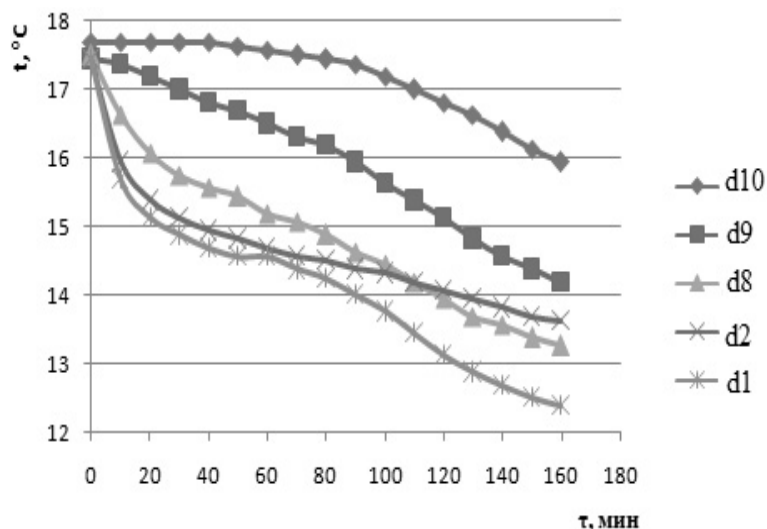


Figure 5. Temperature history distribution (moisture content of 3 %)

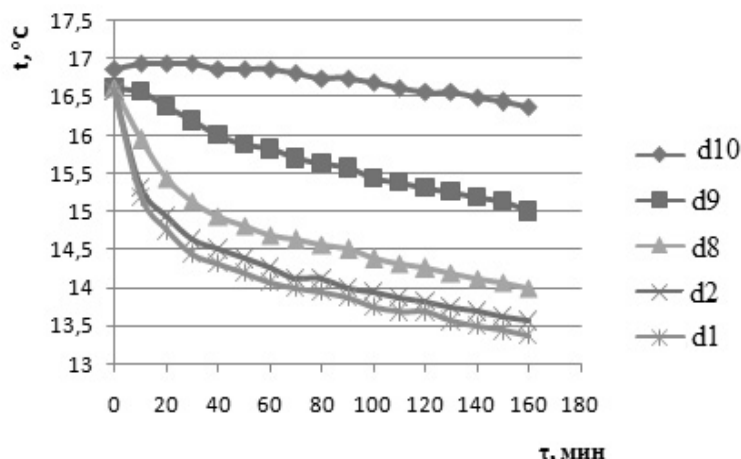


Figure 6. Temperature history distribution (moisture content of 7 %)

As one can see in the figure, the sand temperature gradually decreases, and this means that the sand transfers its heat to the pipe with ice water.

Based on the results of the performed work, the following conclusions can be drawn. In dry sand, the temperature changes within an hour and a half from 19 °C to 15 °C, and in wet sand from 19 °C to 13.5 °C. It follows that wet sand increases heat removal. After half an hour, the temperature change stabilizes. The temperature difference of the sand decreases with increasing moisture content (Fig. 7).

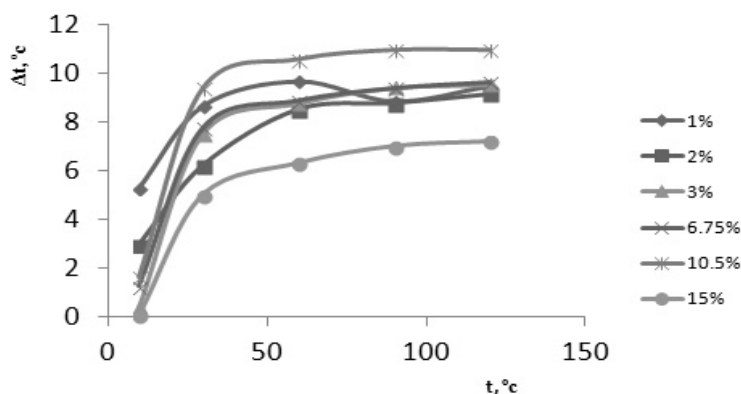


Figure 7. Dependency graph of temperature changes with temperature differences of different moisture content

The figure shows that with increasing moisture content, the temperature difference of the sand gradually increases. The reason for this is that when the sand is wet, water fills the air spaces inside the sand and facilitates the heat exchange. Therefore, when the sand moisture increases, heat is transferred to the pipe. That is, the higher the moisture content, the higher the temperature.

Since at present there are no standard heat exchangers for extracting heat from the ground, such systems should be designed for each specific object separately. It should be noted that from the point of view of thermal physics, ground is a rather complex system. By experimental studies at the test benches, the authors obtained the dependences of temperature histories of dry and wet sand and the temperature distribution in the sand in the vicinity of the polyethylene pipe. The carried out experiments confirmed that the temperature change in dry ground is greater than in wet one.

Thus, in capillary-porous systems, such as the soil mass of the heat removing system, moisture in the pore space has a noticeable effect on the process of heat distribution. The value of the equivalent thermal conductivity of moistened sand is higher than that of moistened clay, and it increases with increasing moisture content from 1 to 7 %. The thermal conductivity of clays varies from 2 to 4 W/(m·°C), and for sand it is from 5 W/(m·°C) and greater. The wetter the sand, the higher the thermal conductivity.

References

- 1 Сибикин Ю.Д. Нетрадиционные и возобновляемые источники энергии: учеб. пособие / Ю.Д. Сибикин, М.Ю. Сибикин. — М.: КНОРУС, 2010. — 232 с.
- 2 Амерханов Р.А. Тепловые насосы и их роль в решении проблем энергосбережения и защиты окружающей среды / Р.А. Амерханов // Менеджер-эколог. — 2008. — № 3. — С. 65–68.
- 3 Шуюшбаева Н.Н. Электрогидроимпульсная технология бурения скважин при различных геологических разрезах / Н.Н. Шуюшбаева, К. Кусаинов, Б.А. Ахмадиев, Г.С. Алтаева, Г.К. Шокимова // Знание. — 2015. — № 11–1. — С. 33–38.
- 4 Kusaiyov K. Study of the Heat-Transfer Processes of Tubular Elements of Ground Heat Exchangers / K. Kusaiyov, N.N. Shuyushbayeva, K.M. Shaimerdenova, Zh.G. Nurgalieva, N.N. Omarov // Journal of Engineering Physics and Thermophysics. — 2015. — Vol. 88, No. 3. — P. 676–680.
- 5 Kusaiyov K. Technical Physics / K. Kusaiyov, N.N. Shuyushbayeva, K.M. Shaimerdenova, B.R. Nusupbekov. — Pleiades Publishing, 2017. — Vol. 62, No. 6. — P. 867–870.

К.М. Шаймерденова, Э.Р. Шрагер, А.С. Тусыпбаева, Ж.К. Наушарбан

Тік орналасқан жылуалмастырғыштардағы жылу алмасу үрдістерін зерттеу

Қазіргі таңда заман ағымына сай көптеген елдерде электр энергиясын әртүрлі жолдармен өндіруде. Жылу энергиясын өндіруде жылу сорғылары технологиясын қолдану ең тиімді энергетикалық әдістердің бірі болып табылады, яғни энергия үнемдеу мақсатында жер қойнауы жылуын, су асты суларын, су қоймаларын, табиғи су ағындарын және т.б. пайдалануға мүмкіндік береді. Бұл технологияның экологиялық тиімділігі, отын жану кезінде пайда болатын парникті газдардың сыртқа толығымен таралып кетуін болдырмауға жағдай туғызатындығынан көрінеді. Сондықтан жүйеде газ және сұйық отындарды пайдалану кезінде ескі қазандықтарды алмастырудан гөрі, жылу сорғыларының жұмыс істеу принциптері басты және өзекті мәселелердің бірі болып табылады. Ол қазу негізінде алынған отынды тұтынудың деңгейін қысқартып қана қоймай, атмосфераға бөлініп шығатын көмірқышқыл газының мөлшерін анағұрлым азайтады. «Дәстүрлі емес энергия көздері» зертханасында топырақ жылу алмастырғышында кездесетін жылу беру процестерін зерттеу үшін эксперименталды сынақ стендіде эксперименттер өткізілді. U-тәрізді топырақ жылу алмастырғыштың маңында температураны бөлу эксперименттік түрде анықталды. Олар жердегі құбырдағы температура өзгерістерін көрсетеді. Алынған деректер бойынша, тәуелділік графиктері құрылды. Температураның өзгеруі құмның ылғалдылығына байланысты анықталды. Әртүрлі ылғалдылықтағы температура айырмашылығына температура өзгерісінің графигі тұрғызылды.

Кілт сөздер: жылуалмастырғыш, жылусорғыш, жер, температура датчигі, жылуалмасу, энергия.

К.М. Шаймерденова, Э.Р. Шрагер, А.С. Тусыпбаева, Ж.К. Наушарбан

Исследование процессов теплообмена на вертикальных теплообменниках

Сегодня во многих странах электроэнергия вырабатывается различными способами, в зависимости от современных тенденций. Использование технологии теплового насоса в тепловой энергии является одним из наиболее эффективных энергетических методов. С целью энергосбережения позволяет использовать подповерхностное тепло подводных вод, водохранилищ, природных водных потоков и т.д. Экологическая эффективность этой технологии заключается в том, что она помогает предотвратить выбросы парниковых газов в результате сгорания. Поэтому использование газа и жидкого топлива в системе является одной из основных и актуальных проблем эксплуатации тепловых насосов, а не замены старых котлов, что не только сократит потребление топлива, но и уменьшит количество выбросов углекислого газа в атмосферу. В лаборатории «Нетрадиционные источники энергии» были проведены эксперименты на собранном экспериментальном стенде для исследования процессов теплообмена, протекающих в грунтовом теплообменнике. Экспериментально определено распределение температуры в окрестности U-образного грунтового теплообменника. Они показывают изменения температуры вокруг трубы в грунте. По полученным данным были построены графики зависимости. Было определено изменение температуры в зависимости от различной влажности песка. Построен график зависимости изменения температуры с разницей температуры различной влажности.

Ключевые слова: теплоотдача, теплообмен, грунт, датчик температуры, теплообменник, энергия.

References

- 1 Sibikin, Yu.D., & Sibikin, M.Yu. (2010). *Netraditsionnye i vozobnovliaemye istochniki enerhii [Unconventional and renewable energy sources]*. Moscow: Knorus [in Russian].
- 2 Amerkhanov, R.A. (2008). Teplovye nasosy i ikh rol v reshenii problem enerhosberezheniia i zashchity okruzhaiushchei sredy [Heat pumps and their role in solving problems of energy saving and environmental protection]. *Menedzher-ekoloh — Environmental Manager*, 3, 65–68.
- 3 Shuyushbaeva, N.N., Kusaiynov, K., Akhmadiev, B.A., Altaeva, G.S., & Shokimova, G.K. (2015). Elektrohidroimpulsnaia tekhnolohiia bureniia skvazhin pri razlichnykh heolohicheskikh razrezakh [An electric hydropulse well drilling technology for various geological sections]. *Znanie — Knowledge*, 11–1, 33–38.
- 4 Kusaiynov, K., Shuyushbayeva, N.N., Shaimerdenova, K.M., Nurgalieva, Zh.G., & Omarov, N.N. (2015). Study of the Heat-Transfer Processes of Tubular Elements of Ground Heat Exchangers. *Journal of Engineering Physics and Thermophysics*, 88, 3, 676–680.
- 5 Kusaiynov, K., Shuyushbayeva, N.N., Shaimerdenova, K.M., & Nusupbekov, B.R. (2017). *Technical Physics*. Pleiades Publishing, 62, 6, 867–870.

I. Hevko¹, O. Lyashuk¹, M. Sokil², L. Slobodian¹, V. Hud¹, Yu. Vovk¹

¹*Ternopil Ivan Puluj National Technical University, Ukraine;*

²*Lviv Polytechnic National University, Ukraine*

(E-mail: oleglashuk@ukr.net)

Resonant oscillation of vertical working part of conveyer-loader

The experimental equipment for testing the screw loader of bulk materials with horizontal and vertical branches was designed and manufactured, which allows to determine the process productivity and power consumption according to the developed methods. Experimental equipment is equipped with laboratory equipment, which ensures the change of investigated processes in wide ranges with high accuracy in the automated control mode with the fixation of necessary research results. On the basis of mathematical models, the dependences of the angular velocity of perturbation on the physico-mechanical and geometric parameters of the system of branches and the angular velocity of SWP are obtained. It was established that the resonance dynamic stresses at significant angular velocities exceed several times the resonant stresses of a «static elastic body» (which does not rotate), which makes it possible to take into account when choosing a dynamic coefficient of strength. With the same physical-mechanical and geometric characteristics of an elastic body, the resonance for larger values of the angular velocity of its rotation takes place for a smaller frequency of external periodic perturbation.

Key words: mathematical model, amplitude, resonance, conveyer.

Introduction

The technical means of continuous transportation of friable materials are the basis of the complex mechanization of loading and unloading operations, which increase the productivity and efficiency of production processes. The specific gravity of spiral conveyors in loading and unloading works of most construction, road, agricultural, processing and other machines, which is about 40–50 %.

It is known that resonant oscillations are the most dangerous modes of operation of machines and equipment. They are characterized by a significant increase in the amplitude of oscillations, and hence dynamic loads. Therefore, these operating modes greatly reduce the operating life of the machine. If, in some cases, resonance phenomena cannot be avoided, then, by choosing the system parameters, they try to provide a minimum amplitude increase during the transition through the resonance. Therefore, the question of resonance oscillation research is of vital importance for the improvement of their structures.

Analysis of recent research and publications. The interaction of auger mechanisms with agricultural materials, as well as the choice of rational parameters of GTTM and their modes of operation, were investigated by M.P. Vasylenko [1], B.M. Gevko [2, 3], P.M. Zaika [4], R.M. Rogatinsky [5, 6], I.M. Zuyev [7], V.L. Kulikovsky [18] and others.

The problems of determining the rational operating modes and constructive parameters of the GTTM are devoted to the work of R.L. Zenkov [8–11], A.M. Grigoriev [12–14], B.M. Gevko [3], K.V. Alferov [8], H.A. Khailis [15], V.I. Plavinsky [16], N.V. Ostapchuk [17, 18], O.R. Rogatinskaya [19], I.M. Khorolsky [20].

Questions of substantiation of the parameters of oscillations of mechanical systems are devoted to the works of I.M. Babakov [21], O.A. Goroshko [22], P.D. Dotsenko [23], M.P. Martyntsev [24], M.A. Pavlovsky [25], S.N. Nikiforov [26], Yu.A. Mitropolsky [27], M.M. Bogolyubov [28], and others. However, issues relating to the improvement of the structures of the spiral mechanisms themselves and their working parts need further research. Investigating the resonant oscillations of the vertical working part of the conveyer loader.

Material and method

For carrying out the experimental researches of productivity of spiral loader with a working part the stand [29] was used, the general view of which is depicted in Figure 1. Stand for the study of the overload of friable materials from a horizontal to a vertical axis, made in the form of a frame 1, a cylindrical horizontal spiral working part 2 with a central shaft 3 and a vertical groove 4 with a vertical spiral working part 5. A cylindrical and horizontal groove of spiral working part 2 is rigidly mounted on the stand 6 on the frame 1. Below there is a vertical groove 4 is a perpendicular to its axis a rotary connection sleeve 7 which, in a known manner, performs the angle of rotation of the vertical groove 4. From above, at the entrance to the cylindrical horizontal spiral working part 2, a bunker 8 with a friable material 9 is rigidly installed.

The stand is equipped with a driven actuator 10 with a cylindrical horizontal spiral working part 2 and a vertical spiral working part 5 through the pass transmissions 11 and 12 and on the additional T-shaped transmission gear 13. At this productivity of the vertical spiral working part 5 should be no less than the productivity of the cylindrical horizontal working part 2, in order not to jamming the technological process. At the top of the vertical groove 4, a loading window 14 with a tray under which the tank 15 is installed for collecting friable material from the vertical section is made. In addition, at the bottom of the cylindrical end the horizontal working part 2, the initial window 16 with a crossbar for measuring the productivity of the horizontal section was made. Under the outlet there is a container 17 for collecting friable material that the horizontal section moves.

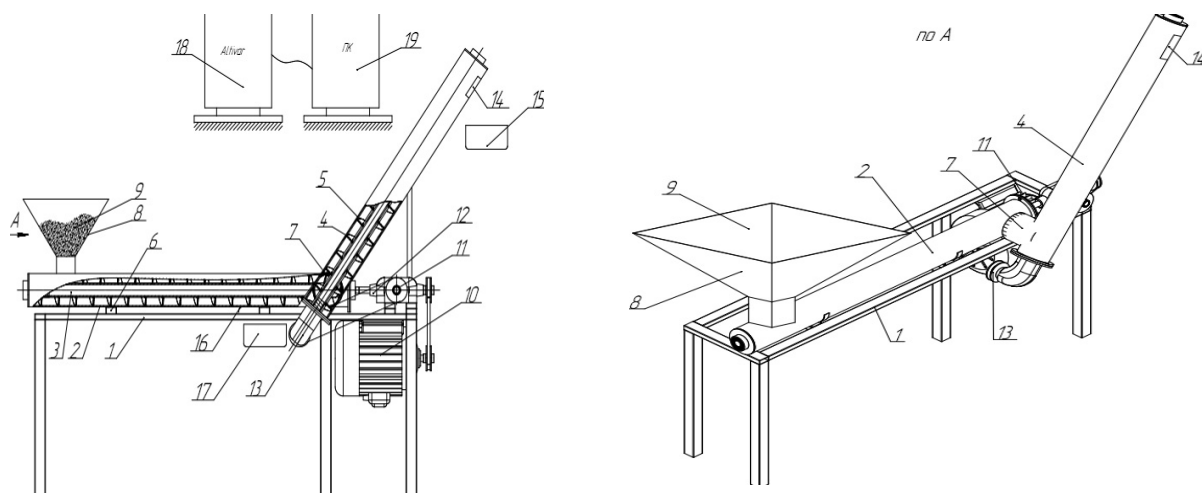


Figure 1. Stand to investigate the overload of friable materials from the horizontal to the vertical line

In addition, the steps of the cylindrical horizontal spiral working part are evenly enlarged in the direction of exit of material from it.

In addition, the stand is equipped with control devices Altivar 7.1 and a personal computer 19 for measuring power, kinematic and technological parameters.

The work of the stand to study the overload of friable materials from a horizontal to a vertical branch is carried out as follows. To study the performance of the horizontal section, open the switch under the capacity of 17, fix the time and determine the performance. To establish the performance of the horizontal and vertical sections, the shutter is closed on the horizontal section and all the friable material is transported through window 14 into a container 15 that weighs and performs the analysis.

The design of the test facility (Fig. 2) includes a spiral-mixer driven from a personal computer (PC) through a frequency converter (Altivar series) 3. The spiral mixer consists of a frame, with the possibility of axial rotation and change of the angle of inclination of the body, in which there is a working part driven by a

three-phase asynchronous electric motor (AIP90L4Y3), is located in relation to the horizon through the support. In the case the bunker and loading and unloading holes are fixed — exits, in which a recessed pipe is installed. The engine is equipped with a sensor for motor shaft rotation frequency (E40S6–10Z4–6L-5) 13.

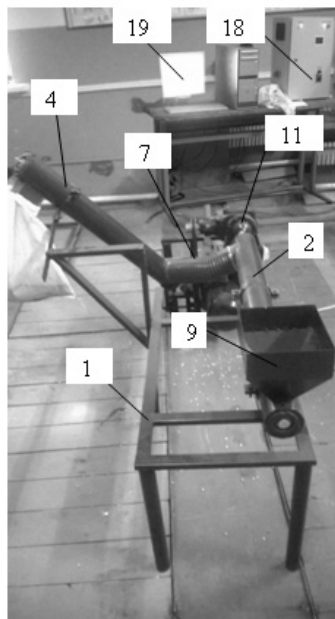


Figure 2. The general view of the spiral loader

It is known [14] that resonant modes of operation of machines and equipment are the most dangerous. They are characterized by a significant increase in the amplitude of oscillations, and hence dynamic loads. Therefore, these operating modes greatly reduce the operational terms of machines (we are not talking about special machines principle of operation of which is based on resonant phenomena). If, in some cases, it is not possible to avoid resonant phenomena, then try at the expense of choosing the system parameters to provide the minimum value (growth) of the amplitude during the transition through the resonance. Where it follows that the study of the resonant phenomena of the horizontal working body of the loader mixer has not only theoretical, but also practical value.

From the condition of existence of resonant oscillations, which for the case of the main bending working part can be written in the form:

$$\nu \approx \Omega - \frac{3\mu \pi^2 a^2}{32 l^2 \Omega} + \left(\frac{\pi}{l}\right)^2 \frac{m}{m + \rho} \frac{u^2}{8\Omega}. \quad (1)$$

Thus, the resonance phenomenon for different values of the velocity of the grain mixture, its linear mass, and the various angular velocities of the rotation of the horizontal working part will occur at different frequencies of external perturbation. As noted above, the real effect of small amplitudes of transverse vibrations of the horizontal box of the mixer loader on its own frequency is negligible. From the above, it follows that the dominant role of entering the resonance is played by: the angular velocity of rotation of the working part, the speed of the grain mixture and its mass. Thus, for different values of these parameters, the amplitude of the transition through the resonance will take different values. In addition, as shown in [14], the amplitude of passage through the resonance depends on the phase difference between the proper and the forced oscillations, in our case $\varphi = \psi - \theta$. The first resonance approximation for the above-described boundary-value problem will be sought in the form of an asymptotic representation, but in contrast to the nonresonance case, the amplitude in the transition through the resonance is determined by the relation of the form

$$\frac{da}{dt} = \mu A_1(a, \phi), \quad (2)$$

$$\frac{d\varphi}{dt} = \Omega - \nu + \mu B_1(a, \varphi), \quad \varphi = \psi - \theta.$$

The problem is to determine this type of functions, taking into account (1), (2), for the first approximation, satisfied the basic equation. Acting in the same way as for a nonresonant case, taking into account (3), we find

$$\begin{aligned} \frac{\partial y}{\partial t} &= \mu A_1(a, \phi) (\cos(\kappa x + \psi) - \cos(\kappa x - \psi)) - \\ &- a(\Omega + \mu B_1(a, \phi)) (\sin(\kappa x + \psi) + \sin(\kappa x - \psi)) + \mu \frac{\partial y}{\partial \theta} \nu + \mu \frac{\partial y}{\partial \psi} \Omega \\ \frac{\partial^2 y}{\partial t^2} &= \mu \frac{\partial A_1(a, \phi)}{\partial \phi} (\Omega - \nu) (\cos(\kappa x + \psi) - \cos(\kappa x - \psi)) - 2\mu \Omega A_1(a, \phi) (\sin(\kappa x + \psi) + \sin(\kappa x - \psi)) + \\ &+ \frac{\partial^2 y}{\partial \psi^2} \Omega^2 + \frac{\partial^2 y}{\partial \theta^2} \nu^2 + 2 \frac{\partial^2 y}{\partial \theta \partial \psi} \nu \Omega. \end{aligned} \quad (3)$$

The resulting ratio let you capture the differential equation that connects the unknown function as

$$\begin{aligned} L\left(\frac{\partial^2 y_1}{\partial \psi^2}, \frac{\partial^2 y_1}{\partial \theta^2}, \dots, \frac{\partial^4 y_1}{\partial x^4}\right) &= aV^2 \left(\frac{\pi}{l}\right)^2 \sin \frac{\pi}{l} x \cos \psi - \\ &- 2V \frac{\pi}{l} \cos \frac{\pi}{l} x \cos \psi + F(x, a, \psi, \theta) + \mu \sin \frac{\pi}{l} x \times \\ &\times \left(\cos \psi \left(-\frac{\partial A(a, \phi)}{\partial \phi} (\Omega - \nu) + 2a\Omega B \right) + \sin \psi \left(a \frac{\partial B(a, \phi)}{\partial \phi} (\Omega - \nu) + 2A(a, \phi) \Omega \right) \right). \end{aligned} \quad (4)$$

Thus, for a resonance case, the function must be a solution of the equation and satisfy homogeneous boundary conditions if represented as their form

$$y_1(x, a, \psi, \theta) = \sum \sin \frac{k\pi}{l} x Y_{1k}(a, \theta, \psi). \quad (5)$$

In this case, the coefficients of its decomposition $Y_{1k}(a, \theta, \psi)$ are bound by differential equations

a) for $k = 1$

$$\begin{aligned} \frac{\partial^2 Y_{11}}{\partial \psi^2} \omega^2 + 2 \frac{\partial Y_{11}}{\partial \psi \partial \theta} \nu \omega + \nu^2 \frac{\partial^2 Y_{11}}{\partial \theta^2} + (\alpha^2 \left(\frac{\pi}{l}\right)^4 + \omega^2) Y_{11} &= \\ = aV^2 \left(\frac{\pi^2}{2l}\right) \cos \psi + \frac{1}{p} \int_0^l \sin \frac{\pi}{l} x F(a, x, \theta, \psi) dx + \\ + \left(\cos \psi \left(-\frac{\partial A(a, \phi)}{\partial \phi} (\Omega - \nu) + 2a\Omega B \right) + \sin \psi \left(a \frac{\partial B(a, \phi)}{\partial \phi} (\Omega - \nu) + 2A(a, \phi) \Omega \right) \right). \end{aligned} \quad (6)$$

b) for $k \neq 1$

$$\begin{aligned} \frac{\partial^2 Y_{1k}}{\partial \psi^2} \omega^2 + 2 \frac{\partial Y_{1k}}{\partial \psi \partial \theta} \nu \omega + \nu^2 \frac{\partial^2 Y_{1k}}{\partial \theta^2} + (\alpha^2 \left(\frac{k\pi}{l}\right)^4 + \omega^2) Y_{1k} &= \\ = aV^2 \frac{(k\pi)^2}{2l} \cos \psi + \frac{1}{p} \int_0^l \sin \frac{k\pi}{l} x F(a, x, \theta, \psi) dx. \end{aligned} \quad (7)$$

In the same way as for a nonresonance case, the conditions for the absence of a function in the schedules $y_1(a, x, \psi, \theta)$, and hence in $Y_{1k}(a, \psi, \theta)$ ($k \neq 1$), the first harmonics ψ allow us to obtain relations that determine the right-hand side of the dependences (6)

$$(\Omega - \nu) \frac{\partial A}{\partial \phi} - 2a\Omega B = \frac{1}{p} \frac{1}{4\pi^2} \sum_s e^{is\phi} \int_0^l \int_0^{2\pi} F(a, x, \psi, \theta) \sin \frac{k\pi}{l} x e^{-is\phi} \cos \psi dx d\psi d\theta \quad (8)$$

$$a \frac{\partial B}{\partial \phi} (\Omega - \nu) - 2A\Omega + V^2 \frac{\pi^2}{l^2} = \frac{1}{p} \frac{1}{4\pi^2} \sum_s e^{is\phi} \int_0^l \int_0^{2\pi} F(a, x, \psi, \theta) \sin \frac{k\pi}{l} x e^{-is\phi} \cos \psi dx d\psi d\theta. \quad (9)$$

In the case when a spiral mixer operates a periodic perturbation which does not depend on its deflection, and small nonlinear forces are determined as for the case of their own oscillations, differential equations in the resonance region can look

$$\frac{da}{dt} = -\frac{\bar{\delta}}{m + \rho} (\Omega)^{s-1} a^s - \frac{2\mu H}{\pi(\Omega + \nu(t))} \cos \varphi \quad (10)$$

$$\frac{d\phi}{dt} = \Omega - \nu - \left(\frac{\pi}{l}\right)^2 \frac{mu^2}{8\Omega(m + \rho)} + \mu \left(\frac{2H}{\pi(\Omega + \nu(t))a} \sin \phi - \frac{3}{32} \frac{\pi^2 a^2}{l^2 \omega} \right).$$

Resonant phenomena of the working part, adversely affect the technological process of loading or moving the grain mixture, while reducing the life of the machine. To avoid it and to investigate the influence of a whole range of parameters on the process of its passage, it is necessary to construct for this case the solution of the mathematical model of the process

$$L_1(\xi, \zeta) = -\delta \left(\frac{\partial \xi}{\partial t} \right)^s - k_1 \frac{\partial^2}{\partial x_1^2} \left(\frac{\partial^2 \xi}{\partial x_1^2} \right)^3 + h \cos \theta, \quad (11)$$

$$L_2(\xi, \zeta) = -\delta \left(\frac{\partial \zeta}{\partial t} \right)^s - k_1 \frac{\partial^2}{\partial x_1^2} \left(\frac{\partial^2 \zeta}{\partial x_1^2} \right)^3 + h \cos \theta.$$

Provided:

$$p\mu \approx q\Omega_k \quad (12)$$

Similarly, as for the horizontal working part of the conveyor-loader, the differential equations describing the laws of variation of the amplitude of oscillations in the transition through the main resonance acquire the form

$$\begin{aligned} \frac{da}{dt} &= \frac{\mu}{4\pi l_1 \Omega} \left(\int_0^l \int_0^{2\pi} \bar{f}_1(a, x_1, \varphi + \theta, \theta) (\cos(\kappa x_1 + \varphi + \theta) - \cos(\kappa x_1 - \varphi + \theta)) d\theta dx_1 \right), \\ \frac{d\phi}{dt} &= \Delta - \frac{\varepsilon}{4\pi l_1 \Omega a} \left(\int_0^l \int_0^{2\pi} \bar{f}_1(a, x, \varphi + \theta, \theta) (\sin(\kappa x + \varphi + \theta) + \sin(\kappa x - \varphi + \theta)) d\theta dx_1 \right), \end{aligned} \quad (13)$$

where Δ — the imbalance between the frequencies of own and forced oscillations, thus $\Delta = \Omega - \mu$, and $\bar{f}_1(a, x_1, \varphi + \theta, \theta)$ correspond to the values of the right-hand sides of equations (11) under the condition that $\xi(x_1, \phi)$ and $\zeta(x_1, \phi)$ take the main values in the asymptotic representation of the solution.

Results

Figure 3 and Table represent the value of the amplitude of transverse oscillations during the transition through the main resonance for various numerical values of the parameters of the investigated system and the angular velocity of the rotation of the working part.

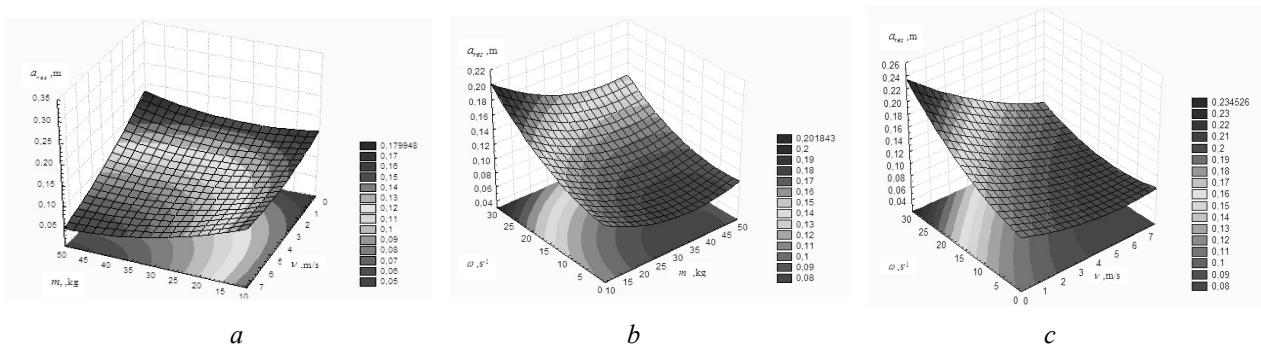


Figure 3. Graphic dependencies of the value of the growth factor of the amplitude when passing through the resonance due to the rotation of the working part

Different numerical values of the parameters of the investigated system and the angular velocity of the rotation of the working part represent the value of the amplitude of the transverse vibrations during the transition through the main resonance

m	ρ	l	w	Ω_{pez}	V = 0		V = 5 m/s		V = 7.5 m/s	
					a_{pez}	$\xi = \frac{a_{\text{pez} \omega=0}}{a_{\text{pez} \omega \neq 0}}$	a_{pez}	$\xi = \frac{a_{\text{pez} \omega=0}}{a_{\text{pez} \omega \neq 0}}$	a_{pez}	$\xi = \frac{a_{\text{pez} \omega=0}}{a_{\text{pez} \omega \neq 0}}$
kg/m	kg/m	m	s ⁻¹	s ⁻¹	m		m		m	
10	10	8	0	37.754	0.1121	–	0.1092	–	0.1023	–
10	10	8	10	27.754	0.1504	1.3427	0.1493	1.3672	0.1336	1.3056
10	10	8	15	22.754	0.1814	1.6184	0.1697	1.5540	0.1504	1.4702
10	10	8	20	17.754	0.2318	2.1240	0.2210	2.0238	0.1523	1.4438
20	10	8	0	31.285	0.1419	–	0.1291	–	0.1183	–
20	10	8	10	21.285	0.2211	1.5674	0.1813	1.4041	0.1451	1.2265
20	10	8	20	11.285	0.2381	1.6881	0.2232	1.7289	0.1961	1.6577
20	10	8	25	6.285	0.3306	2.3447	0.2987	2.3137	0.2510	2.127
10	10	6	0	64.134	0.0621	–	0.0601	–	0.0582	–
10	10	6	10	58.134	0.0731	1.1771	0.0681	1.1331	0.0622	1.0687
10	10	6	20	48.134	0.0884	1.4235	0.0841	1.3993	0.0763	1.3109
10	10	6	30	38.134	0.1101	1.7729	0.1036	1.7238	0.0943	1.6209
30	10	6	0	48.178	0.0938	–	0.0821	–	0.0634	–
30	10	6	10	38.178	0.1263	1.3475	0.1023	1.2434	0.0701	1.056
30	10	6	25	23.178	0.1984	2.1151	0.1381	1.6821	0.0893	1.4085
50	10	6	0	35.337	0.1436	–	0.0788	–	0.0411	–
50	10	6	10	29.337	0.1456	1.0139	0.0843	1.0698	0.0464	1.017
50	10	6	25	14.337	0.3061	2.1362	0.09210	1.1689	0.0493	1.023

Discussion

The obtained results allow asserting the following: the resonant amplitudes depend on the speed of the grain mixture, the angular speed of rotation of the working screw and the rate of change (in the resonant zone) of the frequency of the external periodic perturbation:

- for smaller values of the linear mass of the grain mix, the working screw and the higher speed of the transition through the main resonance, the value of the resonance amplitude is smaller;
- the growth rate of the amplitude in the transition through the resonance for the working part which rotates in comparison with the «stationary» its position is less for the case of more relative movement of the grain mixture.

Conclusion

On the basis of mathematical models, the dependences of the angular velocity of perturbation on the physico-mechanical and geometric parameters of the system of branches and the angular velocity of SWP are obtained. It is established that for larger values of the angular velocity of rotation of a working part, the resonant frequency value is smaller at $L=8$ m, $\Omega=17-40$ s⁻¹. For working parts of greater length, the amplitude of the transition through the resonance is greater than 10^{-25} s⁻¹ $L=8$ m and increases from 0,1121 to 0,2311 m. With an increase in the relative velocity of the transfer of the grain mixture leads to a decrease in the amplitude of the transition through the resonance at $m=50$ kg, the speed within 5...7,5 m/s decreases within 0,1023...0,0701 m. Design of screw loader designs, stand equipment and experimental installation using the Altivar 71 frequency converter and Power Suite v.2.5.0 software allowed to carry out a complex of experimental studies.

References

- 1 Василенко П.М. Механизация и автоматизация процессов приготовления и дозирования кормов / П.М. Василенко, И.И. Василенко. — М.: Агропромиздат, 1985. — 224 с.

- 2 Гевко Б.М. Научные основы разработки винтовых транспортирующим механизмов сельскохозяйственных машин: автореф. дис. ... д-ра техн. наук: спец. 05.20.04 — «Сельскохозяйственные и мелиоративные машины» / Б.М. Гевко. — Ростов н/Д., 1987. — 45 с.
- 3 Гевко Б.М. Винтовые подающие механизмы сельскохозяйственных машин / Б.М. Гевко, Р.М. Рогатынский. — Львов: Высш. шк., 1989. — 176 с.
- 4 Заика П.М. О выборе параметров винтовых транспортеров зерновых комбайнов / П.М. Заика // Сельхозмашины. — 1958. — № 2. — С. 22–24.
- 5 Рогатинский Р.М. Моделирование работы малогабаритного лопастно-винтового смесителя / Р.М. Рогатинский, И.Б. Гевко, Д.В. Дмитров // Сельскохозяйственные машины: сб. науч. ст. — Луцк, 2000. — Вып. 6. — С. 129–135.
- 6 Рогатинский Р.М. Механико-технологические основы взаимодействия шнековых рабочих органов с сырьем сельскохозяйственного производства: автореф. дис. ... д-ра техн. наук: спец. 05.20.01 — «Подъемно-транспортные машины», 05.05.05 «Механизация сельскохозяйственного производства» / Р.М. Рогатинский. — Киев, 1997. — 52 с.
- 7 Зуев И.М. Монтаж, эксплуатация и ремонт машин в животноводстве / И.М. Зуев, Э.П. Сорокин, А.В. Шпыро. — М.: Агропромиздат, 1988. — 447 с.
- 8 Алферов К.В. Бункерные установки / К.В. Алферов, Р.Л. Зенков. — М.: Машиностроение, 1975. — 307 с.
- 9 Зенков Р.Л. Механика насыпных грузов / Р.Л. Зенков. — М.: Машиностроение, 1973. — 220 с.
- 10 Зенков Р.Л. Бункерные устройства / Р.Л. Зенков. — М.: Машиностроение, 1972. — 182 с.
- 11 Зенков Р.Л. Машины непрерывного транспорта / Р.Л. Зенков, И.И. Ивашков, Л.Н. Колобов. — М.: Машиностроение, 1987. — 320 с.
- 12 Григорьев А.М. Комплексная механизация и автоматизация погрузо-разгрузочных и транспортных работ в машиностроении и приборостроении / А.М. Григорьев, П.А. Преображенский. — Киев: Наук. думка, 1967. — 116 с.
- 13 Григорьев А.М. Винтовые конвейеры / А.М. Григорьев. — М.: Машиностроение, 1972. — 184 с.
- 14 Григорьев А.М. Гибкие шнеки / А.М. Григорьев, П.А. Преображенский. — М.: Знание, 1967. — 98 с.
- 15 Хайлис Г.А. Основы теории и расчета сельскохозяйственных машин / Г.А. Хайлис. — Киев: Изд-во УСХА, 1992. — 240 с.
- 16 Машины непрерывного транспорта / под ред. В.И. Плавинского. — М.: Машиностроение, 1969. — 719 с.
- 17 Остапчук Н.В. Оптимизация технологических процессов на землелеперирабатывающих предприятиях / Н. В. Остапчук. — М.: Колос, 1974. — 144 с.
- 18 Остапчук Н.В. Основы математического моделирования процессов пищевых производств / Н.В. Остапчук. — Киев: Вища шк., 1981. — 304 с.
- 19 Рогатинская А.Р. Обоснование параметров нагрузки и конструкций винтовых конвейеров: автореф. дис. ... канд. техн. наук: спец. 05.05.05 — «Подъемно-транспортные машины» / А.Р. Рогатинская. — Тернополь, 2006. — 20 с.
- 20 Хорольский И.М. Динамика цепных систем и замкнутых контуров машин непрерывного транспорта / И.М. Хорольский. — Львов: Изд. ГУ «Львовская политехника», 1999. — 194 с.
- 21 Бабаков И.М. Теория колебаний / И.М. Бабаков. — М.: Наука, 1965. — 560 с.
- 22 Горошко О.А. О продольных колебаниях балки с подвижным экипажем / Горошко О.А. // Прикладная механика. — 1978. — Т. 14, № 8. — С. 70–78.
- 23 Доценко П.Д. В колебаниях и устойчивости прямолинейного трубопровода / П.Д. Доценко // Прикладная механика. — 1971. — Вып. 3. — С. 85–91.
- 24 Мартынцив М.П. Одно обобщение метода Д'Аламбера для систем, которые характеризуются продольным движением / М.П. Мартынцив, М.Б. Сокол // Науч. вестн: сб. науч.-техн. работ. — Львов: УДЛТУ, 2003. — Вып. 13.4. — С. 64–67.
- 25 Павловский М.А. Теоретическая механика / М.А. Павловский, Т.В. Путята. — Киев: Вища шк., 1985. — 328 с.
- 26 Никифоров С.Н. Сопротивление материалов / С.Н. Никифоров. — М.: Высш. шк., 1966. — 584 с.
- 27 Митропольский Ю.А. Асимптотические решения уравнений в частных производных / Ю.А. Митропольский, Б.И. Мосеенков. — Киев: Вища шк., 1976. — 84 с.
- 28 Боголюбов Н.Н. Асимптотические методы в теории нелинейных колебаний / Н.Н. Боголюбов, Ю.А. Митропольский. — М.: Наука, 1974. — 501 с.
- 29 Пат. № 128019. Украина, МПК (2006.01) В65G 33/00. Стенд для исследования перегрузки сыпучих материалов с горизонтальной на вертикальную ветвь / Ляшук А.Л.; Слободян Л.М.; Клендий В.М.; Марунич А.П.; заявители и патентообладатели Ляшук А.Л.; Слободян Л.М.; Клендий В.М.; Марунич А.П. — № u201803752; заявл. 06.04.2018; опубл. 27.08.2018, Бюл. № 16.

И. Гевко, О. Ляшук, М. Сокил, Л. Слободян, В. Гудь, Ю. Вовк

Винттік жұктіегіштің қозғалмалы жұмыс бөлігінің резонанстық тербелісі

Шашылатын нысандар үшін қолданылатын жұктіегіштің, өндіріс үдерісін және энергия шығынын белгілі әдіспен анықтауға мүмкіндік беретін, жылжылмалы бөлігі дайындалған. Эксперимент жүзінде жасалған бөлік зерттелетін үдерістің өзгерісін автоматты түрде аса жоғары дәлдікпен бақылап отыруға мүмкіндік береді. Математикалық әдістер көмегімен қарастырып отырған құрылымның бұрыштық жылдамдығының жүйенің физика-механикалық және геометриялық параметрлеріне тәуелділігі анықталған. Жоғарғы бұрыштық жылдамдыққа резонанстық динамикалық кернеу дененің

резонанстық статистикалық серпімділік кернеуінен бірнеше есе артып құрылғыға қауіп төндіруі мүмкін. Бұл жағдайды құрылғының динамикалық қауіпсіздігін есептегенде еске алу керек.

Кілт сөздер: математикалық модель, амплитуда, резонанс, транспортер.

И. Гевко, О. Ляшук, М. Сокил, Л. Слободян, В. Гудь, Ю. Вовк

Резонансные колебания мобильного рабочего органа винтового загрузчика

Спроектировано и изготовлено экспериментальное оборудование для испытания винтового загрузчика сыпучих материалов с горизонтальной и вертикальной ветками, которое позволяет определять производительность процесса и энергозатраты согласно разработанных методик. Экспериментальное оборудование оснащено лабораторным оборудованием, обеспечивающим изменение исследуемых процессов в широких диапазонах с высокой точностью в автоматизированном режиме управления с фиксацией необходимых результатов исследования. На основе математических моделей получены зависимости угловой скорости возмущения от физико-механических и геометрических параметров системы веток и угловой скорости винтового рабочего органа. Установлено, что резонансные динамические напряжения при значительных угловых скоростях вращения в несколько раз превышают резонансные напряжения «статического упругого тела» (которое не вращается), что предопределяет учёт динамического коэффициента запаса прочности. При тех же физико-механических и геометрических характеристиках упругого тела резонанс при больших значениях угловой скорости его вращения имеет место для меньшей частоты внешнего периодического возмущения.

Ключевые слова: математическая модель, амплитуда, резонанс, транспортер.

References

- 1 Vasilenko, P.M., & Vasilenko, I.I. (1985). *Mekhanizatsiia i avtomatizatsiia protsessov prihotovleniia i dozirovaniia kormov* [Mechanization and automation of the processes of cooking and dosing of fodders]. Moscow: Agropromizdat [in Russian].
- 2 Gevko, B.M. (1987). *Nauchnye osnovy razrabotki vintovykh transportiruiushchikh mekhanizmov selskokhoziaistvennykh mashin* [Scientific bases of development of screw conveying mechanisms of agricultural machines]. *Candidate's thesis*. Rostov-on-Don [in Russian].
- 3 Gevko, B.M., & Rogatynsky, R.M. (1989). *Vintovye podaiushchie mekhanizmy selskokhoziaistvennykh mashin* [Screw feeding mechanisms of agricultural machines]. Lvov: Vysshaia shkola [in Russian].
- 4 Zaika, P.M. (1958). *O vybere parametrov vintovykh transporterov zernovykh kombainov* [On the choice of parameters of screw conveyors of grain combines]. *Selkhoz mashiny — Farm Machines*, 2, 22–24 [in Russian].
- 5 Rogatynsky, R.M., Gevko, I.B., & Dmitrov, D.V. (2000). *Modelirovanie raboty malohabaritnogo lopastno-vintovogo smesitelia* [Modeling of the work of a small-sized lobed-and-screw mixer]. *Selskokhoziaistvennye mashiny — Agricultural machines*. Lutsk, 6, 129–135 [in Russian].
- 6 Rogatynsky, R.M. (1997). *Mekhaniko-tekhnologicheskie osnovy vzaimodeistviia shnekovykh rabochikh orhanov s syrem selskokhoziaistvennogo proizvodstva* [Mechanic-technological bases of interaction of screw working bodies with raw materials of agricultural production]. *Candidate's abstract*. Kiev [in Russian].
- 7 Zuyev, I.M., Sorokin, E.P., & Shpyro, A.V. (1988). *Montazh, ekspluatatsiia i remont mashin v zhivotnovodstve* [Installation, operation and repair of machines in animal husbandry]. Moscow: Agropromizdat [in Russian].
- 8 Alferov, K.V., & Zenkov R.L. (1975). *Bunkernye ustanovki* [Bunker installations]. Moscow: Mashinostroenie [in Russian].
- 9 Zenkov, R.L. (1973). *Mekhanika nasypanykh hruzov* [Mechanics of bulk cargo]. Moscow: Mashinostroenie [in Russian].
- 10 Zenkov, R.L. (1972). *Bunkernye ustroistva* [Bunker devices]. Moscow: Mashinostroenie [in Russian].
- 11 Zenkov, R.L., Ivashkov I.I., & Kolobov L.N. (1987). *Mashiny nepreryvnogo transporta* [Machines of Continuous Transport]. Moscow: Mashinostroenie [in Russian].
- 12 Grigoriev, A.M., & Preobrazhenskii, P.A. (1967). *Kompleksnaia mekhanizatsiia i avtomatizatsiia pohruzo-razhruchochnykh i transportnykh rabot v mashinostroenii i priborostroenii* [Integrated mechanization and automation of cargo handling and transport works in mechanical engineering and instrument making]. Kiev: Naukova dumka [in Russian].
- 13 Grigoriev, A.M. (1972). *Vintovye konveiry* [Screw Conveyors]. Moscow: Mashinostroenie [in Russian].
- 14 Grigoriev, A.M., & Preobrazhenskii, P.A. (1967). *Hibkie shneki* [Flexible screw]. Kiev: Znanie [in Russian].
- 15 Khailis, G.A. (1992). *Osnovy teorii i rascheta selskokhoziaistvennykh mashin* [Fundamentals of the theory and calculation of agricultural machines]. Kiev: USCA Publ. [in Russian].
- 16 Plavinsky, V.I. (Ed.) (1969). *Mashiny nepreryvnogo transporta* [Machines of continuous transport]. Moscow: Mashinostroenie [in Russian].
- 17 Ostapchuk, N.V. (1974). *Optimizatsiia tekhnologicheskikh protsesov na zemlepererabatyvaiushchikh predpriiatiakh* [Optimization of technological processes in land-processing enterprises]. Moscow: Kolos [in Russian].
- 18 Ostapchuk, N.V. (1981). *Osnovy matematicheskoho modelirovaniia protsessov pishchevykh proizvodstv* [Fundamentals of Mathematical Modeling of Food Processes]. Kiev: Vishcha shkola [in Russian].

- 19 Rogatinskaya, A.R. (2006). Obosnovanie parametrov nahruzki i konstruktzii vintovykh konveierov [Justification of the parameters of the load and structures of screw conveyors]. *Candidate's thesis*. Ternopol [in Russian].
- 20 Khorolsky, I.M. (1999). *Dinamika tsepnnykh sistem i zamknytykh konturov mashin nepreryvnoho transporta [Dynamics of chain systems and closed circuits of continuous transport machines]*. Lvov: Izd. GU «Lvovskaia politehnika» [in Russian].
- 21 Babakov, I.M. (1965). *Teoriia kolebanii [The theory of oscillations]*. Moscow: Nauka [in Russian].
- 22 Goroshko, O.A. (1978). O prodolnykh kolebaniikh balki s podvizhnym ekipazhem [On the longitudinal oscillations of the beam with a moving crew]. *Prikladnaia mekhanika — Applied Mechanics*, 14, 8, 70–78 [in Russian].
- 23 Dotsenko, P.D. (1971). O kolebaniikh i ustoichivosti pryamolineinogo truboprovoda [On oscillations and stability of rectilinear pipeline]. *Prikladnaia mekhanika — Applied Mechanics*, 3, 85–91 [in Russian].
- 24 Martyntsev, M.P., & Sokol, M.B. (2003) Odno obobshchenie metoda D'Alemberta dlia sistem, kotorye kharakterizuiutsia prodolnym dvizheniem [One generalization of the D'Alembert method for systems characterized by a longitudinal motion]. *Nauchnyi vestnik — Scientific herald* (Iss. 13.4). Lvov: UDLTIU, 64–67 [in Russian].
- 25 Pavlovsky, M.A., & Putiata, T.V. (1985). *Teoreticheskaia mekhanika [Theoretical mechanics]*. Kiev: Vishcha shkola [in Russian].
- 26 Nikiforov, S.N. (1966). *Soprotivlenie materialov [Materials Resistance]*. Moscow: Vysshiaia shkola [in Russian].
- 27 Mitropolsky, Yu.A., & Moseenkov, B.I. (1976). *Asimptoticheskie resheniia uravnenii v chastnykh proizvodnykh [Asymptotic Solutions of Equations in Private Derivatives]*. Kiev: Vishcha shkola [in Russian].
- 28 Bogolyubov, N.N., & Mitropolsky, Yu.A. (1974). *Asimptoticheskie metody v teorii nelineinykh kolebanii [Asymptotic methods in the theory of nonlinear oscillations]*. Moscow: Nauka [in Russian].
- 29 Lyashuk A.L., et al. (2018). Stend dlia issledovaniia perehruzki sypuchikh materialov s horizontalnoi na vertikalnuiu vetv [Stand for investigation of overload of bulk materials from horizontal to vertical branch]. *Patent № 128019, Ukraine. Bulletin No. 16* [in Russian].

A.A. Kashkanov¹, V.M. Diorditsa², V.Yu. Kucheruk³,
D.Zh. Karabekova⁴, A.K. Khassenov⁴, A.M. Sharzadin⁴

¹*Kharkiv National Automobile and Highway University, Ukraine;*

²*Vinnytsia Research Forensic Centre of the Ministry of Internal Affairs, Ukraine*

³*Vinnytsia National Technical University, Ukraine*

⁴*E.A. Buketov Karaganda State University, Kazakhstan*

(E-mail: a.kashkanov@gmail.com)

Inertial evaluation of the tyre-road interaction during emergency braking

An improved method of evaluation of the parameters of braking efficiency in vehicles of M1 category has been proposed for expert examination of motor vehicle accidents. This method is based on the control of parameters which are able to significantly influence the friction processes in the contact tyre-road area. These parameters were discovered in the course of analysis of theoretical approaches to the evaluation of the quality of tyre-road interaction, analytical formulas used for evaluation of the main braking parameters (deceleration, stopping distance) as well as for experimental evaluation of parameters of inertia braking efficiency. The generalization of study results showed that existing expert methods of evaluation of the parameters of vehicle motion during emergency braking do not take into account the design of modern braking systems, tyres and psychological aspects of control of the braking process by a human operator. After processing experimental data, recommendations have been formed to improve the existing approaches and eliminate the discovered defects. The verification of the proposed recommendations allowed to establish the areas of their efficiency for M1 category vehicles on dry bituminous concrete and confirmed the need to conduct further studies for vehicles of other categories and other types and conditions of road surface within the framework of the developed general approach.

Keywords: friction forces, tyre, road surface, friction process, deceleration, stopping distance, expert examination of motor vehicle accidents.

Introduction

The expansion of volumes and application sphere of motor vehicles raises the possibility of increase in the human and material costs as a result of road accidents. According to the data of the World Health Organization, every year more than 1.35 million people (3700 people per day) die and tens of millions are hurt in road accidents. This organization predicts that in 2020 road accidents (RA) will take the third place in the world as a reason for loss of health after cardiovascular diseases and severe depression. Mortality caused by road accidents is the main reason of death in children and youth aged from 5 to 29 [1].

The motion of a vehicle on the roadway or in another locality can be viewed as an operation of the system «driver – vehicle – roadway – environment» (DVRE). A breakdown in the normal operation of each of the components of DVRE system leads to the loss of efficiency (decrease in the speed of motion, unjustified stops, increase in fuel consumption) or to road accidents (RA). In the majority of cases, braking systems of motor vehicles (MV) [2] are used to prevent road accidents and the efficiency of their work is limited by friction forces during the tyre-road contact. Friction processes in the contact tyre-road area primarily depend on the speed of vehicle motion, type and condition of tyres as well as type and condition of the roadway [3]. The quality of tyre-road interaction is evaluated by the adhesion coefficient (coefficient of static friction) as well as the coefficient of sliding friction (if the wheels are locked up) which is usually lower than the adhesion coefficient [4]. Different methods, means and technologies depending on the purpose and goal of studies are currently used to evaluate tyre-road interaction as well as braking properties of the vehicle.

The ability to evaluate with sufficient accuracy the quality of tyre-road friction is important for improvement of the operation of control and safety systems of the vehicle (anti-lock braking system (ABS), electronic stability program (ESP), adaptive cruise control (ACC), preventive safety systems), traffic control and road maintenance [4–8].

In the USA and Europe the information obtained from the electronic control, safety and comfort systems of vehicles is successfully used to establish the circumstances of road accidents. It became possible due to the development of technologies used to record vehicle motion during a road accident: GPS system for pinpointing vehicle location, Event Data Recorder (EDR) (for recording the data on the accidents) Auto-

mated Crash Notification (CAN) (automated systems for notification of accidents)) [9–11]. Automated systems for recording traffic parameters help to ensure the high accuracy of the initial data in order to establish the mechanisms of certain emergency situations using the basic laws of motion [9, 12].

Practice shows that it is not always possible to use the information from electronic systems which record vehicle motion parameters during road accidents. According to the Best Practice Manual on Road Accident Reconstruction of the European Network of Forensic Science Institutes [15] the evaluation of tyre-road interaction may be performed by conducting an investigatory experiment in road conditions of the scene of action or in similar conditions. The goal of the experiment is to determine the adhesion coefficient and (or) braking efficiency parameters (stopping distance, deceleration) [2, 8, 13, 16] which characterize the friction processes during tyre-road contact.

If it is impossible to conduct an experiment, then the adhesion coefficient, deceleration and stopping distance may be determined according to the reference data of experimental and calculation values [15] or may be accepted as a normative established by the Traffic Rules and the Council Directive 71/320/EEC [4]. Braking efficiency parameters may be determined by calculations using the formulas known in the forensic science practice [16].

Thus, the modelling of the braking efficiency parameters of vehicles during road accident examination is associated with calculations when the expert uses measurement results given to him by an investigator or by the court as well as typical reference data as initial data. Reference data include parameters and coefficients, the numerical values of which are chosen by the expert himself from the special scientific, technical and reference literature based on the nature and conditions of the road accident. The list of such characteristics and parameters includes the indices which characterize the braking efficiency of the vehicle (delay in the brake system response, deceleration increase time, constant deceleration), driver reaction time; indices of quality and condition of the road surface, coefficient of tyre-road adhesion, information on the speed of pedestrian motion, slip angles and radii of road turns etc.

In order to evaluate the braking efficiency, the expert just needs to calculate certain parameters by using formulas known from the theory of the operational characteristics of the vehicle [14, 15, 16]. However, only if the initial data are accurate and the calculation method has been chosen correctly, then it can be said that expert conclusions are valid, objective and accurate and can be used as proof.

The main difference between the braking efficiency in modern vehicles in comparison and the braking efficiency in outdated vehicles which are not even equipped with ABS, is one of the subjects studied in this thesis. The purpose of the study is to improve the quality of vehicle expert examination after road accidents by improving outdated expert methods of evaluation of the vehicle motion parameters during braking based on the analysis of the parameters of tyre-road interaction during emergency braking.

The following tasks were performed to achieve the set goal:

- analysis of theoretical principles of formation of the parameters of tyre-road interaction during braking;
- experimental study of braking efficiency parameters in the operated vehicles;
- processing of experimental study results and issuing recommendations for improvement of the expert methods of evaluation of motion parameters of the modern vehicles during braking.

Analysis of the principles of formation of tyre-road interaction parameters during braking

A tyre is the only element used by the vehicle to interact with the road. The safety of motion is based on the ability to surmount high decelerations during braking and high transverse acceleration with respective lateral slips during a turn as well as on the ability to have minimal inclination for aquaplaning. According to the physical laws of friction, the friction which must be overcome to move an object on a flat surface depends only on the weight of the object (normal force having vertical influence on the surface) and the adhesion of materials between the foundation and the object. The quality of interaction between the foundation and the object is determined by dimensionless quantity, i.e. friction coefficient (μ). The low μ values indicate a smooth slippery surface of adherent materials with low friction. In case of high μ values, friction forces are increased and they must be overcome or transmitted (longitudinal, transversal forces or forces of lateral slips). The friction significantly determines the physics of driving of the vehicle at the beginning of the motion as well as during acceleration, deceleration and turns. The longitudinal and transversal forces are added vectorially to the resulting force transmitted from the tyre to the road (Fig. 1). The higher is the adhesive ability of the roadway and the tyre or the wheel load, the higher is the resulting force.

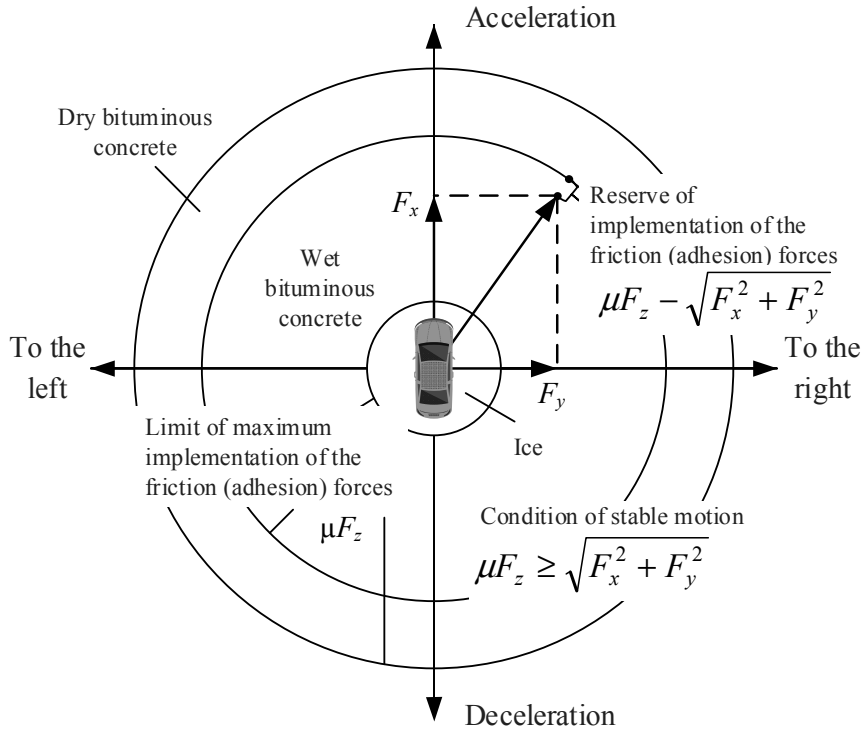


Figure 1. Forces in the tyre friction circle

Based on the Figure 1, the friction coefficient can be determined by using the value of friction forces in the transversal and longitudinal directions as well as the wheel load

$$\mu = \sqrt{F_x^2 + F_y^2} / F_z. \quad (1)$$

If Burkhardt’s method is used [13]

$$\mu = (c_1 \cdot (1 - e^{-c_2 \cdot s}) - c_3 \cdot s) \cdot e^{-c_4 \cdot s \cdot v} \cdot (1 - c_5 \cdot F_z^2), \quad (2)$$

where c_1, c_2, c_3 are coefficients depending on the road surface quality; c_4 is coefficient depending on the maximum vehicle speed; c_5 is coefficient depending on the wheel load; v is vehicle motion speed; s is longitudinal sliding of the wheel.

If the angle of lateral tyre slip γ and lateral tyre stiffness C_γ are known, then the coefficient of lateral friction μ_y is determined by using the following equation

$$\mu_y = \gamma \cdot C_\gamma / F_z. \quad (3)$$

Deceleration during braking is determined by laws of mechanical motion and is limited by the ability of vehicle tyres to adhere to the road surface

$$j = (v_1 - v_2) / t_b = (v_1^2 - v_2^2) / (2S_b) \leq g \cdot (\mu \cdot \cos \alpha \pm \sin \alpha), \quad (4)$$

where v_1, v_2 is initial and final vehicle speed; t_b is braking time; S_b is stopping distance; g is free fall acceleration; α is road incline angle; « \leftarrow » symbol is accepted for downward motion, « \rightarrow » is accepted for upward motion.

The Stopping distance under stable deceleration is determined using the following equation

$$S_{bs} = 0.5 \cdot j \cdot t_b^2 = v_a^2 / (2 \cdot j), \quad (5)$$

and according to the US standard [17] for vehicle speed v_a in km/h

$$S_{bs} = 0.039 \cdot v_a^2 / j. \quad (6)$$

According to the Best Practice Manual on Road Accident Reconstruction of the European Network of Forensic Science Institutes the braking length [15] is determined by using the following formula

$$S_b = (t_a + 0.5 \cdot t_{gd}) \cdot v_a + v_a^2 / (2 \cdot j), \quad (7)$$

where t_a is brake response time; t_{gd} is deceleration increase time.

Antilock braking system became one of the first and most important systems designed to reduce the stopping distance. ABS is a system equipped with control devices giving feedback which prevent the wheels from locking up during braking, as well as help to maintain the controllability and roadholding ability of the vehicle. The point of optimum braking efficiency is between two boundary situations, i.e. free rolling of the wheel and its full lockup. The difference between the speed of the vehicle and the speed of the wheel during braking is called longitudinal wheel slip, its optimum value during adhesion is within the limits of 10–30 % [4].

Results of experimental study of the parameters of vehicle braking efficiency

The stable deceleration is the main parameter used to evaluate the braking efficiency of a vehicle. This parameter allows the expert to objectively evaluate the length of braking (stopping) distance of the vehicle and its speed of motion during emergency braking. Experimental data on vehicle braking dynamics was collected in the period from 2014 to 2018. These data were obtained by using certified special modern devices (Fig. 2): MAHA VZM-100, MAHA VZM-300 as well as the mobile recording and measuring set of Kharkiv National Automobile and Highway University [18] which allows to test the durability, controllability, ride smoothness, as well as aerodynamic, power, braking, hauling and speed properties of motor vehicles under UN Global Technical Rules No. 8 [19]. Experimental studies were mainly conducted with a visit to the scene of a road accident, the road conditions were similar to those of the road accident. Special attention was given to vehicles equipped with ABS and the type of the used tyres. The technical condition of vehicles was in compliance with the traffic rules.

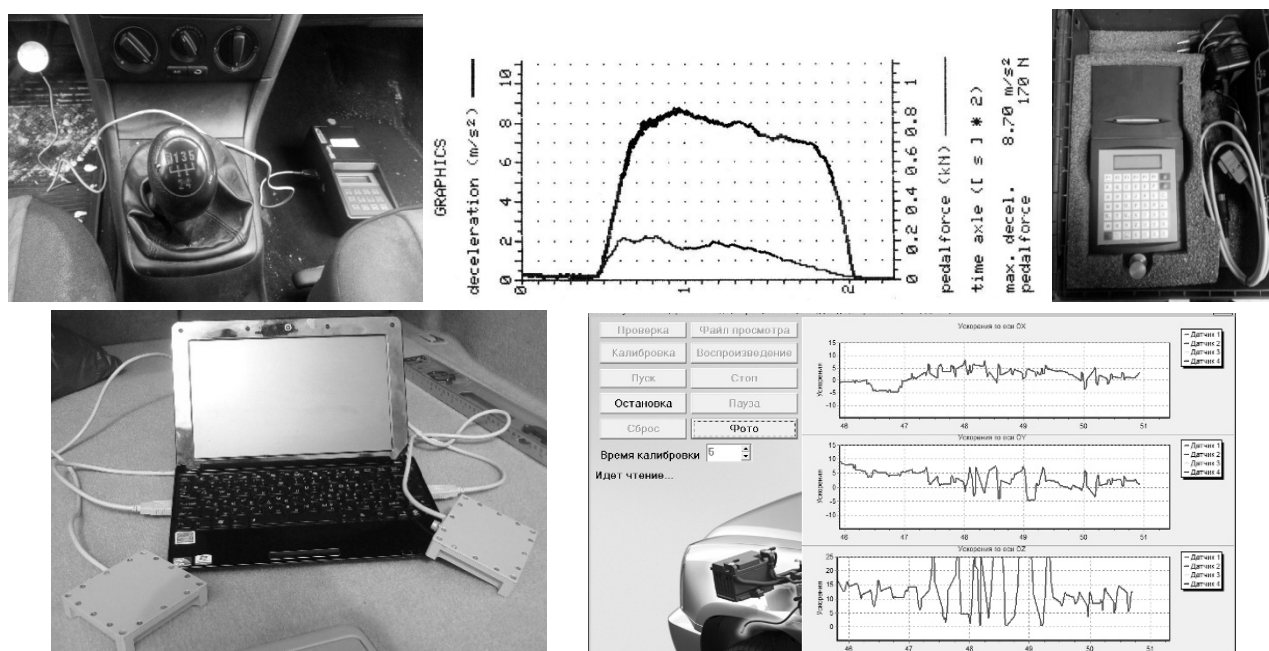


Figure 2. Devices for measuring the dynamics of vehicle braking

The study was conducted on 198 vehicles of M1, M3, N1, N2, N3, N3+O categories on different road surfaces. Model years were from 1975 to 2012. The total number of measurements of the stable deceleration of vehicles and the number of the studied vehicles (in brackets) are shown in Table 1.

Table 1

Number of performed tests (studied vehicles)

Road surface	Vehicle category					
	M1	M3	N1	N2	N3	N3+O
Dry bituminous concrete	306(72)	28(8)	46(12)	44(11)	32(9)	20(6)
Wet bituminous concrete (0,2 mm film)	114(32)	24(7)	22(3)	24(7)	4(1)	–
Smoothed snow	76(18)	–	14(2)	6(1)	–	–
Black ice	28(7)	–	8(1)	4(1)	–	–

The results of generalization of the conducted studies are shown on Figures 3–5 and in Table 2. The results were analysed using MS Excel. The shown parameters were calculated using 95 % confidence level. The processing of study results showed that the process of vehicle braking is stochastic and is very well described by the normal law.

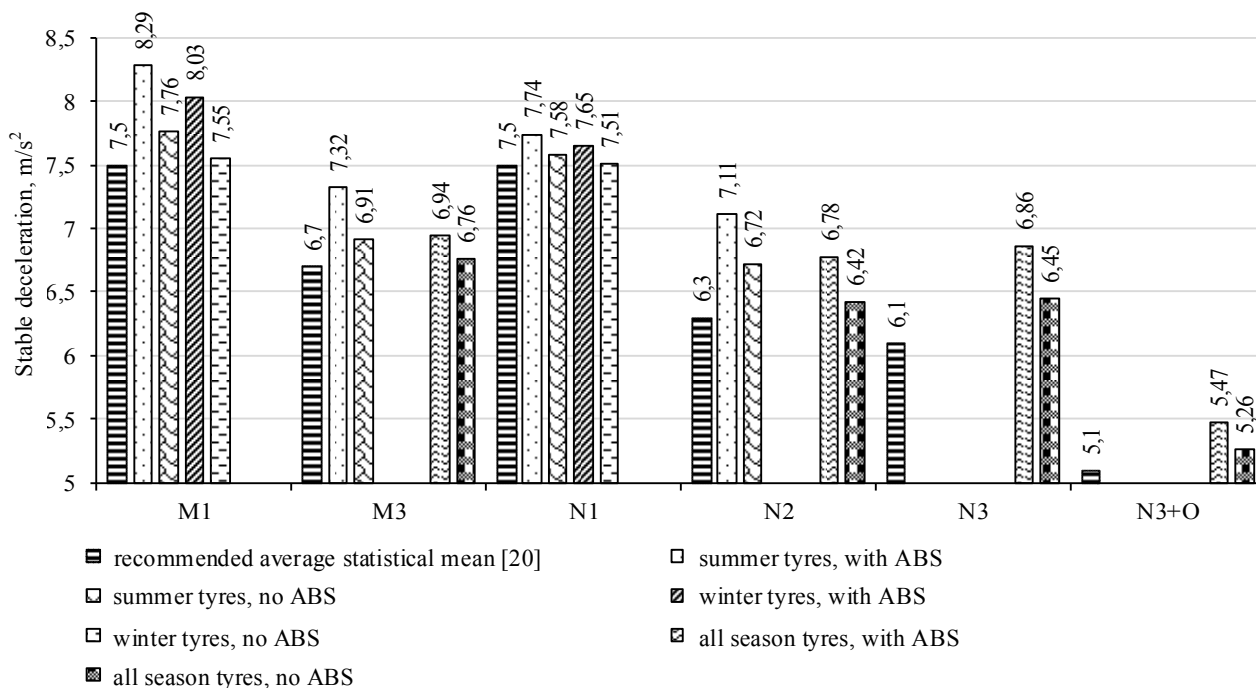


Figure 3. Average indices of stable deceleration on the dry bituminous concrete

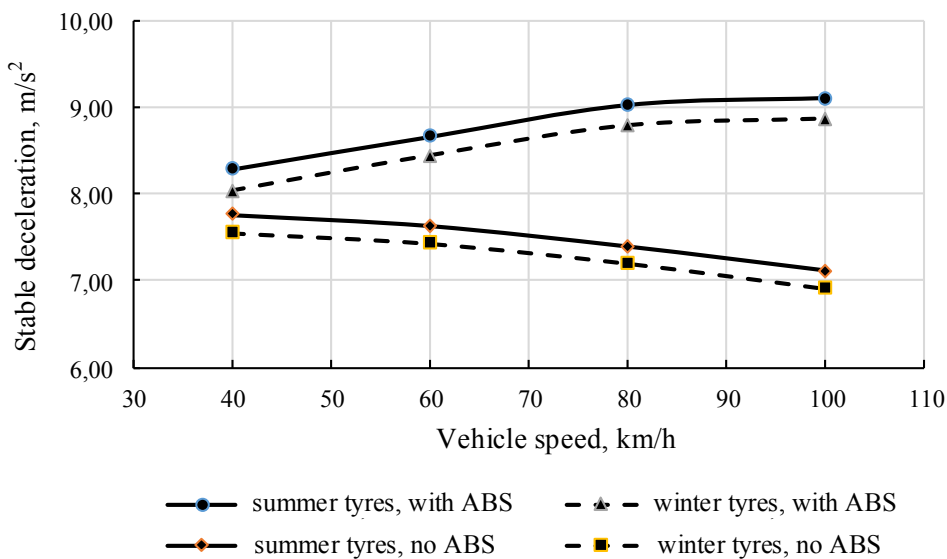


Figure 4. Average indices of stable deceleration in vehicles of M1 category on dry bituminous concrete

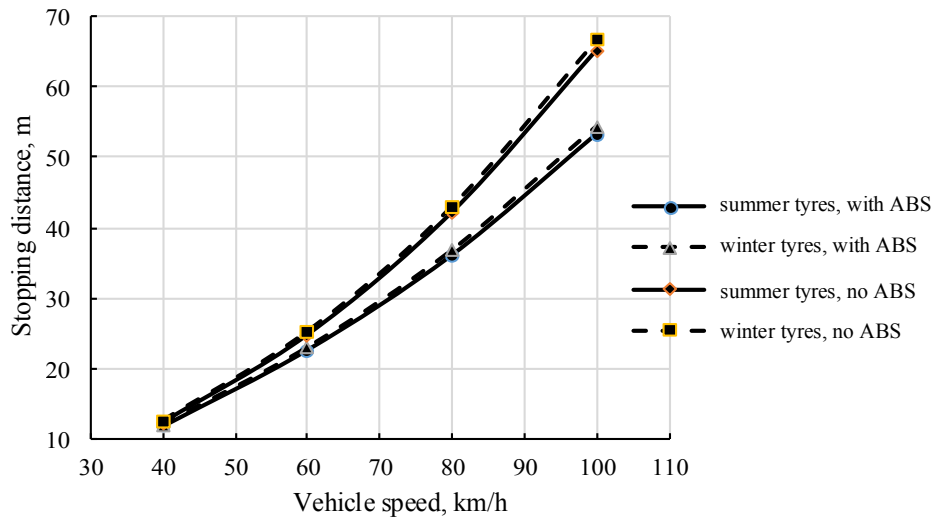


Figure 5. Average indices of stopping distance for vehicles of M1 category on dry bituminous concrete

Table 2

Average indices of stable deceleration of vehicles of M1 category on different types of surface, m/s^2

Road surface	Tyre type, ABS functioning				Recommended value [20]
	Summer tyres		Winter tyres		
	with ABS	without ABS	with ABS	without ABS	
Dry bituminous concrete	8.29	7.76	8.03	7.55	7.5
Wet bituminous concrete (0,2 mm film)	6.71	5.86	6.83	6.14	5
Smoothed snow	–	–	3.11	2.98	2.5
Black ice	–	–	1.7	1.65	1.5

The analysis of the results presented on Figure 3 and in Table 2 shows that the recommended average statistical mean of stable deceleration for expert examination of road accidents are different from average experimental values. The difference between indices is 9.5–26.8 % which is significant enough to form an expert conclusion on a specific road accident. In order to improve the objectivity of an expert examination, the type of tyres and design characteristics of vehicle braking system must be taken into consideration from the point of view of availability and functioning of modern electronic systems (ABS, ESP etc.).

As we can see on Figure 4, the deceleration of vehicles without ABS decreases as the speed of motion increases which correlates well with the data [4, 16]. Vehicles equipped with ABS show the opposite tendency which is explained by the characteristics of the system functioning and the psychology of driving by a human operator during braking [21]. The data obtained for vehicles equipped with ABS correlate well with the results [14]. The difference in the indices for vehicles with ABS and vehicles without ABS makes almost 6 % at the speed of 40 km/h, and 26 % at the speed of 100 km/h. Summer tyres show a 3 % better dynamics on the dry bituminous concrete than winter tyres. In case of wet bituminous concrete (0,2 mm film), there is an opposite tendency: winter tyres show a 3 % better braking dynamics than summer tyres and this tendency increases as long as the thickness of water film grows [4].

The stopping distance in vehicles equipped with ABS is less than in vehicles without ABS (Fig. 5). The difference between indices for vehicles with ABS and vehicles without ABS is almost 4 % at the speed of 40 km/h and 23 % at the speed of 100 km/h. The difference between indices of stopping distances for summer and winter tyres on dry bituminous concrete is within the limits of 0.5 %.

Forming recommendations for improving expert methods of evaluation of motion parameters of modern vehicles during braking

The results of the conducted experimental studies show the need to take into consideration the type of tyres and functioning of ABS during the determination of braking parameters of vehicles which can influence the results of expert examination of vehicles. The equation (7) recommended to determine the stopping distance of a vehicle does not take into consideration the mentioned parameters and must be improved.

The analysis of characteristics of functioning of modern ABS and the results of the conducted studies allows to propose the following range of improvements.

The following equation is proposed to determine the stopping distance in vehicles equipped with ABS

$$S_b = (t_a + 0.5 \cdot t_{gd}) \cdot v_a + \frac{v_a^2 - v_s^2}{2 \cdot j_{ABS}} + \frac{v_s^2}{2 \cdot j} \tag{8}$$

where j_{ABS} is stable deceleration with ABS turned on, j is stable deceleration with ABS turned off; v_s is maximum vehicle speed, its decrease results in ABS turning off, $v_a = 15 \text{ km/h}$ [4].

$$j_{ABS} = j \cdot (1 + (1.7 \ln v_a - 5.9) / j) \tag{9}$$

The following equation can be used to determine the stopping distance for vehicles without ABS

$$S_b = (t_a + 0.5 \cdot t_{gd}) \cdot v_a + \frac{v_a^2}{2 \cdot j_v} \tag{10}$$

where j_v is corrected stable deceleration of motion speed of a vehicle.

$$j_v = j \cdot (1 + (0.54 - 0.0119 \cdot v_a) / j) \tag{11}$$

The results of comparison of experimental data with calculations according to the proposed models (8)–(11) and the current method (7) are shown on Figures 6, 7.

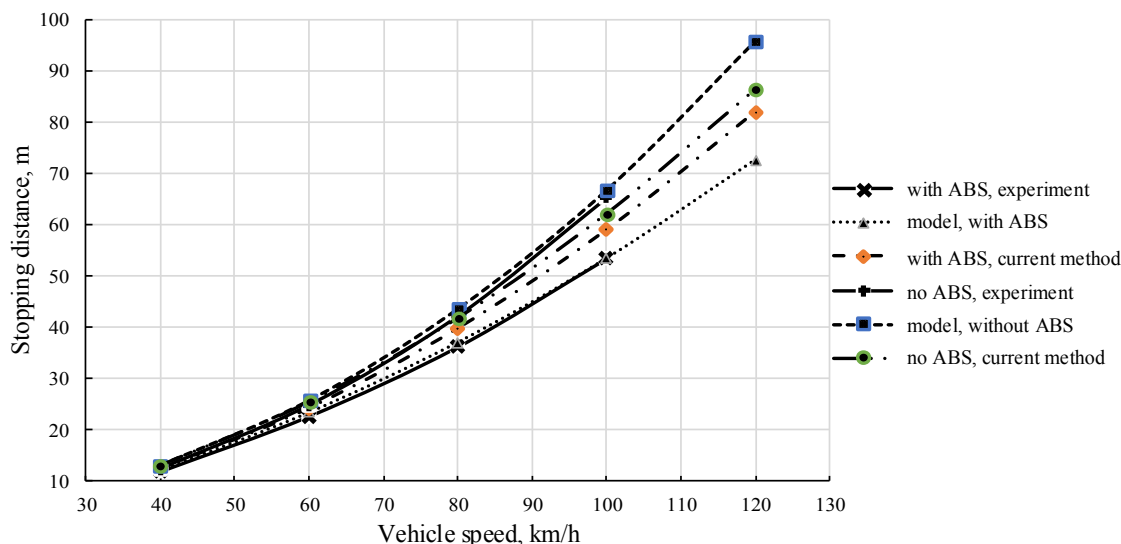


Figure 6. Results of evaluation of the stopping distance in vehicles of M1 category on dry bituminous concrete

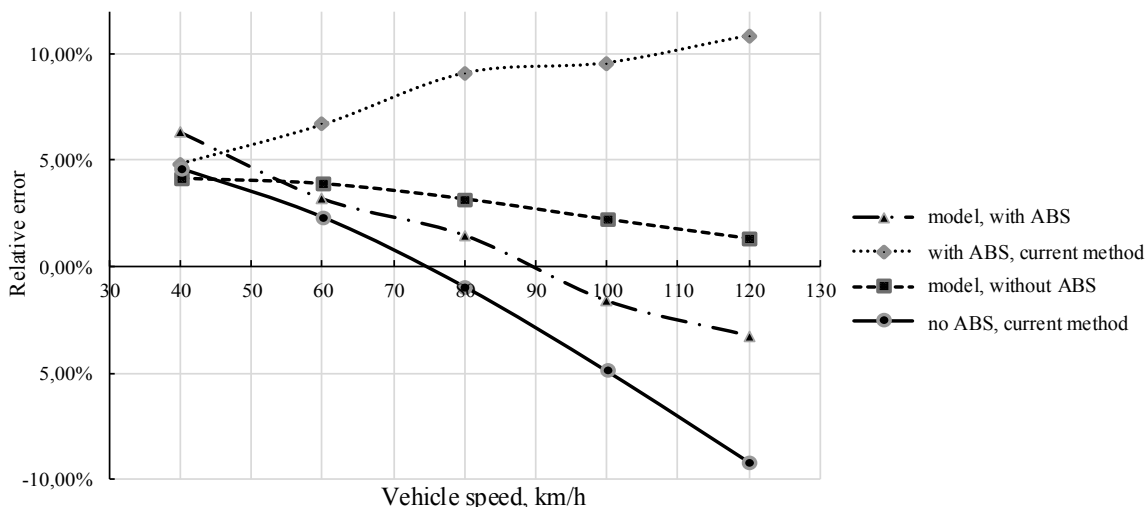


Figure 7. Error in the evaluation of the stopping distance in vehicles of M1 category on dry bituminous concrete

The analysis of modelling results presented on Figures 6, 7 allows to recommend the equations (8) and (9) for vehicles of M1 category equipped with ABS during evaluation of braking efficiency parameters on dry bituminous concrete at the speed of 45 km/h or higher. In case of lower initial speed of braking, it is advisable to apply the current method and use the equation (7). The equations (10) and (11) can be recommended for vehicles of M1 category which are not equipped with ABS during evaluation of braking efficiency parameters on dry bituminous concrete at the speed of 85 km/h or higher. Otherwise, it is advisable to apply the current method and use the equation (7).

Conclusions

Tyre-road interaction during emergency braking is a complex dynamic process of stochastic nature. The quality of description of this process depends upon the full consideration of all ponderable factors: type and condition of road surface, type and condition of tyres, characteristics of vehicle design, initial braking speed, physiological characteristics of the driver etc.

The following conclusions can be drawn after analysing theoretical foundations of formation of the indices of tyre-road interaction during braking and experimental studies of indices of vehicle braking efficiency:

1. The development of vehicle structure and technologies of tyre production results in the improvement of indices of tyre-road interaction and requires regular renewal of the guidelines and methods for evaluation of motion parameters of modern vehicles during braking.
2. A general approach has been developed to improve the evaluation of efficiency parameters of braking in modern vehicles. The verification of this approach showed its efficiency for vehicles of M1 category on dry bituminous concrete, and specifically, for vehicles which are not equipped with ABS at the speed higher than 85 km/h, and for vehicles equipped with ABS at the speed higher than 45 km/h. In other cases, it is advisable to use the current method.
3. Further studies are needed to provide similar recommendations for other categories of vehicles and types of road surface.

References

- 1 World Health Organization. Road traffic injuries [Electronic resource]. — Retrieved from: <http://www.who.int/mediacentre/factsheets/fs358/en/>.
- 2 Кашканов А.А. Оцінка експлуатаційних гальмових властивостей автомобілів в умовах неточності вихідних даних: монографія / А.А. Кашканов, В.М. Ребедайло, В.А. Кашканов. — Вінниця: ВНТУ, 2010. — 148 с.
- 3 Rotshtein A. Fuzzy Expert System for Identification of Car Wheels Adhesion Factor with a Road Surface / A. Rotshtein, A. Kashkanov // Proceeding of the 6-th European Congress on Intelligent Techniques and Soft Computing. — Aachen, Germany. — 1998. — P. 1735–1740.
- 4 Reif K. Bosch Automotive Handbook. 9th Edition / K. Reif, K.H. Dietsche. — Karlsruhe: Robert Bosch GmbH, 2014. — 1544 p.
- 5 Singh K.B. An Intelligent Tire Based Tire-Road Friction Estimation Technique and Adaptive Wheel Slip Controller for Anti-lock Brake System / K.B. Singh, Ali Arat M., S. Taheri // Journal of Dynamic Systems Measurement and Control. — 2013. — 135(3):031002–031002–26. doi:10.1115/1.4007704.
- 6 Singh K.B. Estimation of tire-road friction coefficient and its application in chassis control systems / K.B. Singh, S. Taheri // Systems Science & Control Engineering. — 2015. — № 3:1. — P. 39–61. DOI: 10.1080/21642583.2014.985804.
- 7 Laugier C. Probabilistic analysis of dynamic scenes and collision risks assessment to improve driving safety / C. Laugier, I. E. Paromtchik, M. Perrollaz, J.D. Yoder, C. Tay, M. Yong et al. // IEEE Intelligent Transportation Systems Magazine. — 2011. — No. 3. — P. 4–19.
- 8 Andersson M. Road friction estimation, Part II — IVSS project report [Electronic resource] / M. Andersson, F. Bruzelius, J. Casselgren, M. Hjort, S. Lofving, G. Olsson et al. — Retrieved from: http://fudinfo.trafikverket.se/fudinfoexternwebb/Publikationer/Publikationer_001101_001200/Publikation_001109/IVSS_RFEII_Slutrapport.pdf.
- 9 Кашканов А.А. Автоматизовані системи повідомлення про ДТП та перспективи їх використання / А.А. Кашканов, В.А. Кашканов, О.Г. Грисюк // Сучасні технології в машинобудуванні та транспорті. — Луцьк: Луцький НТУ, 2016. — № 1(5). — С. 78–82.
- 10 Marco P daSilva. Analysis of Event Data Recorder Data for Vehicle Safety Improvement [Electronic resource] / Marco P daSilva. — Retrieved from <http://www.nhtsa.gov/DOT/NHTSA/NRD/Multimedia/PDFs/EDR/Research/811015.pdf>.
- 11 Hynd D. Study on the benefits resulting from the installation of Event Data Recorders [Electronic resource] / D. Hynd, M. McCarthy. — Retrieved from https://ec.europa.eu/transport/sites/transport/files/docs/study_edr_2014.pdf.
- 12 Struble D. Automotive accident reconstruction: practices and principles / Struble D. — Boca Raton: CRC Press, 2013. — 498 p.

13 Kemzuraite K. Investigation of dynamic properties of vehicle in various friction condition simulated with use of skidcar system / K. Kemzuraite, V. Zuraulis, D. Więckowski // The Archives of Automotive Engineering. — 2014. — No. 63(1). — P. 82–102.

14 Nerijus Kudarauskas. Analysis of emergency braking of a vehicle / Kudarauskas Nerijus // Transport. — 2007. — No. 22:3. — P. 154–159. DOI: 10.1080/16484142.2007.9638118.

15 European Network of Forensic Science Institutes. Best Practice Manual for Road Accident Reconstruction, ENFSI, ENFSI-BPM-RAA-01. Version 01 — November 2015 [Electronic resource]. — Retrieved from: http://enfsi.eu/wp-content/uploads/2016/09/4._road_accident_reconstruction_0.pdf.

16 Пучкин В.А. Основы экспертного анализа дорожно-транспортных происшествий: База данных. Экспертная техника. Методы решений / В.А. Пучкин. — Ростов н/Д.: ИПО ПИ ЮФУ, 2010. — 400 с.

17 A Policy on Geometric Design of Highways and Streets. — AASHTO Green Book, 7th Edition, 2018. — 1047 p.

18 Пат. 51031 Україна, МПК G01P 3/00 25.06.2010. Система для визначення параметрів руху автотранспортних засобів при динамічних (кваліметричних) випробуваннях / Подригало М. А., Коробко А.И., Клец Д. М., Файст В.Л.; заявник та патентовласник Харківський нац. автотранспорт. університет. — № у 2010 01136; заявл. 04.02.10; опубл. 25.06.10, Бюл. № 12.

19 The United Nations Economic Commission for Europe. Global technical regulation United Nations № 8 «Electronic stability control systems»: Established in the Global Registry on 26 June 2008 [Electronic resource]. — Retrieved from: <http://www.unece.org/fileadmin/DAM/trans/main/wp29/wp29wgs/wp29gen/wp29registry/ECE-TRANS-180a8e.pdf>.

20 Туренко А.М. Автотехнічна експертиза. Дослідження обставин ДТП: підручник для вищих навчальних закладів / А.М. Туренко, В.І. Клименко, О.В. Сарасв, С.В. Данець. — Харків: ХНАДУ, 2013. — 320 с.

21 Цыганков Э.С. 120 приемов контраварийного вождения / Э.С. Цыганков. — М.: РИПОЛ классик; Престиж книга, 2007. — 320 с.

А.А. Кашканов, В.Н. Диордица, В.Ю. Кучерук,
Д.Ж. Карабекова, А.К. Хасенов, А.М. Шарзадин

Шұғыл тежеу кезінде автокөлік дөңгелектерінің жолмен өзара әрекеттесуін инерциялық бағалау

Апатты жағдайларға автотехникалық сараптама жүргізу кезінде М1 санатындағы көлік құралдарын тежеу тиімділігінің параметрлерін бағалаудың жетілдірілген әдістемесі ұсынылды. Бұл әдістеме шинаның жолмен байланысқан аймағында үйкеліс процестеріне елеулі әсер ететін параметрлерді бақылауға негізделген. Бұл параметрлер автомобиль шиналарының жолмен өзара іс-қимыл сапасын бағалауға теориялық тәсілдерді талдау, тежелудің негізгі көрсеткіштерін (баяулау, тежеу жолы) бағалау және инерциялық әдіспен тежелу тиімділігінің көрсеткіштерін эксперименттік бағалау үшін аналитикалық формулалар негізінде анықталды. Зерттеу нәтижелерін жалпылау шұғыл тежеу кезінде автомобиль қозғалысының параметрлерін бағалаудың қолданыстағы сараптамалық әдістері заманауи автотехникалық жүйелерінің, шиналар конструкциясының дамуын және тежеу процесін оператор-адамды басқарудың психологиялық аспектілерін ескермегенін көрсетті. Тәжірибелік деректерді өңдеу негізінде қолданыстағы тәсілдерді жетілдіру және анықталған кемшіліктерді жою бойынша ұсыныстар жасалды. Ұсынылған ұсынымдарды тексеру құрғақ битуминозды бетонда М1 санатындағы көлік құралдары үшін олардың тиімділік саласын белгілеуге мүмкіндік берді және әзірленген жалпы тәсіл шеңберінде басқа санаттағы көлік құралдары үшін әрі қарай зерттеулер жүргізу қажеттігін және жол жабынының басқа түрлері мен жағдайларын растады.

Кілт сөздер: үйкеліс күші, автомобиль шинасы, жол жабыны, тежеу процесі, баяулау, тежеу жолы, жол-көлік оқиғаларының сараптамасы.

А.А. Кашканов, В.Н. Диордица, В.Ю. Кучерук,
Д.Ж. Карабекова, А.К. Хасенов, А.М. Шарзадин

Инерционная оценка взаимодействия автомобильных шин с дорогой при экстренном торможении

Предложена усовершенствованная методика оценки параметров эффективности торможения транспортных средств категории М1 при проведении автотехнических экспертиз аварийных ситуаций. Данная методика основана на контроле параметров, способных существенно повлиять на процессы трения в зоне контакта шины с дорогой. Данные параметры были выявлены на основе анализа теоретических подходов к оценке качества взаимодействия автомобильных шин с дорогой, аналитических формул для оценки основных показателей торможения (замедление, тормозной путь) и экспериментальной оценки показателей эффективности торможения инерционным методом. Обобщение результатов исследований показало, что существующие экспертные методы оценки параметров движения автомобилей при экстренном торможении не учитывают развития конструкции современных тормоз-

ных систем, шин и психологические аспекты управления человеком-оператором процессом торможения. На основе обработки экспериментальных данных были сформированы рекомендации по усовершенствованию существующих подходов и устранению выявленных недостатков. Проверка предложенных рекомендаций позволила выявить зоны их эффективности для ТЗ категории М1 на сухом асфальтобетоне и подтвердила необходимость проведения дальнейших исследований для других категорий ТЗ и других типов и состояний дорожного покрытия в рамках разработанного общего подхода.

Ключевые слова: силы трения, автомобильная шина, дорожное покрытие, процесс торможения, замедление, тормозной путь, экспертиза дорожно-транспортных происшествий.

References

- 1 World Health Organization. Road traffic injuries. *www.who.int* Retrieved from <http://www.who.int/mediacentre/factsheets/fs358/en/>.
- 2 Kashkanov, A.A., Rebedailo, V.M., & Kashkanov, V.A. (2010). *Otsinka ekspluatatsiynykh halmovyykh vlastyvostei avtomobiliv v umovakh netochnosti vykhidnykh danykh [Estimation of operational braking properties of cars in conditions of inaccuracy of initial data]*. Vinnytsia: VNTU [in Ukrainian].
- 3 Rotshtein, A., & Kashkanov, A. (1998). Fuzzy Expert System for Identification of Car Wheels Adhesion Factor with a Road Surface. *Proceeding of the 6-th European Congress on Intelligent Techniques and Soft Computing* (pp. 1735–1740). Aachen, Germany.
- 4 Reif, K., & Dietsche, K.H. (2014). *Bosch Automotive Handbook. 9th Edition*. Karlsruhe: Robert Bosch GmbH.
- 5 Singh, K.B., Ali Arat, M., & Taheri, S. (2013). An Intelligent Tire Based Tire-Road Friction Estimation Technique and Adaptive Wheel Slip Controller for Antilock Brake System. *Journal of Dynamic Systems Measurement and Control*, 135(3):031002–031002–26. doi:10.1115/1.4007704.
- 6 Singh, K.B. & Taheri S. (2015). Estimation of tire-road friction coefficient and its application in chassis control systems. *Systems Science & Control Engineering*, 3:1, 39–61, DOI: 10.1080/21642583.2014.985804.
- 7 Laugier, C., Paromtchik, I. E., Perrollaz, M., Yoder, J.D., Tay, C., & Yong, M., et al. (2011). Probabilistic analysis of dynamic scenes and collision risks assessment to improve driving safety. *IEEE Intelligent Transportation Systems Magazine*, 3, 4–19.
- 8 Andersson, M., Bruzelius, F., Casselgren, J., Hjort, M., Löfving, S., & Olsson, G., et al. (2010). Road friction estimation, Part II — IVSS project report. *fudinfo.trafikverket.se* Retrieved from http://fudinfo.trafikverket.se/fudinfoexternwebb/Publikationer/Publikationer_001101_001200/Publikation_001109/IVSS_RFEII_Slutrapport.pdf
- 9 Kashkanov, A.A., Kashkanov, V.A., & Hrysyuk, O.G. (2016). Avtomatyzovani systemy povidomlennya pro DTP ta perspektyvy yikh vykorystannya [Automated systems of accidents notification and prospects for their use]. *Suchasny tekhnologiyi v mashynobudubanni ta transpiti — Modern technologies in mechanical engineering and transport*, 1(5), 78–82 [in Ukrainian].
- 10 Marco P daSilva. (2008). Analysis of Event Data Recorder Data for Vehicle Safety Improvement. *www.nhtsa.gov* Retrieved from <http://www.nhtsa.gov/DOE/NHTSA/NRD/Multimedia/PDFs/EDR/Research/811015.pdf>.
- 11 Hynd, D., McCarthy, M. (2014). Study on the benefits resulting from the installation of Event Data Recorders. *ec.europa.eu* Retrieved from https://ec.europa.eu/transport/sites/transport/files/docs/study_edr_2014.pdf.
- 12 Struble, D. (2013). *Automotive accident reconstruction: practices and principles*. Boca Raton: CRC Press, 498.
- 13 Kemzuraite, K., Zuraulis, V., & Więckowski, D. (2014). Investigation of dynamic properties of vehicle in various friction condition simulated with use of skidcar system. *The Archives of Automotive Engineering*, 63(1), 82–102.
- 14 Nerijus, Kudarauskas (2007). Analysis of emergency braking of a vehicle, *Transport*, 22:3, 154–159, DOI: 10.1080/16484142.2007.9638118.
- 15 European Network of Forensic Science Institutes (2019). Best Practice Manual for Road Accident Reconstruction, ENFSI, ENFSI-BPM-RAA-01. Version 01 — November 2015. *enfsi.eu* Retrieved from http://enfsi.eu/wp-content/uploads/2016/09/4_road_accident_reconstruction_0.pdf.
- 16 Puchkin, V.A. (2010). *Osnovy ekspertnoho analiza dorozhno-transportnykh proisshestvii: Baza dannykh. Ekspertnaia tekhnika. Metody reshenii [Basics of expert analysis of road accidents: Database. Expert equipment. Solution Methods]*. Rostov-on-Don: IPO PI YUFU [in Russian].
- 17 A Policy on Geometric Design of Highways and Streets (2018). *AASHTO Green Book 7th Edition*, 1047.
- 18 Podryhalo, M.A., Korobko, A.I., Klets, D.M., & Faist, V.L. (2010). Sistema dlia viznachennia parametriv rukhu avtotransportnykh zasobiv pri dinamichnikh (kvalimetricnikh) viprobuvanniakh [System for determination of parameters of motion of motor transport means at dynamical (qualimetric) tests]. *Patent 51031 Ukraine*, MPK G01P 3/00 25.06.2010; applicant and patent holder Kharkiv National Automobile and Highway University. No u 2010 01136; Decl. 04.02.10; Publ. 25.06.10, Bull. No. 12 [in Ukrainian].
- 19 The United Nations Economic Commission for Europe (2019). Global technical regulation United Nations № 8 «Electronic stability control systems»: Established in the Global Registry on 26 June 2008. *www.unece.org* Retrieved from <http://www.unece.org/fileadmin/DAM/trans/main/wp29/wp29wgs/wp29gen/wp29registry/ECE-TRANS-180a8e.pdf>
- 20 Turenko, A.M., Klymenko, V.I., Sarayev, O.V., & Danecz, S.V. (2013). *Avtotekhnichna ekspertiza. Doslidzhennya obstavin DTP: pidruchnik dlya vishchikh navchalnykh zakladiv [Autotechnical examination. Investigation of accident-related problems]*. Kharkiv: KhNAHU [in Ukrainian].
- 21 Tsygankov, E.S. (2007). *120 priemov kontravariinoho vozhdennia [120 methods of emergency driving]*. Moscow: RIPOL klassik, Prestizh kniga [in Russian].

V.Yu. Kucheruk¹, I.P. Kurytnik², Ye.Z. Oshanov³, P.I. Kulakov¹,
A.A. Semenov¹, D.Zh. Karabekova³, A.K. Khassenov³

¹Vinnitsia National Technical University, Ukraine;

²The W. Pilecki State Higher School, Oswiecim, Poland;

³Ye.A. Buketov Karaganda State University, Kazakhstan

(E-mail: karabekova71@mail.ru)

Computer-measuring system of the induction motor's dynamical torque-speed characteristics

In the article an efficient method of determining the dynamic torque-speed characteristic of induction motors and the computer-measuring system for its realization is considered. In this method, the additional flywheel is used, the dynamic measurements of the angular speed as a function of time are taken at the start, after the end of the transition process, and at during the self-braking mode of the induction motor. For approximating the data that are obtained as a result of the measurements, the moving average algorithm is used. Also, with the help of this system, the inertia moment, angular speed dependence on time, electromagnetic dynamic moment dependence on time, electromagnetic dynamic power dependence on time, mechanical dynamic power dependence on time, and dynamic loss in rotor winds dependence on time are measured. In the article, the results of experimental measurements of the induction motor characteristics using a proposed computer-measuring system are given. The proposed system is experimental; in the future, it can be used to test induction motors during their production processes.

Keywords: computer-measuring system, dynamic torque-speed characteristic, induction motor, moving average algorithm.

The measurement of the dynamical torque-speed characteristic is important in the electrical machine check for all kinds of electrical machines. The three-phase alternating current motors with short-circuit rotors (induction motors) are widely used in a variety of industrial applications due to their rather simple design. Determining the parameters of induction motors by their torque-speed characteristic is important for the proper use of the motors since the torque moment and the mechanical losses must be agree [1]. It is common practice to determine the dependence of the torque moment from the angular speed for the study of a motor characteristics in the static and dynamic modes of its operation.

The authors in [2] consider an efficient method of determining the maximum performance torque-speed characteristic for an induction motor drive. This method is based on a mathematical model that provides a method of calculation for the output power, the apparent power, the power factor, and the efficiency vs the speed. The proposed method is applicable to the analysis of induction motors based on the results of measuring their output characteristics. The authors in [3–6] deal with the practical application of the acceleration method for evaluating induction machine torque-speed and current-speed characteristics. Also, this paper considers the influence of the time measurement on the shape of torque-speed characteristics. However, this method does not take into account the accurate value of the moment of inertia of the electric motor rotor. The authors of [7] describe the measuring method for determining the torque-speed characteristic of an induction machine, which is determined by recording and differentiating the speed signal during the starting of the machine. In the proposed system, the data is gathered using a measuring system based on a digital acquisition card and processed in custom software, built using LabVIEW, on a personal computer. This system does not take into account the mechanical losses on the electric machine shaft and the accurate value of the rotor's moment of inertia. The authors in [7–9] present a measurement method for the determination of the torque-speed characteristics of induction motors, which is in compliance with the IEEE standard test procedure for polyphase induction motors and generators [1]. To implement this method, dynamic measurements of the angular speed as a function of time are carried out. Afterward, digital filtering of the obtained data is carried out, then the dependence of the angular acceleration as a function of time is calculated using digital differentiation. On the basis of this dependence, the torque-speed characteristics are calculated. In this method, the measurements are taken with no load on the motor shaft. The dynamic measurements of the angular speed as a function of time are taken during the start and after the end of the transition process, and the measurements in the process of the self-braking mode are not carried out. The authors in [10, 11] describe the use of a

curve-fitting technique to deduce the nominal torque-speed characteristic of a three-phase induction motor from the speed data obtained in a no-load acceleration test. In paper [12] the authors propose the measuring method of the rotor moment of inertia at the use of various numbers of additional flywheels. In this method, B-splines are used for the processing of measured data obtained during the start. In this case, a determination of the torque-speed characteristics during the self-braking mode is not carried out.

There is a group of methods based on the computation of the torque-speed characteristic on the basis of the induction motor parameters, mathematical model or substitution schemes of the induction motor [13–17]. These methods are often used in automated electric drives, but they do not take into account the exact values of the mechanical losses and the moment of inertia. This is the reason for the additional measurement error.

One of the most labor-consuming operations that electrical machines check is the measurement of the dynamical torque-speed characteristic. The dynamical torque-speed characteristic is a very informative characteristic; it increases the probability of being able to determine certain parameters of the electrical machine, such as the starting, minimum, maximum, nominal, and critical moments. Using synchronous hollows of the dynamical torque-speed characteristic it is possible to analyze the condition of electrical machine isolation. However, due to the lack of necessary measuring devices, the dynamical torque-speed characteristic in some cases is not supervised. The main parameters of the dynamical torque-speed characteristic are the rotor inertia moment and the moment of mechanical losses. Most of the existing means for measuring the dynamical torque-speed characteristic admit, that the moment of mechanical losses is constant when actually, it is a function of the shaft angular speed. The moment of inertia is determined through different means of measurement that are all time-consuming.

Thus, there is a necessity for a more exact and automated measurement of the inertia moment and moment of mechanical losses for determining the dynamical torque-speed characteristic. This requires a computer-measuring system of the induction motor dynamical torque-speed characteristics with improved metrological parameters, which uses various modes of the induction motor operations.

The authors offer a method of measuring the dynamical torque-speed characteristic, which consists of the following.

The dynamical torque-speed characteristic is dependent on the moment on the shaft of the electrical machine M_d at an angular speed:

$$M_{d(\omega)} = J \cdot \frac{d\omega}{dt} + M_{0(\omega)}, \quad (1)$$

where J — rotor inertia moment; M_0 — moment of mechanical losses; ω — angular speed of rotor; and t — time. A necessary condition for its realization is the availability of the additional inertia moment J_m , executed in a kind, simple body of rotation; for example, a disk or a cylinder. The additional inertia moment size is calculated by its geometrical and weight parameters.

First, the dependence of the angular speed on time in two modes of the induction motor operation without an additional inertia moment is measured. During the time of the transient mode (after starting) the dependence of angular speed ω_s on time is measured, at achievement of synchronous speed the induction motor is disconnected from the power supply. Furthermore, during its self-braking mode, the dependence of angular speed ω_{b1} on time is measured.

Third, when the induction motor has been stopped on the shaft end, the additional inertia moment J_m is established; then, the induction motor is started. After achievement of synchronous speed the induction motor is disconnected from the power supply, and during its self-braking mode, the dependence of the angular speed ω_{b2} on time is measured.

Accordingly, the induction motor movement equations without an additional inertia moment and with an additional inertia moment J_m are outlined in the following equation.

$$\begin{cases} M_{el}(\omega) = J \cdot \varepsilon_s(\omega) + M_0(\omega) \\ 0 = J \cdot \varepsilon_{b1}(\omega) + M_{0(\omega)} \\ 0 = (J + J_m) \cdot \varepsilon_{b2}(\omega) + M_{0(\omega)}, \end{cases} \quad (2)$$

where $M_{el}(\omega)$ — electromagnetic moment; $\varepsilon_s(\omega)$ — rotor angular acceleration dependence on the angular speed of the rotor throughout the transient mode (after the start); $\varepsilon_{b1}(\omega)$ — rotor angular acceleration de-

pendence on the angular speed of the rotor during its self-braking mode without the additional inertia moment; $\varepsilon_{b2}(\omega)$ — rotor angular acceleration dependence on the angular speed of the rotor during its self-braking mode with the additional inertia moment.

The methodical basis of an offered method is to decide on a system from three equations (2) with three unknown parameters: $M_{el}(\omega)$, $M_{0(\omega)}$ and J . After moving the unknown parameters of system (2) to the left-hand part, we obtain the following equation:

$$\begin{cases} M_{el}(\omega) - M_{0(\omega)} - J \cdot \varepsilon_s(\omega) = 0 \\ -M_{0(\omega)} - J \cdot \varepsilon_{b1}(\omega) = 0 \\ -M_{0(\omega)} - J \cdot \varepsilon_{b2}(\omega) = J_m \cdot \varepsilon_{b2}(\omega). \end{cases} \quad (3)$$

Having decided on a common second and third equation of a system (3), we obtain the following equation:

$$J = J_m \cdot \frac{\varepsilon_{b2}(\omega)}{\varepsilon_{b1}(\omega) - \varepsilon_{b2}(\omega)}; \quad (4)$$

$$M_{0(\omega)} = J_m \cdot \frac{\varepsilon_{b1}(\omega) \cdot \varepsilon_{b2}(\omega)}{\varepsilon_{b1}(\omega) - \varepsilon_{b2}(\omega)}. \quad (5)$$

Value of inertia moment J is averaged in all ranges of the induction motor angular speed. The electromagnetic moment M_{el} is determined from the first equation of system (3)

$$M_{el}(\omega) = J_m \cdot \frac{(\varepsilon_s(\omega) - \varepsilon_{b1}(\omega)) \cdot \varepsilon_{b2}(\omega)}{\varepsilon_{b1}(\omega) - \varepsilon_{b2}(\omega)}. \quad (6)$$

$M_{el}(\omega)$ is a dynamic electromagnetic moment without a moment of mechanical losses $M_0(\omega)$. The complete dynamic moment $M_d(\omega)$ is determined from

$$M_d(\omega) = M_{el}(\omega) + M_0(\omega) = J_m \cdot \frac{\varepsilon_s(\omega) \cdot \varepsilon_{b2}(\omega)}{\varepsilon_{b1}(\omega) - \varepsilon_{b2}(\omega)}. \quad (7)$$

The offered method can be applied to the determination of the inertia moment J and moment of mechanical losses $M_{0(\omega)}$. For this purpose, it is necessary to conduct two experiences of self-braking and to determine the required parameters under the formulas (4)–(5). The offered method enables the determination of not only the dynamical torque-speed characteristic but other characteristics of the induction motor in a dynamic mode of its work [18], including:

- the electromagnetic dynamic mechanical characteristic $M_{el}(\omega)$;
- the electromagnetic moment $M_{el}(t)$;
- the dynamic mechanical characteristic $M_d(\omega)$;
- the dynamic moment $M_d(t)$;
- the angular speed at the induction motor's various modes $\omega = f(t)$;
- the sliding $s = f(t)$;
- the rotor inertia moment J ; — the electromagnetic dynamic power $P_{el} = f(t)$, $P_{el} = f(\omega)$:

$$P_{el} = M_{el} \cdot \omega; \quad (8)$$

- the mechanical dynamic power $P_m = f(t)$, $P_m = f(\omega)$:

$$P_m = P_{el} \cdot (1 - s); \quad (9)$$

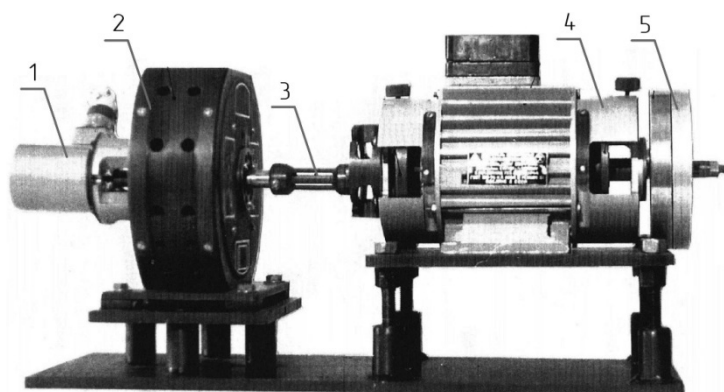
- the dynamic loss in rotor winds $P_l = f(t)$, $P_l = f(\omega)$:

$$P_l = P_{el} \cdot s. \quad (10)$$

Essentially, it enables the expansion of an area to occur using a given method.

To implement this method, an experimental computer-measuring system of the induction motor's dynamical torque-speed characteristics was developed. The appearance of the experimental setup for the computer-measuring system is shown in Figure 1, and the computer-measuring system structural scheme is shown in Figure 2.

Induction motor's rotor (model 4A71A4CY1) with the muff is connected to an angular speed sensor (model BE-178), the output signal of which is fed to a microcontroller unit. In the experimental setup, it is possible to fix two additional flywheels on the motor shaft for implementing the proposed method of measuring the inertia moment. The electromagnetic brake, which is shown in Figure 1, is designed to study the starting characteristics of the motor and not for measuring the inertia moment.



1 — angular speed sensor; 2 — electromagnetic brake; 3 — muff; 4 — investigated induction motor; 5 — additional flywheels for measurement the inertia moment

Figure 1. The appearance of the experimental setup for the computer-measuring system of the induction motor's dynamical torque-speed characteristics

The microcontroller unit uses a microcontroller manufactured by Microchip Technology Inc. and external RAM static memory chips for storing an array of measurement results. Data transfer to a personal computer (PC) is carried out through a USB interface. To convert Universal Synchronous/Asynchronous Receiver/Transmitter (USART) port signals to a USB interface, a Future Technology Devices International (FTDI) converter is used. The microcontroller provides control of the supply driver in turning the motor on and off.

In the offered computer-measuring system of the induction motor's dynamical torque-speed characteristics, the dependence of the angular speed of the motor shaft on time is measured with the aid of a digital angular sensor, which provides the formation of 1,000 pulses per revolution of the motor shaft. The time interval between the two output pulses of this sensor corresponds to the rotation of the motor shaft by $\varphi_0 = 0.36^\circ$. The average angular speed over a time interval between two pulses is defined as the ratio of angle φ_0 to this time interval.

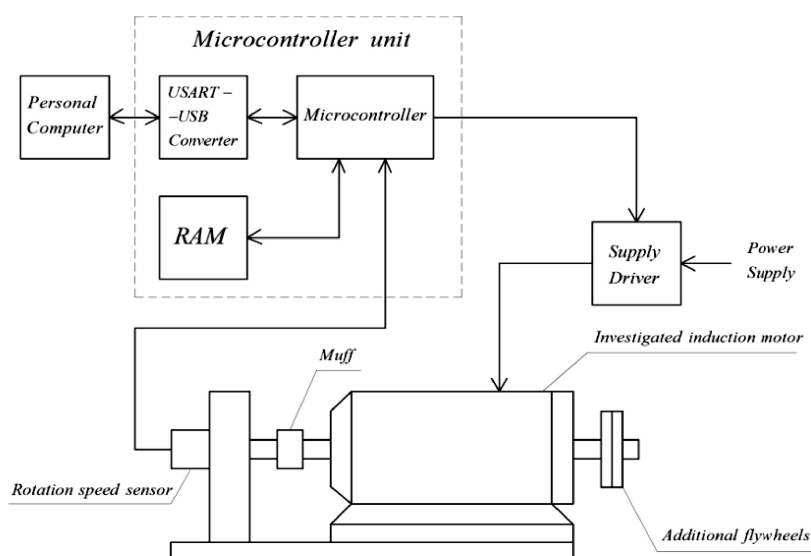


Figure 2. The structural scheme of the computer-measuring system of the induction motor's dynamical torque-speed characteristics

In general, the algorithm of the computer-measuring system of the induction motor's dynamical torque-speed characteristics is as follows:

1. Formation of a signal to control the supply driver to turn on the motor.
2. Measuring the carrying out angular speed dependence on time during the starting of the motor.
3. Formation of a signal to control the supply driver to turn off the motor.
4. Measuring the carrying out angular speed dependence on time during the motor's self-braking mode.
5. Transfer of measurement results to a PC.
6. Attaching an additional flywheel to the motor shaft to measure the moment of inertia.
7. Repeat steps 1–5 with the additional flywheel installed.
8. Processing of measurement information on a PC.

Figure 3 shows the experimental measurement results of the angular speed dependence on time during the starting of the motor. Figure 4 shows the experimental measurement results of the angular speed dependence on time during the motor's self-braking mode.

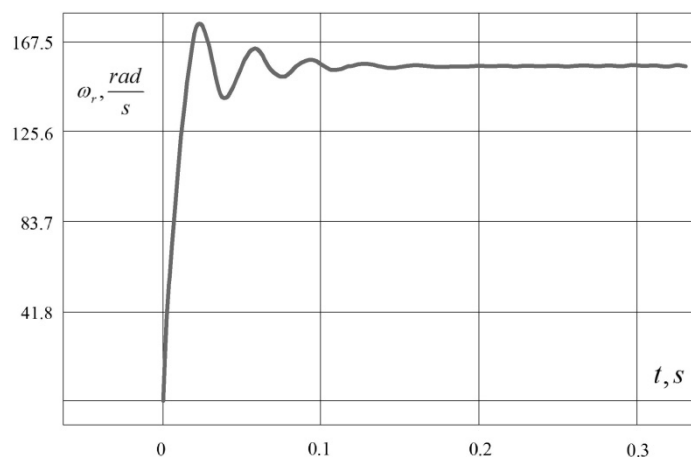


Figure 3. Experimental measurement results of the angular speed dependence on time during the starting of the motor

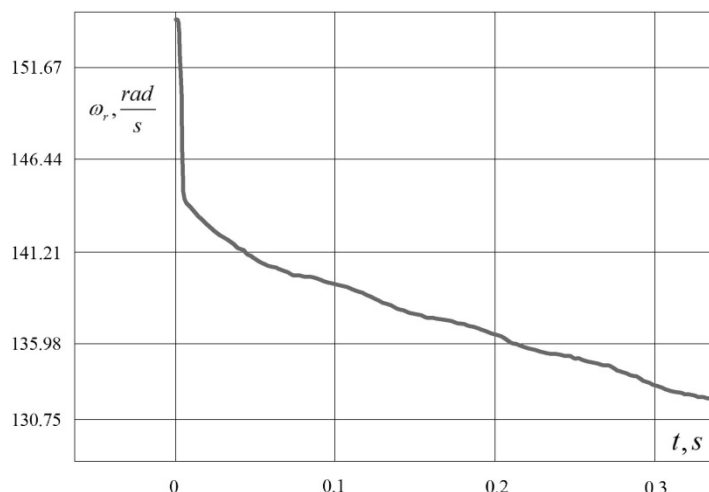


Figure 4. Experimental measurement results of the angular speed dependence on time during the starting of the motor

To determine the dependence of the angular acceleration on time for further calculation of the dynamical torque-speed characteristics, it is necessary to differentiate the dependence of the angular speed on time. Because the output signal of the sensor has a discrete character, the result of the direct differentiation of the angular speed dependence on time has a very high error. To reduce this error, it is necessary to average the results of the angular speed measurements. In our case, a moving average algorithm is used. This algorithm

is a popular way of measuring approximate results [19]. With digital signal processing, this algorithm is very effective at suppressing parasitic high-frequency components in the measuring signal. It also does not require a large number of calculations (such as spline-approximation), which allows it to be used in real time mode. The digital processing of the angular speed measurement results is carried out as follows [19]. The additive noise $n(k)$, which has a mathematical expectation $E\{n(k)\}$, is added to the angular speed value s . Thus, the measurement value is described by the following expression:

$$y(k) = s + n(k), \quad (11)$$

where k — the measurement number; y — the measurement value of the angular speed.

To determine the assessment of the signal using the method of least squares with the loss function:

$$V = \sum_{i=1}^N [y(k) - s]^2, \quad (12)$$

where N — number of measurements.

From the condition $\frac{dV}{ds} = 0$, we obtain the following expression for the average value of the measurement results:

$$\hat{s}N = \frac{1}{N} \sum_{k=1}^N y(k), \quad (13)$$

To obtain a recursive variant of the algorithm from expression (13), the previous estimate $\hat{s}(N-1)$ is subtracted, as outlined in the following equation:

$$\hat{s}(k) = \hat{s}(k-1) + \frac{1}{k} [y(k) - \hat{s}(k-1)]. \quad (14)$$

With an increasing value of k , the influence of the individual measurement results on the $\hat{s}(k)$ decreases. If the parameter $k_\omega = \text{const}$ is used instead of the parameter k in expression (14), the effect of all subsequent measurements will be same, and Expression (14) will take the form

$$\hat{s}(k) = \hat{s}(k-1) + \frac{1}{k_\omega} [y(k) - \hat{s}(k-1)] = \frac{k_\omega - 1}{k_\omega} \hat{s}(k-1) + \frac{1}{k_\omega} y(k) \quad (15)$$

By experimentally selecting the k_ω parameter's value, the necessary averaging degree of the series of measurements is established.

Below are the results of the experimental measurements of the induction motor's dynamical torque-speed characteristic (Fig. 5), electromagnetic dynamic moment's dependence on time (Fig. 6), electromagnetic dynamic power's dependence on time (Fig. 7), mechanical dynamic power's dependence on time (Fig. 8), and dynamic loss in rotor wind's dependence on time (Fig. 9). The graphs show the measurement results in a thin line without using the moving average algorithm, in a thick line using the moving average algorithm.

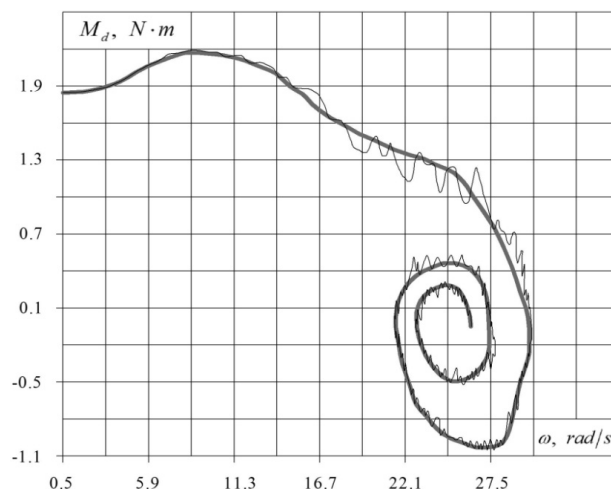


Figure 5. The induction motor's dynamical torque-speed characteristic measurement result

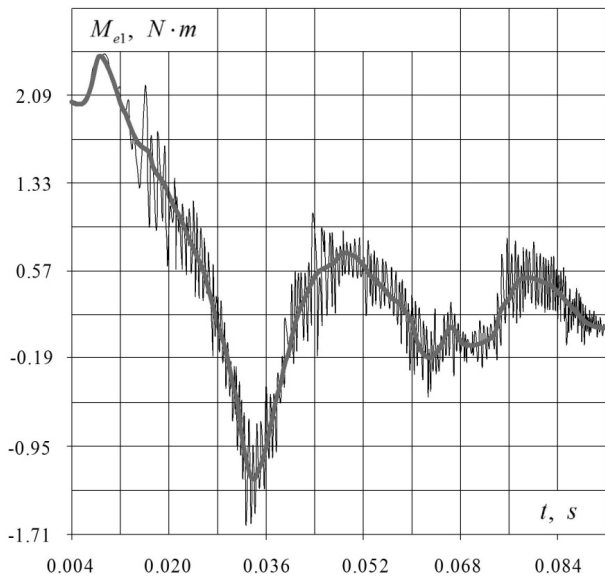


Figure 6. The electromagnetic dynamic moment's dependence on time

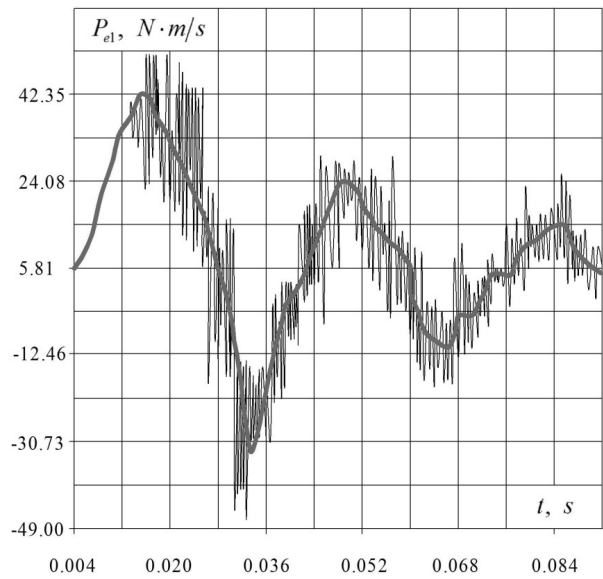


Figure 7. The electromagnetic dynamic power's dependence on time

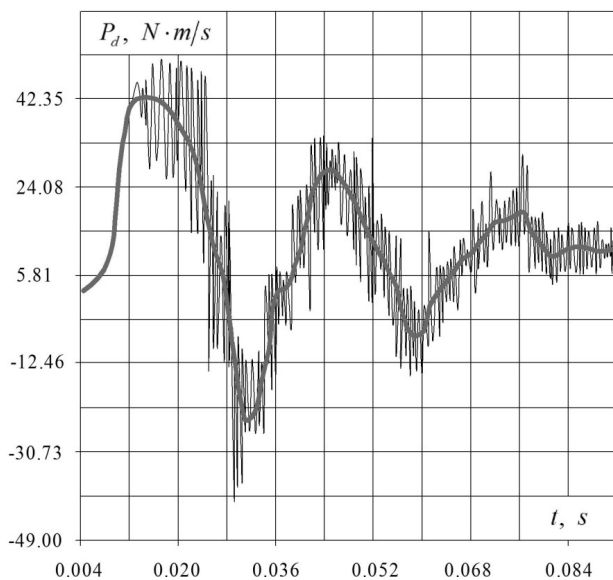


Figure 8. The mechanical dynamic power's dependence on time

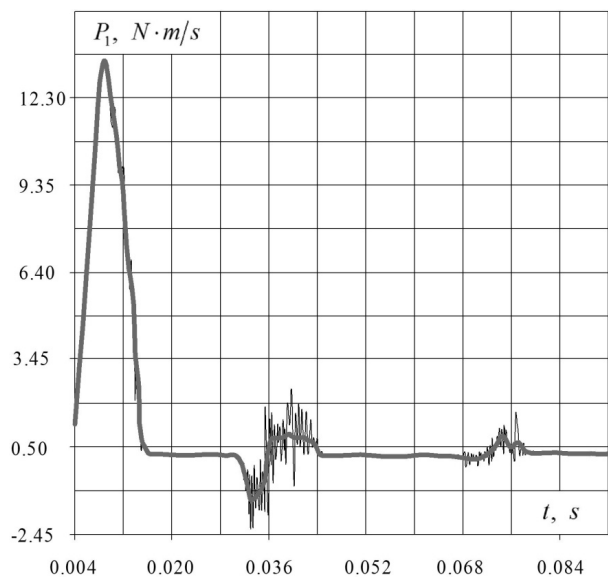


Figure 9. The dynamic loss in rotor winds' dependence on time

An experimental version of the computer-measuring system of the induction motor's dynamical torque-speed characteristics was developed. With the help of this system, the dynamical torque-speed characteristic, inertia moment, angular speed's dependence on time, electromagnetic dynamic moment's dependence on time, electromagnetic dynamic power's dependence on time, mechanical dynamic power's dependence on time, and dynamic loss in rotor winds' dependence on time were measured. The proposed system had the following basic metrological characteristics:

- Lower limit of angular speed measurement: 3 rad/s;
- Upper limit of angular speed measurement: 370 rad/s;
- Error of angular speed measurement < 1.5 %;
- Lower limit of dynamic moment: 0 Nm;
- Upper limit of dynamic moment: 30 Nm;
- Error of dynamic moment measurement < 2.5 %;
- Lower limit of inertia moment measurement: 0.0004 kg·m²;

- Upper limit of inertia moment measurement: $0.005 \text{ kg} \cdot \text{m}^2$;
- Error of inertia moment measurement $< 5 \%$.

The measuring method of the rotor moment of inertia at the use of an additional flywheel and the angular speed's dependence on time during the motor self-braking mode were proposed and implemented.

To reduce the error of direct differentiation of the angular speed's dependence on time a moving average algorithm was used. This enabled the improvement of the characteristics of the system in comparison with analogues.

References

- 1 IEEE Standard Test Procedure for Polyphase Induction Motors and Generators (2004). *IEEE Std 112–2004 from 12th May 2004 (Revision of IEEE Std 112–1996)*. New York: American National Standard Institute.
- 2 Anuchin, A., Shpak D., Zharkov, A., Ostrirov, V., & Vagapov, Y. (2017). A method of determining the maximum performance torque-speed characteristic for an induction motor drive over its entire speed range. *IEEE 58th International Scientific Conference on Power and Electrical Engineering of Riga Technical University* (12–13 October, pp. 1–5).
- 3 Toman, M., Cipin, R., Mach, M., & Vorel, P. (2017). Application of acceleration method for evaluation of induction motor torque-speed characteristics. *IEEE International Conference on Environment and Electrical Engineering and IEEE Industrial and Commercial Power Systems Europe* (6–9 June, pp. 1–4).
- 4 Bodolai, T. (2010). Computer-aided Measurement Method for Determination of Torque-Speed Characteristics of Electrical Motors Used in Practical Education. *Journal of Physics*, 1, 1–7.
- 5 Natrasevski, A. (1971). Installation and Method of Recording Electric Motor's Torque-Speed Curve Under Steady-State and Dynamic Regimes. *IEEE Transactions on Industry and General Applications*, 7, 500–503.
- 6 Selim H., & Girgis, G.A. (1986). Microprocessor-Based Digital Accelerometer and its Application in an Instrument for Motor Torque-Speed Characteristic Display During the Transient Interval. *IEEE Transactions on industrial electronics*, 44–48.
- 7 Buinac, R., & Tomljenovic, V. (2013). Determination of the torque-speed characteristic of induction motor in electric machinery education. *36th International Convention on Information and Communication Technology, Electronics and Microelectronics* (20–24 May, pp. 765–769).
- 8 Szabados, B., Dableh, J.H., Findlay, R.D., & Stafford, D. (1989). A new approach for measurement of the torque-speed characteristics of induction motors. *Fourth International Conference on Electrical Machines and Drives* (13–15 September, pp 246–350).
- 9 Szabados, B., Dableh, J.H., Findlay, R.D., Obermeyer, G.M., & Draper, R.E. (1990). Measurement of the torque-speed characteristics of induction motors using an improved new digital approach. *EEE Transactions on Energy Conversion*, 5, 565–571.
- 10 Chan, T.F. (1993). Determination of the Torque-Speed Characteristic of an Induction Motor Using a Curve-Fitting Technique. *International Journal of Electrical Engineering Education*, 366–373.
- 11 Bellini, A., Figalli, G., & Ulivi, G. (1986). A Microcomputer-Based Optimal Control System to Reduce the Effects of the Parametric Variations and Speed Measurement Errors in Induction Motor Drives. *IEEE Transactions on Industry Applications*, 22, 42–50.
- 12 Cipin, R., Patocka, M., & Vondrus, J. (2011). Acceleration method of the IM torque-speed characteristics measurement. *International Conference on Power Engineering, Energy and Electrical Drives* (11–13 May, pp. 1–5).
- 13 Aree, P. (2016). Analytical approach to determine speed-torque curve of induction motor from manufacturer data. *Procedia Computer Science*, 293–296.
- 14 Niu, S., Ho, S.L., & Fu, W. (2015). Fast Computation of Torque-Speed Characteristics of Induction Machines. *IEEE International Magnetism Conference* (11–15 May, p. 1).
- 15 Emmrich, K., Brune, A., & Ponick, B. (2014). Evaluation of an Analytical, Efficiency-Optimized Torque-Speed Characteristic of Induction Machines Coupled with a Thermal-Electromagnetic Energy Consumption Calculation. *International Conference on Electrical Machines* (2–5 September, pp. 762–767.).
- 16 Pflingsten, G., & Hameyer, K. (2017). Highly efficient approach to the simulation of variable-speed induction motor drives. *Science Measurement & Technology IET*, 11, 793–801.
- 17 Kojooyan-Jafari, H., Monjo, L., Corcoles, F., & Pedra, J. (2014). Parameter Estimation of Wound-Rotor Induction Motors From Transient Measurements. *IEEE Transactions on Energy Conversion*, 29, 300–308.
- 18 Podzharenko, V.O., & Kucheruk, V.Y. (1996). Computer-Measuring System of the Mechanical Characteristics of Electrical Drives. *Conference of Electrical Drives and Power Electronics* (1–3 October 1996, pp. 633–637).
- 19 Iserman, R. (1981). *Digital Control Systems*. Berlin: Springer-Verlag.

В.Ю. Кучерук, И.П. Курытник, Е.З. Ошанов, П.И. Кулаков,
А.А. Семенов, Д.Ж. Карабекова, А.К. Хасенов

Асинхронды қозғалтқыштың айналмалы моментінің динамикалық сипаттамаларын компьютерлік-өлшеу жүйесі

Мақалада асинхронды қозғалтқыштардың және оны іске асыру үшін компьютерлік-өлшеу жүйесінің айналмалы моментінің динамикалық сипаттамасын анықтаудың тиімді әдісі қарастырылды. Бұл әдіс қосымша маховикті қолданып және бұрыштық жылдамдықты динамикалық өлшеу, бастапқы, өтпелі процесс аяқталғаннан кейін және асинхронды қозғалтқыштың өзін-өзі тежеу режимінде орындалатын уақыт функциясы ретінде қолданылды. Өлшеу нәтижесінде алынған деректерді аппроксимациялау үшін жылжымалы орта алгоритмі пайдалынды. Сонымен қатар бұл жүйенің көмегімен инерция моменті, бұрыштық жылдамдықтың уақытқа тәуелділігі, электрмагниттік динамикалық моменттің, электрмагниттік динамикалық қуаттың, механикалық динамикалық қуаттың, және ротор желдеріндегі динамикалық шығындардың уақытқа тәуелділіктері өлшенеді. Мақалада ұсынылған компьютерлік-өлшеу жүйесін пайдалана отырып, асинхронды қозғалтқыштың сипаттамаларын эксперименттік өлшеу нәтижелері келтірілген. Ұсынылған жүйе эксперименттік болып табылады және одан әрі оларды өндіру процесінде асинхронды қозғалтқыштарды сынау үшін пайдаланылуы мүмкін.

Кілт сөздер: компьютерлік-өлшеу жүйесі, динамикалық жылдам-жылдамдық сипаттамасы, асинхронды қозғалтқыш, жылжымалы орта алгоритмі.

В.Ю. Кучерук, И.П. Курытник, Е.З. Ошанов, П.И. Кулаков,
А.А. Семенов, Д.Ж. Карабекова, А.К. Хасенов

Компьютерно-измерительная система динамических характеристик крутящего момента асинхронного двигателя

В статье рассмотрен эффективный метод определения динамической характеристики вращательного момента асинхронных двигателей и компьютерно-измерительной системы для его реализации. В этом методе использованы дополнительный маховик, динамические измерения угловой скорости, как функции времени, выполняющегося в начале, также после окончания переходного процесса и в режиме самоторможения асинхронного двигателя. Для аппроксимации данных, полученных в результате измерений, применен алгоритм скользящего среднего. Кроме того, с помощью этой системы измеряются момент инерции, а также зависимости (от времени) угловой скорости, электромагнитного динамического момента, электромагнитной динамической мощности, механической динамической мощности и динамических потерь в ветрах ротора. В статье приведены результаты экспериментальных измерений характеристик асинхронного двигателя с использованием предложенной компьютерно-измерительной системы. Предложенная система является экспериментальной и в дальнейшем может быть использована для испытаний асинхронных двигателей в процессе их производства.

Ключевые слова: компьютерно-измерительная система, динамическая моментно-скоростная характеристика, асинхронный двигатель, алгоритм скользящего.

B.R. Nussupbekov¹, G.T. Kartbaeva¹, M. Stoev²,
A.K. Khassenov¹, D.Zh. Karabekova¹, A.K. Muratova¹

¹*Ye.A. Buketov Karaganda State University, Kazakhstan;*

²*Neofit Rilski South-West University, Blagoevgrad, Bulgaria
(E-mail: ayanbergen@mail.ru)*

Electrohydroimpulse method of extracting bone grease

The extraction of fat is the most important stage of the technological process of production of animal fats. The task of the study is to ensure the extraction of fat from fat cells of adipose tissue. Therefore, there are various technological methods that allow to influence the adipose tissue in such a way as to separate the fat contained in them from the fat cells. Electrohydroimpulse method of extracting bone grease for the production of gelatin was developed. Electrohydroimpulse method of extracting grease from bone mass, characterized in that the bone mass is not subjected to mechanical shock. In the mixture, a shock wave is formed, which is created by an electrohydroimpulse installation. Tests of the experimental electrohydroimpulse installation for the extraction of grease from the bone mass of cattle were carried out for various bones of cattle. The article shows a diagram of the crushing host of electrohydroimpulse plants for the extraction of grease from bone mass. In laboratory studies, the work on degreasing the crushed bone has been done at different values of the capacitor bank electrohydroimpulse installation, the discharge voltage, the length of the discharge gap on the switching device, the temperature of the mixture and set effective parameters for optimal degreasing of bone mass.

Keywords: bone grease extraction, crushing unit, electrohydraulic method, switching device, length of discharge gap.

Introduction

Extraction of bone grease is the most important task of the technological process of edible animal grease production affecting both the quantitative and qualitative characteristics of the grease processing method. The grease contained in the bone is a great nutritional value, because of its highly digestibility, and contains many unsaturated and polyunsaturated fatty acids and lecithin, and its latter is several times more than in other animal greases.

Regardless of the using final products the technology of processing food bone material firstly provides bone dehydration. The simplest way to extract grease from bone and bone residue is to heat it at atmospheric pressure in open boilers. The degreasing process takes place at a temperature of 90–100 °C in an aqueous medium. Contact with water eliminates the possibility of adsorption of grease on the surface of particles and reduces its retention in the capillaries of the bone material [1, 2].

The boilers are heated with water or steam through the casing, since direct contact of the hot steam with the bone promotes the formation of emulsion and increase in the loss of protein substances with the broths. Removable baskets are provided for the mechanization of loading and unloading raw materials.

The raw material varies depending on the temperature and duration of heating. First of all this refers to gluten which is formed from collagen, and its hydrolysis, which leads to the depletion of bone collagen.

The soft mode of sweating is caused by the need to preserve the mechanical strength of the tubular bone as an ornamental material. In addition, high temperature and prolonged contact of grease with heated bone lead to a deterioration in the organoleptic characteristics of the final product. This explains the moderate temperature conditions not exceeding 90–100 °C of the bone heating in the open boilers.

Removing grease from the grease source by heating in the open boilers is not completely reached. The greaves consisting of 30–35 % the mass of raw materials contains up to 20 % grease. Greaves degreased on special equipment which requires certain material costs. Grease grade decreases during secondary degreasing of greaves.

As sweating grease in batch apparatus, two thermal methods of obtaining grease are used: dry and wet. The essence of grease extraction by the dry method lies in the fact that the moisture contained in the grease raw material evaporates into the atmosphere or is removed under vacuum after unwelding and during the dehydration process. In this case, the grease contained in the raw material is partially excreted by forming a two-phase system: dry fatty greaves — grease [3, 4].

For the final extraction of grease from the greaves we apply pressing or centrifugation. The dry method is practiced when it is necessary to ensure a high yield of benign grease and greaves, and the taste and smell of grease are secondary importance. The adipose tissue is in direct contact with hot water or live steam used to heat the raw materials during the heat treatment process in the wet method of processing fat raw materials. At the same time, most proteins mainly collagen are welded and hydrolyzed to form gluten (broth). The grease released from the raw materials is also partially emulsified. As a result of heat treatment the three-phase system is obtained: grease — greaves — grease.

However this method is quite complex in terms of hardware, and leads to loss of bone collagen during grease extraction which leads to a decrease in yield and deterioration in the quality of glue and gelatin produced from skimmed bone. Owing to the duration of the process of draining, grease may acquire the taste and smell of weakly roasted raw materials. At the dry method of grease draining requires a large consumption of steam, cold water and electricity. Complete and thorough destruction of cells and tissue as a whole is achieved only when the raw material is heated to temperatures above 100 °C and the quality of fat deteriorates sharply in this method. The main disadvantage of dry and wet methods is using equipment of large dimensions and metal with a small heat transfer surface, low heat transfer coefficient [5].

A particularly high degree of grease extraction from bone mass is necessary in case of its subsequent use for the production of photogelatin: the residual grease content in the bone tissue should not exceed 1 % by weight of the bone, therefore it is necessary to remove at least 95 % of the grease originally contained in it. A given degree of grease extraction can be achieved by repeatedly passing the bone through hydromechanical impulse devices, however as long as decrease of the greaset content in the aquatic environment makes it difficult to allocate. The big disadvantage of the pulse hydromechanical method is the strong grinding of the bone with rotating hammers. With a single pass through the apparatus about 30 % of the bone mass is so crushed that it can no longer be used in gelatin production, and with repeated passing the losses increase to 50 % [6, 7].

In this regard, electrohydroimpulse method of extracting greese from bone mass is developed in the laboratory of hydrodynamics and heat exchange of Y.A. Buketov Karaganda State University, differ from the bone mass that is not subjected to mechanical shock. A shock wave is formed in the mixture which is created using an electrohydroimpulse installation [8, 9].

Results and discussions

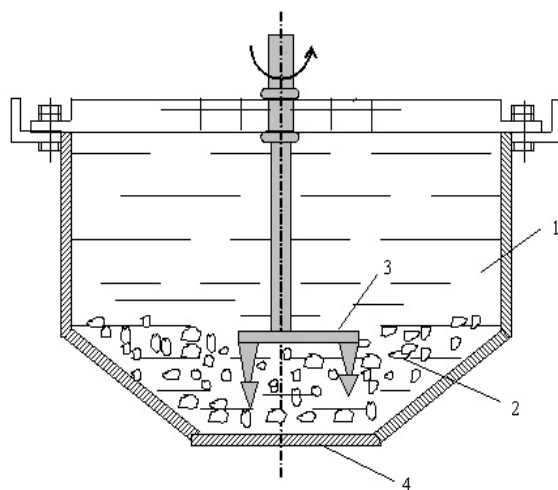
So far, it is not established which of the possible known methods (hydromechanical pulsed, extraction, etc.) of raw bone degreasing ensures the achievement of the greatest economic effect. An experimental electrohydroimpulse installation and the working part of the crushing unit were designed and assembled to study the effect of the underwater spark discharge on crushing and extracting grease from the bone mass and protein from the bone matrix.

Figure shows the diagram of the crushing unit of an electrohydroimpulse installation for extracting grease from bone mass. Before carrying out laboratory work it is necessary to prepare the bone mass of medium fatness. Preliminary preparation of the electrohydroimpulse installation for the performance of work is carried out when disconnected from the network following the rules of safe operation. A negative grounded electrode is connected to the body of the crushing and grinding unit by means of a tire, the cross section of which (for copper) is at least 30 mm², and the points of direct connection must have a good contact. After that, the control panel of the electrohydroimpulse installation is grounded. Install protective fences to prevent accidental contact with the voltage of workers in the workshop.

Tests of an experimental electrohydroimpulse unit for extracting grease from the bone mass of cattle were carried out for various bones of cattle taken separately in the sausage shop of «Tulpar» JSC in Karaganda. According to the technological estimates of the laboratory of the «Tulpar» JSC workshops, organic compounds (bones) had a small and medium fatness.

Standard differential thermocouples calibrated by temperature, are mounted in the CGU (crushing and grinding unit) to determine the temperature of the mixture. Before conducting the experiments, 20 kg of the bone material obtained after pressing was crushed to the size of 5–10 mm, divided into certain fractions and weighed on special electronic scales. Then the bone mass was placed in a special container with technical water and left for 6 hours. After the treatment, the impregnated bones were weighed to determine the mass. The bone mass connected to water and heated to a temperature of 32–50 °C enters the crushing and grinding unit through a guide cone receiver. The mass is subjected to the impact of a shock wave arising from a spark discharge after tightly closing the flap. The intensity of the degreasing process and the possibility of wide

regulation directly in the course of the process being carried out is achieved by rotating the CGU case relative to the central electrode. The CGU housing is rotated by a motor with an angular speed of 15 rpm... In this case, the working electrode is supplied with a specific energy equal to 2.0×10^4 J/m with a pulse repetition rate of 5...14 Hz. The defatted bone from the spark gap falls on the discharge conveyor, and the grease floats up and is further processed through the drainage along with the water. The residual grease content in the bone is about 1.0–1.4 % in the process of a single treatment in the installation.



1 — working capacity; 2 — organic mass; 3 — high voltage double electrode; 4 — negative electrode

Figure. Diagram of the crushing unit of an electrohydroimpulse installation for extracting grease from bone mass

When exposed to a pulse repetition rate of $7 \div 15$ Hz, shock waves arise in the aquatic environment, and water penetrating into the bone contributes to the destruction of the structure of the grease source which contains grease displacing it. In this regard, the effect of destruction of the bone structure and the transition of fat mass in the solution. The frequency range is set on the basis of experimental studies.

The temperature in the range of 32–50 °C allows to destroy the grease and remove from it a valuable component — fat. At temperatures below 32 °C, part of the grease is retained by the destroyed tissue (pits) as a result of adsorption and capillarity. The viscosity and surface tension of the grease increase, and the extraction process slows down.

Studies of the electro-impulse method shows that impulses arising due to the electrohydraulic effect are sufficient to destroy the bonds that keep fat cells in the tissue.

The impact of the underwater spark discharge on the degree of degreasing was investigated at a voltage on the switching device of 10 kV; capacitor capacitance 0,1; 0,2; 0,25; 0,4; 0,5 μ F. The experiments were carried out with bones of cattle (Table 1) with the following parameters.

Table 1

The main parameters of bone mass

Bone name	Components, %				
	grease	collagen	other proteins	ash	water
Spine	20	12	6	25	37
Chest bone	14	9	10	16	51
Pelvic bone	22	13	4	32	29

Bone degreasing occurs under the influence of an underwater spark discharge and cavitation of a gas bubble, with a high-voltage discharge in water. The degree of extraction depends on the electrical parameters of the electrohydroimpulse installation and the temperature of the mixture in the crushing and grinding unit. Tables 2–6 present quantitative data on the effect of capacitor battery capacity on the degree of extracting grease from bone mass at various values of voltage U , discharge gap length l_p at the switching device, and mixture temperature.

Table 2

The effect of the capacitance battery of an electrohydroimpulse unit for the degreasing of crushed bone
(at $U = 10$ kV, $l_p = 7$ mm, $t_{mix} = 32$ °C)

Bone name	Initial data of bone mass $d_{frac} = 10$ mm				
	% grease before processing	% release of grease after processing			
		0.2 μ F	0.25 μ F	0.4 μ F	0.5 μ F
Spine	20	12.7	13.3	14.1	14.5
Chest bone	14	8.8	9.0	9.0	8.9
Pelvic bone	22	14.5	15.7	16.1	16.2

Table 3

The effect of the capacitance battery of an electrohydroimpulse unit for the degreasing of crushed bone
(at $U = 15$ kV, $l_p = 7$ mm, $t_{mix} = 32$ °C)

Bone name	Initial data of bone mass $d_{frac} = 10$ mm				
	% grease before processing	% release of grease after processing			
		0.2 μ F	0.25 μ F	0.4 μ F	0.5 μ F
Spine	20	14.6	14.6	16.3	16.5
Chest bone	14	9.7	10.0	10.3	10.6
Pelvic bone	22	16.6	17.5	18.2	18.2

Table 4

The effect of the capacitance battery of an electrohydroimpulse unit for the degreasing of crushed bone
(at $U = 20$ kV, $l_p = 7$ mm, $t_{mix} = 32$ °C)

Bone name	Initial data of bone mass $d_{frac} = 10$ mm				
	% grease before processing	% release of grease after processing			
		0.2 μ F	0.25 μ F	0.4 μ F	0.5 μ F
Spine	20	15.0	15.1	17.1	17.2
Chest bone	14	10.2	10.4	11.0	11.3
Pelvic bone	22	17.2	18.0	19.0	18.2

Таблица 5

The effect of the capacitance battery of an electrohydroimpulse unit for the degreasing of crushed bone
(at $U = 10$ kV, $l_p = 7$ mm, $t_{mix} = 32$ °C)

Bone name	Initial data of bone mass $d_{frac} = 10$ mm				
	% grease before processing	% release of grease after processing			
		0.2 μ F	0.25 μ F	0.4 μ F	0.5 μ F
Spine	20	15.0	15.1	17.1	17.2
Chest bone	14	10.1	10.6	11.2	11.2
Pelvic bone	22	17.4	18.1	19.0	18.1

Table 6

The effect of the capacitance battery of an electrohydroimpulse unit for the degreasing of crushed bone
(at $U = 25$ kV, $l_p = 9$ mm, $t_{mix} = 38$ °C)

Bone name	Initial data of bone mass $d_{frac} = 10$ mm				
	% grease before processing	% release of grease after processing			
		0.2 μ F	0.25 μ F	0.4 μ F	0.5 μ F
Spine	20	15.3	15.5	17.4	17.2
Chest bone	14	10.4	10.8	11.4	11.3
Pelvic bone	22	17.8	18.4	19.0	18.7

Table 7

The effect of the capacitance battery of an electrohydroimpulse unit for the degreasing of crushed bone
(at $U = 25$ kV, $l_p = 10$ mm, $t_{\text{mix}} = 42$ °C)

Bone name	Initial data of bone mass $d_{\text{frac}} = 10$ mm				
	% grease before processing	% release of grease after processing			
		0.2 μF	0.25 μF	0.4 μF	0.5 μF
Spine	20	16.5	16.8	18.1	18.0
Chest bone	14	11.1	11.4	12.0	11.9
Pelvic bone	22	18.3	18.7	19.6	19.4

Table 8

The effect of the capacitance battery of an electrohydroimpulse unit for the degreasing of crushed bone
(at $U = 25$ kV, $l_p = 12$ mm, $t_{\text{mix}} = 44$ °C)

Bone name	Initial data of bone mass $d_{\text{frac}} = 10$ mm				
	% grease before processing	% release of grease after processing			
		0.2 μF	0.25 μF	0.4 μF	0.5 μF
Spine	20	17.0	17.3	18.5	18.4
Chest bone	14	11.7	11.9	12.4	12.3
Pelvic bone	22	19.1	19.3	20.0	19.8

Table 9

The effect of the capacitance battery of an electrohydroimpulse unit for the degreasing of crushed bone
(at $U = 30$ kV, $l_p = 12$ mm, $t_{\text{mix}} = 44$ °C)

Bone name	Initial data of bone mass $d_{\text{frac}} = 10$ mm				
	% grease before processing	% release of grease after processing			
		0.2 μF	0.25 μF	0.4 μF	0.5 μF
Spine	20	17.1	17.3	18.6	18.7
Chest bone	14	11.8	12.0	12.4	12.4
Pelvic bone	22	19.5	19.3	20.1	19.9

Conclusion

From the obtained laboratory data it can be seen that the voltage on the switching device should be $U = 25$ kV, the length of the discharge gap, $l_p = 12$ mm, and the mixture temperature $t_{\text{mix}} = 44$ °C, the optimal value of the capacity of capacitor battery is about $C = 0.4$ μF for maximum greave extraction from the bone mass. The repetition rate of the discharges was established from experimental data of 7 Hz for optimal defatting of the bone mass.

References

- 1 Соколов А.А. Технология мяса и мясопродуктов: учебник / А.А. Соколов. — М.: Пищ. пром-сть, 1970. — 740 с.
- 2 Стабников В.Н. Процессы и аппараты пищевых производств: учебник / В.Н. Стабников, В.И. Баранцев. — М.: Агропромиздат, 1985. — 509 с.
- 3 Лысянский В.М. Экстрагирование в пищевой промышленности: учебник / В.М. Лысянский, С.М. Гребенюк. — М.: Агропромиздат, 1987. — 187 с.
- 4 Либерман С.Г. Производство пищевых животных жиров на мясокомбинатах: учебник / С.Г. Либерман. — М.: Пищ. пром-сть, 1982. — 256 с.
- 5 Джафаров А.Ф. Производство желатина: учебник / А.Ф. Джафаров. — М.: Агропромиздат, 1990. — 287 с.
- 6 Нусупбеков Б.Р. Влияние температуры на электрогидравлический способ извлечения жира из костной массы / Б.Р. Нусупбеков, А.Ж. Сатыбалдин, Г.Е. Сейсенбек // Вестн. Караганд. ун-та. Сер. Физика. — 2001. — № 1(21). — С. 103–106.
- 7 Kusainov K.K. An electrohydraulic metod of removal of fat from bones / K.K. Kusainov, B.R. Nusupbekov, G.E. Seisenbek // Eurasian Physical Technical Journal. — 2007. — Vol.4, No. 2(8). — P. 57–61.

8 Сейсенбек Г.Е. Энергетические характеристики электрогидроимпульсного способа извлечения жира и белка из костной массы / Г.Е. Сейсенбек, Б.Р. Нусупбеков, К. Кусаиынов // Вестн. Евразийск. нац. ун-та им. Л.Н. Гумилева. Сер. физическая. — 2008. — № 2(62). — С. 165–173.

9 Нусупбеков Б.Р. Способ обезжиривания костного сырья / Б.Р. Нусупбеков, Г.Е. Сейсенбек, Г.М. Шаймерденова, Р.С. Турлыбекова // Научная жизнь. — 2009. — № 2. — С. 30–33.

Б.Р. Нусупбеков, Г.Т. Картбаева, М. Стоев,
А.К. Хасенов, Д.Ж. Карабекова, А.К. Муратова

Сүйек майын алудың электргидроимпульстік әдісі

Майды бөліп алу тағамдық мал майларын өндірудің технологиялық процесінің маңызды сатысы болып табылады. Зерттеудің міндеті май тінінің жасушаларынан майды алуды қамтамасыз ету болып табылады. Сондықтан май жасушаларынан өнімді бөліп алу үшін май ткандарына әсер ететін әртүрлі технологиялық тәсілдер қолданылуы мүмкін. Желатин өндіру үшін сүйек майын алудың электргидроимпульстік әдісі әзірленді. Сүйек массасынан май алудың электргидроимпульстік әдісі сүйек массасының механикалық соққысына ұшырамауымен ерекшеленеді. Қоспада электргидроимпульсті қондырғымен қалыптасатын соққы толқыны пайда болады. Ірі қара малдың сүйек массасынан май алу бойынша тәжірибелік электргидроимпульстік қондырғыны сынау ірі қара малдың түрлі сүйектері үшін жүргізілді. Мақалада сүйек массасынан май алу үшін электргидроимпульсті қондырғының ұнтақтау торабының схемасы келтірілген. Зертханалық зерттеулер кезінде электргидроимпульсті қондырғының конденсатор батареясы сыйымдылығының, разряд кернеуі мәндерінің, коммутациялық құрылғыдағы разряд аралықтың ұзындығының, қоспа температурасының әртүрлі мәндерінде ұсақталған сүйекті майсыздандыру жұмыстары орындалып, сүйек массасын оңтайлы майсыздандыру үшін тиімді параметрлер тағайындалды.

Кілт сөздер: сүйек майын алу, ұсақтау торабы, электргидравликалық әдіс, коммутациялық құрылғы, разряд аралығының ұзындығы.

Б.Р. Нусупбеков, Г.Т. Картбаева, М. Стоев,
А.К. Хасенов, Д.Ж. Карабекова, А.К. Муратова

Электрогидроимпульсный метод извлечения костного жира

Извлечение жира является важнейшей стадией технологического процесса производства пищевых животных жиров. Задача исследования заключается в обеспечении извлечения жира из жировых клеток жировой ткани. Поэтому возможны различные технологические приемы, позволяющие воздействовать на жировую ткань таким образом, чтобы выделить из жировых клеток содержащийся в них жир. Разработан электрогидроимпульсный метод извлечения костного жира для производства желатина который отличается тем, что костные массы не подвергаются механическим ударам. В смеси образуется ударная волна, которая создается с помощью электрогидроимпульсной установки. Испытания экспериментальной электрогидроимпульсной установки по извлечению жира из костной массы крупного рогатого скота проводились для различных костей крупного рогатого скота. В статье приведена схема дробильного узла электрогидроимпульсной установки для извлечения жира из костной массы. При лабораторных исследованиях выполнены работы по обезжириванию измельченной кости при различных значениях емкости конденсаторной батареи электрогидроимпульсной установки, значений напряжения разряда, длины разрядного промежутка на коммутирующем устройстве, температуры смеси и установлены эффективные параметры для оптимального обезжиривания костной массы.

Ключевые слова: извлечения костного жира, дробильный узел, электрогидравлический метод, коммутирующее устройство, длина разрядного промежутка.

References

- 1 Sokolov, A.A. (1970). *Tekhnolohiia miasa i miasoproduktov [Meat and meat products technology]*. Moscow: Pishchevaia promyshlennost [in Russian].
- 2 Stabnikov, V.N., & Barantsev, V.I. (1985). *Protessy i apparaty pishchevykh proizvodstv [Processes and apparatus of food production]*. Moscow: Ahropromizdat [in Russian].
- 3 Lysyanskiy, V.M., & Grebenyuk, S.M. (1987). *Ekstrahirovanie v pishchevoi promyshlennosti [Extraction in the food industry]*. Moscow: Ahropromizdat [in Russian].

- 4 Liberman, S.G. (1982). *Proizvodstvo pishchevykh zhyvotnykh zhirov na myasokombinatakh [Production of animal fats in meat processing plants]*. Moscow: Pishchevaia promyshlennost [in Russian].
- 5 Dzhafarov, A.F. (1990). *Proizvodstvo zhelatina [Gelatin production]*. Moscow: Agropromizdat [in Russian].
- 6 Nusupbekov, B.R., Satybaldin, A.Zh., & Seysenbek, G.E. (2001). Vliianie temperatury na elektrohivavlicheskiy sposob izvlecheniia zhira iz kostnoi massy [The effect of temperature on the electrohydraulic method of extracting fat from bone mass]. *Vestnik Karahandinskoho universiteta. Seriya Fizika — Bulletin of the Karaganda University. Physics series, 1(21)*, 103–106 [in Russian].
- 7 Kusainov, K.K., Nusupbekov, B.R., & Seisenbek, G.E. (2007). An elektrohydraulic metod of removal of fat from bones. *Eurasian Physical Technical Journal, 4, 2(8)*, 57–61.
- 8 Seysenbek, G.E., Nusupbekov, B.R., & Kusainov, K. (2008). Enerheticheskie kharakteristiki elektrohivavliivnogo sposobu izvlecheniia zhira i belka iz kostnoi massy [Energy characteristics of the electrohydroimpulse method for extracting fat and protein from bone mass]. *Vestnik Evraziiskoho natsionalnogo universiteta imeni L.N. Gumilyova. Seriya fizika — Bulletin of L.N. Gumilyov Eurasian national University, Physics series, 2(62)*, 165–173 [in Russian].
- 9 Nusupbekov, B.R., Seysenbek, G.E., Shaymerdenova, G.M., & Turlybekova, R.S. (2009). Sposob obezhirivaniia kostnogo syria [Method of degreasing bone raw materials]. *Nauchnaia zhizn — Scientific life, 2*, 30–33 [in Russian].

N.K. Tanasheva², A.N. Dyusembaeva^{1, 2}, B.R. Nussupbekov¹,
L.L. Min'kov³, Zh.G. Nurgalieva¹, K.K. Sadenova¹

¹*Ye.A. Buketov Karaganda State University, Kazakhstan;*

²*Institute of Applied Mathematics, Karaganda, Kazakhstan;*

³*Tomsk State University, Russia*

(E-mail: nazgulya_tans@mail.ru)

The study of the aerodynamic coefficients of rotating cylinders

In the course of the research, the theoretical knowledge on the aerodynamic characteristics of coiled cylinders in rotary motion was reviewed and the cylinders in circular motion on the working part of the aerodynamic pipe were studied. During the studying the dependence of the aerodynamic characteristics of rotating motion cylinders on the distance change, several cases of rotation of the cylinders were considered. When the direction of rotation of the cylinders changes, it is determined that frictional coefficient and the lifting force coefficient are changed. At the same time, the distance at which the aerodynamic parameters will have the highest value is determined. The rotation of rotating moving cylinders is determined by the aerodynamic pumps of the cylinders in the horizontal direction of the airflow due to the air velocity, the number of cylinders and the distance between the two cylinders. An increase in the velocity of the airflow is determined by the reduction of the coefficient of the friction coefficient and the lifting force of the cylinders in rotary motion; The aerodynamic characteristics of the coiled cylinders were first detected to increase the distance between the cylinders and reach them at a later distance. The aerodynamic characteristics of the cylinders with diameters 10 cm in diameter, that is the rotary motion, is determined by the maximum value with the coefficient of lifting force and the frontal impedance coefficient. These results are useful for us in practice, as these results can be used in smaller wind speed engines. In the local economy, the use of local wind power is a convenient, affordable, and environmentally friendly, with a minimal wind speed engine focused on reducing the deficit of electricity, which is one of the key issues in rural areas.

Keywords: rotary cylinders, magnus effect, angular barrier and lifting coefficients, Reynolds number.

Introduction

The main technical policy of the state for the further development of the energy sector is the launch of alternative energy sources. Kazakhstan is one of the countries with the alternative energy sources, such as water, wind, and solar energy. However, in addition to partial hydroenergy use, these alternative sources of power are not activated in the country. One of the main reasons for this is the fact that the country has a large concentration of energy resources.

Electricity can be divided into two: traditional and non-traditional. The most important source of traditional energy is coal, natural gas, peat and uranium. At first, the energy they have is coming from, but it is still an inexhaustible source of energy.

It's called irreversible because every year, only a small amount of solar energy becomes the energy of irreparable sources, and how many millions of years it takes to make a small amount of coal, ore, gas and uranium recovered. And non-traditional power sources include wind, water, solar energy, and so on. The use of renewable energy sources in energy consumption does not affect the overall heat balance here and does not lead to global warming. The energy coming from the ground and leaving the ground does not change. We take energy from the use of the newest generation of wind energy within this unhealthy electricity source. The first value of these sources of energy is that they do not harm nature. Renewable energy sources regularly replenish their energy and reaches millions of years until the wind reaches them. This is their second preferential.

The main importance of this research is to investigate the aerodynamic characteristics of the crankshafts' cylinders on the increase of power generation capacities of low-speed air flow motors. The wind speeds up to 4–5 m/s in Karaganda. So far, low wind speed engines were identified with two shaft and three swing motors based on the Magnus effect. However, the electricity generated by them can not fully compensate for losses [1–5]. Therefore, in order to reduce the flow of these motor drives, we need to consider the mutually advantageous location of the blades, in particular the cylinders, which are their main mechanisms.

Using our rotary motion cylinders, we set ourselves a goal to study how changes in their aerodynamic parameters affect the flow velocity, the number of cylinders, and the cylinder axes.

The main purpose of this research is to determine the effective location of the cylindrical blades, which relates to the basic elements of the wind turbines based on the Magnus Effect at low wind velocity and their dependence on other variables.

Methods of research

Research works at the aerodynamic pipeline are cheap and reliable. Therefore, the study of the aerodynamic patterns of the thing in the cylindrical form was carried out on the simple T-I-M aerodynamic pipe, located in the Aerodynamic measurement laboratory of the Department of Engineering Thermophysics named after professor Zh.S. Akylbayev. The aerodynamic pipe which is tested is an aerodynamic pipe with an open working zone in the closed circuit.

The coiled cylinders are located horizontally in the direction of air flow into the working part of the aerodynamic tube. For the study of the aerodynamic characteristics, lengths 31 cm are taken from 10 cm in diameter from two cylinders 3 and secured to bearing by means of the shaft 3. A roller bearing is fitted to the rotary motion of the cylinder to prevent obstacle of friction force.

The cylinders are rotated by means of the electromotor 5. In order to increase the rotation of the electromotor valve, it connects to the laboratory autotransformer with connecting wires. The rotary motion of one cylinder is supplied to the second cylinder by the belt pulleys 2 and the belt. Image of this mechanism is shown in Figure 1.



Figure 1. Figure of the workpiece video clip attached to the cylinders attached to the aerodynamic pipe

It is observed how the aerodynamic parameters of the cylinders change depending on the flow velocity, the rotation number and the distance between the two cylinders when the cylinders in the rotating motion are flowing horizontally. The results obtained from the experiments are as follows.

Results of research

Reduction of aerodynamic coefficients in speed of flowing air in a horizontal direction of cylinders with rotary motion is revealed in experiment.

The dependence of the barrier coefficient from the velocity of the airflow, i.e. the Reynolds number, is shown in Figure 2.

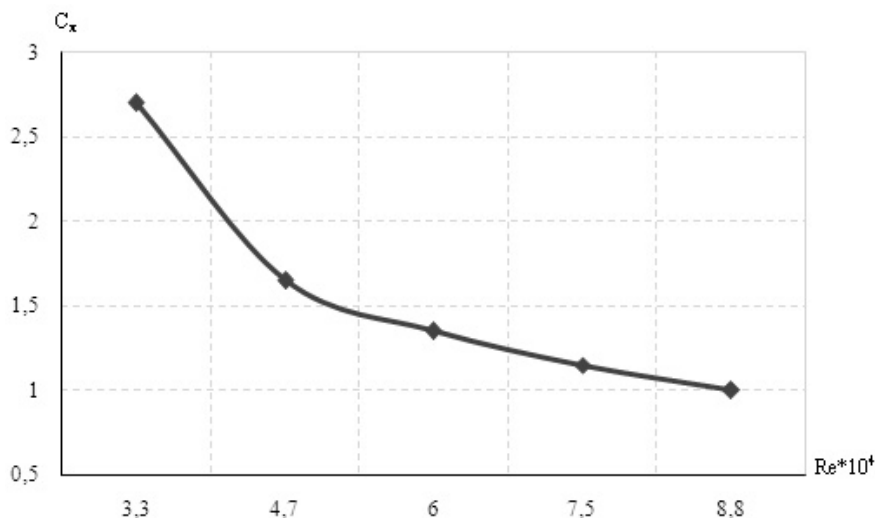


Figure 2. A graph of the Reynolds number dependence of the frontal barrier coefficient of cylinders with a diameter of 10 cm and 5 cm with a rotating moving distance when the engine is 120 V

As you can see from the dependence, the coefficient of frictional resistance decreases as the value of Reynolds increases. If we recall the formula for the calculation of the coefficient of the angle barrier, then we see that the angle barrier is inversely proportional to the square of the velocity. In the equation, along with the velocity, the force of the angle barrier directly proportional to the coefficient varies. But its change is less than the square of speed. Therefore, the angular barrier coefficient decreases when the velocity of air flow increases.

Figure 3 illustrates the dependence of the lifting force coefficient of the cylinders with a diameter of 10 cm in distance of 5 cm in the constant rotation of the cylinder.

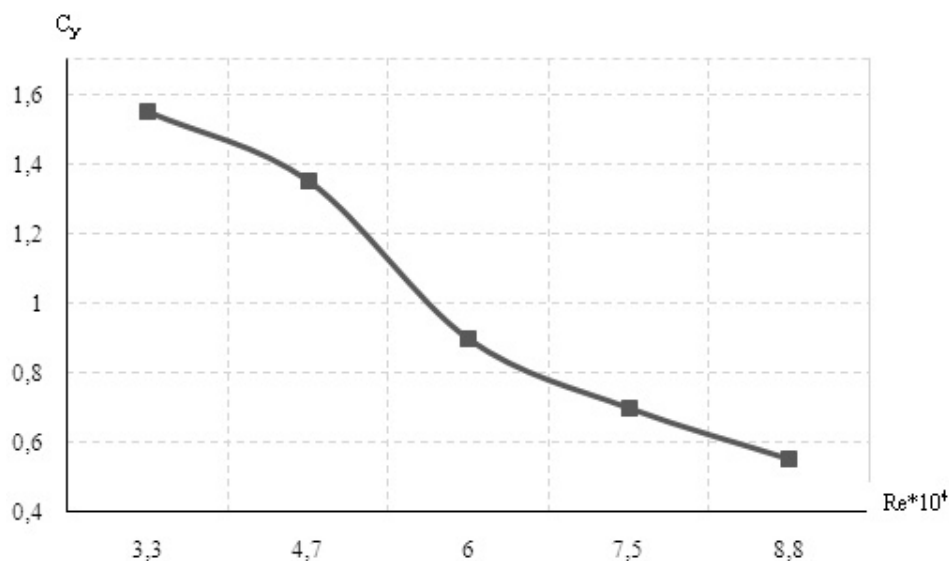


Figure 3. Dependence of lifting force on the Reynold number

As shown by the dependence on Figure 3, the lifting force of the double cylinders in rotating motion decreases as the number of Rheinolds increases. Because the lifting force is inversely proportional to the quadratic air velocity corresponds to the equation, and the Reynolds ratio is directly proportional to the velocity of the airflow, the lifting factor is proportional to the value of the Reynolds. Therefore, when the speed of the air flowing in the rotating motion of the cylinders in the orbital direction increases, the lifting force coefficient decreases.

The dependence of the friction coefficient of the rotating motion cylinders on the number of rotation of the cylinders is shown in Figure 4.

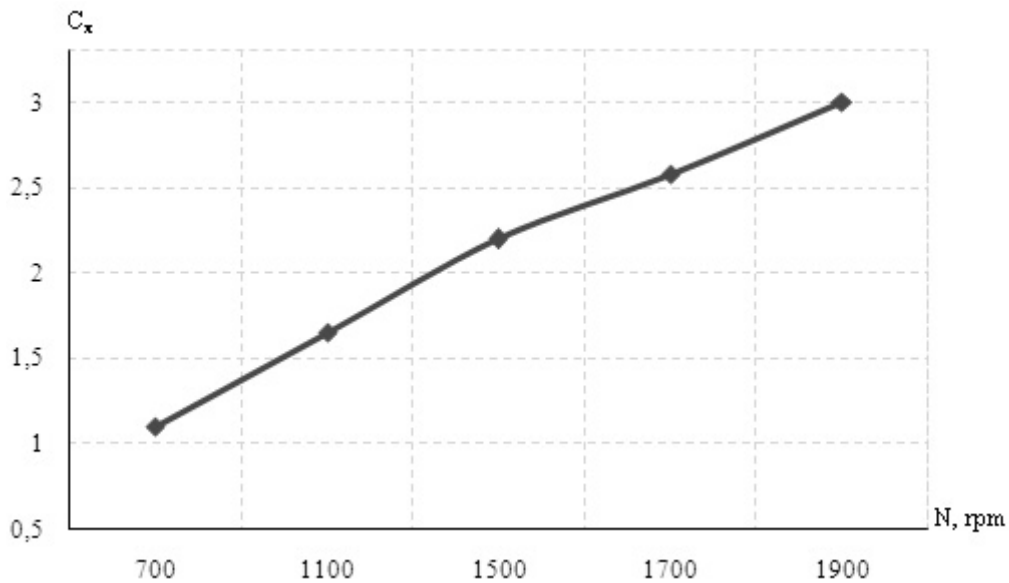


Figure 4. The dependence of the obstacle impedance on the number of rotations

As shown by the dependence, the angular barrier coefficient of rotating-acting cylinders with 10 cm in diameters 5 cm in distance horizontally oriented to the air flow varies directly proportionally to the number of rotation of the cylinders, i.e. the angle barrier coefficient increases as the number of rotations increases. The reason can be explained this way from a scientific point of view. At the back of the cylinders, the vortex area emerges when the air flows into the cylinder. Under the influence of these vortices, the pressure behind the cylinder decreases, the air rarely. When the rotating motion of the cylinder moves, the associated flow on the surface of the cylinder obstructs the movement of the incoming particles and starts to move them to the front surface of the cylinder. The air flows to the front of the cylinder under the influence of the direct flow. The energy of sealed air particles is greater than the energy of the absorbed air. As the number of cylinders revolves increasing, the compression of air particles on the front surface increases to a certain extent. This leads to the increased resistance of the cylinders. Therefore, when the number of rotation of the cylinders increases, the correlation coefficient also increases.

The following Figure 5 depicts the dependence of the cylinder rotation factor on the lifting force coefficient of rotating moving cylinders with a distance of 5 cm and a diameter of 10 cm, horizontally positioned to the direction of the air flow of 7 m/s.

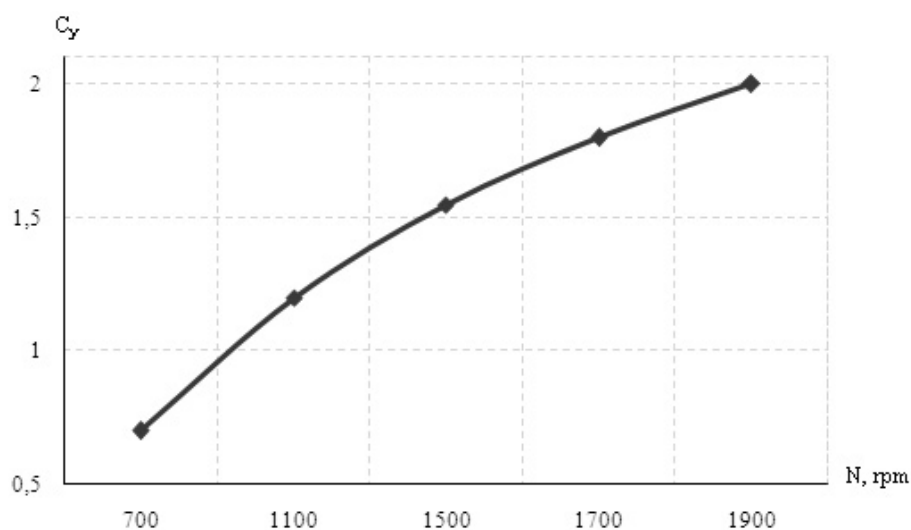


Figure 5. Graphs of dependence of the lifting force coefficient of cylinders with 10 cm in diameter of 10 cm with diameter of 5 cm with a velocity of 7 m/s

As you can see from Figure 5, the lifting force of the cylinders in rotary motion is decreasing with the increase in the number of cylinders. The reason for this is scientifically explained as follows. When the flow of rotating moving things flows horizontally, the Magnus effect is applied vertically to the cylinders, i.e. the reduced pressure zone is formed at the opposite direction to the air flow from the adjacent stream of the rotating cylinder on the surface of the rotating cylinder, and the associated flow to the upstream where there is an overpressure zone.

As a result, the cylinders move to the lower zone under the influence of forces in the high pressure zone. As the turnover increases, the force that affects the cylinders decreases in the reduced pressure zone and increases in the high pressure zone. Accordingly, the lifting force of the cylinders in the rotating motion increases. That is why the lifting force factor increases when the number of rotating cylinders increases.

Conclusion

The values obtained from the experiments can make a great contribution to increasing the power of the electric motors produced at low wind speeds. The results from the study of changes in the aerodynamic characteristics of the cylinders, especially between the cylinders that are blended, allow us to determine the effective location of the rotary cylinders, which are the main elements of the motor. The effective range of the spindle blades, that is, the cylinders, produces and consumes more electricity than the wind energy uses less energy. And with low cost and more energy-efficient engines, it is a good solution to reduce energy deficit in rural areas, far from central power plants.

This work was supported by project AP05131520.

References

- 1 Болотов А.В. Развитие ветроэнергетики Республики Казахстан, энергетические системы электроснабжения автономных объектов / А.В. Болотов, С.Е. Соколов, С.А. Болотов // Вестник АИЭС. — 2009. — № 3. — С. 11–18.
- 2 Бычков Н.М. Ветродвижитель с эффектом Магнуса. 2. Расчетные характеристики ветроколеса / Н.М. Бычков // Теплофизика и аэромеханика. — 2008. — Т. 15, № 2. — С. 583–596.
- 3 Kusaiynov K. Numerical simulation of a flow past a triangular sail-type blade of a wind generator using the ANSYS FLUENT software package / K. Kusaiynov, N.K. Tanasheva, L.L. Min'kov, B.R. Nusupbekov, Y.O. Stepanova, A.V. Rozhkova // Technical Physics. — 2016. — Vol. 61, Iss. 2. — P. 299–301.
- 4 Tanasheva, N.K. Effect of a rough surface on the aerodynamic characteristics of a two-bladed wind-powered engine with cylindrical blades / N.K. Tanasheva, T.O. Kunakbaev, A.N. Dyusembaeva, N.N. Shuyushbayeva, S.K. Damekova // Technical Physics. November 2017, Volume 62, Issue 11, pp 1631–1633.
- 5 Tanasheva N.K. Investigation of aerodynamic characteristics from the airflow angle of the rotating cylinder / N.K. Tanasheva, A.N. Dyusembaeva, L.L. Min'kov // Bulletin of the Karaganda University. Physics series. — 2018. — No. 1(89). — P. 88–92.

Н.К. Танашева, А.Н. Дюсембаева, Б.Р. Нусупбеков,
Л.Л. Миньков, Ж.Г. Нургалиева, К.К. Саденова

Айналмалы қозғалыстағы цилиндрлердің аэродинамикалық коэффициенттерін зерттеу

Мақалада орындау барысында айналмалы қозғалыстағы қосақталған цилиндрлердің аэродинамикалық сипаттамалары туралы теорияларға шолу жасалып, алынған теориялық білімдерге сүйене отырып, аэродинамикалық құбырдың жұмыстық бөлігінде айналмалы қозғалыстағы қосақталған цилиндрлер зерттелді. Айналмалы қозғалыстағы қосақталған цилиндрлердің аэродинамикалық сипаттамаларының арақашықтықтың өзгерісінен тәуелділігін зерттегенде цилиндрлердің айналу бағыттарының бірнеше жағдайы қарастырылды. Цилиндрлердің айналу бағыты өзгергенде олардың маңдайлық кедергі мен көтеру күші коэффициенттерінің өзгеретіндігі анықталды. Сонымен қатар аэродинамикалық параметрлер ең үлкен мәнге ие болатын арақашықтық белгілі болды. Айналмалы қозғалатын қосақталған цилиндрлерді ауа ағыны көденең бағытта аққан кездегі цилиндрлердің аэродинамикалық сипаттамаларының ауа жылдамдығына, цилиндрлердің айналу санына және екі цилиндрдің арасындағы қашықтыққа байланысты өзгерісі анықталды. Ауа ағының жылдамдығы артқанда айналмалы қозғалыстағы қосақталған цилиндрлердің маңдайлық кедергі мен көтеру күші коэффициенттерінің азаятындығы анықталды. Қосақталған цилиндрлердің аэродинамикалық сипаттамаларының, алдымен, цилиндрлердің арақашықтығы белгілі бір мәнге жеткенге дейін өсіп,

одан кейінгі арақашықтықтарда қайтадан кемитіндігі анықталды. Айналымды қозғалыс жасайтын, диаметрлері 10 см қосақталған цилиндрлердің аэродинамикалық сипаттамалары, яғни көтеру күші және маңдайлық кедергі коэффициенттері ең үлкен мән қабылдайтын арақашықтық анықталды. Бұл нәтижелер тәжірибеде қолдануға пайдалы болып саналады, себебі оларды аз жел жылдамдығында жұмыс істейтін желқозғалтқыштарында қолдануға болады. Ал аз жел жылдамдығында жұмыс істейтін желқозғалтқышын ауылдық жерлердегі шешілмеген негізгі мәселелердің бірі болып есептелетін электр энергияның тапшылын азайту бағытында жергілікті шаруашылықта қолдану ыңғайлы, сонымен қатар экологиялық жағынан тиімді болып табылады.

Кілт сөздер: айналымды цилиндрлер, Магнус тиімділігі, көтеру күші және маңдайлық коэффициенттері, Рейнольдс саны.

Н.К. Танашева, А.Н. Дюсембаева, Б.Р. Нусупбеков,
Л.Л. Миньков, Ж.Г. Нургалиева, К.К. Саденова

Исследование аэродинамических коэффициентов вращающихся цилиндров

Проведен обзор теоретических знаний об аэродинамических характеристиках спиральных цилиндров при вращательном движении и изучены цилиндры при круговом движении на рабочей части аэродинамической трубы. В ходе исследования рассмотрены зависимости аэродинамических характеристик цилиндров вращательного движения от изменения расстояния. При изменении направления вращения цилиндров определяется изменение коэффициентов трения и подъемной силы. Определены расстояния, на которых аэродинамические параметры имеют наибольшее значение. Вращение движущихся цилиндров определяется аэродинамическими насосами цилиндров в горизонтальном направлении воздушного потока за счет скорости воздуха, количества цилиндров и расстояния между двумя цилиндрами. Увеличение скорости воздушного потока определяется уменьшением коэффициента трения и подъемной силы цилиндров при вращательном движении; аэродинамические характеристики спиральных цилиндров были впервые обнаружены для увеличения расстояния между цилиндрами и достижения их на более позднем расстоянии. Аэродинамические характеристики цилиндров диаметром 10 см, т.е. вращательное движение, определяются максимальными значениями коэффициентов подъемной силы и лобового сопротивления. Эти результаты полезны на практике, так как они могут быть использованы для разработки двигателей, работающих при меньшей скорости ветра. В местной экономике использование ветроэнергетики является удобным, доступным и экологически чистым способом получения энергии. Двигатель ориентирован на снижение дефицита электроэнергии, что является одним из актуальных вопросов в сельской местности.

Ключевые слова: вращающиеся цилиндры, эффект Магнуса, коэффициенты лобового сопротивления и подъемной силы, число Рейнольдса.

References

- 1 Bolotov, A.V., Sokolov, S.E., & Bolotov, S.A. (2013). Razvitie vetroenerhetiki Respubliki Kazakhstan, enerheticheskie sistemy elektrosnabzheniia avtonomnykh obektov [Wind power development of Kazakhstan, energy power supply system of autonomous objects]. *Vestnik AIES — Bulletin AIPET*, 3(6), 11–18 [in Russian].
- 2 Bychkov, N.M. (2008). Vetrodvihatel s efektom Mahnusa. 2. Raschetnye kharakteristiki vetrokolesa [Wind turbine with Magnus. 2. Characteristics of the rotating cylinder]. *Teplofizika i aeromekhanika — Thermophysics and Aeromechanics*, 1, 583–596 [in Russian].
- 3 Kusainov, K., Tanasheva, N.K., Min'kov, L.L., Nusupbekov, B.R., Stepanova, Y.O., & Rozhkova, A.V. (2016). Numerical simulation of a flow past a triangular sail-type blade of a wind generator using the ANSYS FLUENT software package, *Technical Physics*, 61, 2, 299–301.
- 4 Tanasheva, N.K., Kunakbaev, T.O., Dyusembaeva, A.N., Shuyushbayeva, N.N., & Damekova S.K. (2017). Effect of a rough surface on the aerodynamic characteristics of a two-bladed wind-powered engine with cylindrical blades, *Technical Physics*, 62, 11, 1631–1633.
- 5 Tanasheva, N.K., Dyusembaeva, A.N., & Min'kov, L.L. (2018). Investigation of aerodynamic characteristics from the air-flow angle of the rotating cylinder, *Bulletin of the Karaganda University. Physics series*, 1(89), 88–92.

АВТОРЛАР ТУРАЛЫ МӘЛІМЕТТЕР СВЕДЕНИЯ ОБ АВТОРАХ INFORMATION ABOUT AUTHORS

- Arinova, E.T.** — Physics teacher, Gimnasium No. 1, Karaganda, Kazakhstan.
- Arkhipov, V.V.** — Candidate of physical and mathematical sciences, G.F. Morozov Voronezh State Forestry University, Russia.
- Chirkova, L.V.** — Candidate of technical sciences, Associate professor, Ye.A. Buketov Karaganda State University, Kazakhstan.
- Diorditsa, V.M.** — Forensic expert, Head of the automotive research sector, Research forensic center at the Department of the Ministry of internal affairs in Vinnitsa region, Vinnitsa, Ukraine.
- Dyusembaeva, A.N.** — PhD student, Ye.A. Buketov Karaganda State University, Kazakhstan.
- Erdybaeva, N.K.** — Doctor of physical and mathematical sciences, Professor, D. Serikbayev East Kazakhstan State Technical University, Ust-Kamenogorsk, Kazakhstan.
- Eremin, E.N.** — Doctor of technical sciences, Professor, Omsk State Technical University, Russia.
- Ermaganbetov, K.T.** — Professor, Candidate of physical and mathematical sciences, Ye.A. Buketov Karaganda State University, Kazakhstan.
- Hevko, I.** — Doctor of technical sciences, Professor, Ternopil Ivan Pul'uj National Technical University, Ukraine.
- Hud, V.** — Candidate of technical sciences, Docent, Ternopil Ivan Pul'uj National Technical University, Ukraine.
- Ibraev, N.Kh.** — Doctor of physical and mathematical sciences, Professor, Ye.A. Buketov Karaganda State University, Kazakhstan.
- Ispulov, N.A.** — Candidate of physical and mathematical sciences, Associate professor, S. Toraighyrov Pavlodar State University, Kazakhstan.
- Kamalova, G.B.** — Master student, Ye.A. Buketov Karaganda State University, Kazakhstan.
- Kasimov, S.S.** — Candidate of physical and mathematical sciences, Docent, Ye.A. Buketov Karaganda State University, Kazakhstan.
- Karabekova, D.Zh.** — PhD, Assistant professor, Ye.A. Buketov Karaganda State University, Kazakhstan.
- Karthbaeva, G.T.** — Candidate of biological sciences, Head of the Department, Ye.A. Buketov Karaganda State University, Kazakhstan.
- Kashkanov, A.A.** — Associate Professor, Candidate of technical sciences, Doctoral student, Kharkiv National Automobile and Road University, Kharkiv, Ukraine.
- Kazhikenova, S.Sh.** — Doctor of technical sciences, Associate professor, Head of the Department, Karaganda State Technical University, Kazakhstan.
- Khassenov, A.K.** — PhD, Assistant professor Ye.A. Buketov Karaganda State University, Kazakhstan.
- Kucheruk, V.Yu.** — Professor, Doctor of science (Engineering), Head of the Department, Vinnytsia National Technical University, Ukraine.
- Kulakov, P.I.** — Professor, Doctor of science (Engineering), Vinnytsia National Technical University, Ukraine.
- Kurmash, A.** — Master student, Ye.A. Buketov Karaganda State University, Kazakhstan.
- Kurytnik, I.** — Professor, Doctor of science (Engineering), Head of Department, The W. Pilecki State Higher School, Oswiecim, Poland.

- Kylyshkanov, M.K.** — Doctor of physical and mathematical sciences, Professor, «Ulba Metallurgical Plant» JSC, Ust-Kamenogorsk, Kazakhstan.
- Laurinas, V.Ch.** — Candidate of physical and mathematical sciences, Docent, Ye.A. Buketov Karaganda State University, Kazakhstan.
- Lyashuk, O.** — Doctor of technical sciences, Professor, Ternopil Ivan Pul'uj National Technical University, Ukraine.
- Makhanov, K.M.** — Candidate of physical and mathematical sciences, Docent, Ye.A. Buketov Karaganda State University, Kazakhstan.
- Min'kov, L.L.** — Doctor of physical and mathematical sciences, Tomsk State University, Russia.
- Mukazhan, A.E.** — Master student, Ye.A. Buketov Karaganda State University, Kazakhstan.
- Muratova, A.K.** — Master student, Ye.A. Buketov Karaganda State University, Kazakhstan.
- Nausharban, Zh.K.** — Master student, Ye.A. Buketov Karaganda State University, Kazakhstan.
- Nussupbekov, B.R.** — Professor, Candidate of technical sciences, Dean, Ye.A. Buketov Karaganda State University, Kazakhstan.
- Nurgalieva, Zh.G.** — Senior lecturer, Ye.A. Buketov Karaganda State University, Kazakhstan.
- Omarov, N.N.** — PhD student, Ye.A. Buketov Karaganda State University, Kazakhstan.
- Oshanov, Y.Z.** — PhD student, Ye.A. Buketov Karaganda State University, Kazakhstan.
- Pogrebnyak, A.D.** — Doctor of physical and mathematical sciences, Professor, Sumy State University, Ukraine; Chief specialist of Center for Priority Development «VERITAS», D. Serikbayev East Kazakhstan State Technical University, Ust-Kamenogorsk, Kazakhstan.
- Ranova, G.A.** — Junior researcher, Ye.A. Buketov Karaganda State University, Kazakhstan.
- Rozhkova, K.S.** — Master, Teacher, Ye.A. Buketov Karaganda State University, Kazakhstan.
- Sadenova, K.K.** — Senior lecturer, Ye.A. Buketov Karaganda State University, Kazakhstan.
- Sakenova, R.E.** — PhD student, D. Serikbayev East Kazakhstan State Technical University, Ust-Kamenogorsk, Kazakhstan.
- Schrager, E.R.** — Doctor of physical and mathematical sciences, Professor, National Research Tomsk State University, Russia.
- Seliverstova, E.V.** — PhD, Senior lecturer, Ye.A. Buketov Karaganda State University, Kazakhstan.
- Semenov, A.A.** — Candidate of technical sciences, Professor, Vinnitsa National Technical University, Ukraine.
- Shaimerdenova, K.M.** — Candidate of technical sciences, Associate professor, Head of the Department, Ye.A. Buketov Karaganda State University, Kazakhstan.
- Shaltakov, S.N.** — PhD student, Ye.A. Buketov Karaganda State University, Kazakhstan.
- Sharzadin, A.M.** — Candidate of pedagogical sciences, Associate professor, Ye.A. Buketov Karaganda State University, Kazakhstan.
- Skubnevskii, E.V.** — Candidate of physical and mathematical sciences, Institute of Semiconductor Physics named after av. Rzhanov, Siberian Branch, Russia.
- Slobodian, L.** — Assistant, Ternopil Ivan Pul'uj National Technical University, Ukraine.
- Sokil, M.** — PhD, Associate professor, Lviv Polytechnic National University, Ukraine.
- Stoev, M.** — Associate Professor, PhD, Doctor engineering, Southwestern University «Neophyte Rilski», Blagoevgrad, Bulgaria.
- Tanasheva, N.K.** — PhD, scientific Secretary, Institute of Applied Mathematics, Karaganda, Kazakhstan.
- Tleukenov, S.K.** — Doctor of physical and mathematical sciences, Professor, L.N. Gumylev Eurasian National University, Nur-Sultan, Kazakhstan.
- Tussyphaeva, A.S.** — Master student, Ye.A. Buketov Karaganda State University, Kazakhstan.
- Vovk, Yu.** — PhD, Associate professor, Ternopil Ivan Pul'uj National Technical University, Ukraine.
- Yurov, V.M.** — Candidate of physical and mathematical sciences, Docent, Ye.A. Buketov Karaganda State University, Kazakhstan.

Zeinolla, B.K. — Master student, Ye.A. Buketov Karaganda State University, Kazakhstan.

Zhukenov, M.K. — Candidate of physical and mathematical sciences, Associate Professor, S. Toraighyrov Pavlodar State University, Kazakhstan.

Zhumabekov, A.Zh. — PhD student, Ye.A. Buketov Karaganda State University Kazakhstan.